Infection dynamics and virus-induced apoptosis in influenza virus A infected adherent and suspension MDCK cells

Dissertation

zur Erlangung des akademischen Grades

doctor rerum naturalium

(Dr. rer. nat.)

von Dipl.-Biochem. Britta Peschel
geb. am 06.07.1984 in Göttingen

genehmigt durch die Fakultät für Verfahrens- und Systemtechnik
der Otto-von-Guericke-Universität Magdeburg

Promotionskommission:

Prof. Dr. rer. nat. Dieter Schinzer (Vorsitz)
Prof. Dr.-Ing. Udo Reichl (Gutachter)
Prof. Dr. rer. nat. Bettina Weiß (Gutachterin)
Prof. Dr. rer. nat. Wolfgang Marwan (Gutachter)

eingereicht am: 27.11.2014
Promotionskolloquium am: 17.04.2015

Forschungsberichte aus dem Max-Planck-Institut
für Dynamik komplexer technischer Systeme

Band 44

Britta Peschel

Infection dynamics and virus-induced apoptosis in influenza virus A infected adherent and suspension MDCK cells

Shaker Verlag
Aachen 2015

Bibliographic information published by the Deutsche Nationalbibliothek
The Deutsche Nationalbibliothek lists this publication in the Deutsche Nationalbibliografie; detailed bibliographic data are available in the Internet at http://dnb.d-nb.de.

Zugl.: Magdeburg, Univ., Diss., 2015

Printed in Germany.

ISBN 978-3-8440-3738-8
ISSN 1439-4804

Shaker Verlag GmbH • P.O. BOX 101818 • D-52018 Aachen
Phone: 0049/2407/9596-0 • Telefax: 0049/2407/9596-9
Internet: www.shaker.de • e-mail: info@shaker.de

Abstract

Besides the classical production in embryonated chicken eggs, influenza vaccines can also be produced in cell culture-based processes. These cell culture processes have many advantages over egg-based processes such as a higher flexibility regarding lead times of production campaigns and as an alternative for vaccine manufacturing in case of avian influenza epidemics. To optimise productivity of cell culture processes not only improved cell growth but also the understanding of virus host cell interaction is of crucial importance. Thereby, limiting steps and starting points for optimisation of upstream processing can be identified. In order to contribute to this understanding, aim of this thesis was to characterise influenza virus infection dynamics and virus-induced apoptosis of host cells. Flow cytometric staining of the influenza virus NP protein was used to monitor the time course of infection and a TUNEL assay to characterise progress of apoptosis.

Firstly, studies on statistical analysis of flow cytometric data including the choice of cytometric control samples were carried out. Secondly, infections of adherent Madin-Darby canine kidney (MDCK) cells with different influenza virus strains at several multiplicity of infection (MOI) were performed, followed by studies on defective interfering particles (DIPs). Thirdly, infections of adherent MDCK cells were additionally performed in stirred tank bioreactors (STR). Finally, the MDCK.SUS2 suspension cell line was characterised for influenza virus propagation. Analysis of virus-induced apoptosis and infection dynamics both in dependence of virus strain and MOI as well as for an adherent and a suspension cell line are unique features of this thesis. In addition, data obtained in this work were used in research collaborations for stochastic as well as deterministic mathematical models of influenza virus propagation in cell culture.

At MOI 10^{-4} all influenza virus strains tested in adherent MDCK cells in T25-flasks (A/PR/8 from the Robert Koch Institute (RKI) and from the National Institute for Biological Standards and Control (NIBSC), A/Uruguay/716/2007-like high growth reassortant (HGR) and A/Wisconsin/67/2005-like HGR) showed few strain-specific differences in haemagglutination (HA) titre and Tissue Culture Infective Dose 50 ($TCID_{50}$) and a late apoptosis induction. In MOI 3 infections with influenza A/PR/8 NIBSC an early and strong apoptosis induction and no increase in $TCID_{50}$ was observed. For all strains, except for the Wisconsin-like HGR, maximum HA titre was not affected by the MOI, with 3.0 $\log_{10}$ HAU/100 µL as highest HA titre obtained in infections with the Uruguay-like HGR. In contrast, maximum $TCID_{50}$ decreased with increasing MOI, probably caused by DIPs. Overall, these data demonstrate the importance of low MOI infection conditions in virus production to obtain high infectious virus titres.

The influence of DIPs on infection dynamics, HA titre, and $TCID_{50}$ was demonstrated in infections of adherent MDCK cells with influenza A/PR/8 NIBSC seed virus containing 5.4 x 10^6 to 1.0 x 10^9 infectious virus particles (IVP)/mL (0.2% to 21.3% IVP of total virus particles). A high percentage (21.3%) in the seed virus resulted in maximum $TCID_{50}$ of 3.2 x 10^9 IVP/mL, while in infections with virus seeds containing low amounts of IVP (0.2%) no increase in $TCID_{50}$ was observed. This demonstrates that virus seeds have to be carefully controlled to guarantee high yield virus production.

Infections of adherent MDCK cells with influenza virus A/PR/8 NIBSC in STR showed a 4 h earlier onset of infection with a 0.6 $\log_{10}$ HAU/100 µL lower final HA titre, compared to infections with influenza A/PR/8 RKI. Influenza Uruguay-like and Wisconsin-like HGRs did not reach final HA titres and maximum $TCID_{50}$ of infections with A/PR/8 RKI (3.3 $\log_{10}$ HAU/100 µL, 1.3 x 10^9 IVP/mL). A low MOI infection (10^{-5}) of MDCK cells with influenza A/PR/8 RKI resulted in an increased maximum $TCID_{50}$ of 2.4 x 10^9 IVP/mL compared to MOI 0.025 infections. In addition, infection of adherent MDCK cells with influenza A/PR/8 RKI in serum-free medium without washing steps was performed that showed final HA titre, maximum $TCID_{50}$, and infection dynamics comparable to infections with washing steps. Thus, direct infection was successfully demonstrated to be a possible alternative for influenza virus propagation.

As an alternative to the use of adherent MDCK cells, the suspension cell line MDCK.SUS2 was characterised for influenza virus A propagation in serum-free medium. Testing different medium exchange strategies revealed a 1:2 dilution of the culture broth at time of infection as optimal to achieve fast onset of infection and to obtain high HA titres. MOI 10^{-5} infections of MDCK.SUS2 cells with influenza A/PR/8 RKI showed lower HA titres and $TCID_{50}$ and more pronounced virus-induced apoptosis levels compared to adherent MDCK cells. Future studies will have to clarify whether the increased apoptosis of MDCK.SUS2 cells is related to changes in cellular factors during the cell line adaptation process.

In summary, this work demonstrated low MOI infection conditions to be beneficial for optimisation of $TCID_{50}$ yields in influenza A virus production. Infection dynamics depended, however, on virus strain, especially in terms of virus-induced apoptosis. In addition, presence of DIPs in seed virus strongly influenced infectious virus yields. Finally, a MDCK suspension cell line was demonstrated to be an alternative to adherent MDCK cells, offering a production process that is easier to scale-up. Still, in infections with adherent MDCK cells higher HA titre and $TCID_{50}$ were obtained. Concluding, this work contributed to the understanding of influenza virus propagation in cell culture, and provided valuable insights for optimisation of upstream processing in influenza vaccine production.

Kurzfassung

Als Alternative zur Produktion in bebrüteten Hühnereiern werden Influenza Vakzine heute teilweise bereits in zellkulturbasierten Prozessen hergestellt. Diese Prozesse bieten einige Vorteile wie eine hohe Flexibilität der Produktionsvorlaufzeiten und sind eine Alternative zur Vakzinproduktion im Falle von Vogelgrippeausbrüchen. Zahlreiche Zelllinien werden in der Literatur als zur Influenzavirusvermehrung geeignet beschrieben. Zur Erhöhung der Produktivität dieser zellkulturbasierten Prozesse ist nicht nur die Verbesserung des Zellwachstums von Bedeutung, sondern auch das Verständnis der Virus-Wirtszell-Interaktion. Dies ermöglicht das Auffinden limitierender Schritte und Ansatzpunkte zur Optimierung des *Upstream Processing*. Ziel dieser Arbeit war durch die Charakterisierung von Influenza Virus Infektionsdynamiken und virusinduzierter Apoptose einen Beitrag hierzu zu leisten. Dazu wurden eine durchflusszytometrische Färbung eines Virusproteins sowie ein TUNEL Assay zur Apoptosemessung durchgeführt.

Zunächst wurde die statistische Auswertung durchflusszytometrischer- und Virustiter-Daten sowie die Wahl der Kontrollproben für die Zytometrie untersucht. Dann wurde in statischen Kulturgefäßen der Einfluss der *multiplicity of infection* (MOI) sowie die Rolle von *defective interfering particles* (DIPs) analysiert. Im Anschluss wurden Rührkesselversuche mit adhärenten Zellen durchgeführt. Schließlich wurde eine Suspensionszelllinie zur Influenzavirusvermehrung charakterisiert. Die Analyse von Infektionsdynamik und virusinduzierter Apoptose in Abhängigkeit der MOI und des Virusstammes sowie im Vergleich einer adhärenten mit einer Suspensionszelllinie sind Alleinstellungsmerkmale dieser Arbeit. Darüber hinaus wurden Daten dieser Arbeit zur mathematischen Modellierung der Influenzavirusvermehrung in Zellkultur im Rahmen von Forschungskooperationen genutzt.

Infektionen adhärenter *Madin-Darby canine kidney* (MDCK) Zellen in T-Flaschen bei MOI 10^{-4} zeigten geringe Unterschiede in Hämagglutinations (HA) Titer und *Tissue Culture Infective Dose 50* ($TCID_{50}$) und eine späte virusinduzierte Apoptose aller getesteten Virusstämme (A/PR/8 vom Robert-Koch-Institut (RKI) und vom *National Institute for Biological Standards and Control* (NIBSC), A/Uruguay/716/2007-like *high growth reassortant* (HGR) und A/Wisconsin/67/2005-like HGR). Infektionen mit Influenza A/PR/8 NIBSC zeigten bei MOI 3 eine frühe und starke Apoptoseinduktion sowie keinen Anstieg im $TCID_{50}$. Außer für Wisconsin-like zeigten die finalen HA Titer keine Abhängigkeit von der MOI; der höchste Titer 3.0 $\log_{10}$ HAU/100 µL wurde in Infektionen mit Uruguay-like HGR erzielt. Im Gegensatz zum HA Titer nahm der maximale $TCID_{50}$ mit zunehmender MOI ab, vermutlich durch die Anreicherung von DIPs bei hohen MOI. Die Daten zeigen damit, dass niedrige MOI eine besondere Rolle für hohe $TCID_{50}$ spielen.

Der Einfluss von DIPs auf Infektionsdynamik und Virustiter wurde weiter in einer Studie mit verschiedenen Chargen A/PR/8 NIBSC Saatvirus untersucht, die $TCID_{50}$ zwischen 5.4×10^6 und 1.0×10^9 infektiöse Viruspartikel (IVP)/mL (0.2 bis 21.3% IVP) besitzen. Saatvirus mit hohem Anteil an IVP (21.3%) erzielte einen maximalen $TCID_{50}$ von 3.2×10^9 IVP/mL, wohingegen Saatvirus mit geringem Anteil an IVP (0.2%) keinen Anstieg im $TCID_{50}$ bewirkte. Dies zeigt, dass die Saatviruszusammensetzung kontrolliert werden muss, um hohe Virustiter in der Influenzavakzinproduktion zu erhalten.

Rührkesselinfektionen adhärenter MDCK Zellen mit A/PR/8 NIBSC zeigten einen um 4 Stunden früheren Anstieg und einen um 0.6 $\log_{10}$ HAU/100 µL niedrigeren HA Titer im Vergleich zu A/PR/8 RKI Infektionen. Auch mit Influenza Uruguay-like und Wisconsin-like HGRs wurden nicht so hohe Titer wie mit A/PR/8 RKI (3.3 $\log_{10}$ HAU/100 µL, 1.3×10^9 IVP/mL) erreicht. Infektionen mit A/PR/8 RKI bei niedriger MOI (10^{-5}) zeigten im Vergleich zu MOI 0.025 einen erhöhten maximalen $TCID_{50}$ von 2.4×10^9 IVP/mL. Außerdem zeigte eine direkte Infektion in serumfreien Medium ohne Waschschritte kaum Veränderungen in HA Titer, $TCID_{50}$ und Infektionsdynamik verglichen mit Infektionen mit Waschschritten. Damit wurde eine komplett serumfreie Virusvermehrung als gute Alternative zu Prozessen mit Zellwachstum in serumhaltigem Medium aufgezeigt.

Als Alternative zu adhärenten Zellen wurde die Suspensionszelllinie MDCK.SUS2 zur Virusvermehrung in serumfreiem Medium charakterisiert. Der Vergleich verschiedener Mediumswechselstrategien zeigte, dass eine direkte Infektion ohne Waschschritte zwar möglich, eine 1:2-Verdünnung zum Zeitpunkt der Infektion aber optimal ist, um eine schnelle Infektionsdynamik und hohe Virustiter zu erzielen. MOI 10^{-5} Infektionen zeigten allerdings niedrigere HA Titer und $TCID_{50}$ sowie eine deutlich verstärkte virusinduzierte Apoptose als bei adhärenten MDCK Zellen beobachtet. Weitere Studien werden klären müssen inwieweit die verstärkte Apoptose mit zellulären Veränderungen durch den Adaptationsprozess zusammenhängt.

Zusammenfassend hat diese Arbeit den positiven Einfluss niedriger MOI auf infektiöse Virustiter in der zellkulturbasierten Influenzavermehrung dargelegt. Der Einfluss der MOI hing dabei stark vom Virusstamm ab, besonders in Hinblick auf virusinduzierte Apoptose. Des Weiteren wurde gezeigt, dass DIPs die infektiöse Virusausbeute beeinflussen. Schließlich wurde die MDCK.SUS2 Zelle als leicht hochzuskalierende Alternative zur adhärenten MDCK Zelle getestet. Allerdings blieben HA Titer und $TCID_{50}$ unter denen adhärenter MDCK Zellen. Damit trägt diese Arbeit zum Verständnis der Virusvermehrung in Zellkultur bei und zeigt wertvolle Möglichkeiten zur Optimierung des *Upstream Processing* der Influenzavakzinproduktion auf.

Preface

The work presented in this thesis was conducted during my time as scientific employee at the Max Planck Institute for Dynamics of Complex Technical Systems in Magdeburg from October 2008 until September 2013.

My special thanks are directed to Prof. Dr.-Ing. Udo Reichl (Max Planck Institute for Dynamics of Complex Technical Systems and Otto von Guericke University Magdeburg) for the supervision, the interesting topic, and the possibility to participate at numerous national and international conferences. In addition, special thanks go to PD Dr. rer. nat. habil. Yvonne Genzel (Max Planck Institute for Dynamics of Complex Technical Systems Magdeburg) for the supervision, fruitful discussion, and advice. Additional thanks I owe to Prof. Dr. rer. nat. Bettina Weiß (University of Applied Sciences Esslingen), Prof. Dr. rer. nat. Wolfgang Marwan, and Prof. Dr. rer. nat. Dieter Schinzer (both Otto von Guericke University Magdeburg) for evaluating my thesis as referees and for taking the chair of the commission, respectively.

In completing this work I benefited from the help of M.Sc. Tanja Laske and M.Sc. Sarah Frentzel who conducted their bachelor thesis within my supervision. I like to thank you for your contribution to our good work.

I greatly value the time I could spend with my colleagues at the MPI, especially of the Bioprocess Engineering Group. Here, I want to specially thank the whole Upstream Team and the Molecular Biology Team for the great collaboration inside and outside the lab.

I also gratefully acknowledge the collaborations with Dr.-Ing. Thomas Müller, Dipl.-Ing. Robert Dürr, and Dr.-Ing. Stefan Heldt, the fruitful discussions and successful publications. Furthermore, I want to thank Dr.-Ing. Robert Flassig for support with the statistical analysis of my data.

Furthermore, I am truly grateful for the support and encouragement of my family and my dear friends throughout the course of the thesis. Finally, there are no words to express my thanks to my husband Andreas who always encouraged me, who never stopped believing in me and without whose help, love, and support I would not have completed this thesis.

Britta Peschel Wolfratshausen, April 2015

Content

List of abbreviations

Abbreviation	Meaning
1:2dil	Infection with 1:2 dilution at toi
ATF	Alternating tangential flow
ATP	Adenosine triphosphate
BAD	B cell lymphoma 2-associated death promoter
BAEE	N-α-benzoyl-L-arginine ethyl ester
BAK	Homologous antagonist killer
BAP	Biological active particle
BAPNA	N-α-benzoyl-DL-arginine-4-nitroanilide
BAX	B cell lymphoma 2-associated X protein
Bcl-2	B cell lymphoma 2
BHK	Baby hamster kidney
BP	Band-pass filter
BSA	Bovine serum albumin
ca	Cold-adapted
CAD	Caspase-activated DNAse
CAP	CEVEC's amniocyte production
CHO	Chinese hamster ovary
CHOP	Deoxyribonucleic acid damage-inducible transcript 3
cRNA	Complementary ribonucleic acid
CTL	Cytotoxic T lymphocytes
DI	Defective interfering
DIP	Defective interfering particle
DISC	Death-inducing signalling complex
DNA	Deoxyribonucleic acid
ECACC	European Collection of Cell Cultures
EDTA	Ethylenediaminetetraacetic acid
ER	Endoplasmic reticulum
FADD	Fas-associated protein with death domain
FasL	Fas ligand
Fc	Fragment crystallisable
FCS	Foetal calf serum
FDA	US Food and Drug Administration
FI	Fluorescence intensity
FITC	Fluorescein isothiocyanate
FL	Fluorescence light
fMLP	Formyl-methionine-leucine-phenylalanine
FSC	Forward scatter channel
GMEM	Glasgow's Minimum Essential Medium

HA	Haemagglutinin
HAU	Haemagglutination units
HEK-293	Human embryonic kidney
HEPES	4-(2-hydroxyethyl)-1-piperazineethanesulfonic acid
HGR	High growth reassortant
hpi	Hours post infection
h	Hour
IgG	Immunoglobulin G
IRF7	Interferon regulatory factor 7
IVP	Infectious virus particles
LAIV	Live attenuated influenza vaccines
M1	Matrix protein 1
M2	Matrix protein 2
MDCK	Madin-Darby canine kidney
MESF	Molecules of equivalent soluble fluorochrome
min	Minute
MOI	Multiplicity of infection
mRNA	Messenger ribonucleic acid
NA	Neuraminidase
NEP	Nuclear export protein
NFκB	Nuclear factor κ-light-chain-enhancer of activated B cells
NIBSC	National Institute for Biological Standards and Control
niCKP	Non-infectious cell-killing particles
NP	Nucleoprotein
NS1	Non-structural protein 1
NS2	Non-structural protein 2
PARP	Poly adenosine diphosphate ribose polymerase
PB1	Polymerase basic 1
PB2	Polymerase basic 2
PBS	Phosphate buffered saline
PCR	Polymerase chain reaction
PFP	Plaque-forming particles
PI3K	Phosphatidylinositide 3-kinase
PMT	Photomultiplier tube
pNA	p-nitroaniline
PR	Puerto Rico
PS	Phosphatidylserine
RdRp	ribonucleic acid-dependent ribonucleic acid polymerase
RIG-1	Retinoic acid-inducible gene 1
RKI	Robert Koch Institute
RNA	Ribonucleic acid

ROS	Reactive oxygen species
SD	Standard deviation
SOP	Standard operation procedure
SSC	Side scatter channel
STR	Stirred tank bioreactor
TCID50	Tissue culture infective dose 50
TdT	Terminal deoxynucleotidyl transferase
TMR	Tetramethylrhodamine
TNF	Tumour necrosis factor
toi	Time of infection
TPCK	Tosyl phenylalanyl chloromethyl ketone
TRAIL	TNF-related apoptosis-inducing ligand
TUNEL	TdT-mediated dUTP nick end labelling reaction
WHO	World Health Organization
wME	Infection with medium exchange
w/oME	Infection without medium exchange
VLP	Virus-like particle
vRNA	Viral ribonucleic acid
vRNP	Viral ribonucleoprotein complex

1 Introduction

Motivation and scope

Influenza is an illness of the upper respiratory tract annually causing epidemics with a severe economic burden. Especially in children, elderly, or immune suppressed people, influenza can also be fatal. Though therapeutics like neuraminidase inhibitors can suppress spreading of most influenza virus strains if taken very early after infection, the best means for protection against influenza is vaccination. For more than 50 years influenza vaccines are produced in embryonated chicken eggs, as a broad spectrum of influenza virus strains can be propagated in that way. The latter aspect is of great importance, as the influenza virus, i.e. the pathogen causing influenza, has a high mutation rate, resulting in the need of an annually adapted vaccine that matches the current circulating virus strains (Pleschka 2013).

However, the production of influenza vaccines in chicken eggs has some severe drawbacks such as being very labour-intensive, depending on a reliable egg supply, and being inapplicable for people with allergies against chicken proteins, although recent studies now put this hypothesis to question (reviewed by Kelso 2014). Therefore, cell culture-based processes were developed for influenza virus propagation since the mid-1990s. These processes aim at speeding up the production, becoming independent from egg supply, being closer to the original virus isolate and other benefits (Feng *et al.* 2011; Gregersen *et al.* 2011).

Nowadays, few cell culture-produced influenza vaccines are available on the market, produced in mammalian or baculovirus-insect cell systems (Chan and Tambyah 2012; Reynales *et al.* 2012; Doroshenko and Halperin 2009; Yang 2013), and there is still room for optimisation of the production process. In cases of pandemics, production capacities are not sufficient, emphasising the need for increased product yields. Most importantly, high virus titre yielding production cell lines that are able to propagate a broad range of virus types are needed to meet short term demands. Therefore, understanding of virus-host cell interaction and virus propagation is of major importance in order to identify potential starting points for optimisation. Several methods are being used for this purpose; in this work the very sensitive method flow cytometry, widely used in immunology, will be used to evaluate influenza virus propagation and virus-induced apoptosis. This method enables a simultaneous detection of several parameters, thereby creating highly interesting data sets that are basis for development of optimisation strategies of cell culture-based vaccine production processes and mathematical modelling approaches.

Nowadays, several cell lines are in use for industrial cell culture-based influenza vaccine production and influenza virus propagation with research interests, like mammalian, avian or insect cell lines. Besides Vero cells or Per.C6 cells, the adherent Madin-Darby canine kidney (MDCK) cell line was found to be a suitable substrate for influenza virus propagation. Because the production process with adherent cells requires microcarriers, the cultivation is laborious and especially scale-up is cumbersome. For these reasons suspension cell lines are an interesting alternative, enabling a production process that is easier to scale-up.

Structure of the thesis

First aim of this work is to characterise different influenza A virus strains at various multiplicities of infection (MOI) in adherent MDCK cells in terms of infection dynamics, virus-induced apoptosis, and virus titres. As bioreactor systems are not feasible for this purpose, firstly a smaller screening system is to be found, tested, and established. The influence of the change in MOI is to be investigated, in order to better understand its effect on infection dynamics and virus-induced apoptosis; and to demonstrate if different influenza virus A strains react differently to a change in MOI.

The infection study with different MOIs revealed defective interfering particles (DIPs) to play an important role in our infection experiments, as being present in all seed virus preparations, influencing especially infectious virus titres. For this purpose, studies should be performed investigating the influence of these DIPs on infection dynamics and virus-induced apoptosis.

The influenza virus strains tested in adherent MDCK cells in the small screening system should also be propagated in stirred tank bioreactors. In addition, the influence of lowering the MOI as well as a direct infection without washing steps on infection dynamics, virus-induced apoptosis, and cell-specific virus yields was to be investigated.

Furthermore, as an alternative to adherent cells, a suspension cell line should be characterised for influenza virus propagation. The MDCK.SUS2 cell line was shown by Lohr *et al.* (2010) to be a substrate for influenza virus propagation. It was chosen for characterisation of virus yields, infection dynamics, and virus-induced apoptosis, as it had been directly derived from the high virus titre-yielding adherent MDCK cell line. After an optimisation of infection conditions, two influenza A virus strains are characterised regarding virus titres, infection dynamics, and virus-induced apoptosis. In addition, a comparison to the parental adherent MDCK cell line is performed.

Summarising, this thesis investigates the influence of virus strains and infection conditions on virus infection dynamics, virus-induced apoptosis, and viral yields; thereby contributing

to the understanding of virus-host cell interaction in the upstream part of a cell culture-based influenza vaccine production process. Findings of this work help to optimise virus propagation through optimal low MOI infection condition and demonstrate the importance of DIPs in seed virus preparations. Furthermore, a suspension cell line as an alternative to adherent producer cell lines is presented, enabling an easy to handle and scale-up virus propagation process.

2 Theoretical background

In the following chapter, the theoretical background of influenza virus (section 2.1), influenza virus propagation in cell culture (section 2.2), and apoptosis is presented (section 2.3). Furthermore, the interplay of influenza virus replication and apoptosis is illustrated. Finally, flow cytometry, as a valuable method for analysis of influenza virus propagation in mammalian cells and influenza virus-induced apoptosis, is introduced (section 2.4).

2.1 Influenza virus

Influenza is an infection of the upper respiratory tract with symptoms of fever, muscle or body aches, and coughing. Especially with infants and people of poor health, or weakened prior to the infection, influenza can lead to death. The World Health Organization (WHO) reports of 250.000–500.000 annual deaths of influenza (WHO 2014). Annually, up to 500 million people suffer from influenza but generally recover, resulting in a total economic burden of estimated US$ 87.1 billion (confidence interval: $47.2, $149.5) for the US in 2003 (Molinari *et al.* 2007).

Three types of influenza viruses are known: influenza virus A, B, and C. Influenza virus A is the most abundant type being able to infect different hosts, like human, avian, swine, or equine. Influenza B viruses are limited to humans, but cause less intense symptoms compared to influenza A. The third type, influenza C, is the less abundant type causing only mild common-cold symptoms in humans. In this thesis, focus is on influenza A virus as the most common and for humans most dangerous type.

Through its high mutation rate and new genetic combinations influenza virus A induces new epidemics every year. From time to time influenza viruses with high infectivity emerge causing epidemics, or even pandemics. This is due to the ability of the virus to use different animals as hosts. When different strains infect the same host cell simultaneously, the virus can form new genetic combinations (termed reassortment). For example, the outbreak of the pandemic influenza H1N1 virus in 2009 was traced back to be a reassorted strain from avian and human origin that mixed in swine before passing to humans (Trifonov *et al.* 2009; Smith *et al.* 2009).

The best way for protection against influenza epidemics is vaccination of the population. The International Federation of Pharmaceutical Manufacturers & Associations calculated the annual worldwide demand for trivalent vaccine doses to exceed 400 million (Ifpma 2013). Vaccines for human use have to fulfil strict regulatory requirements regarding

efficacy, potency, and safety. The task of adequate vaccine supply is challenged by the constant mutations and reassortment of the virus. Furthermore, potential pandemics can cause short term demands for vaccine doses. Also, the costs for an influenza vaccine dose should be affordable to improve vaccine availability even in developing countries.

2.1.1 Influenza virus A: structure and replication

The influenza virus A is part of the *Orthomyxoviridae* family, and is a negative-stranded enveloped ribonucleic acid (RNA) virus (Figure 2-1). Within its lipid envelope it carries eight gene segments which code for—to date known—15 proteins (Vasin *et al.* 2014). These gene segments are present as ribonucleoprotein complexes (vRNPs), consisting of the RNA segment that is coupled to nucleoproteins (NP) and a heterotrimeric polymerase complex (Noda and Kawaoka 2012; Moeller *et al.* 2012; Zheng and Tao 2013).

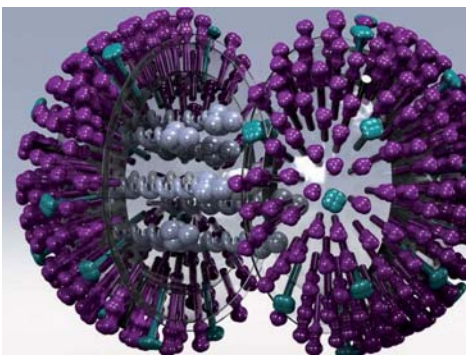

Figure 2-1 Structure of an influenza virus A particle: on the outside haemagglutinin (HA) (purple) and neuraminidase (NA) (turquoise) molecules are located. Within the virus eight vRNPs (grey) are present. See text for details (source: bioprocess engineering group MPI Magdeburg).

In the viral envelope the proteins haemagglutinin (HA) and neuraminidase (NA) are located. Haemagglutinin is responsible for attachment of the virus to the host cell by its ability to bind sialic acids on host cell membranes (Luo 2012). Neuraminidase is described to play a role in early infection and during the endocytic pathway (Matrosovich *et al.* 2004; Suzuki *et al.* 2005; Ohuchi *et al.* 2006). In the later course of infection NA is responsible for the release of virus particles from the cellular membrane (Palese and Compan 1976). As both envelope proteins project from the surface of the virus they are the immunogenic part of the virus and thus mainly used as antigens in classical influenza vaccines.

To date, 18 different subtypes of HA and 11 different NA are known, according to which classifications are made (Knipe and Howley 2013). H17N10 and H18N11 viruses were just recently discovered in bats (Wu *et al.* 2014a). Most abundant are influenza viruses A types H1N1, H3N2, and the avian H5N1 and H5N7. New virus variants also emerge in humans, like the avian H10N8 that was reported to be responsible for death of at least one person in December 2013 (To *et al.* 2014; Parry 2014; Chen *et al.* 2014; García-Sastre and Schmolke 2014).

Also located in the viral membrane are the virus matrix proteins 1 and 2 (M1 and M2). M1 is a capsid protein and M2 an ion channel protein responsible for proton transport into the virus particle when the virus is internalised by endocytosis and later in the virus life cycle. The other viral proteins are the very numerous nucleoprotein (NP), 3 polymerases, called polymerase basic 1 (PB1), polymerase basic 2 (PB2), and polymerase acidic (PA) (forming the heterotrimeric RNA-dependent RNA polymerase (RdRp)), the non-structural protein 1 (NS1) (Schneider and Wolff 2009), and the nuclear export protein (NEP, also termed non-structural protein 2 (NS2)) (Paterson and Fodor 2012). Since 2001 several proteins resulting from frameshifts of the polymerases-coding gene segments were identified: PB1-F2 (Chen *et al.* 2001), PB1-N40 (Wise *et al.* 2009), PA-X (Jagger *et al.* 2012), and just recently PA-N155 and PA-N182 (Muramoto *et al.* 2013). Additionally, M42 (Wise *et al.* 2012) and NS3 (Selman *et al.* 2012), resulting from alternative splicing of the matrix proteins-coding gene segment 7, and the NS proteins-coding segment 8, were described. An overview of the recently discovered proteins is given by Vasin *et al.* (2014).

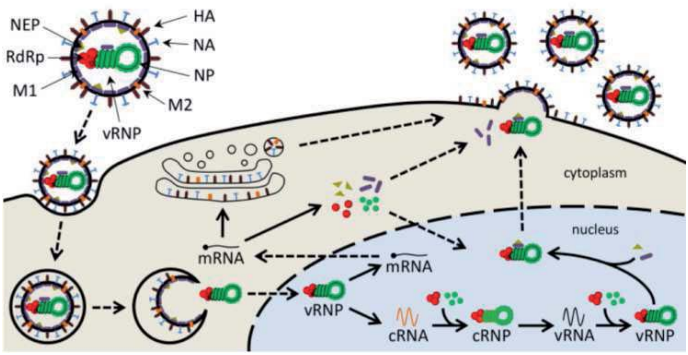

Figure 2-2 Overview influenza virus A replication cycle (for the sake of clarity only one virus particle containing only one vRNP is shown): upon binding the virus is internalised, the viral genome is released into the cytoplasm and transported into the nucleus where vRNPs are transcribed into messenger RNA and complementary RNA molecules. The former is used for transcription into viral proteins; the latter is used for formation of new vRNPs. Finally, budding of new virus particles takes place via the cytoplasmic membrane. See text for more details. Adapted from Heldt *et al*. (2012).

The replication cycle is schematically shown in Figure 2-2. To infect a host cell HA needs to be cleaved into the HA1 and HA2 subunits by a protease. Afterwards, the HA protein binds to alpha 2,3 or 2,6-linked sialic acids present on host cell membrane proteins followed by internalisation of the virus into the cell by endocytosis. After acidification of the endosome the virus membrane fuses with the endosomal membrane and through uncoating the virus content is released into the cytoplasm. Within the nucleus negative-stranded viral RNA ((-)vRNA) are transcribed into positive-stranded viral messenger RNA ((+)mRNA) and positive complementary RNA ((+)cRNA) molecules. The viral mRNAs serve as templates for virus proteins using the host cell's protein synthesis machinery. NA and HA pass the Golgi apparatus to become glycosylated before being transported to the host cell membrane. The (+)cRNA is transcribed again into (-)vRNA to provide RNA segments to be complexed with several NPs and the RdRp to form vRNPs that are transported to the cell membrane and packaged into the newly forming virus particles. To finally release the budding virus particle neuraminidase activity is necessary to cut the sialic acid residues that still link the virus to the host cell membrane.

As the viral RdRp lacks a proofreading function the virus is subjected to a high genetic variability, termed antigenic drift. Due to these point mutations the antigenic epitopes change and the virus is not easily recognised by the mammalian immune system. Furthermore, when a cell is infected by two or more virus strains at a time, the nature of a segmented genome allows new combinations of viral gene segments (termed reassortment) of different virus strains, resulting in completely new virus variants (antigenic shift). Together, both effects result in new virus strains emerging every season, potentially causing epidemics or even pandemics. Hence, for an adequate protection of the population the seasonal influenza vaccine is annually adapted.

2.1.2 Influenza vaccines: classical production and new developments

Advantages and Disadvantages of egg-based vaccine production

Since the 1950s influenza vaccines are produced in a process that uses the ability of influenza viruses A and B to replicate in the allantoic cavity of embryonated hen's eggs. This process is well established with a long history of success for seasonal influenza vaccines with proved safety and efficacy and low technical hurdles. These optimised and robust processes are able to meet the global demand of seasonal influenza vaccines (Lee and Hu 2012).

Although this process is well established, it holds some severe drawbacks. Firstly, the process relies on a sufficient supply with pathogen-free chicken eggs, which could be at

risk in cases of avian influenza epidemics in chicken flocks. Furthermore, dependency on chicken eggs reduces the process' flexibility, as eggs cannot be produced quickly. Thus, in case of influenza epidemics or pandemics with a high demand for supply of vaccine doses, limitations could occur (Gerdil 2003; Partridge and Kieny 2013). Another aspect to consider regarding egg-based processes is the increasing proportion of people developing allergies against chicken proteins (Zeiger 2002), although a recent review disagrees with that (Kelso 2014). Furthermore, virus isolates generated using cell culture are clinically more relevant than the egg-derived isolates, as egg passaging favours mutations in the HA that influence receptor-binding capacity, antigenicity, and immunogenicity of the strain (Robertson *et al.* 1987; Robertson 1993). Overall, the egg-based process is very time-consuming with vaccine producers usually starting in February and March production of the next seasonal influenza vaccine for the northern hemisphere.

Influenza vaccine developments

Currently, seasonal influenza vaccines contain H1 and H3 antigens of two influenza virus A and of one influenza virus B strains, termed trivalent vaccines. Typically, they contain 15 µg of HA of each strain per vaccine dose. Ongoing development is to include a second influenza B strain in order to create quadrivalent vaccines (Reed *et al.* 2012; Nafziger and Pratt 2014; Ambrose and Levin 2012). The need for quadrivalent vaccines is emphasised by the WHO which recommends quadrivalent influenza vaccines since the beginning of the 2013-2014 northern hemisphere influenza season (WHO 2014).

Besides the most common inactivated split or subunit influenza vaccines, other vaccine strategies are under investigation to achieve better immune responses, especially in the elderly (reviewed by Shaw 2012). Live attenuated influenza vaccines (LAIV) using cold-adapted (*ca*) virus strains, for example, are considered to induce a cell-mediated immune response. One example is FluMist® (based on the influenza virus A and B Ann Arbor strains) by the company MedImmune that got approval for the US market by the Food and Drug Administration (FDA) in 2003. Unfortunately, the desired broadened immune response was only demonstrated in young people (Ohmit *et al.* 2006).

Other strategies include reverse genetic approaches (Suphaphiphat *et al.* 2010), DNA-based vaccines (Petsch *et al.* 2012), or immune-stimulating complexes (ISCOMs) (Sanders *et al.* 2005) for vaccination. Also, virus-like particles (VLPs), as successfully generated for different viruses in insect cells (Arif and Pavlik 2013; Fernandes *et al.* 2013), have been investigated for influenza vaccine preparation. In 2013, the first trivalent influenza VLP vaccine produced in baculovirus-infected insect cells received approval (FDA 2013). Furthermore, researchers investigated universal vaccines (Roose *et al.* 2009; Du *et al.* 2010), by addressing conserved sequences, e.g. of the external domain of M2 (M2e) or the

HA stalk region. Adar *et al.* (2009) described the use of a universal influenza vaccine directed against six different conserved virus epitopes in order to broaden the effectiveness against multiple influenza virus strains in mice. In addition, adjuvants like aluminium salts or MF59 and AS03 (both based on squalene) are used to improve the immunogenicity, prolong the exposure time of the antigen, and stimulate immunological signalling cascades of influenza vaccines (reviewed by Tetsutani and Ishii 2012). Finally, vaccine administration using other ways than intramuscular injection, like intradermal administration, are hoped to increase vaccination efficiency (reviewed by Young and Marra 2011).

2.1.3 High growth reassortant virus strains

As early as in the late 1960s so-called high growth reassortant (HGR) virus strains were introduced (Kilbourne 1969) enabling more reliable influenza virus propagation and an improved matching of the vaccine strain to the circulating virus strain.

As different influenza virus strains replicate with different efficiencies, the WHO proposed high growth reassortant strains for usage in influenza vaccine production in order to simplify the production process. The reassortment is possible due to the segmented nature of the influenza virus genome. This enables the combination of segments of different virus strains to be packaged into the same virus particle in cases of co-infected cells (Figure 2-3).

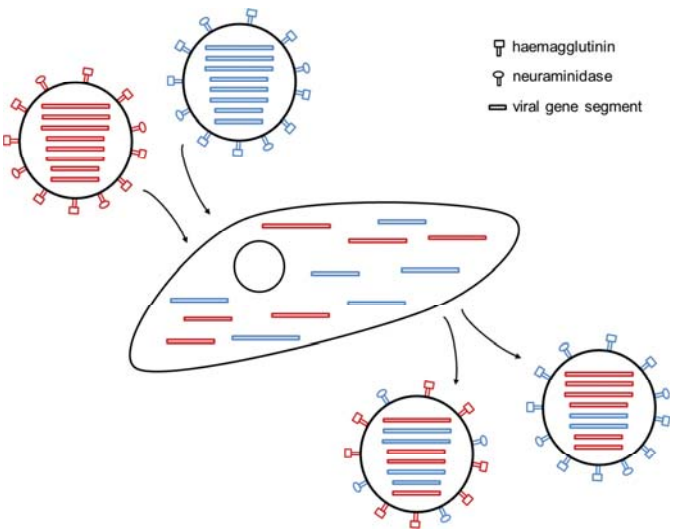

Figure 2-3 Scheme of influenza virus reassortment: upon co-infection with different influenza virus strains (coloured in blue and red) gene segments can be mixed resulting in new virus variants.

For influenza vaccines, so-called 6:2 reassortants are desired that contain influenza gene segments 4 and 6 coding for the immune-relevant proteins HA and NA of the desired seasonal strain and the other six gene segments of a well-characterised high titre-yielding laboratory strain (referred to as backbone, mostly influenza virus A/Puerto Rico/8/34 (A/PR/8)) (Baez *et al.* 1980). Influenza HGR strains can be generated by either of the two methods: the classical method, which is the method currently used for generation of all seasonal influenza vaccines, uses a co-infection of two influenza virus strains in eggs (Kilbourne *et al.* 1971). Afterwards, those strains with the two surface glycoproteins from the field strain are selected. In addition to the classical method, reverse genetic approaches can be used in which Vero cells are transfected with virus-coding plasmids to generate so-called rescued viruses (Hoffmann *et al.* 2002; Neumann *et al.* 2005; Li *et al.* 2013). Currently, only viruses grown in eggs can be used as vaccine virus strains.

Because comparisons of reassorted virus strains with wild type influenza virus strains are performed in this work, literature on this topic is reviewed in the subsequent paragraphs.

Voeten *et al.* (1999) determined time courses for titres of H1N1- and H3N2-based influenza virus reassortants and their wild type background strains in MDCK-SF1 cells that were grown in serum-free EpiSerf medium. They generated reassortants by dual infections of A/PR/8 or A/Hong Kong/2/68 (H3N2) with three strains each and subsequent plaque purification for the correct surface proteins. Genomic composition was analysed for the reassortants with an A/PR/8 backbone. All nine variants had the polymerase and matrix gene segment, and four had a complete A/PR/8 backbone. In most cases, they found higher titres for the reassortants when infecting at MOI 1 x 10^{-3}, 1 x 10^{-4}, 1 x 10^{-5}, and 1 x 10^{-6}. The reassortant with the complete A/PR/8 backbone and HA and NA from A/Wuhan/359/95 showed faster infection dynamics and higher final virus titres for all four tested MOIs compared to infections with its wild type strain, and the highest HA titre of all tested six reassortants. However, strains with a backbone that did not contain all A/PR/8 gene segments also showed better growth characteristics than wild type strains in infection experiments.

Another usage of reassorted influenza virus strains is the generation of virus strains for LAIV production. For this purpose, a virus strain with a *ca* phenotype serves as a backbone. Aggarwal *et al.* (2011) compared 25 different *ca* reassorted influenza virus strains based on the live attenuated master strain A/Ann Arbor/6/60 or B/Ann Arbor/01/64 backbone. They were interested in optimisation of the LAIV production process and performed infections at MOI 1 x 10^{-2}, 1 x 10^{-3}, 1 x 10^{-4}, 1 x 10^{-5}, and 1 x 10^{-6} in shake flasks using adherent MDCK CCL-34 cells. By varying the process parameters time of infection (toi), harvest time and MOI, they optimised LAIV propagation processes to higher infectious virus titres and improved productivities.

2.1.4 Defective interfering virus particles

Due to the high genetic variability and the necessity of eight gene segments to be correctly packaged into new virions, the smallest proportion of virions released by a cell are intact and infectious. For example, Brooke *et al.* (2013) described 90% of the released virus population to be not capable of generating infectious descendants, with most produced viruses lacking at least one essential protein. This might be caused by non-sense or lethal mutations, an unsuccessful transcription of incoming vRNPs, internal deletions resulting in defective interfering RNAs, or virions failing to package one or more vRNP segments. In contrast to the latter finding Chou *et al.* (2012) published data suggesting influenza virus packaging to be highly efficient.

As early as in the 1950s von Magnus described non-infectious influenza virus particles that are not able to replicate on their own, termed von-Magnus-particles (von Magnus 1954). In the following decades a characterisation of this heterogeneous non-infectious virus population was performed (Marcus 1982; Ngunjiri *et al.* 2008; Marcus *et al.* 2009). Biological active particles (BAP) were divided into non-infectious cell-killing particles (niCKP), interferon-inducing particles, and DIPs. While DIPs need an intact helper virus to be replicated they suppress the replication of intact particles in favour of defective particles. In most cases, the presence of DIPs is caused by deletions in different viral gene segments (especially the large segments 1–3 of 2233 to 2341 base pairs coding for the polymerases) with central deletions (Nayak *et al.* 1985). Those shorter gene segments seem to have an advantage in replication because of their length, as well as in packaging. Thus, a co-infected cell will almost solely produce defective particles. In consequence, high MOI conditions lead to a higher probability of co-infections of intact and defective virus particles, thereby favouring the production of DIPs. As they influence the viral outcome of infectious particles, DIPs are an important factor to be considered in influenza seed virus generation and virus production. Especially for production of live attenuated virus strains preventing DIP formation would be crucial. For processes aiming at a continuous virus production, DIPs have to be considered, too. Dilution rates in such processes should be chosen so that low MOI conditions are present most of the time to minimise DIP formation (Frensing *et al.* 2013).

Defective interfering (DI) viruses are also described as a therapeutic and prophylactic drug against influenza virus A infections (Dimmock 2007; and reviewed recently by Dimmock and Easton 2014). Cloned DI viruses were shown to protect mice from acute influenza diseases; however, as shown with immune-deficient mice, the adaptive immune response is necessary to fully clear the infection (Scott *et al.* 2011). Eventually, also ferrets were protected from influenza virus infections with the pandemic influenza virus A/California/04/09 through treatment with DI virus (Dimmock *et al.* 2012).

2.2 Influenza virus propagation using cell culture

In the following sections influenza virus propagation using mammalian cell culture and important factors for this process are described. In section 2.2.1 the procedure of cell culture-based influenza vaccine production is presented, followed by description of cell lines used for virus propagation (section 2.2.2). Finally, the role of the enzyme trypsin for influenza virus propagation in cell culture is explained (section 2.2.3).

2.2.1 Cell culture processes

Some disadvantages of egg-based influenza vaccine production can be overcome by using mammalian cell culture for virus propagation instead of chicken eggs. Nowadays, continuous cells can easily be grown in up to several thousand litres bioreactors, offering high production capacities. For production of recombinant proteins, cell culture is used since the 1980s, with especially Chinese hamster ovary (CHO) cells playing an important role (Wurm 2004; Jayapal *et al.* 2007; Hacker *et al.* 2009). And also for vaccines cell culture is a well-established system, like Vero cells for production of rabies vaccine (Toovey 2007) or poliomyelitis vaccine (Montagnon 1989; Thomassen *et al.* 2014), or PER.C6 cells for poliomyelitis vaccine (Sanders *et al.* 2013).

For influenza virus propagation cell culture-based processes are independent from avian influenza epidemics and eliminate eventual problems concerning people's intolerance against chicken proteins. Another advantage is that the glycosylation pattern of the produced virus is closer to the original isolate than for egg-passaged virus strains. Today's knowledge on the function of the human immune system suggests a different immune response for differentially glycosylated antigens, thus, analysis of glycosylation patterns of proteins used for vaccination is gaining importance (Vigerust and Sheperd 2007; de Vries *et al.* 2012; Hütter *et al*. 2013).

Since the mid-1990s cell-culture techniques are used to propagate influenza virus (Merten *et al.* 1996) in a five step production process (Genzel *et al.* 2014a) (Figure 2-4):

1. Growth of cells up to production scale bioreactor (scale-up)

2. Addition of seed virus to propagate in the cells (virus replication)

3. Separation of the virus from the cells by clarification centrifugation

4. Purification by chromatographic means (downstream processing)

5. Chemical inactivation of the virus; split up to gain only the antigenic relevant parts; blending and filling of the final vaccine

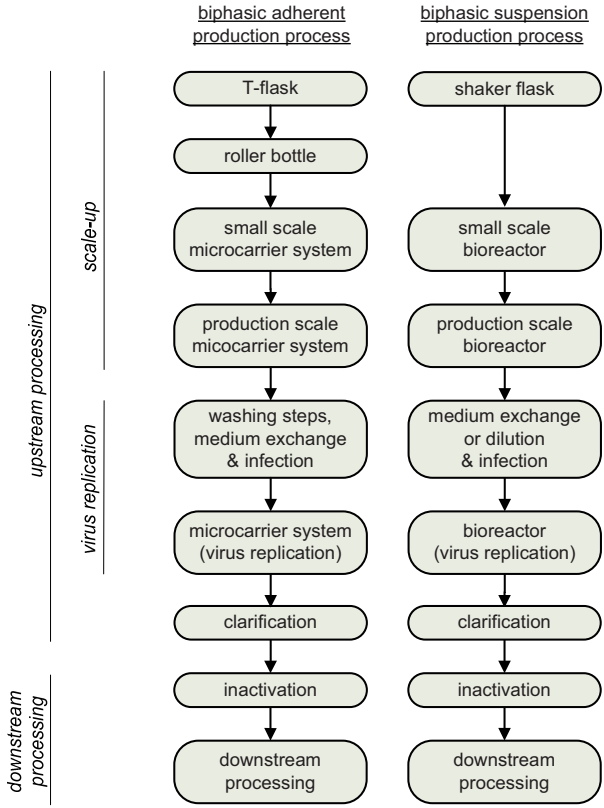

Figure 2-4 Scheme of a cell culture-based influenza vaccine production process using adherent or suspension cells (modified from Genzel *et al.* 2014a).

Vaccines for human use are subjected to many regulations by authorities. Manufacturers have to supply documentation of manufacturing, testing, quality, safety, and efficacy of their product. Besides requirements for the final vaccine (e.g. less than 10 ng of cellular DNA per human dose or not more than 100 µg of total protein per virus strain per human dose), also cell substrates have to be free of contaminants before being approved for usage in vaccine manufacturing. Regulations of cell substrates for human vaccine production are reviewed by Hess *et al.* 2012. Furthermore, vaccine manufacturing should aim at serum-free and animal component-free processes.

To date the following cell culture-generated influenza vaccines were licenced by the European Medicines Agency or FDA. In 2001 and 2007 two influenza vaccines for use in human produced in MDCK cells were licensed for usage in the Netherlands and Europe:

Influvac TC® by Solvay (Brands *et al.* 1999) and Optaflu® by Novartis Behring (Doroshenko and Halperin 2009). In 2009 two pandemic influenza vaccines produced in Vero and MDCK cells, respectively, were licenced (Celvapan® by Baxter and Celtura® by Novartis) (Reynales *et al.* 2012). In November 2012 Novartis received the FDA approval for Flucelvax®, a seasonal influenza vaccine (Chan and Tambyah 2012), and in January 2013 Protein Sciences received FDA approval for Flublok®, a VLP vaccine.

2.2.2 Cell lines for influenza vaccine production

Several cell lines are in use or considered for influenza virus propagation and are discussed in the following sections, with special focus on adherent and suspension MDCK cell lines.

2.2.2.1 Adherent MDCK cell lines

In the 1950s, MDCK cells were isolated by Madin and Darby (1958) from kidney epithelium of an adult cocker spaniel. Later, they were shown to be a possible substrate for influenza virus propagation yielding high virus titres of several influenza virus strains (Gaush and Smith 1968; Tobita 1975; Tobita *et al.* 1975).

Nowadays, two MDCK cell lines are most widely used and commercially available: the MDCK CCL-34 cell line offered by the American Type Culture Collection, and the MDCK 84121903 cell line by the European Collection of Cell Cultures (ECACC). Both cell lines grow adherently, and can thus be cultivated in static cultivation systems like T-flasks and roller bottles up to 1.6×10^5 cells/cm^2. For cultivation in stirred bioreactor systems microcarrier beads (e.g. made of polydextran), are necessary to offer a growth surface. To passage adherent cells and for scale-up, detachment of the cells from the surface with proteases like trypsin is necessary. Conventionally, adherent MDCK cells are grown in serum-containing medium (like foetal calf serum (FCS)-supplemented Glasgow's Minimum Essential Medium (GMEM)). Consequently, prior to influenza virus propagation washing with phosphate buffered saline (PBS) and medium exchange to serum-free virus maintenance medium is needed in order to enable efficient HA cleavage by trypsin. Adherent MDCK cells yield HA titres of up to 3.3 $\log_{10}$ haemagglutination units (HAU)/100 µL (up to 30000 virions/cell), and tissue culture infective dose 50 ($TCID_{50}$) of up to $2–3 \times 10^9$ infectious virus particles (IVP)/mL (1000–2000 IVP/cell) in infections with the common laboratory influenza virus strain A/PR/8 (Genzel *et al.* 2010; Schulze-Horsel *et al.* 2009; Genzel and Reichl 2009).

Studies have shown high cell concentration to result in lower cell-specific yields in cell culture-based virus propagation (Wood *et al.* 1982; Lindsay and Betenbaugh 1992; Wong *et al.* 1996; Maranga *et al.* 2003). By using perfusion and repeated batch modes and up to 12.5 g/L microcarriers for adherent MDCK cell cultivations, Bock *et al.* (2011) were able

to reach up to 1.1 x 10^7 cells/mL. When infecting with influenza A/PR/8 from the Robert Koch Institute (RKI) and the National Institute for Biological Standards and Control (NIBSC) titres of up to 3.7 $\log_{10}$ HAU/100 µL were obtained. Cell-specific yields were comparable to control cultivations with low microcarrier density, thus, the so-called "high-cell density effect" was avoided.

To generate energy, MDCK cells metabolise glucose via the glycolysis into pyruvate. Normally, pyruvate enters the citric acid cycle as acetyl coenzyme A. MDCK cells, however, reduce most of the pyruvate to form lactate. Genzel *et al.* (2004) determined yield coefficient $Y'_{lac/gluc} = 1.65$ during cell growth of adherent MDCK cells. Thus, 90 % of consumed glucose was directly converted into lactate. Besides for energy generation, MDCK cells deaminate glutamine to glutamate, forming ammonia. Afterwards, glutamate is further metabolised via α-ketoglutarate. Genzel *et al.* (2004) determined $Y'_{NH4/gln} = 1.06$ during cell growth of adherent MDCK cells, thus, glutamine was converted in equimolar amounts of ammonia. This glucose and glutamine overflow-metabolism is typical for continuous cell lines and results in formation of large amounts of lactate and ammonia.

Efforts are made to genetically optimise MDCK cells for even higher virus yields. For example Hamamoto *et al.* (2013) steadily knocked down the canine equivalent to the human interferon regulatory factor (IRF) 7 gene in MDCK cells with short hairpin RNAs. Thereby, a 3–5-fold increased amount of viral RNA (relative to untransfected MDCK cells) was detected in the supernatant after infection with influenza virus A/PR/8 and A/Narita/1/2009.

Handling of adherent MDCK cells in bioreactors requires usage of microcarriers. This facilitates cell retention and washing steps. However, for scale-up cumbersome cell detachment steps using proteases have to be performed. This is one major disadvantage for usage of adherent MDCK cells in production processes.

2.2.2.2 MDCK suspension cell lines

The alternatives to adherent cell lines are suspension cell lines. Cultures of suspension cell lines can easily be scaled-up to several thousand litre volumes. Through their adaptation to growth under serum-free medium conditions suspension cells enable a direct infection process without washing steps. The omitting of serum improves lot-to-lot variability, reduces costs and minimises risks of contaminations with viruses, mycoplasmas, and prions. For those reasons adherent MDCK cell lines were adapted to growth in suspension by several groups using different strategies.

The company Novartis Vaccines and Diagnostics holds patents for MDCK suspension cells (named MDCK 33016-PF) that are currently used for production of the influenza vaccines Optaflu® and Celtura® (Doroshenko and Halperin 2009; Reynales *et al.* 2012).

Van Wielink *et al.* (2011) described the generation of a suspension MDCK cell line (termed MDCK-SFS) using the CCL-34 adherent MDCK cell line growing in serum-free medium. MDCK-SFS cells grew to a cell concentration of 2.2 x 10^6 cells/mL, with a maximum specific growth rate of 0.029 h^{-1}. HA titres of MOI 0.01 infections with eight different influenza A strains of H1N1 and H5N7 subtypes ranged between 1.8 and 2.6 $\log_{10}$ HAU/100 µL at 72 hours post infection (hpi). $TCID_{50}$ titres were 3.5 x 10^4 (H5N7)–6.3 x 10^8 (H1N1) IVP/mL at 72 hpi.

A different approach was used by Chu *et al.* who transfected MDCK cells with the human *siat7e* gene coding for a type II membrane sialyltransferase (Chu *et al.* 2009; Chu *et al.* 2010). High *siat7e* expression led to reduced cell adhesion. They hypothesised that the additional negative charges due to more sialic acids promote electrostatic repulsion and thereby facilitate suspension growth. Four different influenza virus strains were investigated for their yields in MDCK-*siat7e* cells. Their specific HA production was 20 times higher than in the parental adherent cell. The authors also performed shake flask infections with three different influenza virus A strains and one influenza virus B strain, namely influenza virus A/California/07/2009 X-179A (H1N1), A/Brisbane/59/2007 IVR-148 (H1N1), A/Uruguay/716/2007 X-175C (H3N2), and B/Brisbane/60/2008 at MOI 0.01 to 0.25. Maximum HA titres were 1:256 (8 $\log_2$ HA/50 µL = 2.7 $\log_{10}$ HAU/100 µL) for the A strains, and 1:2048 (11 $\log_2$ HA/50 µL = 3.6 $\log_{10}$ HAU/100 µL) for the B strain; maximum $TCID_{50}$ were between 1 x 10^6 and 1 x 10^8 IVP/mL. In perfusion cultivations they reached between 1:512 and 1:5790 HAU/50 µL (approximately 3.0 and 3.9 $\log_{10}$ HAU/100 µL). Furthermore, they showed HA titres for three of the four tested influenza virus strains to be higher in 2 L bioreactor cell cultivations compared to propagation in chicken eggs.

Tsutsumi *et al.* (2006) described the adaptation of adherent MDCK cells to suspension growth by incubation of the cells with a metalloendopeptidase purified from *Streptomyces griseus* over a period of 6 months. The resulting suspended cell population was named 6 M-4 cells and shown to proliferate in an anoikis-resistant way. By clonal selection they chose a subpopulation termed 6 M-4-TR7. In infections of 6 M-4-TR7 cells with influenza virus A strains A/New Caledonia/20/1999 (H1N1), A/Panama/2007/1999 (H3N2), and A/Morioka/O-68N/2000 (H3N undefined) in the presence of metalloendopeptidase, HA titres of 64–1024 HA/50 µL (2.1 to 2.7 $\log_{10}$ HAU/100 µL) at MOI 0.001 or 0.002 were obtained.

In this work, the MDCK.SUS2 cell line was used for infection experiments with different influenza virus A strains. This cell line was adapted to growth in suspension using the adherent MDCK 84121903 cell line in cooperation with K. Scharfenberg of FH Emden/Leer (Lohr *et al.* 2010). For this purpose, serum-containing medium was stepwise replaced by a chemically-defined medium over a period of 10 weeks in T25-flasks (Figure 2-5). Afterwards, the suspended single cells and spheroids were transferred to a stirred spinner flask system with the stirrer speed being stepwise increased over the passages of 10 weeks. This process generated a cell line, named MDCK.SUS1, showing a doubling time of >50 hours (h) with a tendency to cell clogging at higher cell concentration. Therefore, faster growing cell fractions were further passaged. Thereby, doubling times could be reduced to 36 h. This cell line was named MDCK.SUS2.

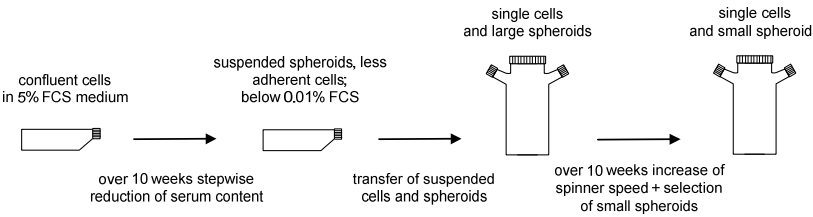

Figure 2-5 Scheme for the adaptation process of adherent MDCK cells to growth in suspension. For details of the adaptation process refer to Lohr *et al.* 2010.

Cultivations of MDCK.SUS2 cells were performed in stirred tank bioreactors and in wave bioreactors, and infections performed with influenza virus B/Malaysia and A/PR/8, respectively (Lohr *et al.* 2010). Maximum viable cell concentration reached 1.9 and 2.3 x 10^6 cells/mL, maximum HA titres achieved 2.75 and 2.9 $\log_{10}$ HAU/100 µL at 72 and 48 hpi for stirred tank and wave bioreactors, respectively. This corresponded to a cell-specific virus yield of 5000 and 7000 virions/cell. $TCID_{50}$ reached its maximum of 7.6 x 10^8 and 1.8 x 10^8 IVP/mL at 60 and 36 hpi. Metabolic profiles showed glucose uptake and lactate release for both, cell growth and infection phase, with a final lactate concentration of 42.8 and 27.4 mmol/L, respectively. Glutamine was taken up during cell growth and virus infection. Ammonia was released during cell growth up to concentration of 4 mmol/L, and further increased up to 5.5 and 6.5 mmol/L by the end of infection. MDCK.SUS2 cells differed in amino acid metabolism from the parental adherent cell line, e.g. by consuming leucine and releasing alanine; whereas adherent MDCK cells showed a lower uptake of leucine and an uptake of alanine (Genzel *et al.* 2006a). However, MDCK.SUS2 cells were grown in a different medium than adherent MDCK cells. At this point it cannot be answered whether those differences are caused by changes of the cells through the adaptation process or the use of different cultivation media.

MDCK.SUS2 cells can grow in serum-free and even protein-free medium. Thus, this cell line can easily be scaled-up and directly infected with no need for a medium exchange. However, like other suspension cell lines MDCK.SUS2 cells tend to cell clogging. This can pose problems in terms of nutrient and oxygen supply. The changes in cell polarisation that happened during adaptation have yet to be investigated. Here, the questions are whether the cells still have an apical and basal side, and whether the virus is released over the complete cell surface, or only over membrane parts that correspond to lipid rafts.

2.2.2.3 Other cell lines

In addition to the MDCK cell line other cell lines from different species are described to be promising substrates for influenza virus propagation and cell culture-based vaccine production.

Vero cells from the African green monkey are adherent cells yielding high influenza virus titres (Govorkova *et al.* 1996; Kistner *et al.* 1998; Genzel and Reichl 2009). Like the suspension MDCK cells, there are also suspension Vero cells described (Paillet *et al.* 2009) and tested for influenza virus H1N1 propagation (Paillet *et al.* 2011). Compared to adherent MDCK cells, Vero cells seem only to replicate a smaller range of influenza virus strains (Genzel and Reichl 2009). Before usage for influenza virus replication this cell line was already licenced for inactivated polio vaccine production. There are some Vero cell culture-derived influenza vaccines licenced: the company Baxter acquired licences for their Vero-derived seasonal influenza vaccine InfluJect® (in 2002), the pandemic vaccine Celvapan® (in 2009), and for PreFluCel® (in 2010) as another seasonal influenza vaccine (Chan and Tambyah 2012; Montomoli *et al.* 2012). Additionally, the prepandemic H5N1 vaccine Vepacel® was approved for usage in the EU (Plosker 2012; Keating *et al.* 2012). An overview of Vero cell culture-derived vaccines is given by Barrett *et al.* (2013).

In 2001 Pau *et al.* showed the human cell line Per.C6 derived from embryonic retina and immortalised by transfection with the adenovirus E1 minigene to be a substrate for influenza virus propagation. The Per.C6 cell line was tested for the production of an H7N1 influenza vaccine. Cox *et al.* (2009) reported about a Phase I study, but found the humoral immune response to be not sufficient to meet regulatory requirements. In another study a recombinant influenza virus vaccine produced in Per.C6 cells induced strong serum antibody response and protected mice from a highly pathogenic influenza H5N1 challenge (Koudstaal *et al.* 2009). The company Crucell is currently aiming at bringing a Per.C6 cell-derived seasonal influenza vaccine to licensure (Crucell 2014).

Other designer cell lines are AGE1.CR and AGE1.CR.pIX cells isolated from duck retina and immortalised with adenovirus type 5 E1 genes (Sandig and Jordan 2005). These cells were specifically designed for vaccine production and growth in serum-free medium. Lohr

et al. (2009) described this cell line to be able to replicate influenza virus A/PR/8 to titres of 2.1 $\log_{10}$ HAU/100 µL with maximum $TCID_{50}$ of 1.8 x 10^8 IVP/mL. Thus, with this cell line only moderate HA titres were reached, while maximum $TCID_{50}$ were comparable to other cell lines. Consequently, this cell line is especially interesting for live attenuated influenza virus propagation. In a different study, Lohr *et al.* (2012) showed the *ca* influenza virus H1N1 A/Singapore/1/57 *ca* x A/Singapore/2339/2000 to yield a maximum of 1 x 10^8 IVP/mL in AGE1.CR.pIX cell bioreactor cultivations.

Relatively new cell lines are the CEVEC's amniocyte production (CAP) cell line of human origin. Genzel *et al.* (2013) showed this cell line growing in serum-free medium to be a substrate for influenza virus replication. After seed virus adaptation of several influenza virus strains infections in shake flask and stirred tank bioreactor systems were carried out. Shake flask infections showed low HA titres when infected without a medium exchange at toi. Adjustment of a 1:2 dilution at toi increased HA titres about 0.4 $\log_{10}$ HAU/100 µL. In bioreactor infections CAP cells reached titres of 2.5 $\log_{10}$ HAU/100 µL and 7.5 x 10^7 IVP/mL (with a strong decrease after reaching peak titre) after direct infection with CAP cell-adapted influenza A/PR/8 seed virus at MOI 0.025 only adding trypsin, glucose, glutamine, and pyruvate at toi.

The company Vivalis generated a non-transformed duck embryonic stem cell line (named EB66®) that was used for monoclonal antibody production, but also influenza virus replication (Mehtali *et al.* 2006; Brown and Mehtali 2010). In March 2014 the approval for a human pandemic influenza vaccine produced in EB66® cells by Valneva and GlaxoSmithKline was announced (Valneva 2014).

Finally, the human embryonic kidney cell line (HEK)-293 was also shown to be a promising substrate for influenza virus propagation. Le Ru *et al.* (2010) showed a suspension HEK-293 cell line growing under serum-free conditions to replicate different influenza virus A strains (A/PR/8, A/WS/33, A/Aichi/2/68, A/Hong Kong/8/68) as well as influenza virus B/Lee/40. In 3 L bioreactor systems they reached 2.81 x 10^9 IVP/mL (corresponding to 643 IVP/cell) and HA titre of up to 10240 HA/mL (4.01 $\log_{10}$ HAU/mL).

Besides these mammalian and avian cell lines also baculovirus-based vector systems in insect cells were considered for virus protein expression as well as *E. coli* bacteria. An influenza vaccine produced in a baculovirus-insect cell system, Flublok® by the company Protein Science, was approved by the FDA in January 2014 (Cox and Hashimoto 2011; Cox and Hollister 2009; Yang 2013; FDA 2013). Furthermore, plant cells are used in research for influenza vaccine antigen production (Shoji *et al.* 2012). Main problem with proteins produced in non-mammalian cells is the different—and in case of *E. coli* even absent—glycosylation of the HA protein, which most likely will have a significant impact on the induced immune response. Thus, analysis of glycosylation and induced immune

response of influenza antigens produced in non-mammalian cells is of special interest. Importantly, when comparing differentially glycosylated HA from insect and mammalian cells, de Vries *et al.* (2012) found lower HA inhibition antibody titres for HA proteins carrying terminal mannose moieties (such as those that are produced in insect cells) compared to HA proteins with complex glycans or single N-acetylglucosamine side chains. And HA N-glycosylation patterns of three different insect cells and the human HEK-293 cells were described by An *et al.* (2013) to differ quantitatively and qualitatively. Finally, despite its missing glycosylation, *E. coli*-derived HA induced production of neutralising antibodies and showed a protective activity in ferrets (Aguilar-Yáñez *et al.* 2010).

2.2.3 Role of trypsin for influenza virus replication in cell culture

As described in section 2.1.1, influenza virus haemagglutinin H0 needs to be cleaved into its subunits HA1 and HA2 to be able to bind sialic acid residues on host cell membrane for successful infection. In human and animal infections extracellular proteases in the mucosa perform this necessary activation of HA. In cell culture systems efficient influenza virus infection relies on external addition of a protease (Klenk *et al.* 1975; Kaverin and Webster 1995). For this purpose, most commonly the protease trypsin is added together with the virus seed in cell culture influenza virus infections. Mostly, bovine and porcine pancreas-derived trypsin is used for this purpose, but alternatives from non-animal origin, like recombinant trypsin produced in bacterial, yeast, or plant cells, are described (Yee and Blanch 1993; Pau and Uytdehaag 2003). As trypsin cleaves proteins at the carboxy side of the amino acids lysine and arginine, it is a very unspecific protease, also described to digest itself (Bier *et al.* 1956).

Bovine serum—included in most growth media—contains many proteins that impair efficient trypsin-mediated cleavage of HA. Consequently, cell culture processes for influenza virus propagation using serum-containing cell growth medium (like for adherent MDCK cells) require washing steps with PBS and a change to serum-free medium prior to seed virus and trypsin addition. Furthermore, MDCK and other cells are known to secrete protease inhibitors (Nishiyama *et al.* 2008), which influence the effective trypsin activity and usually an optimisation of the trypsin activity is necessary to achieve high virus titres. In a direct comparison of adherent MDCK cells and Vero cells for influenza virus production, influenza virus propagation in Vero cells in a serum-free medium process without washing step appeared to be sensitive to trypsin activity (Genzel *et al.* 2010). Still, also for infections of adherent MDCK cells in serum-free medium trypsin activity should be optimised.

To measure trypsin activity, substrates resulting in coloured products upon hydrolysis, e.g. N-α-benzoyl-L-arginine ethyl ester (BAEE), are very useful (Erlanger *et al.* 1961).

Thereby, trypsin activity can be determined using spectroscopic methods (Sacks *et al.* 1971). Alternatively, arginine-derivatives and other molecules were described to be good artificial substrates for trypsin (Somorin *et al.* 1979; Kawabata *et al.* 1988). Importantly, N-α-benzoyl-DL-arginine-4-nitroanilide (BAPNA) was demonstrated to be a powerful trypsin substrate leading to the formation of the yellow dye p-nitroaniline (pNA), especially in presence of the chymotrypsin inhibitor tosyl phenylalanyl chloromethyl ketone (TPCK) (Luchini *et al.* 1996; Tudela *et al.* 1986).

2.3 Apoptosis

In the following section the programmed cell death, apoptosis (section 2.3.1) is described, as it is also induced by influenza viruses and influences infection dynamics as well as virus yields. Finally, the connection between influenza virus and host cell apoptosis induction (section 2.3.2) as well as methods for apoptosis detection are introduced (section 2.3.3).

2.3.1 Pathways of apoptosis induction

In the 1960s researchers realised that the dying of a cell follows a specific program resulting in self-destruction and the term programmed cell death was introduced (reviewed by Lockshin and Beaulaton 1974). In 1972 the term apoptosis was introduced by Kerr *et al*. (1972). Morphologically, apoptotic cells are characterised by cell deformation, cell shrinkage, nuclear condensation, and formation of so-called apoptotic bodies. Central part of this process is a cascade of enzymes called cysteine-dependent aspartate-specific proteases (caspases) functioning as initiators and executioners of apoptosis. Inactive caspases are present in the cytoplasm and become activated from the zymogen procaspase by transcatalytic cleavage to form heterodimers. Besides this caspase-dependent apoptosis execution, there are also caspase-independent ways described in literature. Apoptosis results in the activation of different proteolytic enzymes that lead to cleavage of DNA into oligonucleosomal fragments (180–200 base pairs), and cleavage of substrates that determine cytoplasm and organelle integrity (Saraste and Pulkki 2000). In humans apoptosis plays a role in cell differentiation, disposal of infected or mutated cells as well as in tissue homeostasis. Defects in apoptosis can result in cancer or autoimmune diseases. Importantly, apoptosis (of non-tumour cells) is tolerogenic, i.e. non-immunogenic.

A special case of apoptosis induction resulting from the loss of survival signals transmitted through adhesion molecules and followed by detachment of adherent cells is termed anoikis (Frisch and Francis 1994).

There do exist other types of cell death than apoptosis, namely (macro-)autophagy and necrosis. However, since they are not in the scope of this work, they are not reviewed in this section.

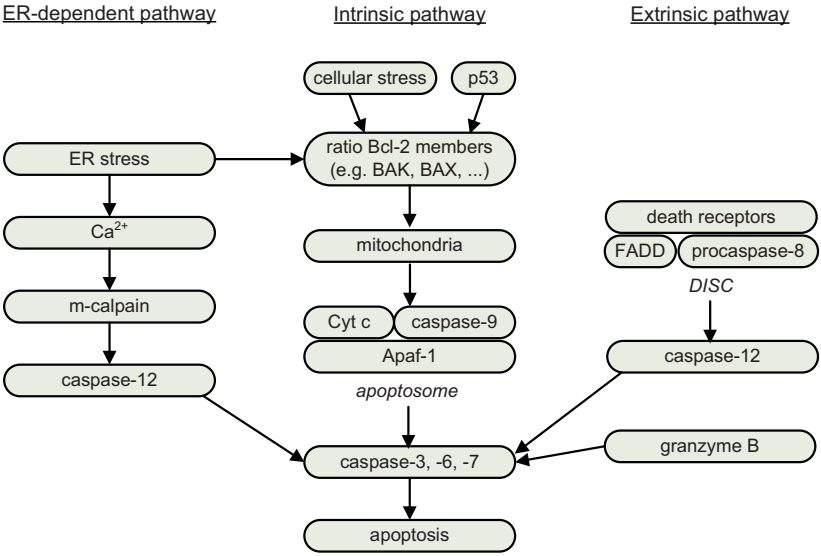

Figure 2-6 Overview of apoptotic pathways: intrinsic apoptosis induction, endoplasmic reticulum (ER)-dependent apoptosis induction and extrinsic apoptosis induction.

In the following, the three principal pathways of apoptosis induction, namely intrinsic, extrinsic, and endoplasmic reticulum (ER)-dependent apoptosis induction are described (Figure 2-6).

2.3.1.1 Intrinsic apoptosis induction

The intrinsic way of apoptosis induction is triggered by intracellular stimuli; key elements are the mitochondria. Of importance is the delicate balance between pro- and antiapoptotic factors of the B cell lymphoma 2 (Bcl-2) protein family (comprising about 20 family members). On the one hand, growth factors enhance expression of antiapoptotic factors of this family; on the other hand, activation of the proapoptotic molecules Bcl-2-associated X protein (BAX) and/or Bcl-2 homologues antagonist killer (BAK) results in the destruction of the mitochondria membrane integrity. This induces the release of cytochrome c and other molecules from the intermembraneous space into cytoplasm. Cytochrome c, apaf-1, adenosine triphosphate (ATP), and procaspase-9 form the so-called apoptosome. This cleaves procaspase-9 into its active form caspase-9, which subsequently cleaves and thereby activates effector caspases-3, -6, and -7. Those effector caspases further mediate,

amplify and execute apoptosis events, namely: chromatin condensation (through caspase substrates lamins), chromatin margination, DNA fragmentation, cell shrinkage, externalisation of phosphatidylserine (PS), membrane blebbing (through caspase substrate ROCK1), or formation of apoptotic bodies. DNA fragmentation for example is performed by caspase-activated DNAse (CAD) through cleavage of its inhibitor ICAD by effector caspases (Sakahira *et al.* 1998).

2.3.1.2 Extrinsic apoptosis induction

Besides internal triggers, apoptosis can be induced via external signals like binding of special ligands to their receptors. Ligands can be tumour necrosis factor (TNF-α), Fas Ligand (FasL), or TNF-related apoptosis-inducing ligand (TRAIL). Their receptors are death receptors of the tumour-necrosis factor receptor superfamily that harbour so-called death domains at their cytoplasmic side. Upon ligand-binding to the receptor, Fas-associated death domain (FADD) is recruited to the death domain, as well as procaspases-8 and -10 forming the death-inducing signalling complex (DISC). At the DISC, procaspase-8 is cleaved into its active form (caspase-8) that eventually directly activates effector caspases (caspases-3, -6, -7). In some cell types additional signals from the mitochondria-induced apoptosis pathway are needed to proceed. Those activated effector caspases are the same as in the intrinsic way, thus both ways are cross-linked.

Additionally to receptor stimulation, cytotoxic T lymphocytes (CTLs) can insert granzyme B through perforin channels in the cell membrane into the cytoplasm. Granzyme B leads to activation of caspase-3 and subsequent apoptosis execution.

2.3.1.3 ER-dependent apoptosis induction

The third way of apoptosis induction is ER stress (reviewed by He 2006 and Mei *et al.* 2013). ER stress includes misfolded and aggregated proteins, inhibition of protein glycosylation, reduced disulphide bonds, defects in protein expression and transport to the Golgi, and other forms of stress. Three ways of ER stress resulting in apoptosis are described. Firstly, transcriptional induction of DNA damage-inducible transcript 3 (CHOP) leads—amongst other effects—to down-regulation of Bcl-2. Secondly, signalling of the IRE1, a type I transmembrane endonuclease localised in the ER membrane, results in kinase activation and subsequent apoptosis induction. The third way for ER-dependent apoptosis is calcium-induced activation of m-Calpain that activates caspase-12. All three ways finally result in executioner caspases activation. Release of calcium of the ER also contributes to increase of reactive oxygen species (ROS). A certain ROS level alters mitochondrial membrane permeability leading to release of cytochrome c. Thereby, this pathway is cross-linked to the mitochondrial apoptosis induction way (Oyadomari *et al.* 2002; Arden and Betenbaugh 2006).

2.3.2 Influenza virus infection and apoptosis

Influenza proteins influence cellular apoptosis pathways

It is known for more than 20 years that influenza viruses induce apoptosis in host cells (Takizawa *et al.* 1993). Especially, influenza virus proteins NS1, PB1-F2, and M2 are today known to manipulate the host cell's apoptosis pathways (Gannage *et al.* 2009; Zhang *et al.* 2011; Krumbholz *et al.* 2011):

- **NS1** was described to induce apoptosis (Schultz-Cherry *et al.* 2001) and to down-regulate apoptosis (Zhirnov *et al.* 2002). The effect of NS1 seems to depend on other proteins and viral replication (Herold *et al.* 2012). NS1 inhibits the serine/threonine kinase PKR, thereby preventing blocking of protein synthesis (Hatada *et al.* 1999; Li *et al.* 2006). Furthermore, NS1 activates the phosphatidylinositide 3-kinase (PI3K) pathway (Ehrhardt *et al.* 2006; Ehrhardt *et al.* 2007; Hale *et al.* 2006) which results in apoptosis-suppression.

- **PB1-F2**, the +1 open reading frame of the PB1 gene, functions in a strain-dependent manner proapoptotic during later stages of the viral life cycle (Chen *et al.* 2001). In influenza virus A/PR/8 infections PB1-F2 led to permeabilisation of the outer mitochondria membrane (Zamarin *et al.* 2005). In addition, it was described that PB1-F2 cooperates with NS1 to inhibit the host cell's interferon response (Varga *et al.* 2011).

- **M2** was shown to inhibit macroautophagy, resulting in an accumulation of autophagosomes that do not fuse with lysosomes (Gannage *et al.* 2009).

While apoptosis of infected cells helps the organism to limit viral spread, several studies demonstrated the influenza virus to utilise host cell apoptosis. It was shown that overexpression of Bcl-2 resulted in decreased virus titres (Hinshaw *et al.* 1994; Olsen *et al.* 1996) as did inhibition of caspase-3 (Wurzer *et al.* 2003). In those cases and in case of nuclear factor κ-light-chain-enhancer of activated B cells (NFκB) inhibition, retention of vRNP in the nucleus was observed. Zhirnov and Klenk (2007) showed antiapoptotic signalling to occur in early phases of influenza virus replication, but to provoke apoptosis at late phases of infection. Thus, in the early phase of the infection virus-induced activation of the Akt/PKB way (through NS1 binding to PI3K subunit p83) negatively regulates proapoptotic factors (like caspases-3, -9, and Bcl-2-associated death promoter (BAD)); in the late phase of infection virus-induced NFκB activation results in activation of proapoptotic factors (Fas, FasL, TRAIL) enabling extrinsic apoptosis induction with subsequent caspase activation. This possibly leads to widened nuclear pores enabling an increased export of vRNPs from the nucleus (Herold *et al.* 2012).

In vivo, the above described complex pathways are additionally influenced by immune cells. Cellular detectors like retinoic acid-inducible gene 1 (RIG-I) result in activation of the interferon system. In different organisms, cell death of virus-infected cells can also be induced externally, for example by cytotoxic $CD8^+$ T cells that detect virus antigens presented on the host cell's outer membrane in a perforin or Fas-dependent manner (Topham *et al.* 1997). Through this mechanism further spreading of the virus is prevented. For example, dendritic cells in the lymph node (and other immune cells) release FasL/TRAIL, thereby activating CTLs that stimulate death receptors on virus-infected lung cells (Legge and Braciale 2005; Langlois and Legge 2010). In addition, influenza virus infected cells themselves express Fas, enabling detection by immune cells. In mouse tracheal epithelial cells influenza virus infection resulted in ER stress and caspase-12-mediated apoptosis (Roberson *et al.* 2012).

Manipulation and usage of apoptosis in cell culture

Different studies showed that in some cell culture systems manipulation of apoptosis can be used to improve product yields. Especially in the production of recombinant proteins, inhibition of apoptosis results in an extended productive lifetime and thereby higher product yields. This can either be achieved by optimising media composition or by applying genetic engineering strategies. Media supplementation can involve addition of nutrients, but also anti-apoptotic chemicals. Suramin, insulin, transferrin, galactose, glutamine, glycine, asparagine, threonine, or caspase inhibitors are only some examples for additives described to be beneficial for increasing yields in CHO, Vero, or hybridoma cultures (reviewed by Arden and Betenbaugh 2004). Genetic strategies comprise expression of *bcl-2* or *bcl-*x_L in NS0, CHO, baby hamster kidney (BHK), and hybridoma cells aiming at inhibiting cell death. Also, expression of catalytically inactive caspase variants, caspase inhibitors, or mutated versions of Bcl-2 or Bcl-$_{xL}$, lacking the caspase cleavage site that prevents their conversion into proapoptotic variants were utilised for this purpose (Sitailo *et al.* 2002; Jendrossek *et al.* 2003). NS0 myeloma fusion partner cells overexpressing heat shock protein 70 that protects cells from stress, showed delayed apoptosis induction and increased number of hybridoma fusions in an antibody production system (Lasunskaia *et al.* 2003). The positive impact on antibody titres was described to be a 40% increase for Bcl-2-expressing CHO cells (Tey *et al.* 2000) and adenoviral gene E1B-19K-expressing hybridomas (Mercille *et al.* 1999; Mercille and Massie 1999). Expression of Aven and E1B-19K genes led to increased maximum antibody titres by 40–55% in CHO cell bioreactor cultivations (Figueroa *et al.* 2007), and improved survival in recombinant factor VIII-expressing BHK cells (Nivitchangyong *et al.* 2007).

Above examples describing inhibition of apoptosis to positively influence product yields were performed in recombinant protein production (Arden and Betenbaugh 2004).

Manipulating apoptosis for higher yields in influenza virus propagation seems to be more complex because of both, positive and negative effects of apoptosis on influenza virus replication. An approach by Schulze-Horsel (2011) tested apoptosis inducing chemicals (staurosporine, gossypol, and valinomycin) and apoptosis inhibitors (betaine, zinc sulphate, and caspase inhibitors) for improving viral yields through manipulation of apoptosis. Adherent MDCK cells were infected with influenza A/Wisconsin/67/2005-like at MOI 0.001 in 6-well plates, and two bioreactor cultivations at MOI 0.001 and 0.002. The chemicals were added at toi in different concentration. Betaine showed a not reproducible increase of cell-specific virus production, 10 µM gossypol led to an increase in cell-specific viral yield; however, considering the standard deviation (SD) of the biological replicates the increase was calculated to be not significant.

2.3.3 Methods for apoptosis detection

Apoptosis can be monitored with different methods. A simple approach is detection of apoptosis-caused DNA fragments from cell lysates using gel electrophoresis, first described by A. H. Wyllie in 1980 (Wyllie 1980). This results in a DNA ladder pattern with bands with size differences of about 180 base pairs—characteristic for late apoptosis. Main advantage is the simplicity of this method. Disadvantages are the poor sensitivity (approximately 1 x 10^6 cells), and the fact that only qualitative results are obtained.

Alternatively, western blot techniques can be used to identify activated caspases or poly(adenosine diphosphate-ribose)polymerase (PARP) (which is a DNA repair-sensing enzyme), using specific antibodies (Kaufmann *et al.* 1993). Similar to the detection of DNA ladder pattern using gel electrophoresis, quantitative results are hard to achieve with this method and no single cell results are obtained as gel electrophoresis-based methods average results over the cell population.

The morphological changes accompanying apoptosis, like cell shrinkage or membrane blebbing, can also be identified microscopically (Kerr *et al.* 1972). Disadvantage of this method is that only a small number of cells is analysed. Thus, no information about distribution in the cell population is gained. For a more specific method fluorescence microscopy using antibodies directed against apoptosis-specific targets can be used. Still, main disadvantage of microscopic methods is the small number of analysed cells.

Above mentioned methods of apoptosis measurements are only delivering qualitative results or analyse too small cell populations. Thereby, no statistically relevant information is obtained. Consequently, these methods are not suited for quantitative monitoring of time courses of apoptosis in infected cell cultures and do not allow generation of data for

quantitative mathematical modelling (as described in section 2.4.4). Thus, another assay had to be chosen for apoptosis measurements in this work.

A more sophisticated approach for apoptosis measurements is usage of flow cytometry. It allows analysis of cellular attributes on single-cell level, thus, avoiding averaged results over the cell population. Through measurement of at least 10000 cells, information on cell population level is available, as well as proportions of positive and negative cells. Another advantage of flow cytometry is that different targets can be addressed in parallel. For example, by staining cellular targets like virus proteins or DNA fragmentation flow cytometry allows determination of quantitative information on infected/uninfected as well as apoptotic/non-apoptotic cell populations. This information can be used to determine correlations between virus-induced apoptosis and infection status of cells. In addition, the qualitative and quantitative influence of infection parameters such as MOI on apoptosis can be investigated and used for industrial production optimisation at a later stage. Furthermore, these quantitative data can be used for mathematical modelling (described in section 2.4.4). These arguments led to the decision to use flow cytometry as method of choice for apoptosis detection in this work. Hence, flow cytometry and flow cytometric methods for apoptosis detection are explained in more detail in section 2.4.

2.4 Flow cytometry for virus-infected host cells

In the following section the general working principle of a flow cytometer is introduced (section 2.4.1), followed by examples for application of flow cytometry in cell cultures infected with influenza virus (section 2.4.2). Finally, remarks on flow cytometric data evaluation are given (section 2.4.3), and the role of flow cytometric data for mathematical modelling is addressed (section 2.4.4).

2.4.1 Basic principle of flow cytometry

A flow cytometer analyses fluorochrome-labelled cells by excitation through a laser and detection of the emitted light by photomultiplier tubes (PMT) (Figure 2-7). For this purpose, antigen-specific antibodies that are conjugated to fluorophores or labelled by a second conjugated antibody, which is directed against the fragment crystallisable (Fc) region of the primary antibody, are used. Additionally, staining can be performed using DNA dyes. In case of surface antigens, cells only have to be incubated with the antibody solution. In case of intracellular targets, usually a membrane permeabilisation step with detergents is performed to improve uptake of the antibody into the cell.

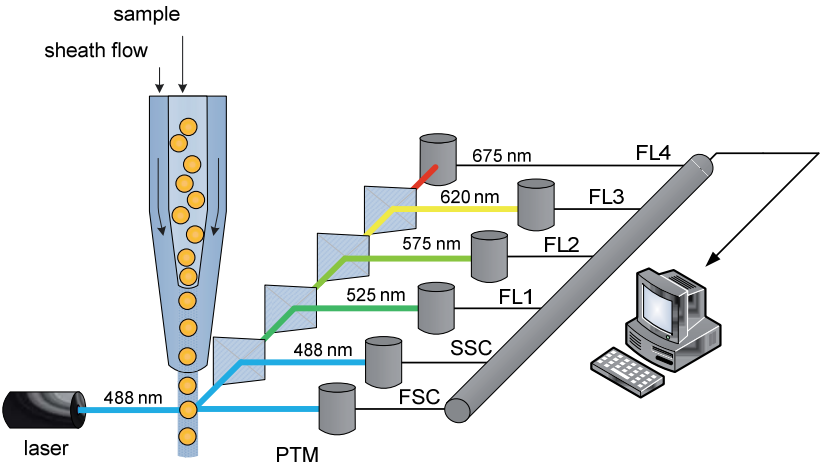

Figure 2-7 Working principle of a flow cytometer: labelled samples are excited by a laser and emit light to photomultiplier tubes (PMT). Through a set-up with semi-permeable mirrors several fluorescent dyes can be analysed in parallel. FSC = forward scatter channel, SSC = side scatter channel, FL1–4 = fluorescence light channels 1–4. Modified from Rollié (2010).

In the flow cytometer stained cells are aligned by hydrodynamic focusing through injection of a sheath fluid stream. This single stream of particles is then passed through a 488 nm argon ion elliptical focused laser beam that excites the fluorophore(s). The emitted light is collected by PMTs or silicon photodiodes. Light scattered in line or in narrow angles to the laser beam is collected in the forward scatter channel (FSC). This signal roughly corresponds to the particle size, and can be used, e.g., for discrimination of intact cells from cell debris. At a 90° angle the side scattered light is collected into the side scatter channel (SSC). This signal correlates with the granularity of a cell and can be used to distinguish, e.g., granulocytes from other lymphocytes. Through 45° positioned dichroic mirrors light of wavelengths between 505 and 545 nm (525 nm band-pass filter (BP)) is conducted to the fluorescence light (FL)-1 channel PMT, light of 560–590 nm (575 nm BP) to the FL-2 channel, light of 605–635 nm (620 nm BP) to the FL-3 channel, and light of 660–700 nm (675 nm BP) to the FL-4 channel. Through this set-up it is possible to detect green, yellow, orange, and red light emitted from the fluorochrome independently, meaning a simultaneous detection of four different targets.

The Epics XL flow cytometer used in this work excites stained samples with a 15 mW argon laser (laser beam spot size: 10 µm high by 80 µm wide) and has a fluorescence sensitivity of <1000 molecules of equivalent soluble fluorochrome (MESF). Particles of a size from 0.5 µm to 40 µm can be analysed with a maximum measurement speed of 3300 cells/second.

If the emission spectra of simultaneously measured fluorochrome overlap and hit the same detector, compensation of the detected signals is necessary. For this purpose, single and multiple stained control samples are evaluated prior to measurement of experimental samples. Thereby, the proportion of light spilling over in the other detector channels is determined.

For analysis, data can be displayed individually for every detector in single-parameter histogram plots (number of events over the fluorescence intensity), or in 2D plots in which the fluorescence signal of one channel is plotted over the fluorescence signal of another channel. For 2D plots the most commonly used display modes are dot or contour plots. Additionally, so-called gates or regions can be set to choose or exclude specific subpopulations from further analysis. Generally, read-out is the proportion of positive and negative cells in percentage. However, by usage of cell count beads it is possible to determine absolute numbers of (positive) cells. Also calibration beads can be used to calculate the fluorescence intensity into fluorescent molecules. Summarising, flow cytometry is a valuable method enabling multi-parameter analyses on the single-cell level even in a quantitative way.

Mostly used in immunology as diagnostic tool and for differentiation of various immune cells, flow cytometry is nowadays used for many diverse applications that also include analysis of bacteria species and VLPs.

2.4.2 Flow cytometry for measuring apoptosis and infection in cell culture

Most common flow cytometric methods for apoptosis detection

One flow cytometric method for apoptosis detection is a caspase assay. Key step is the addition of a fluorochrome-conjugated pan caspase inhibitor. It contains three amino acids, including an activated caspase binding aspartate residue that is linked to a fluoro-methyl-ketone (Bedner *et al.* 2000). Through formation of a thio-methyl-ketone with the cysteine in the active site is binds irreversibly to the active site, thereby inactivating the caspase. This inhibition prevents detection of only shortly activated caspases. Advantage of the method is its detection of early apoptotic signals, disadvantages are concerns and doubts regarding the specificity of the pseudo substrate and the fact that the overall fluorescence intensity of apoptotic cells labelled with the caspase inhibitor does not reflect unique binding to caspase active centres (Kuzelova *et al.* 2007; Pozarowski *et al.* 2003), and that there are caspase-independent apoptosis pathways described. Also, Elmore (2007) emphasised that caspase activation not necessarily indicates that apoptosis will occur and that the tremendous overlap in substrate preferences of caspases affects the specificity.

Generally, the assay should be performed with fresh, non-fixed samples to prevent unspecific signals.

Another option is the staining of the membrane lipid PS that appears on the outer cell membrane during apoptosis with fluorescent-labelled Annexin V in a flow cytometric assay (van Engeland *et al.* 1998). It is a highly sensitive assay, however, interpretation of Annexin V assay results might be difficult after mechanical or enzymatic treatment of the cells (e.g. trypsin), as it influences PS flipping. Accordingly, this is a major drawback for using the Annexin V assay in trypsin-treated influenza infection samples.

Staining of DNA fragments using the terminal deoxynucleotidyl transferase (TdT)-mediated dUTP nick end labelling reaction (TUNEL) is another approach for detection of late apoptosis with flow cytometry (Gavrieli *et al.* 1992). The TUNEL assay uses the ability of the enzyme TdT to incorporate labelled deoxyuridines at 3'OH-termini of DNA strand breaks forming polydeoxynucleotide polymers. Today's procedures include a fixation with (para-)formaldehyde with subsequent postfix/permeabilisation and storage in 70% ethanol (Loo 2011). This is especially advantageous for infectious samples (like samples from influenza virus infections) as ethanol and (para-)formaldehyde inactivate the sample which simplifies later sample treatment. Another advantage of this assay is its high sensitivity of as few as 100 cells that can be detected. Main disadvantages are the high costs, that it is not quantitative, and necrotic cells are potentially stained as well.

Finally, changes in scattered light by cell size and shape can be recorded with flow cytometry without fluorescent dyes. Also, lysosome function can be measured using dyes such as acridine orange that are acidophilic and concentrate in areas of high lysosomal and phagocytic activity. As this is not apoptosis-specific, additional validating methods should be performed in parallel. In addition, assays are available detecting changes in mitochondrial membrane potential, calcium flux, or cytochrome c release (reviewed by Christensen *et al.* 2013).

Apoptosis detection in influenza virus infected cell cultures

For apoptosis detection of bioreactor and small-scale cultivation samples of adherent and suspension MDCK cells an assay was required that is usable with fixed cell samples. Fixation directly inactivates the samples and enables a parallel staining and evaluation of an infection experiment series. Additionally, this improves comparability between samples from one infection experiment. Furthermore, a method was soughed that is independent of the way of apoptosis induction, as apoptosis induced via different pathways might not be captured with pathway-specific assays. The TUNEL assay fulfils these requirements and was hence chosen as method of choice for apoptosis detection in this work. Additionally,

Schulze-Horsel *et al.* (2009) described the non-apoptotic infected cell population (determined with a TUNEL assay) to be the productively virus releasing population, as with onset of apoptosis induction a drop in productivity was observed. Thus, the TUNEL assay with its detection of late apoptotic cells is a good method to determine the time point when an influenza infected culture becomes unproductive.

A parallel caspase assay was not performed because of the aforementioned drawbacks of the assay. More importantly, caspases activation and DNA fragmentation correlate and proceed in a small time window. Bedner *et al.* (2000) investigated parallel samples of human leukaemia cells treated with the apoptosis-inducing agent camptothecin using a caspases assay and the TUNEL assay. Subsequent regression plot analysis showed an excellent correlation of the two methods. Also, the same group described detection of PARP cleavage and DNA fragmentation to appear only with a 30 minutes (min) delay (Li and Darzynkiewicz 2000). This is also in agreement with the finding that the full apoptosis process from initiation to completion occurs within 2 h (Elmore 2007). When considering samples from influenza infection experiments to be taken in several hours intervals, a resolution of early apoptosis (with caspase assays) and late apoptosis (with TUNEL assay) seems not feasible.

Other methods like determination of membrane integrity, PS exposure (Annexin V assay) or dissipation of mitochondrial membrane potential cannot be used for apoptosis detection with fixed and stored samples (Wlodkowic *et al.* 2011), as fixating agents (like methanol or formaldehyde) influence the measured cellular parameters (e.g. by crosslinking or denaturing proteins). Thus, these methods cannot be used for detection of apoptosis in samples that were stored during infection experiments and were thus not used for apoptosis measurements in this work.

The eventual detection of necrotic cells by a TUNEL assay is not a hindering in statements concerning productive life span of cells in cell culture, because in cell culture systems secondary necrosis is observed (Elmore 2007). Influenza virus infected cell cultures will most likely become apoptotic due to the virus infection; however, without phagocytes in the culture infected apoptotic cells undergo necrosis.

Detection of influenza virus infection in cell culture

Monitoring of influenza virus propagation with flow cytometry was performed by several groups in different ways. Steele-Mortimer *et al.* (1990) measured time courses of influenza virus C (Johannesburg/1/66) infected MDCK cells using virus-specific polyclonal serum from infected rabbits and a second incubation with fluorescein isothiocyanate (FITC)-conjugated anti-rabbit immunoglobulin G (IgG) antibody. Nichols *et al.* (1993) described

an FITC-labelled NA and HA-containing influenza virus that could be detected with flow cytometry. They analysed monocytes-macrophages having bound influenza virus and internalised the virus. Lonsdale *et al.* (2003) showed usage of antibodies directed against influenza virus A and B nucleoprotein for determination of percentage of infected cells. They chose NP as target for infection detection as it is after M1 the most abundant structural influenza virus protein. Furthermore, NP was described to be highly conserved between viruses of the same type (Walls *et al.* 1986). Schulze-Horsel *et al.* (2008) described staining of influenza virus proteins M1 and NP for detection of virus propagation. M1-fluorescence appeared to be much lower compared to NP-fluorescence. Consequently, in parallel stained samples discrimination of M1-positive and negative cells was not as clear as in NP-stained samples. Thus, NP staining for influenza virus infection detection is preferable to M1 staining.

Combining flow cytometric staining of infection and apoptosis

Additional information can be gained by combining different flow cytometric stainings. A combination of virus protein staining and apoptosis staining enables to distinguish uninfected and infected apoptotic cells. Chaïbi *et al.* (2005) performed a simultaneous staining of rotavirus-infected Caco-2 cells (MOI 10, 10 hpi) for a viral antigen and a TUNEL assay to distinguish infected and apoptotic infected cells. However, as TUNEL-fluorescence was not much higher than their mock-infected control, no clear separation between non-apoptotic and apoptotic infected cells was possible. Also, the analysis was only conducted at one time point, thus, no information about the dynamic of apoptosis induction upon rotavirus infection was obtained.

Double staining of virus proteins and apoptosis together with measurement of virus titres offers valuable information to determine the time point when (productive) infected cells become apoptotic and are lost as virus producing cells. Schulze-Horsel *et al.* (2009) used parallel staining of influenza virus NP and the TUNEL assay for detection of influenza virus propagation and virus-induced apoptosis in bioreactor infections of adherent MDCK cells using two influenza virus A/PR/8 strains from different suppliers, the RKI and the NIBSC, respectively. Additionally, they used the influenza virus A/Wisconsin/67/2007-like reassortant strain for a bioreactor infection experiment.

In this work staining of viral NP was used in combination with a TUNEL assay to discriminate uninfected non-apoptotic, infected non-apoptotic, apoptotic infected, and apoptotic uninfected cell populations with flow cytometry in influenza virus infected cell cultures.

2.4.3 Flow cytometric gates and controls

Flow cytometric data can be analysed individually for every detection channel in form of histograms or the information of two channels obtained from multiple staining can be combined in 2D plots. Histograms contain the information of the population distribution and can be analysed for type of distribution, mean, and SD. In 2D plots so-called gates or regions can be drawn to discriminate populations with different fluorescent levels. Those gates can be drawn in a polygonal manner, however, especially if drawn manually this analysis holds the drawback of being very subjective, as the decision to set the barrier strongly depends on personal estimation. A more objective way for analysis is the setting of quadrant gates.

The most important decision in an infection staining is to distinguish negative from positive events. The first basis for this is an optimal antibody concentration. Therefore, for establishing a flow cytometric staining procedure, it is important to titrate the needed amount of antibody. This guarantees optimal separation of negative and positive populations during analysis. In immunology, Fc receptor blocking is performed during flow cytometric surface staining to prevent unspecific antibody binding. This is possible, because immune cells like B cells, natural killer cells, monocytes, macrophages, or platelets express Fc receptors. Hence, for influenza virus protein staining in MDCK cells this is not possible. The second basis for a correct decision between negative and positive events is the right choice of control samples. In immunology an isotype control is performed to detect background fluorescence in flow cytometric stainings, again, for influenza virus protein staining this is not possible as MDCK cells do not express Fc receptors.

2.4.4 Role of flow cytometric data for mathematical modelling of influenza infection

To perform in depth analyses of biological data and to explain biological phenomena, mathematical models are valuable tools. Several models of the dynamics of influenza virus A on the population level as well as to understand virus kinetics were developed (reviewed by Beauchemin and Handel 2011; Smith and Parelson 2010). These models of influenza virus kinetics are helpful, e.g. to develop treatment strategies or to improve epidemiological models.

Mathematical models depend on reliable data to fit the model's parameter and to verify model predictions. Flow cytometric data on virus infected cells and apoptotic cell populations, with their single-cell information of at least 10000 measured cells, are very useful for mathematical models on influenza virus kinetics in cell culture. Together with virus titre data and cell concentration valuable information on virus propagation and virus

spreading in the culture can be used for parameter fitting, thereby giving insights in intracellular virus propagation and extracellular virus release.

Flow cytometric data together with cell concentration as well as infectious and total virus titres gained in this work were used in two approaches for mathematical modelling of influenza virus propagation and apoptosis in cell culture. One approach was deterministic modelling of virus replication in single cells that was integrated into a model for transmission of virus between host cells. Furthermore, population balance modelling using population distributions gained by flow cytometric measurements was performed. Both approaches are described in the following paragraphs.

In a first model Heldt *et al.* (2012) described the complete intracellular viral life cycle. One result was that number of virus proteins and viral genomes produced and replicated in the host cell would allow release of larger numbers of virus particles. Thus, other processes than transcription and translation, like formation of eight gene segment-containing complexes at the plasma membrane, transport of vRNPs to the plasma membrane, or virus budding are potential bottlenecks. For prediction of virus yields in cell culture, however, this single-cell model is not suited and was therefore successfully expanded for virus spreading in cell culture. Thereby, the single-cell model is an essential component of the model for virus spreading.

A follow-up study described the extension of the single-cell model to cell-to-cell transmission of influenza virus in cell culture (Heldt *et al*. 2013). In this approach flow cytometric data on the infection and apoptosis status of the cell population was used in combination with data on viral RNA species. For this purpose, flow cytometric data and infectious virus titres of influenza virus A/PR/8 RKI infections at MOI 1 x 10^{-4}, 0.1, and 3 in adherent MDCK cells was provided from this work. These data enabled an integrated modelling approach which links intracellular processes to the spreading of the virus between cells. The model can predict how the inhibition of specific steps in the viral life cycle affects virus propagation. Concretely, inhibition of viral transcription, replication, protein synthesis, nuclear export, as well as virus assembly and virus release were found to have strong negative effects on virus propagation. Consequently, these processes should not be limited in cell culture-based influenza virus propagation. Furthermore, in their simulations most cells died before the end of the virus production phase, thus indicating that a delay of apoptosis induction might improve virus titres. Thus, the model by Heldt *et al.* (2013) helped to understand virus propagation in cell culture. However, the model was mainly intended for drug targeting and hence did not provide concrete suggestions for improvement of influenza virus propagation in cell culture. Further studies that apply such models aiming at increasing the number of released virions could give concrete evidences

on how yields in cell culture-based virus propagation can be improved and that could be validated experimentally afterwards.

Population balance modelling constitutes another approach to address the distribution dynamics of infected cells as measured by flow cytometry. In particular, the approach of Müller *et al.* (2011 and 2013) comprises three coupled distributed cell populations (uninfected, infected, and apoptotic cells) and two lumped virus species (active and inactive) to perform population balance modelling of virus-host cell interactions during virus propagation in cell culture. Time courses of these populations were directly obtained from cytometric data and provided for the modelling approach of Müller and Dürr (Müller *et al.* 2011 and 2013; Dürr *et al.* 2012). Flow cytometric raw data had to be transformed into adequate data forms before being handed over to the modellers:

- Single fluorescence channel information in histograms was transformed into vectors
- 2D plots of apoptosis fluorescence against infection fluorescence were transformed into matrices

These transformations enabled further calculations in different mathematical programs (like MATLAB®).

Above transformed flow cytometric measurements were used by T. Müller and R. Dürr to explain characteristic dynamic phenomena like transient multimodality and the reversal of propagation direction in a distributed modelling approach. Experimental data on 1.2 L cultivations of adherent MDCK cells infected with influenza A/PR/8 RKI, A/PR/8 NIBSC, and A/Wisconsin/67/2005-like at MOI 0.025 were used to determine kinetic parameters for infection, apoptosis, and other relevant processes (Müller *et al.* 2011 and 2013). In addition, Dürr *et al.* (2012) showed that the agreement between the model and experimental data can be improved—especially for later time points of infection—by considering a nonlinear dependency of the kinetic parameters on the degree of fluorescence (internal coordinate). Currently, flow cytometric data, cell concentration, and virus titre courses are used to improve the established model and the included assumptions in order to perform validations and adaptations.

3 Material and Methods

In this chapter all applied methods and used materials are described. These comprise cell culture techniques including infection experiments and seed virus adaptation. Furthermore, analytical methods for cell concentration, virus titre, extracellular metabolite concentration, and trypsin activity determination are described. Finally, usage of flow cytometry for influenza virus and virus-induced apoptosis measurement is depicted. Lists of used equipment, consumable, and chemicals are given in sections 8.1 and 8.2; a list of the used standard operation procedures (SOPs) is given in the appendix (section 8.3).

3.1 Cell culture

In this work an adherent and a suspension MDCK cell line were cultivated in different cultivation systems. The performed cultivation procedures are presented subsequently. SOPs applied are summarised in section 8.3.

3.1.1 Cultivation of adherent MDCK cells

For preculture adherent MDCK cells (ECACC #84121903) were grown in GMEM containing 2 g/L peptone and 10% foetal calf serum (Z medium) (Table 3-1 and SOP M/02) in static T-flasks (25, 75, or 175 cm^2) or roller bottles in a 5% CO_2 atmosphere at 37°C. Cells were passaged weekly up to 20 passages. For this purpose, flasks were washed twice with PBS (Table 3-2 and SOP M/01) and cells were detached after 15 min incubation with trypsin/Ethylenediaminetetraacetic acid (EDTA) solution (Table 3-3 and SOP M/07). The reaction was stopped by addition of at least the same volume of Z medium, and single cells were obtained by pipetting. Cell concentration was determined in a Vi-Cell™ XR cell counter (Beckman Coulter). Finally, 7 x 10^4 cells/cm^2 were seeded in fresh Z medium into a new flask.

Table 3-1 Composition GMEM Z medium.

Compound	Amount
GMEM basis medium[a]	890 mL
Lab-M-peptone (20%)	10 mL
Foetal calf serum	100 mL

Components were mixed under sterile conditions and stored at 4°C.

[a] GMEM basis medium was prepared according to SOP M/03

Table 3-2 Composition PBS.

Compound	Amount
NaCl	8.00 g/L
KCl	0.2 g/L
KH_2PO_4	0.2 g/L
Na_2PO_4	1.15 g/L
	ad 1.0 L dH_2O

Solution was autoclaved and stored at room temperature.

Table 3-3 Composition trypsin/EDTA solution (10-fold concentrated).

Compound	Amount
PBS	100 mL
Trypsin (775 Units/mg)	0.5 g
EDTA	0.2 g

The solution was sterile-filtered after mixing of the components and stored at 4°C. Single-concentrated trypsin/EDTA solution was generated through dilution with PBS.

Table 3-4 Overview of vessels used for adherent MDCK cell cultivation.

Cultivation vessel	Working volume	Temperature via	Gas supply
Petri dishes	2 mL	Incubator	5% CO_2 via membrane
T-flasks (T25, T75, T175)	10, 50, and 125 mL	Incubator	5% CO_2 via membrane
Spinner flask	250 mL	Incubator	5% CO_2 via membrane
1 L CellFermPro (DasGip)	1000 mL	Heater band	40% DO via dip tube
1.2 L Biostat (Sartorius)	1000 mL	Water jacket	40% DO via dip tube
5 L BiostatC™ (Sartorius)	5000 mL	Peltier element	Sparger

For stirred tank bioreactor cultivations 1 L DasGip, 1.2 L Biostat, or 5 L BBraun cultivation vessels were used, all equipped with temperature, pH, stirring, and aeration control. Prior to the start of the cultivation a two point pH calibration (pH 7.0 and 9.21) was performed. 2.5 x 10^5 cells/mL from roller bottle precultures were seeded in Z medium containing 2 g/L cytodex® 1 microcarrier. Prior to the experiment a stock solution with 40 g/L microcarriers was prepared and sterilised. Stirring was adjusted to 65 rpm, temperature was set to 37°C, aeration to 40% dissolved oxygen (DO), and pH to 7.3. Cells were grown to confluence or indicated adherent cell concentration. An overview of

cultivation vessels used for infection experiments with adherent MDCK cells is given in Table 3-4.

3.1.2 Cultivation of MDCK.SUS2 cells

MDCK.SUS2 cells obtained through a collaboration with K. Scharfenberg (FH Emden/Leer), were grown in 100 or 250 mL vented shake flasks (with baffles) in Smif8 medium supplemented with 22.3 mmol/L $NaHCO_3$, 106.7 mmol/L NaCl, 0.805 mmol/L $CaCl_2$, 0.01‰ Pluronic-F68, 0.017 mmol/L ethanolamine, 1.6 mmol/L L-glutamic acid, and 20.3 mmol/L D-(+)-glucose (Table 3-5 and SOP M/03.3). Prior to usage, the medium was freshly supplemented with 4 mmol/L glutamate and 4 mmol/L pyruvate (if not indicated differently). Cells were cultivated at a temperature of 37°C in a 5% CO_2 atmosphere and 180 rpm shaking. MDCK.SUS2 cells were passaged every 4 to 5 days. For this purpose, after trypsinisation to reduce cell clogging, cell concentration was determined in a Vi-Cell™ XR. For inoculation 5×10^5 cells/mL were seeded in glutamate and pyruvate supplemented Smif8 medium with 10% of the culture volume of the supernatant from the previous passage (termed: conditioned medium). A list of utilised cultivation vessels for infection experiments of MDCK.SUS2 cells is given in Table 3-6.

Table 3-5 Composition Smif8 medium.

Compound	Amount
Smif 8 powder medium	30.41 g
$NaHCO_3$ (22.3 mmol/L)	20.00 g
NaCl (106.7 mmol/L)	62.38 g
$CaCl_2$ (0.805 mmol/L)	1.184 g (pre-dissolved in 500 mL dH_2O)
Pluronic F-68 (0.01‰)	100 mL (10% stock solution)
Ethanolamine (0.017 mmol/L)	10 µL (98% stock solution)
L-glutamic acid (1.6 mmol/L)	2.42 g
(D)-(+)-glucose (water free) (20.33 mmol/L)	36.62 g
	ad 10 L dH_2O

Components were mixed, sterile-filtered and stored at 4°C. Prior to usage Smif8 medium was supplemented with 4 mmol/L glutamate and 4 mmol/L pyruvate.

For stirred tank bioreactor cultivations a 1.2 L Biostat Bplus reactor equipped with SCADA MFCS/win software for bioreactor operation and data recording was used. Controlled parameters were temperature, pH, stirring, and oxygen supply. Prior to inoculation a two-point-calibration of the pH sensors was performed. MDCK.SUS2 cells were seeded in glutamate and pyruvate supplemented Smif8 medium at 7×10^5 cells/mL

(10% conditioned medium). Stirring was adjusted to 75 rpm, temperature was set to 37°C, aeration to 40% DO, and pH set to 7.3.

Table 3-6 Cultivation vessels used for MDCK.SUS2 cell cultivation.

Cultivation vessel	Working Volume	Temperature via	Gas supply
1.2 L Biostat	1000 mL	Water jacket	40% DO via dip tube
Shake flask	100 mL, 250 mL	Incubator	5% CO_2 via membrane
Spinner flask	250 mL	Incubator	5% CO_2 via membrane
Vented reaction tube	20 mL	Incubator	5% CO_2 via membrane

3.2 Infections with influenza virus A

Adherent MDCK cells and MDCK.SUS2 cells were used for infection experiments with four different influenza virus A strains. Influenza A/PR/8 seed virus was used from two different suppliers, the RKI in Berlin (Amp. 3138) and the NIBSC in Hertfordshire, United Kingdom (#06/114). Furthermore, the two HGRs A/Uruguay/716/2007-like (NYMC X-175c) and A/Wisconsin/67/2005-like (NYMC X-161b), both H3N2 type strains with an A/PR/8 backbone were used for infection experiments. In Table 3-7 an overview of all influenza seed virus preparations utilised in this work is given.

Table 3-7 Influenza A seed virus strains used in this work: virus strain, subtype, $TCID_{50}$, and date of preparation.

Influenza virus strain	Subtype	$TCID_{50}$ (IVP/mL)	HA titre (log_{10} HAU/100µL)	Date of preparation
A/PR/8 NIBSC	H1N1	1.30×10^7	2.60	01.06.2006
A/PR/8 NIBSC	H1N1	5.43×10^6	2.10	16.07.2009
A/PR/8 NIBSC	H1N1	6.32×10^6	2.08	06.11.2007
A/PR/8 NIBSC	H1N1	9.20×10^8	2.80	17.02.2010
A/PR/8 NIBSC	H1N1	1.00×10^9	2.37	02.03.2011
A/PR/8 RKI	H1N1	4.00×10^7	2.30	05.10.2006
A/PR/8 RKI	H1N1	5.17×10^8	2.63	15.07.2009
A/Uruguay/716/2007-like HGR	H3N2	9.82×10^7	2.45	17.12.2008
A/Uruguay/716/2007-like HGR*	H3N2	1.00×10^9	2.72	20.06.2012
A/Wisconsin/67/2005-like HGR	H3N2	2.28×10^8	2.41	30.05.2007

All strains are adherent MDCK cell-adapted, except for A/Uruguay/716/2007-like HGR* which is MDCK.SUS2 cell-adapted.

3.2.1 Infection of adherent MDCK cells

For T25-flasks infection experiments adherent MDCK cells were grown for 5 days until confluence in Z medium. After washing twice with PBS, 10 mL virus maintenance medium (Table 3-8) containing 5 units trypsin/mL and the seed virus (according to the target MOI) was added for infection. Afterwards, samples were taken in 8–12 h intervals to measure supernatant and adherent cell concentration. Furthermore, infection supernatant was stored at -80°C for later virus titre determination, and aliquots of 1 x 10^6 cells for later flow cytometric staining and analysis (section 3.2.3) were taken.

Table 3-8 Composition virus maintenance medium.

Compound	Amount
GMEM basis medium	990 mL
Lab-M-peptone (20%)	10 mL

Components were mixed under sterile conditions and stored at 4°C.

For infections of 3.5 cm diameter petri dishes, 1.5 x 10^6 cells were seeded 24 h prior to infection. Infection was performed in a reduced volume to improve virus binding to the cells. Therefore, seed virus and trypsin were added in a volume of 500 µL, and after an incubation of 1 h at 37°C filled up to 2 mL. Three dishes at every sampling time point were harvested: one for cell concentration determination, a second one for sample generation for flow cytometric analyses (section 3.2.3), and a third for RNA measurements (performed by C. Seitz, MPI Magdeburg, Bioprocess Engineering Group).

For infections of adherent MDCK cells in stirred systems (spinner and bioreactor), stirring was stopped to allow settling of microcarriers. Then, carriers were washed twice with PBS and a medium exchange to serum-free virus maintenance medium, containing 2 x 10^{-5} units/cell trypsin and seed virus, was performed. In time intervals from 5 to 12 h samples were taken to cross check for the pH and to determine supernatant and adherent cell concentration. Furthermore, culture supernatant was stored for later analysis of total and infectious virus titres. Samples for later measurement of extracellular metabolite concentration were incubated at 80°C for 3 min to inactivate virus. Finally, 1 x 10^6 cells were fixed and stored for later flow cytometric analysis (section 3.2.3).

When adherent MDCK cells were cultivated in serum-free EpiSerf medium, no medium exchange was performed before infection. Instead, seed virus, trypsin, and glucose at a final concentration of 10 mmol/L were added directly to the culture broth at toi. Sample taking and preparation for later analysis of virus titres and flow cytometric analysis of infection status and apoptosis induction were performed as in medium exchange infections.

3.2.2 Infection of MDCK.SUS2 cells

For shake flask infections of MDCK.SUS2 cells three different infection procedures were used: firstly, direct infections were performed, with 5 mmol/L glucose, 1 x 10^{-5} units/cell trypsin, and seed virus being directly added to the culture broth; secondly, a 1:2 dilution at toi was performed by discarding half of the culture and replacing it with the same volume of fresh medium containing 1 x 10^{-5} units/cell trypsin and the seed virus; thirdly, culture broth was centrifuged at 300 x g for 10 min and resuspended in fresh medium containing seed virus and 1 x 10^{-5} units/cell trypsin (full medium exchange).

MDCK.SUS2 cells grown in spinner flasks were infected directly with influenza A/PR/8 RKI through addition of seed virus (MOI 0.025) and 1 x 10^{-5} units/cell trypsin or with a medium exchange or 1:2 dilution prior to infection at MOI 1 x 10^{-4}.

For infection in reduced volume (increased cell and virus concentration) shake flask cultures of MDCK.SUS2 cells were grown in Smif8 medium supplemented with 4 mmol/L glutamate and 4 mmol/L pyruvate. Prior to infection culture broth was centrifuged and half of the supernatant stored at 4°C. Resuspended cells were infected with influenza virus A/PR/8 RKI at MOI 0.025. At 1 hpi the stored culture supernatant was added again to the infected cells.

Stirred tank bioreactor infections (1 L working volume (wv)) of MDCK.SUS2 cells were carried out either by direct infection without medium exchange or with a 1:2 dilution prior to infection. For the direct infection, cell concentration was determined twice and the needed volume of seed virus (calculated with the seed virus' $TCID_{50}$ to adjust the indicated MOI) and 1 x 10^{-5} units/cell trypsin was calculated. Afterwards, 5 mmol/L glucose, trypsin, and seed virus were added directly to the culture broth using a syringe via a septum. For infections with 1:2 dilutions prior to infection, the culture broth was diluted with the actual reactor working volume of fresh Smif8 medium containing 1 x 10^{-5} units/cell trypsin and the seed virus. Every 8 h samples were taken to measure pH, cell concentration, virus titres, extracellular metabolite concentration, and to prepare cells for later flow cytometric analysis (see subsequent section 3.2.3).

3.2.3 Sample preparation for flow cytometric analysis

For flow cytometric analysis aliquots of 1 x 10^6 cells were prepared. For this purpose, in adherent cell infections supernatant and trypsinised adherent cells were pooled; in MDCK.SUS2 cell infections a sample of the culture broth was directly taken and mixed with a final concentration of 1% paraformaldehyde (1:2 dilution of paraformaldehyde stock solution, Table 3-9 and SOP M/08). After incubation on ice for 30 min, cells were pelleted and dissolved in PBS. The volume containing 1 x 10^6 cells was finally aliquotted

in 4.5 mL ice cold 70% ethanol. To guarantee fast and homogeneous distribution the tubes were vortexed during aliquotation. Until staining for flow cytometric analysis samples were stored at -20°C.

Table 3-9 Composition 2% paraformaldehyde solution.

Compound	Amount
Paraformaldehyde	10 g
PBS	500 mL
NaOH (5 mol/L)	to solve paraformaldehyde powder
HCl (5 mol/L)	volume equivalent to used volume NaOH
	adjust at pH 7.0 with HCl

After mixing PBS and paraformaldehyde NaOH was added until complete solution of the paraformaldehyde. Afterwards, pH was adjusted to 7.0 using HCl.

Prior to measurement, negative control samples were generated by performing a mock infection. For this purpose, a T175-flask confluently covered with adherent MDCK cells in GMEM was washed twice with PBS. Then, a medium exchange to 100 mL virus maintenance medium, containing 5 units/mL trypsin but no seed virus, was performed. Mock-infected cells were incubated for 15 min at 37°C. Afterwards, supernatant was discarded, cells were washed twice with PBS, and detached by 15 min incubation with trypsin/EDTA solution. Trypsinisation reaction was stopped and cell concentration determined, followed by fixation in 1% paraformaldehyde for 30 min on ice. After centrifugation (300 x g, 6 min, 4°C) and resuspension in PBS aliquots of 1 x 10^6 cells in 4.5 mL ice cold 70% ethanol were stored at -20°C until further usage as control samples.

For generation of positive control samples, a confluent roller bottle with MDCK cells was washed twice with PBS. Then, cells were infected by a medium exchange to 100 mL virus maintenance medium containing 12.5 units/mL trypsin and 5 x 10^5 IVP/mL A/PR/8 seed virus (RKI, $TCID_{50}$ = 4 x 10^7 IVP/mL) in a volumetric infection with no MOI adjustment. The bottle was incubated at 37°C until total supernatant cell concentration exceeded 5 x 10^5 cells/mL. Subsequently, the supernatant was harvested, centrifuged, and resuspended in PBS. Cell concentration was determined, and cells were fixed in 1% paraformaldehyde for 30 min on ice, centrifuged (300 x g, 10 min, 4°C), and resuspended again in PBS. Finally, fixation of 1 x 10^6 cells each in 4.5 mL ice cold 70% ethanol and storage at -20°C until staining was performed.

3.3 Adaptation of seed virus

In the next two subsequent sections two adaptation protocols to generate seed virus master and working banks are described. The first protocol (section 3.3.1) was performed for all strains used for adherent MDCK cell infections; the second protocol (section 3.3.2) was only used for influenza A/Uruguay/716/2007-like HGR adaptation to MDCK.SUS2 cells.

3.3.1 Volume-based adaptation

Purchased virus aliquots were adapted to adherent MDCK cells as described below. First, the lyophilised virus was dissolved in dH_2O and the complete vial was used together with 500 µL trypsin (500 U/mL) to infect a T75-flask (wv: 50 mL) of confluent MDCK cells. 24 hpi 200 µL supernatant plus 500 µL trypsin were taken to infect a new T75-flask. Again 24 hpi, 200 µL supernatant and 500 µL trypsin were taken to infect a new T75-flask. Finally, 48 hpi supernatant was harvested and aliquots were stored as virus master seed bank. From this master seed $TCID_{50}$ and HA titre were determined.

To generate a working seed of this adapted virus, a confluent grown roller bottle of MDCK cells (wv: 250 mL) was infected with 1 mL master bank seed virus together with 2.5 mL trypsin (500 U/mL). Harvest and aliquotation (1.8 mL) was performed 24–36 hpi, and $TCID_{50}$ and HA was determined of the stored vials. Virus master- and working seeds were stored at -80°C.

3.3.2 Low MOI adaptation

To improve infection dynamics of the Uruguay-like HGR strain in MDCK.SUS2 cells an adaptation of the seed virus to the cell line was performed using a low MOI adaptation strategy (Figure 3-1). For this purpose, serial dilutions of the seed virus of 10^{-1}, 10^{-2}, 10^{-3}, and 10^{-4} in Smif8 medium were performed. Then, 200 µL of the dilutions were used to infect 2 x 10^7 MDCK.SUS2 cells in 20 mL Smif8 medium in vented 50 mL reaction tubes. Calculated MOI in this passage were 9.8 x 10^{-2} to 9.8 x 10^{-5}. At 72 hpi, infection supernatants were analysed for HA titre, and the two dilutions showing the highest titres were stored in aliquots at -80°C as passage 1 (P1). The supernatant showing the highest titre was diluted 10^{-2}, 10^{-3}, 10^{-4}, and 10^{-5}, and 200 µL were used to infect four new reaction tubes with 2 x 10^7 cells (corresponding to MOI 4.2 x 10^{-3} to 4.2 x 10^{-6}). 48 hpi HA titre was checked and the two best supernatants were stored in aliquots as passage 2 (P2). The best P2 supernatant was diluted 10^{-3}, 10^{-4}, 10^{-5}, and 10^{-6}, and used for the next passage. This procedure was repeated for five passages in which the dilutions used for infections were stepwise reduced down to 10^{-8}, resulting in MOI of 7.5 x 10^{-5} to 7.5 x 10^{-8}. After

supernatants of all five passages had been collected, HA titre as well as $TCID_{50}$ were measured.

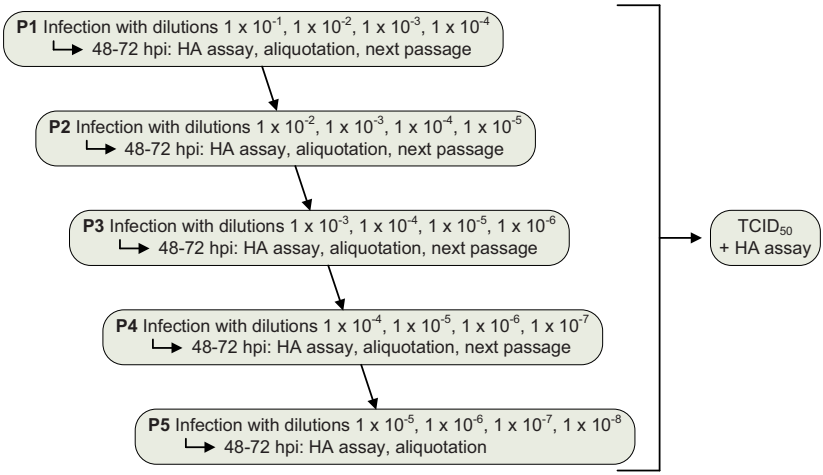

Figure 3-1 Scheme of low MOI adaptation procedure. Four reaction tubes with 2 x 10^7 cells in 20 mL medium each are infected with dilutions of the seed virus for five passages (P1–P5). Afterwards, $TCID_{50}$ and HA titre of all stored samples are determined.

3.4 Analytical methods

3.4.1 Determination of cell concentration

3.4.1.1 Cell concentration of adherent MDCK cells

Supernatant cells in adherent MDCK cultivations were counted with a Vi-Cell™ XR. For static cultivations supernatant was directly measured, for microcarrier cultivations cell suspension was filtered through a 50 µm cell mesh (Partec CellTrics®). The standard deviation of the method was determined to be 14% (Bock *et al.* 2009). The measuring program included taking of 100 photos and counting of cells with diameters between 8 and 25 µm. Through a trypan blue staining read-out was viable and total cell concentration.

For determination of adherent cell concentration 1 mL of culture sample was taken, supernatant discarded, and settled microcarriers were washed three times with PBS. Afterwards, 100 µL of microcarrier suspension was mixed with 100 µL trypsin/EDTA solution in 96-well plates. After microscopic pictures at 10 x magnification for later counting of microcarriers had been taken, the plate was incubated for 20 min at 37°C to detach all cells from microcarriers. Finally, cell suspension was 1:2 diluted with trypan

blue solution (Table 3-10 and SOP M/15) and counted in a Fuchs-Rosenthal chamber. Adherent cell concentration was then calculated as the product of the number of attached cells per microcarrier (X_{MC}) and the number of microcarriers per mL (N_{MC}). With

$$X_{MC} = \frac{\text{absolute number of cells}}{\text{absolute number of microcarriers}} \quad (1)$$

and

N_{MC} = 8000 microcarriers/mL. Adherent cell concentration of every sample was determined three times using three wells in parallel.

Table 3-10 Composition 1% trypan blue solution.

Compound	Amount
Trypan blue	10 g
NaCl	18 g
	ad 1000 mL dH_2O

Components were mixed, sterile-filtered and stored at room temperature. Prior to usage stock solution was diluted 1:2.

3.4.1.2 Cell concentration of MDCK.SUS2 cells

For MDCK.SUS2 cell concentration determination a Vi-Cell™ XR was used. Prior to cell counting samples were treated as follows: 1 mL of cell suspension was centrifuged at 600 x g for 1 min at room temperature. From the supernatant 950 µL were discarded, and the cell pellet was resuspended in 450 µL of trypsin/EDTA solution. After incubation for 10 min at 37°C, trypsinisation was stopped through addition of 500 µL of FCS. Finally, the cell suspension was homogenised by intensive pipetting and inserted into the Vi-Cell™ XR for cell concentration determination. The measuring programs included taking of 100 photos and detection of cells with diameters between 7 and 50 µm. Through a trypan blue staining read-out was viable and total cell concentration.

3.4.2 HA assay

For measurement of HA content as total virus titre, an HA assay was performed according to Kalbfuss *et al.* (2008) (SOP V/05): 1:2 serial dilutions of infection supernatants in 96-well plates were mixed with 100 µL erythrocytes solution (adjusted to $2 \times 10^7 \pm 0.1 \times 10^7$ cells/mL). After 3 h incubation at room temperature haemagglutination was checked by absorbance measurement at 700 nm using a Tecan plate reader. Sigmoid fitting of the absorbance over the negative decimal logarithm of the dilution was then used to calculate $\log_{10}$ HAU/100 µL. This read-out can be used to estimate numbers of virions/mL

assuming the ratio virus particles/erythrocytes is one at the highest dilutions showing haemagglutination by:

$$conc_{virus} = conc_{erythrocytes} \times 10^{\log_{10} \text{HAU/100 µL value}}. \quad (2)$$

The limit of detection is 0.15 $\log_{10}$ HAU/100 µL and the standard deviation is 0.03 $\log_{10}$ HAU/100 µL which is the dilution error. For calculation of cell-specific total virus yield maximum HA titre was divided by the overall maximum cell concentration.

3.4.3 50% Tissue Culture Infectious Dose ($TCID_{50}$)

For determination of infectious virus concentration a $TCID_{50}$ assay was used (performed according to SOP V/08). Briefly, 1:10 serial dilutions of medium supernatant were used to infect adherent MDCK cells in 96-well plates. One plate per sample was used to perform an 8-fold determination. After 2 days incubation at 37°C cells were fixed with paraformaldehyde and staining of viral HA was performed using a monoclonal antibody and a secondary Alexa-Fluor488-labelled antibody. Fluorescence was analysed microscopically at 10-fold magnification, checking for the dilution showing only one positive event. Calculation of IVP/mL was then performed according to the method of Spearman and Kärber (Mahy and Kangro 1996):

log(virus 100%) + 0.5 – (cumulative 100%/number of tests per dilution) (3)
= log virions/100 µL

with "log(virus 100%)" being the dilution showing 100% positive wells, "cumulative 100%" being the number of positive wells, and "number of tests per dilution" being eight (as one 96-well plate was used for each sample).

Cell-specific yields of IVP were calculated as the ratio of $TCID_{50}$ to maximum cell concentration.

Percentage of IVP was calculated by:

% IVP = 100 / (HA in virions/mL) x ($TCID_{50}$ in IVP/mL). (4)

3.4.4 Metabolite concentration

Extracellular metabolite concentration of glucose, lactate, ammonia, glutamate, and glutamine in culture supernatants were determined with a BioProfile® Plus. With every set of samples, standards in three concentrations of all metabolites were measured, and this standard curve was used to correct measured values. Samples and standards were measured randomised to prevent an influence on metabolite determination in case of a systemic drift

of the sensors. Relative standard deviations and validated measuring ranges are given in Table 3-11. If measured values exceeded the indicated validated ranges, dilutions were prepared and samples were measured again.

Table 3-11 Validated measuring ranges, standard deviations of the method, and limits of quantitation for the BioProfile® Plus. In cases of homogeneous variances absolute standard deviation in mmol/L is given; for inhomogeneous variances relative standard deviations in percentage is given.

	Glucose	Lactate	Ammonia	Glutamine	Glutamate
Validated measuring range (mmol/L)	1.11–41.08	2.22–33.40	0.20–5.20	0.20–2.60	0.20–2.60
Standard deviation	0.39 mmol/L[a]	0.30 mmol/L[a]	4.54%[b]	12.81%[b]	0.02 mmol/L[a]
Limit of quantitation (mmol/L)	3.91	2.98	0.15	0.82	0.29

[a] homogeneous variances

[b] inhomogeneous variances

Based on determined extracellular concentration of glucose and lactate the yield coefficient $Y'_{lac/gluc}$ was calculated as the ratio of amount produced lactate and consumed glucose. The same calculation was performed to determine the ammonia yield coefficient from glutamine ($Y'_{NH4/gln}$).

3.4.5 Trypsin activity

Trypsin activity of infection supernatants and stock solutions used for infection were determined using the trypsin activity colorimetric assay kit (BioVision) according to the manufacturer's instructions. Briefly, 5 µL sample was mixed with 45 µL assay buffer and 1 µL chymotrypsin inhibitor in 96-well plates and incubated for 10 min. Afterwards, 50 µL reaction mix containing 48 µL assay buffer and 2 µL substrate were added, quickly mixed, and absorbance measured at 405 nm in 20 min intervals in a Tecan plate reader. In parallel, a pNA standard curve was generated by filling up 0, 2, 4, 6, 8, and 10 µL of pNA stock solution to 50 µL with assay buffer. Calculation of trypsin activity was performed by

$$A_{Try} = \frac{B}{\Delta t \times V} \times F_D \quad (5)$$

with A_{Try} being trypsin activity in pNA mU/mL, B the pNA content in nmol generated with the standard curve, Δt the time difference between the measurements in min, V the volume of sample added in mL, and F_D the dilution factor if samples were diluted prior to activity measurements.

With

1 pNA Unit = 312 BAEE Units (6)

the read-out pNA U/mL could be converted into the more common BAEE U/mL.

3.4.6 Flow cytometric staining

Flow cytometry was used to investigate infection status of influenza virus infected cells with a FITC-labelled anti-NP antibody (AbD Serotec, #MCA400) in parallel to apoptosis detection with the in situ cell death detection kit (Roche, tetramethylrhodamine (tmr) red-labelled). The latter is based on addition of deoxyribonucleotides through the enzyme TdT to open 3' OH-ends, a hallmark of late apoptosis-induced DNA fragmentation.

For a flow cytometric double staining with FITC-labelled anti-NP antibody and the TUNEL assay, collected samples of infection courses (stored at -20°C) containing 1 x 10^6 cells were pelleted at 300 x g at 4°C for 10 min and washed twice with FACS washing buffer (Table 3-12 and SOP M/12). Then, cell pellets were permeabilised by 2 min incubation with 100 µL permeabilisation buffer (Table 3-13) on ice. After two subsequent washing steps, 50 µL TUNEL reaction mix containing 45 µL labelling solution and 5 µL TdT enzyme solution were added per sample. After 60 min incubation at 37°C samples were washed twice with FACS washing buffer (Table 3-12). 25 µL NP antibody solution was added and again incubated for 60 min at 37°C. After a final washing step with FACS washing buffer samples were suspended in 500 µL FACS washing buffer.

In addition to infection experiment samples, control samples to adjust compensation settings for the flow cytometric analysis were treated as follows. For an apoptosis positive control sample a previously generated mock-infected sample was treated with the nuclease benzonase for 10 min in a benzonase-mix (Table 3-14) containing 98 µL 4-(2-hydroxyethyl)-1-piperazineethanesulfonic acid (HEPES) buffer (Table 3-15), 1 µL benzonase, and 1 µL $CaCl_2$ on ice. This created DNA fragments that resulted in a positive signal when analysed with the TUNEL assay. As a negative control a mock sample was stained with the reaction mix without enzyme addition (labelling solution without TdT addition) in order to detect the fluorescence background caused by the fluorescent nucleotides. For infection positive control samples a roller bottle was infected and supernatant cells (assumed all being infected) were stored in aliquots and single stained for NP. Because, as mentioned above, no isotype control can be performed when staining MDCK cells for influenza virus infection, unstained samples of infected cells were taken as negative controls.

Measurements were performed with an EpicsXL™ flow cytometer equipped with Expo™32 acquisition software, using a 488 nm argon laser for excitation and FL1 (505 to 545 nm) and FL3 (605 to 635 nm) channels for detection of the emitted FITC and tmr red fluorescence. Prior to measurement of infection experiment samples, compensation settings were adjusted using the four single stained control samples.

Table 3-12 Composition washing buffer for flow cytometric staining.

Compound	Amount
Glycine	10 g
Bovine serum albumin (BSA)	0.5 g
	ad 500 mL PBS

Components were mixed, sterile-filtered and stored at 4°C.

Table 3-13 Composition permeabilisation buffer.

Compound	Amount
Triton X-100 (0.1%)	0.5 mL of 10% stock
Sodium citrate dihydrate (0.1%)	50 mg
	ad 50 mL dH_2O

Components were mixed, sterile-filtered and stored at 4°C.

Table 3-14 Composition benzonase solution used for generation of DNA strand breaks for positive control samples in TUNEL assay.

Compound	Amount
Benzonase (3.5 units/µL)	1 µL
HEPES buffer	98 µL
$MgCl_2$ (2 mmol/L)	1 µL from 200 mmol/L stock

Table 3-15 Composition HEPES buffer used for preparation of benzonase solution.

Compound	Amount
HEPES (20 mmol/L)	476.6 mg
NaOH pellets	900 mg
NaCl	2922 mg
	ad 1 L dH_2O

Components were mixed, sterile-filtered and stored at 4°C.

3.4.7 Flow cytometric analysis

To check the correct optical alignment and fluidic stability of the flow cytometer, Flow-Check™ Fluorospheres (Beckman Coulter) were used in a weekly routine. These beads are labelled with different dyes, whose emission ranges from 525 nm to 700 nm when excited at 488 nm. Half-peak coefficient of variation values for Flow-Check™ fluorospheres of less than 2% for forward scattered light and FL1–FL4 confirm proper working of the flow cytometer.

Flow cytometric list mode data files were analysed in different manners using FlowJo (Treestar Inc.) and Expo™32 (Beckman Coulter) evaluation software. Firstly, monomeric cells were gated by checking scatter versus auxiliary signal/peak height to area ratio. Those gated cells were plotted as histogram plots (TUNEL-fluorescence and NP-fluorescence, respectively) as well as 2D dot plots (TUNEL-fluorescence over NP-fluorescence). The sample taken directly after infection (0 hpi) was then used to set gates for infection and apoptosis. In particular, gates for uninfected/infected and non-apoptotic/apoptotic cell populations were set to obtain a 1% false-positive signal.

Flow cytometric staining of influenza virus showed background fluorescence, meaning that already the 0 hpi sample showed some low fluorescence intensity. Still, the staining worked properly, as during the infection a population of bright fluorescent cells could be detected. The analysis with individually set gates was compared to the analysis using quadrants, but manual polygonal regions appeared to be subjective and population percentage was much lower than expected. For these reasons, for analysis of stainings a quadrant analysis was used with setting of the barrier between negative and positive events using the 0 hpi sample (with 1% false-positive). For experiments in which cells were infected without a medium exchange prior to infection a substantial apoptotic uninfected cell population was present 0 hpi. For those data sets no 1% false positive gate for apoptotic cells could be set. Instead, the barrier between non-apoptotic and apoptotic cells was manually set in the minimum between the two populations.

For experimental data used for subsequent stochastic modelling, Quantum™ FITC-5 MESF High Level calibration beads (Bangs Laboratories) were measured twice together with infection experiment samples. These beads contain distinct MESF units that can be calibrated to resulting fluorescence intensities. Thereby, MESF units can be calculated from fluorescence intensities of experimental samples. For this purpose, a standard calibration curve was generated by plotting the MESF versus median fluorescence intensities for beads with known MESF values. Linear regression delivers the calibration curve equation in which measured fluorescence intensities of unknown samples can be inserted to calculate the according MESF unit value. An example of such a calibration curve generated with the Quantum™ FITC-5 MESF beads measured twice in an

EpicsXL^{TM} flow cytometer is shown in Figure 3-2. As can be seen from the figure, the calibration can be reproduced very well and the linear relationship holds true for the whole fluorescence range of the beads.

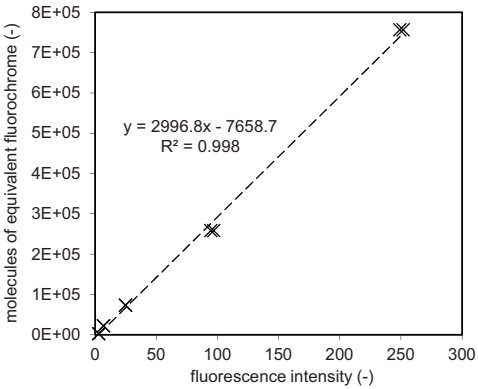

Figure 3-2 Example of a standard calibration curve generated with Quantum^{TM} FITC MESF beads to enable a quantitative usage of infection data for population balance modelling approaches.

4 Results and discussion

In the following chapter remarks on statistical data analysis of cell culture infection experiments are made (section 4.1) followed by investigations on control samples for flow cytometric measurements (section 4.2). Afterwards, results from infection experiments of adherent MDCK cells in different cultivation vessels are shown and discussed (sections 4.3–4.5) as well as MDCK.SUS2 cells tested for influenza virus propagation (section 4.6).

4.1 Statistical data analysis

There are many reasons for variations in repeated biological experiments, especially when working with cell cultures. Loewer and Lahav (2011) reviewed reasons for non-genetic heterogeneity, like stochastic fluctuation of cellular components, cellular states, and the microenvironment. In literature there are also several approaches to describe biological noise quantitatively. Arriaga (2009) summarised these ways to determine intrinsic and extrinsic biological noise by single-cell techniques (like time lapse microscopy and flow cytometry). Snijder *et al.* (2009) soughed for explanations for the origin of heterogeneity pattern of cellular activities in adherent cell populations. For infections with rota virus, dengue virus, mouse hepatitis virus, and simian virus 40 they found many processes within one cell population to be heterogeneous: much of the variation in virus infection, endocytosis, and lipid composition of the cell surface is determined by the cell's population context, especially population size, local cell density, and cell islet edges. Snijder and Pelkmans (2011) emphasised moreover that cell-to-cell variability in cellular activities is the consequence of complex and robust regulatory networks from the cell population context.

Besides biological noise, experiment errors (like measuring errors) also contribute to variations in experiment repetitions. Especially, experimental conditions like different passages of cells, different batches of medium, pipetting errors, and other experimental errors result in variations between repeated experiments. However, variations like time delays observed in repeated infection experiments performed in this work were too large to be solely caused by measuring errors. Instead, reasons for inhomogeneity are more likely different passages of cells, different lots of medium, error in $TCID_{50}$ of seed virus, and pipetting errors (especially at very low MOI).

4.1.1 Variations in infection experiments and statistical data analysis for data sets in this thesis

For experiment repetitions performed in this work especially differences in the onset of infection (increase in HA, $TCID_{50}$, and NP positive cells) were observed (an example is shown in Figure 4-1). In the following the handling of such data sets is demonstrated.

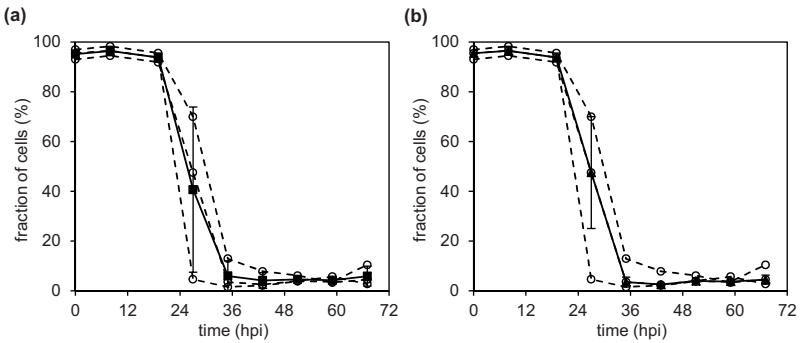

Figure 4-1 Mean versus median of uninfected non-apoptotic cells determined with flow cytometry. Courses of three times repeated bioreactor cultivation of MDCK.SUS2 cells infected with influenza virus A/PR/8 from RKI at MOI 1 x 10^{-5}. Open symbols indicate single courses of uninfected non-apoptotic cells determined with flow cytometry. Filled symbols are calculated mean and SD (a) and median and median absolute deviation (MAD) (b).

In Figure 4-1 one example of the uninfected cell population as measure for progress of infection in a three times independently repeated infection of adherent MDCK cells in a stirred tank bioreactor system is shown. Usually, for such data sets calculation of mean and SD with subsequent t-test for determination of significance to other experiments is performed (Figure 4-1a). Importantly, a requirement for performance of a t-test is data sets to be normally distributed and to have homogeneous variances. Especially for small sample sizes, fulfilment of the constraints is very important (Rudolf and Kuhlisch 2008).

Thus, in a first step, normality of example data was assessed via Kolmogorov-Smirnov test, while homogeneity of variances was tested with a Levene's test (both performed with MATLAB® 2012 software (MathWorks)). A level of significance $\alpha = 0.05$ was chosen, corresponding to an allowed maximum probability of error of 5%. Calculated p-values for a three times repeated bioreactor cultivation of adherent MDCK cells with subsequent infection with influenza virus A/PR/8 are shown in Table 4-1. At significance level α = 5%, normality and homogeneity of variances for most of the time points have to be rejected. Similar results were obtained for the same analysis of a three times repeated infection experiment of MDCK.SUS2 cells in bioreactors and shake flasks comparing different culture conditions (data not shown).

Table 4-1 p-values of virus titre and cell population data from bioreactor infections of adherent MDCK cells: three independent replicates were tested for null hypotheses that normal distribution and homogeneity of variances are given ($\alpha = 0.05$). Numbers in red indicate $p < \alpha$, thus, rejection of the null hypothesis; numbers in green mark $p > \alpha$, thus, acceptance of the null hypothesis.

		p-values for					
	hpi	HA titre	$TCID_{50}$	uninfected cells	infected cells	apoptotic cells	infected apoptotic cells
Test for normality	0	3.33×10^{-1}	n.a.	-4.44×10^{-16}	1.90×10^{-2}	5.87×10^{-2}	1.76×10^{-1}
	8	3.33×10^{-1}	n.a.	-4.44×10^{-16}	2.47×10^{-1}	1.90×10^{-2}	3.33×10^{-1}
	19	3.33×10^{-1}	-4.44×10^{-16}	-4.44×10^{-16}	4.74×10^{-5}	5.38×10^{-6}	1.20×10^{-1}
	27	1.30×10^{-3}	-4.44×10^{-16}	-4.44×10^{-16}	-4.44×10^{-16}	4.99×10^{-3}	4.13×10^{-2}
	35	5.80×10^{-6}	-4.44×10^{-16}	-8.88×10^{-16}	-4.44×10^{-16}	5.87×10^{-2}	1.90×10^{-2}
	43	2.70×10^{-6}	-4.44×10^{-16}	-6.66×10^{-16}	-4.44×10^{-16}	2.83×10^{-2}	6.49×10^{-10}
	51	4.70×10^{-7}	-4.44×10^{-16}	-6.66×10^{-16}	-4.44×10^{-16}	2.83×10^{-2}	2.22×10^{-13}
	59	2.10×10^{-7}	-4.44×10^{-16}	-1.11×10^{-15}	-4.44×10^{-16}	1.90×10^{-2}	-4.44×10^{-16}
	67	6.70×10^{-8}	-4.44×10^{-16}	-2.22×10^{-16}	-4.44×10^{-16}	5.87×10^{-2}	-1.11×10^{-15}
	96	3.00×10^{-8}	-4.44×10^{-16}	n.a.	n.a.	n.a.	n.a.
Test for homogeneity of variances		3.55×10^{-2}	3.75×10^{-2}	7.16×10^{-3}	1.04×10^{-2}	4.82×10^{-2}	1.13×10^{-2}

The consequence of this violation of parametric tests' constraints was refusal of presenting mean and SD for repeated data sets and using a t-test for determination of significance. Instead, non-parametric methods were used for analysis of independently repeated data sets. Examples are the Wilcoxon or Friedmann test. These tests compare rank series and do not require to assume a specific distribution of the data set. Additionally, these tests are resilient to outliers and are more suitable for small sample sizes (Rudolf and Kuhlisch 2008).

When the distribution condition is violated the median is better in reflecting the central tendency of data sets than the mean. The median plus MAD as statistical dispersion correspond to the rank based character of non-parametric tests.

For these reasons, median and MAD were used to present three times performed bioreactor and shake flask infection experiments in this work (Figure 4-1b). Testing for statistical significance was not performed, as with sample size n = 3 the according non-parametric tests are of too limited power.

4.1.2 Discussion

Usually in biological sciences calculation and presentation of mean and SD for repeated data sets is performed. However, in cases of shown timely shifted infection dynamics this will not only result in huge error bars, but also in mis-interpretation when constraints for the data's distribution of parametric tests are not fulfilled.

Filip *et al.* (2013) evaluated cells from chronic lymphocytic leukaemia patients regarding cell viability and apoptosis in co-culture experiments with other cells and anti-leukaemia drugs. They used presentation of median and MAD for flow cytometric data on cell viability and apoptosis after testing for normality with a Shapiro-Wilk test. To evaluate statistical significance of differences between dependent samples they used the Wilcoxon matched pair test, and for independent samples the Mann-Whitney U test. Before, median and MAD were used by Seitz *et al.* (2012) for gene expression data, after testing for normality and homogeneity of variances were negative. Disadvantage of calculating median and MAD is the loss of information about extreme values. Also, non-parametric methods are not recommended in case the requirements for parametric tests are fulfilled (Rudolf and Kuhlisch 2008).

Performance of a normalisation of data sets—as method to reduce variances in data repetitions—is not suitable for comparisons performed in this work. But a ratio apoptotic infected/infected cells determined with flow cytometry was performed in order to ease the comparison of apoptosis induction and presence of apoptotic cells between infection studies using different influenza virus strains, different cells, or different cultivation conditions. The alternative to show representative runs is avoided when possible, as the information on the variance is lost. For data sets of T25-flask infection studies that had been repeated three times representative runs are shown, as due to variations in sampling points no calculation of median and MAD was possible.

Summarising, testing of normality and homogeneity of variances of example data sets from this work showed that usage of parametric methods (like calculation of mean, SD, and t-test) is not correct for these data sets. Instead, non-parametric methods that are independent of the data set's distribution are the correct way to present data sets of repeated infection experiments that are not normally distributed with non-homogeneous variances. In cases of small sample sizes like $n = 3$ they react less on extreme values and help to better identify trends. Thus, for presentation of three times repeated experiments median and MAD are used. Non-parametric tests for significance for $n = 3$ do not deliver reliable results and were therefore omitted.

4.2 Investigation of flow cytometric control samples

As control samples are of great importance for a correct interpretation of results from flow cytometric measurements, in this chapter studies regarding controls for influenza virus staining and differentiation between cell populations are presented (section 4.2.1). In addition, under certain conditions fluorescence intensity distributions shifted, which is presented in section 4.2.2. Finally, in section 4.2.3 results are discussed.

4.2.1 Decision between uninfected and infected cell populations

In flow cytometric measurements control samples determine the validity of the recorded data. In this work, a FITC-labelled antibody against influenza virus NP was used to follow virus propagation using flow cytometry. For setting the infection gate NP-stained mock-infected, unstained infected, and NP-stained 0 hpi samples were tested for their FL1-fluorescence (Figure 4-2). Through the overlay of several histograms in one diagram no cell counts on the y-axis are given in Figure 4-2 to Figure 4-4.

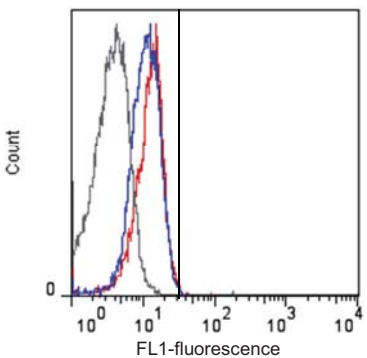

Figure 4-2 Comparison of histograms of FL1-fluorescence of potential samples for setting the infection gate. NP-stained 0 hpi infection samples (red curve), NP-stained mock-infected samples (blue curve), and unstained infected samples (grey curve) of adherent MDCK cells. The vertical line indicates 1% false-positive gate for the NP-stained control samples. Through the overlay of histogram distributions a normalisation of the distribution height is performed by the software, thus, no count values can be given on the y-axis.

Unstained samples showed median fluorescence intensities too low to use them for the gating procedure. In contrast, there is a relatively high background fluorescence of the intracellular NP staining. NP-stained mock-infected samples showed the same upper limit in FL1-fluorescence as NP-stained infected 0 hpi samples (Figure 4-2). Thus, mock-

infected and infected 0 hpi samples are equally suitable for setting the upper limit of background fluorescence.

The option of always performing parallel mock infections and using these samples to set the infection gate was discarded as the samples showed a constant background fluorescence over the infection phase (Figure 4-4). Manual polygonal gates are very dependent on the analysing person; therefore, quadrant evaluation of 2D flow cytometric data was preferred. Consequently, for analysis of infection time series shown in this work NP-stained 0 hpi samples were used to set a 1% false-positive infection gate (black vertical line, Figure 4-2) and gates were kept constant during evaluation of infection series samples.

4.2.2 Shifting cell populations

Depending on the influenza virus strain and the MOI used for infection, a shift in fluorescence intensities of uninfected and infected cell populations was sometimes observed in late infection. One extreme example is shown in Figure 4-3. At 32 hpi the population becomes bimodal, with a second FL1-fluorescence peak additionally to the uninfected low FL1 peak. This is most likely caused by cells that have just started to accumulate virus protein. At 52 hpi this infected cell population shifts to higher FL1-fluorescence intensities when virus replication has progressed.

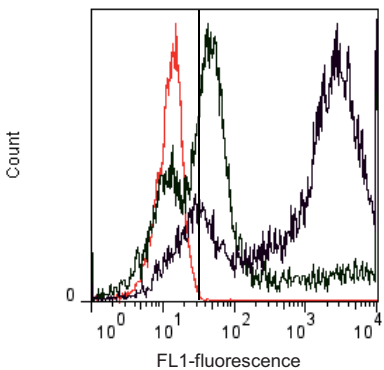

Figure 4-3 Example of shifts in FL1-fluorescence intensities of uninfected and infected cell populations of MDCK cells infected with influenza virus A/PR/8 RKI at MOI 0.016. Red curve: 0 hpi, green curve: 32 hpi, violet curve: 52 hpi. The black vertical line indicates the 1% false-positive gate set with the 0 hpi sample. Through the overlay of several histogram distributions no cell count can be given on the y-axis.

To clarify whether the shifting of the low FL1-fluorescence population was caused by the virus or the cells, autofluorescence of unstained infected cells was measured up to 72 hpi.

Furthermore, NP-stained mock-infected samples were measured for up to 72 hpi to exclude shifting in fluorescence being caused by the medium exchange performed at toi.

Time series of unstained samples showed only a very minor shift in fluorescence at very late time points in infection (Figure 4-4a), probably due to the higher proportion of apoptotic cells present late in infection. NP-stained mock-infected samples showed no shift of their upper fluorescence limit over 72 h (Figure 4-4b). Thus, the observed shift in NP-fluorescence of the uninfected population during infection is not caused by a changing auto- or background fluorescence of the cells. The data show that the fluorescence shift must be caused by the virus itself, e.g. through absorption of virus particles to the cell surface or virions released into the cytoplasm.

For these reasons, the gate between uninfected and infected samples (set with the 0 hpi infected NP-stained sample) was kept constant for all sampling time points during analysis of infection time series. This is also in agreement with gating procedures in evaluation of immunologic flow cytometric data, and with previous flow cytometric detection of influenza virus infection (Nichols *et al.* 1993).

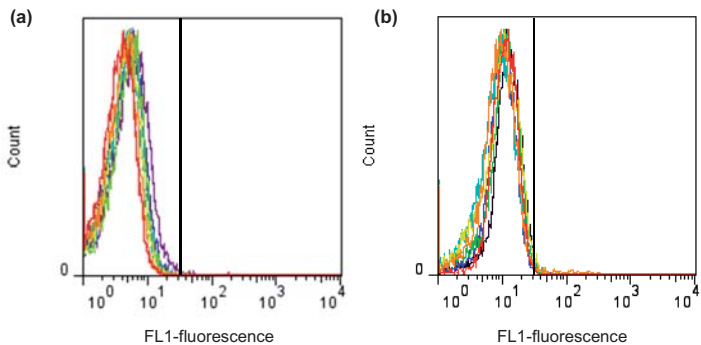

Figure 4-4 Histogram distributions of NP-fluorescence intensities of (a) unstained infected samples and (b) NP-stained mock-infected samples of adherent MDCK cells. Analysed time points: 0 (red), 8 (orange), 16 (yellow), 24 (light green), 32 (dark green), 40 (light blue), 52 (dark blue), and 72 (violet) hpi. The black vertical line indicates the 1% false-positive gate. Through the overlay of several histogram distributions no absolute count values on the y-axis can be given.

4.2.3 Discussion

Shifts in histogram fluorescence intensities are not an unusual observation. In fact, there are several studies described in literature that make use of shifts in fluorescence intensities in order to address various questions.

Wu *et al.* (2014b) used a proteinase K assay to investigate whether selected FITC-labelled DNA aptamers interact with certain surface proteins on a glioma cell line overexpressing an epidermal growth factor receptor. As the digestion time with proteinase K increases, a decrease in fluorescence signal intensity occurred reflecting the decreasing interaction between the aptamer and the surface protein.

Ikeda *et al.* (2000) used decreasing fluorescence intensity as a measure for a murine leukaemia virus binding to a glycoprotein at the surface of different murine cell lines in dependency of temperature: an increase from 4°C to 37°C resulted probably in a conformational change of the glycoprotein resulting in a loss in fluorescence from the cell-glycoprotein-labelled antibody complex.

Liu *et al.* (2007) investigated the effect of Flex-Het drugs on mitochondrial swelling and membrane integrity in ovarian cancer cells and non-cancerous cells. Therefore, they used the cationic dye JC-1 that accumulates in mitochondria to form aggregates. In case of a loss of mitochondrial membrane integrity or potential, a shift in fluorescence was monitored over drug treatment time.

The uptake of FITC-labelled dextran as a model for antigen uptake by dendritic cells was used by Porter *et al.* (2007). Monitoring the increase in mean fluorescence intensity they performed a quantitation of the time-dependent functional uptake of FITC-dextran up to 90 min.

The ability of a receptor at the surface of cells to be internalised was measured as a decrease in fluorescence intensity in a flow cytometer (Gavina *et al.* 2010). Rat leukaemia cells transfected with a HA-tagged receptor for the formyl-methionine-leucine-phenylalanine (fMLP) peptide were stimulated with fMLP peptide and stained with an anti-HA antibody and a secondary fluorescent-labelled goat-anti-mouse antibody. The decrease in fluorescence intensities was monitored at three time points up to 30 min.

Steele-Mortimer *et al.* (1990) evaluated time series of MDCK cells infected with influenza C/Johannesburg/1/66 using flow cytometry up to 72 hpi. Therefore, they incubated cells with virus-specific polyclonal serum followed by incubation with a FITC-labelled secondary antibody. Percentage of infected cells reached a maximum around 30 hpi and decreased afterwards. However, as the authors do not provide histograms it cannot be decided if a shift in fluorescence intensity might be responsible for the decrease in percentage of positive cells.

Finally, Nichols *et al.* (1993) distinguished internalised from bound FITC-labelled influenza virus A/AA/Marton/43 (H1N1) in monocyte-macrophages. Percentage of cells positive for influenza virus after infection at MOI 3 increased up to 30 min, but decreased

afterwards. They hypothesised that this decrease in positive cells is due to loss in FITC-fluorescence which is caused by the change in pH when the virus enters the cell's endosomes. However, when treating cells with inhibitors for vacuolar acidification no significant influence on the percentage of cells positive for internalised virus was detected. They also present histograms in which a bimodal distribution is visible for internalised virus 20 min after infection, indicating an uninfected and an infected cell population. Interestingly, the left peak of uninfected cell slightly shifts to higher fluorescence intensities, especially after 50 min. This shift of the uninfected cell population is comparable to that observed in influenza virus stainings and flow cytometric analyses performed in this work. However, a direct comparison of the histogram data is not possible, due to the different virus-host cell system and different staining strategy (Nichols *et al.* use labelled virus, whereas in this work viral NP is labelled after sample taking). Also, they do not comment on this shifting cell population. Still, this study is an additional indicator that cell populations with intracellular influenza virus detected with flow cytometry do not have strict constant fluorescence intensity.

4.3 Influenza virus replication in adherent MDCK cells using static cultivation systems

In this section results from T25-flask infections of adherent MDCK cells with different influenza virus A strains are shown. Aim of these studies was investigation of the effect of a change in MOI on virus infection dynamics, virus-induced apoptosis, and viral yields. For this purpose, infections with influenza A/PR/8 RKI and NIBSC, the HGR strains Uruguay-like and Wisconsin-like at MOI 0.0001, 0.1, and 3 were performed. These data (sections 4.3.1 and 4.3.3) plus the according discussion were published previously as "Isken B, Genzel Y, Reichl U. 2012. Productivity, apoptosis, and infection dynamics of influenza A/PR/8 strains and A/PR/8-based reassortants. *Vaccine* **30**: 5253–5261".

4.3.1 T25-flasks as small screening system

To investigate the influence of different infection parameters on infection dynamics and virus-induced apoptosis in cell culture-based influenza virus propagation, stirred tank bioreactor cultivations are time consuming and material expensive. In particular, for comparison of several virus strains at various MOIs in parallel, bioreactor systems would not be feasible. In order to overcome these limitations, T25-flasks were chosen as culture system enabling parallel investigation of different infection conditions. Aiming at analysing infection status and apoptosis with flow cytometry, petri dishes were considered to be too small, as at least 3 aliquots with 1×10^6 cells each should be stored for measurements. Thus, T25-flasks with an infection volume of 10 mL were investigated as

screening system. Firstly, dynamics of infection progression and HA titre should be compared to 1 L stirred tank bioreactor systems. A cultivation using adherent MDCK cells in GMEM infected with influenza virus A/PR/8 NIBSC at MOI 0.025 was compared to an A/PR/8 NIBSC MOI 0.025 infection in T25-flasks. For this purpose, multiple T25-flasks were inoculated from the same cell pool in parallel and grown to confluence for 5 days. Afterwards, flasks were washed with PBS and infected in parallel using 10 mL serum-free virus maintenance medium containing 50 units trypsin and seed virus to adjust an MOI of 0.025. The general preparation steps for later flow cytometric evaluation like trypsinisation of adherent cells, pooling of trypsinised cells with cells from supernatant, and double fixation were performed as with bioreactor samples.

In Figure 4-5 the comparison of stirred tank to T25-flask infection dynamics is shown. In T25-flask infections HA titre increased at 24 hpi (Figure 4-5a). This is about 12 h later compared to the bioreactor infection performed with the same strain at the same MOI.

Comparing maximum percentage of infected non-apoptotic cells in T25-flasks to bioreactors, it appeared that in T-flasks maximum percentage were 16.4% lower than in the bioreactor infection under similar conditions (data not shown), and maximum total virus titres were 0.14 $\log_{10}$ HAU/100 µL lower in T25-flask infections (Figure 4-5a), which is in the assay's error range. Consequently, specific virus yields per cell (calculated from maximum cell numbers and maximum HA titres) were in the same range for both systems: 9325 and 11259 virions/cell in bioreactor and T25-flask infections, respectively.

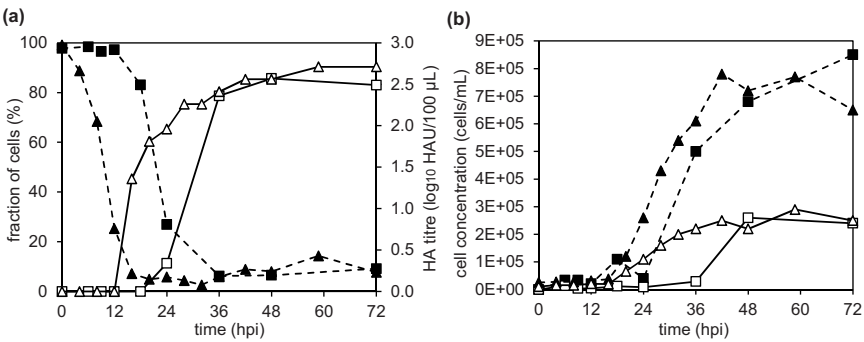

Figure 4-5 Comparison of infection dynamics and HA titre of a 1 L stirred tank reactor infection (triangles) to a T25-flask infection (squares) of adherent MDCK cells infected with influenza virus A/PR/8 NIBSC at MOI 0.025. (a) uninfected cells (dashed lines) and HA titre (solid lines); (b) total (dashed lines) and viable (solid lines) cell concentration in supernatant.

Cell concentration in supernatant (Figure 4-5b) showed a comparable time shift as seen in HA titre time courses and infection dynamics. Equal cell concentration was reached in

T25-flask 50 hpi. Thus, T25-flasks offer an easy to handle infection system, which is especially useful for comparison of multiple infection conditions.

As a final remark, T25-flask infections were performed directly through addition of 10 mL virus maintenance medium containing trypsin and seed virus: no low volume incubation to improve virus attachment to the cells and to achieve a synchronous infection was performed. Furthermore, scouting experiments performed within the scope of this thesis have shown that such a low volume incubation does not result in a synchronous infection in terms of NP-fluorescence measured by flow cytometry (data not shown).

4.3.2 Biological variation within and between T25-flask experiments

Next aim was to identify variations of infected T25-flasks within one experiment. For this purpose, a parallel infection of three T25-flasks was performed followed by analysis of cell concentration in supernatant, HA titre, and infected and apoptotic cell populations. Confluent adherent MDCK cells were infected in 10 mL serum-free virus maintenance medium containing influenza virus A/PR/8 RKI at MOI 0.016 and three parallel T25-flasks were analysed at every time point (Figure 4-6). Both, total and viable cell concentration in the supernatant started to increase at 30 hpi, with the total cell concentration steadily increasing up to 8.7–9.3 x 10^5 cells/mL, and the viable cell concentration up to 2.8–3.1 x 10^5 cells/mL at 72 hpi (Figure 4-6a). Variations at 8 and 16 hpi in total cell concentration might be caused by the lower detection limit of the Vi-Cell™ XR of 6 x 10^4 cells/mL. Generally, at all time points the variations between the three parallel flasks were below 6 x 10^4 cells/mL.

When comparing HA titre time courses of the three parallel T25-flasks a similar picture as in cell concentration measurement appeared, with very similar HA titres at all time points (Figure 4-6b). Finally, variations in flow cytometric determination of infection status and apoptosis should be compared between parallel infected T25-flasks (Figure 4-6c). Again, differences between the three parallel analysed T25-flasks were very low, at maximum 9.7% at 40 hpi. Summarising, parallel infected T25-flasks showed excellent agreement regarding courses of cell concentration, HA titre, and flow cytometric evaluation of infection status and virus-induced apoptosis. Thus, for comparison of multiple infection conditions T25-flasks offer an easy to handle infection system with low inter-experimental variations.

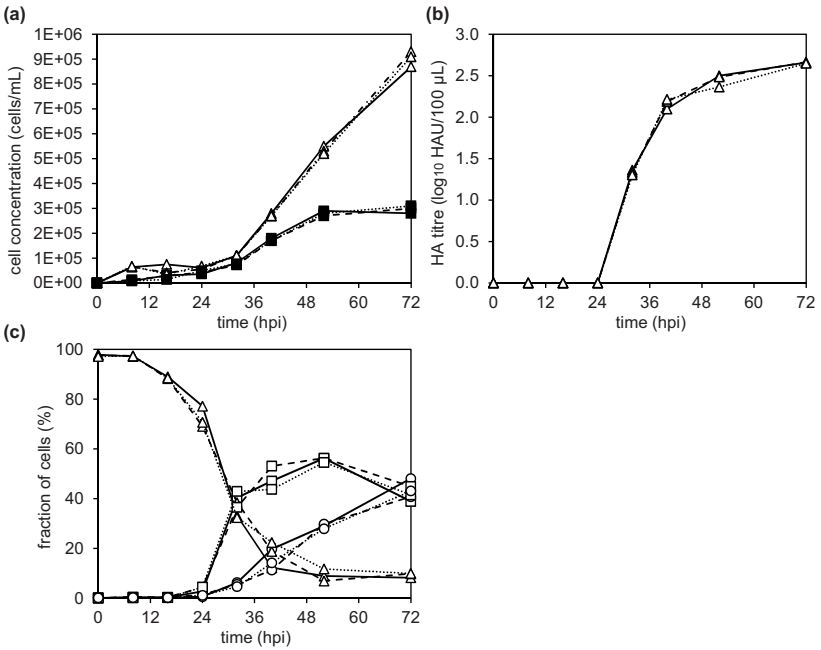

Figure 4-6 Three parallel infected T25-flasks of confluent adherent MDCK cells infected with influenza virus A/PR/8 RKI at MOI 0.016. (a) total (triangles) and viable (squares) cell concentration in the supernatant; (b) HA titre; (c) cell populations of uninfected (triangles), infected (squares) and apoptotic infected (circles) cells determined with flow cytometry.

The next step was analysis of biological reproducibility over time. In Figure 4-7 a T25-flask infection run that has been performed three times in completely independent experiments is shown. Supernatant cell concentration, HA titre, and percentage of uninfected cells of the three experiments are plotted as single runs. All three experiments fit together very well, showing a deviation of only few hours in the course of infection. The delay of onset of HA titre increase was 10.2 ± 2.1 h (median ± MAD). This value was determined by calculating the intersection between the initial HA titre and the linear regression of the exponential HA titre increase. This small delay might reflect errors in MOI adjustment through cell counting or pipetting errors.

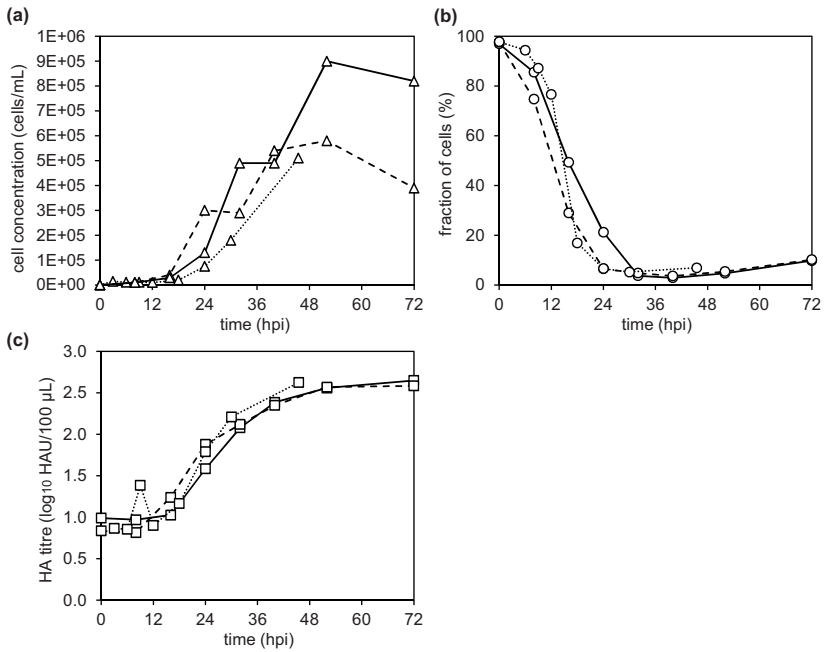

Figure 4-7 Comparison of biological repetitions of infection experiments in T25-flasks. Adherent MDCK cells infected with influenza A/PR/8 RKI at MOI 3: analysis of (a) supernatant cell concentration, (b) percentage of uninfected cells determined with flow cytometry, and (c) HA titre.

Furthermore, histograms of NP-fluorescence distributions of the three independent experiments were compared. In particular, the infected cell population of NP-fluorescence histogram distributions of 24, 32, and 40 hpi samples of three times performed T25-flask infections of MDCK cells with influenza A/PR/8 RKI at MOI 3 were fitted with a Gaussian distribution using MATLAB® software. In Figure 4-8 results of this MATLAB® analysis are shown, comparing mean and SD of the fitted distributions. A list of the determined values for mean fluorescence intensities, SD, and confidence intervals of SD of this three times repeated T25-flask infection can be found in the appendix (Table 8-4). All analysed samples showed mean fluorescence intensities between 1662 and 3635 fluorescence units (Figure 4-8a). Importantly, no significant differences neither between the repeated experiments nor the evaluated time points appeared. Also, no tendencies for fluorescence intensities to increase from 24 to 40 hpi were visible. Nevertheless, a factor that might influence absolute fluorescence intensities is the ratio of antibody molecules per cell that can vary due to cell losses during the staining procedure.

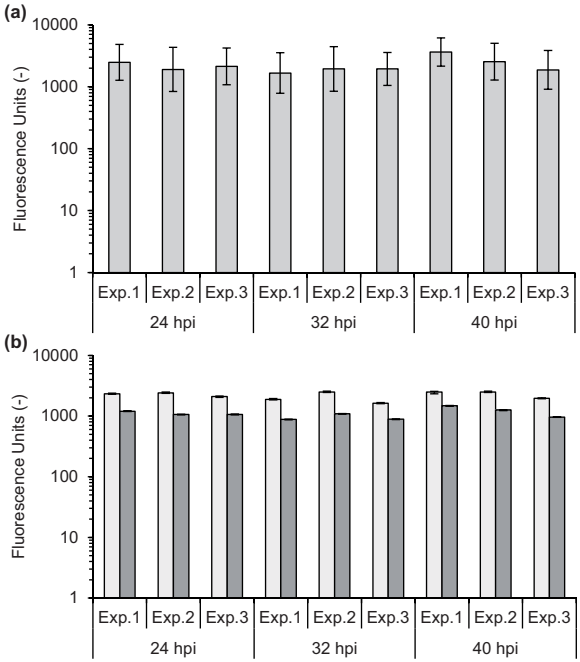

Figure 4-8 Three times performed infection of adherent MDCK cells in T25-flasks infected with influenza A/PR/8 RKI at MOI 3. (a) Analysis of mean fluorescence intensities of NP-fluorescence histograms with corresponding SD; (b) calculation of positive (light grey bars) and negative (dark grey bars) SD with corresponding 95% confidence interval. Analysis of three independent experiments (Exp.1–3) analysed at 24, 32, and 40 hpi.

While mean fluorescence values of the distributions did not differ much, the SD—representing the width of the distributions—varied between the samples. This is shown in Figure 4-8b by plotting SD plus its 95% confidence interval (light grey bars: SD in positive direction, dark grey bars: SD in negative direction). Clearly, the widths of the distributions do not only differ between experiment repetitions but also between time points within one experiment. Importantly, no correlation between sampling time point and distribution width was identified. Similar results were obtained when analysing NP-fluorescence distributions of parallel infected T25-flasks (shown in Table 8-5 in the appendix). Concluding, flow cytometric analysis of NP-fluorescence in MDCK cells infected in T25-flasks delivers reproducible mean fluorescence intensities even for independent experiment repetitions.

4.3.3 Influence of MOI on virus titres, infection dynamics, and apoptosis induction

Typically, each virus strain has its specific productivity, which can be different depending on the virus-host cell system. Moreover, the replication of some virus strains is restricted to few or even one host cell line. Some influenza virus strains show an MOI dependency, leading to higher virus titres at low MOI (Voeten *et al.* 1999; Aggarwal *et al.* 2011). In-depth analysis of progress of infection and characterisation of corresponding cell population distributions (i.e. degree of infection, apoptosis) can help to better understand these variations in productivity, and give hints towards seed virus and strain optimisation.

Former infections in the upstream team of the bioprocess engineering group had been performed at MOI 0.025 (Schulze-Horsel *et al.* 2009; Genzel *et al.* 2004; Genzel *et al.* 2005; Bock *et al.* 2011). Thus, the newly established T25-flask system should be used to investigate the influence of lower and higher MOI on infection and apoptosis dynamics as well as on virus titres. At the same time different high and low yield virus strains (wild type and HGR) should be compared. For this purpose, parallel T25-flasks were infected with four influenza A virus strains at MOI 0.0001, 0.1, and 3. An overview of the used seed virus preparations including their $TCID_{50}$, HA titre, and percentage of infectious particles is given in Table 4-2. Results shown in this section are discussed afterwards in section 4.3.4. For estimation of virions/mL based on HA titre, equation (2) (section 3.4.2) was used.

Table 4-2 Influenza seed viruses used for T25-flask infection experiments of adherent MDCK cells (seed virus adapted to adherent MDCK cells). In addition, virus subtype, seed virus titres, and percentage infectious particles is given.

Influenza virus strain	Subtype	$TCID_{50}$ (IVP/mL)	HA titre (virions/mL)	% infectious particles
A/PR/8 NIBSC	H1N1	0.13×10^8	7.96×10^9	0.16
A/PR/8 RKI	H1N1	0.40×10^8	3.99×10^9	1.00
A/Uruguay/716/2007-like HGR	H3N2	0.98×10^8	5.64×10^9	1.74
A/Wisconsin/67/2005-like HGR	H3N2	2.28×10^8	5.14×10^9	4.44

Effects of variations in MOI on HA titre and $TCID_{50}$

First, the T25-flask infections with influenza A/PR/8 RKI, A/PR/8 NIBSC and the HGRs Uruguay-like and Wisconsin-like at MOI 0.0001, 0.1, and 3 were analysed for infectious and total viral particle concentration by $TCID_{50}$ and HA assay, respectively. As expected, HA titres increased earlier the higher the MOI used for infection (Figure 4-9a, c, e). Due to

the comparatively low $TCID_{50}$ value of the seed virus (Table 4-2), a HA titre of 1.6 log_{10} HAU/100 µL was measured in A/PR/8 NIBSC infections at 0 hpi. The two tested HGR strains always showed the earliest increase in HA while the two A/PR/8 wild type strains showed comparable dynamics. The Uruguay-like HGR showed the earliest increase in HA titre of all tested strains at the tested MOIs. In addition, using the Uruguay-like HGR strain very high end titres up to 3.1 log_{10} HAU/100 µL were achieved independent of the MOI. Interestingly, the Wisconsin-like HGR reached the highest HA titres at MOI 0.0001 and significant lower HA titres at MOI 3 indicating an MOI dependency.

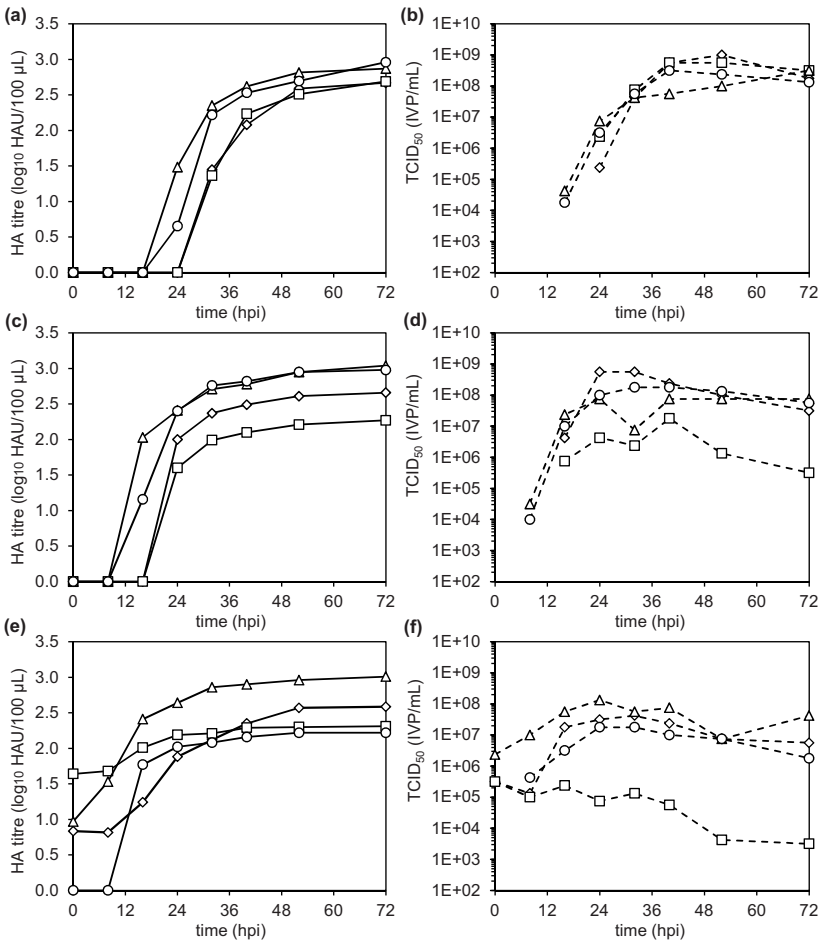

Figure 4-9 Courses of HA titre (a, c, d) and $TCID_{50}$ (b, d, f) of T25-flask infections of adherent MDCK cells with influenza A/PR/8 RKI (diamonds), A/PR/8 NIBSC (squares), Uruguay-like HGR (triangles), and Wisconsin-like HGR (circles) at MOI 0.0001 (a, b), 0.1 (c, d), and 3 (e, f).

Time courses of the $TCID_{50}$ were similar at MOI 0.0001 for all tested strains, with influenza A/PR/8 RKI increasing a few hours later than the other three strains (Figure 4-9b). With higher MOI the dynamics of $TCID_{50}$ varied more between the strains (Figure 4-9d, f). Remarkably, the A/PR/8 NIBSC did not show any increase in infectious particle concentration with MOI 3. Generally, the dynamic patterns of HA and $TCID_{50}$ appeared to be more comparable between the tested strains at low MOI.

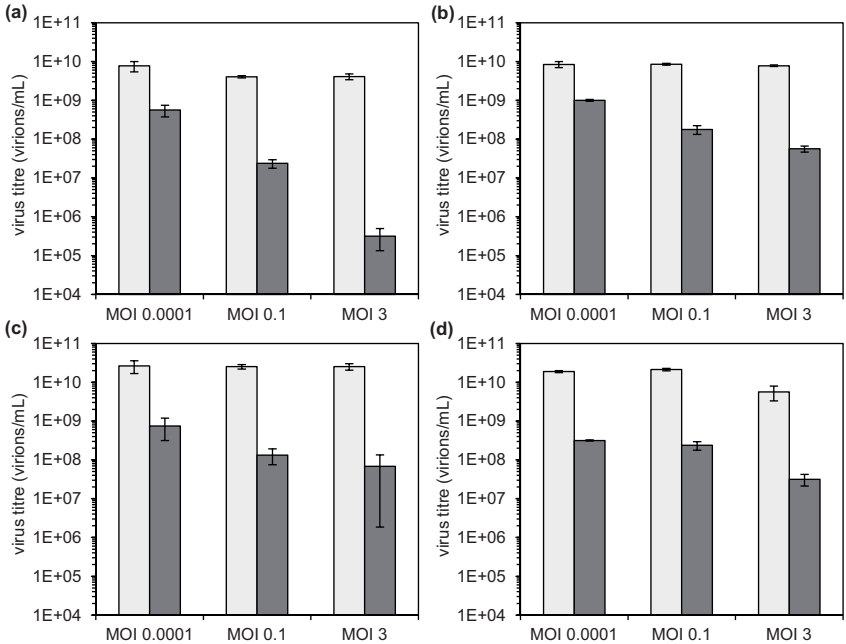

Figure 4-10 Maximum HA titre (dark grey bars) and $TCID_{50}$ (light grey bars) of adherent MDCK cells infected with influenza (a) A/PR/8 NIBSC, (b) A/PR/8 RKI, (c) Uruguay-like, and (d) Wisconsin-like HGRs at MOI 0.0001, 0.1, and 3. Shown are median ± MAD from at least three independent experiments.

In addition, the maximum number of virus particles obtained via HA assay and $TCID_{50}$ was analysed (Figure 4-10). This allowed a statistical evaluation of the results, verifying reproducibility of the T25-flask set-up. It can clearly be seen that for the Uruguay-like HGR as well as for the two A/PR/8 wild type strains a change in MOI did not lead to significant differences in the maximum number of virus particles released (Figure 4-10a, b, c: light grey bars). Only infections with the Wisconsin-like HGR at MOI 3 resulted in significant lower values than at MOI 0.0001 and 0.1 (Figure 4-10d) thus confirming an MOI dependency of the maximum number of virus particles (HA values) obtained. Maximum $TCID_{50}$ decreased with increasing MOI used for infection (Figure 4-10, dark

grey bars) especially for the tested wild type strains. Most strikingly, for influenza A/PR/8 NIBSC infections the maximum $TCID_{50}$ titre at MOI 0.0001 was 5 magnitudes higher than at MOI 3. Apparently, no infectious virus particles were produced in MOI 3 infections, or virus stability was very low. For A/PR/8 RKI and Wisconsin-like HGR infections the $TCID_{50}$ at MOI 3 were more than ten times below maximum titres reached in MOI 0.0001 infections.

The composition of the seed viruses used for infections ranged from 0.16% (A/PR/8 NIBSC) to 4.44% (Wisconsin-like HGR) for the ratio of infectious virus particles to total virus particles (Table 4-2). The highest number of virions produced per cell at MOI 3 infections was observed for the Uruguay-like HGR with a total number of 47000 virions/cell and 231 IVP/cell, respectively (Table 4-3). In contrast, A/PR/8 NIBSC produced only 7400 virions/cell and 0.6 IVP/cell at MOI 3. Percentage values of maximum $TCID_{50}$ to maximum HA titre at MOI 3 revealed for A/PR/8 NIBSC a 60-fold lower proportion compared to A/PR/8 RKI. At MOI 0.0001 in Uruguay-like infections almost 40000 virions were released per cell, however, A/PR/8 RKI had the highest percentage of infectious virus particles produced (11.48%). Interestingly, the MOI increase had a much more severe effect on proportions of infectious virus particles for the two wild type strains and especially the A/PR/8 NIBSC than for the two tested HGR strains (factor 21.5 and 920.5 for A/PR/8 RKI and NIBSC, factor 2.8 and 5.8 for the HGRs, respectively). Finally, as shown in Table 4-3, high MOI infections generally led to decreased numbers of infectious virus particles released per cell (0.6–230.9 IVP/cell at MOI 3 and 474.5–1451.4 IVP/cell at MOI 0.0001).

Table 4-3 Overview of yields of T25-flask infections of adherent MDCK cells.

Virus strain	Yield MOI 0.0001			Yield MOI 3			Fold reduction high vs low MOI
	Total virions/cell	Infectious virions/cell	% infectious virions	Total virions/cell	Infectious virions/cell	% infectious virions	
A/PR/8 NIBSC	11696.8	868.6	7.43	7437.5	0.6	0.01	920.5
A/PR/8 RKI	12644.9	1451.4	11.48	13017.1	69.4	0.53	21.5
Uruguay-like HGR	39959.9	474.5	1.19	46996.5	230.9	0.49	2.4
Wisconsin-like HGR	26885.4	479.5	1.78	9998.6	30.5	0.31	5.8

Infected and uninfected cell populations in low and high MOI infections

In many studies, e.g. Voeten *et al.* (1999) on influenza virus HGR characterisation, only an HA assay is used for virus quantification. Experimental data based on infectivity or HA assays are only elucidating the time course of virus release and the accumulation of virus particles. To optimise influenza vaccine production, additional information concerning the physiological status of the host cells at toi as well as the progress of infection and virus-induced apoptosis is useful.

Thus, in addition to virus titre measurements, flow cytometric analysis of virus accumulation in cell populations at different MOIs was performed. As expected, the decrease in the percentage of uninfected cells (Figure 4-11a, c, e) correlated well with increase in infected cell populations (Figure 4-11b, d, f). At MOI 0.0001, the two HGRs Uruguay-like and Wisconsin-like showed faster infection dynamics compared to the two tested wild type strains. All strains reached the maximum in percentage of infected cells between 24 and 32 hpi with a slight decrease afterwards (Figure 4-11b). When raising the MOI to 0.1, increases in percentage of infected cells started earlier compared to lower MOI, similar to the shifts in HA titres (Figure 4-9a, c, e). Again the HGRs showed the fastest dynamics while progress of infection of A/PR/8 RKI was the slowest. Interestingly, the A/PR/8 NIBSC revealed a dynamic behaviour more comparable to the HGR strains than to A/PR/8 RKI at this MOI. Furthermore, A/PR/8 NIBSC showed the strongest response to MOI variation. Also noticeable is the change in the percentage of infected cells after the maximum: while the Wisconsin-like HGR stayed at a constant high level, A/PR/8 NIBSC showed a striking decline in percentage of infected cells from 65% to 30% within 8 h (Figure 4-11d). At the higher MOI of 3 the A/PR/8 NIBSC infection was as fast as the HGR infection and showed an even more severe drop in the percentage of infected cells from its maximum of 80% down to 25% (Figure 4-11f). Interestingly, maximum percentage values of infected cells were independent of the MOI always ranging between 60% and 80% for all tested strains. Infection with higher MOI generally led to a shift to earlier time points, however, the extent of this shift varied for the different strains.

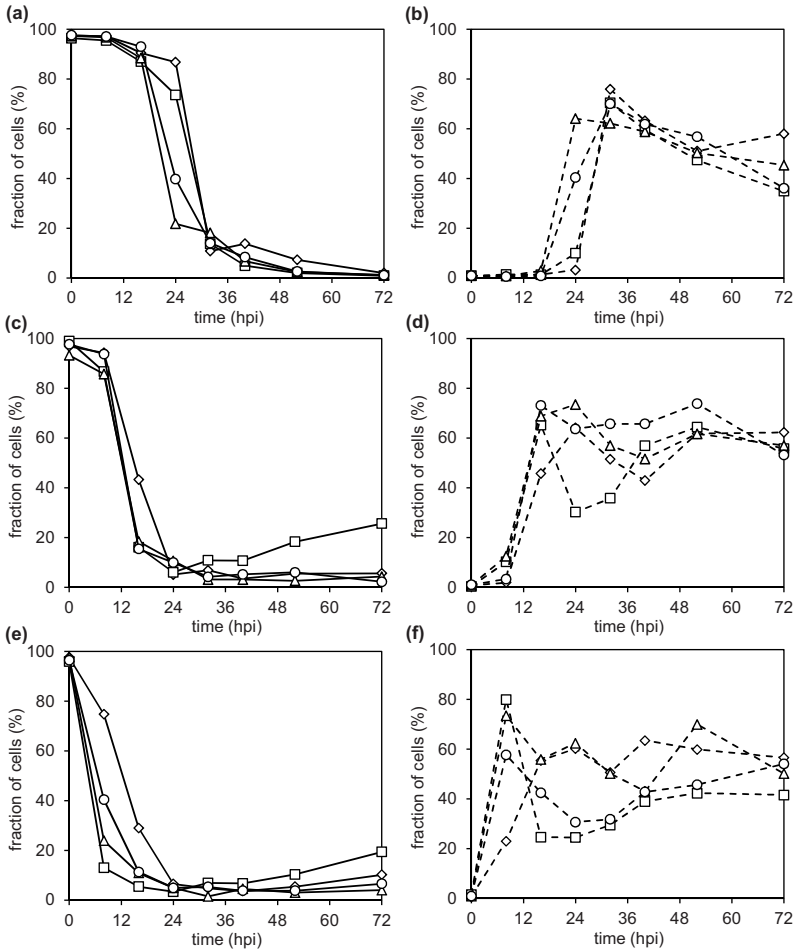

Figure 4-11 Fractions of uninfected (a, c, e) and infected (b, d, f) cells determined with flow cytometry of a T25-flask infection experiment with adherent MDCK cells using influenza A/PR/8 RKI (diamonds), NIBSC (squares) and the HGRs Uruguay-like (triangles) and Wisconsin-like (circles) at MOI 0.0001 (a, b), 0.1 (c, d), and 3 (e, f).

Dynamics of virus-induced apoptosis is strain- and MOI-dependent

Influenza virus infections are known to induce apoptosis in their host cell, which has a significant influence on the number of virus producing cells and therefore on yields in vaccine manufacturing (Schulze-Horsel *et al.* 2009; Möhler *et al.* 2005; Petiot *et al.* 2011). Thus, in addition to the infection status, cell populations were analysed by flow cytometry with respect to apoptosis induction.

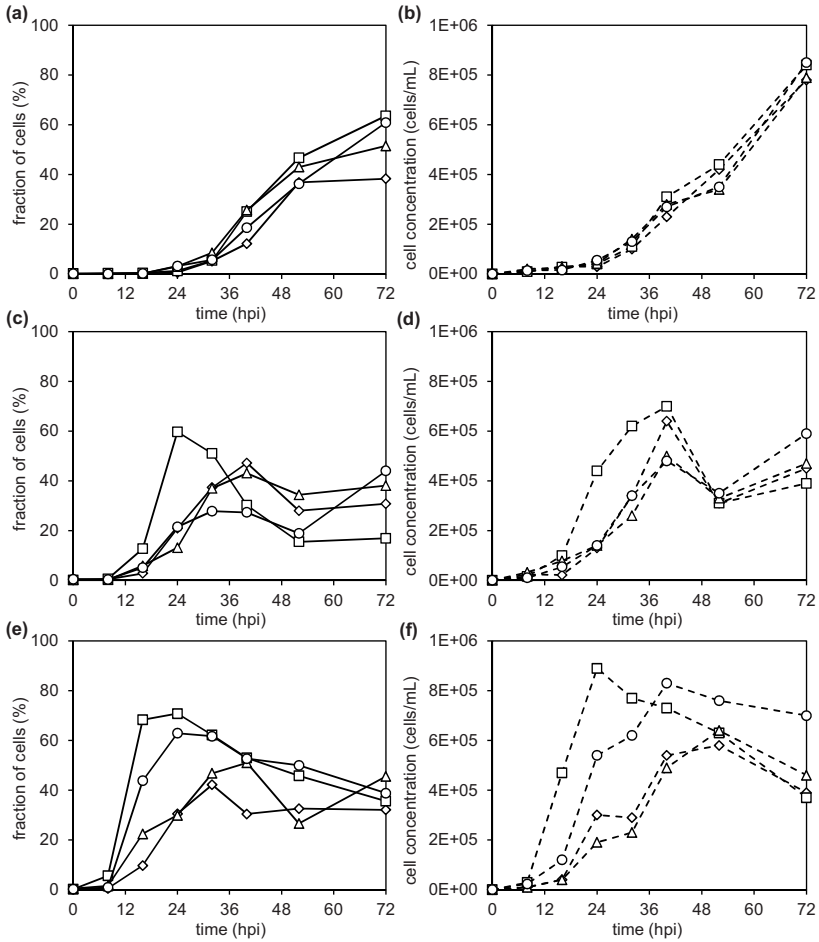

Figure 4-12 Flow cytometric determination of apoptotic infected cell populations (a, c, e) and supernatant cell concentration (b, d, f) of MOI 0.0001 (a, b), 0.1 (c, d), and 3 (e, f) infections of adherent MDCK cells grown to confluence in T25-flasks. Virus strains used for infection: influenza A/PR/8 RKI (diamonds), A/PR/8 NIBSC (squares) and the HGRs Uruguay-like (triangles) and Wisconsin-like (circles).

For the low MOI of 0.0001 the percentage of apoptotic infected cells constantly increased for all tested strains in a comparable range and correlated very well with the time course of cell concentration in the supernatant (Figure 4-12a, b). With increasing MOI, the fraction of apoptotic cells in Uruguay-like HGR and A/PR/8 RKI infections showed similar dynamics, while the A/PR/8 NIBSC showed a much earlier and stronger increase in the percentage of apoptotic infected cells up to 60% (Figure 4-12c). This fast apoptosis induction became even stronger at infections with MOI 3 (maximum of 71% apoptotic

infected cells) (Figure 4-12e). Interestingly, at MOI 3, the Wisconsin-like HGR also strongly induced apoptosis (maximum of 63%) (Figure 4-12e).

Most time courses of the percentage of apoptotic infected cells declined after a maximum was achieved. This is most likely due to cell lysis, as cell concentration in the supernatant decreased in a comparable manner. Generally, the time courses in supernatant cell concentration (Figure 4-12b, d, f) correlated very well for all MOIs with percentage in apoptotic infected cells (Figure 4-12a, c, e). Importantly, not only did infections with higher MOI lead to an earlier and stronger induction of apoptosis, the tested strains also responded quite differently to higher MOIs. While the A/PR/8 NIBSC and Wisconsin-like HGR strain strongly induced apoptosis especially at higher MOI (Figure 4-12e), the A/PR/8 RKI and Uruguay-like HGR only led to a moderate increase in the percentage of apoptotic infected cells. Comparing dynamics of infected cells (Figure 4-11b, d, f) with apoptosis induction it appears that infections with influenza A/PR/8 NIBSC result in a fast progress of infection and a fast onset of apoptosis, while the Uruguay-like HGR strain infected cultures very fast, but induced apoptosis much later and in a less pronounced way. A/PR/8 RKI responded generally very little to MOI variation, and the Wisconsin-like HGR strain showed only at the high MOI of 3 a stronger induction of apoptosis. Remarkably, the differences between the strains became only distinct at higher MOI, while at lower MOI the dynamics of apoptosis induction was similar for all tested strains.

4.3.4 Discussion

Different influenza virus strains perform very differently when propagated in cell culture. Some virus strains replicate well to high titres while others exhibit an MOI dependency, grow to only low titres, or will not propagate at all. To better understand differences between high and low yield influenza virus strains, infections with different influenza virus strains at various MOIs should be performed. As infections in bioreactor systems are too laborious and cost-intensive for such studies, a T25-flask infection system was established. Thereby, infection experiments comparing up to four different virus strains or four different MOIs in parallel can be performed. Comparing infection dynamics and HA titres in T25-flasks to those obtained in bioreactor systems, T25-flask infections showed a later onset of infection. Reason for this time delay might be related to diffusion-limited spreading of the virus and the different flow conditions in T25-flasks compared to STR. In the T25-flask system, virus seed added for infection in 10 mL virus maintenance medium and, in particular, released virions must spread through the system mainly by diffusion. In the STR system, virus particles are transported by convective mass transport induced by stirring, in addition to diffusion. This seems to accelerate the infection waves resulting in an earlier detectable onset of infection in stirred systems compared to static cultivation systems.

In addition, the cultivation system has an impact on the cellular metabolic activity. For example, shear stress is present in stirred systems, but absent in static cultivation systems. An altered metabolic activity of adherent MDCK cells that showed higher glutamate and glutamine uptake rates in stirred systems than in static systems even in the stationary phase was described by Wahl *et al.* (2008) and Rehberg *et al.* (2013). Wahl *et al.* (2008) described influenza virus replication not to be a burden for cellular metabolism; however, cells on microcarriers (that are exposed to shear stress) might show cell growth (and metabolic activity) at a low specific rate which is believed being beneficial for virus replication.

In order to analyse variations between T25-flask infections, parallel infected T25-flasks as well as independently repeated infection experiments in T25-flasks were compared. Courses of cell concentrations and HA titre in parallel T25-flasks showed only minor variations. Also, flow cytometric analysis of infection dynamics and apoptosis showed differences of very maximum 9.7% in the highly dynamic part of the infection. Independent experiment repetitions demonstrated at maximum few hours delay in percentage of uninfected cells and first increase of HA titre. Finally, analysis of NP-fluorescence distributions showed a good reproducibility of cytometric stainings even in independent experiment repetitions. Concluding, T25-flasks demonstrated to be a useful system with good reproducibility, similar final HA titres and cell-specific virus yields compared to stirred tank bioreactor (STR) infections. Hence, T25-flasks were used for studies aiming at comparing different virus strains at different MOI.

Subsequently, T25-flask infections of adherent MDCK cells with two wild type A/PR/8 strains and two A/PR/8-based HGR strains were conducted at MOI 0.0001, 0.1, and 3. As expected, the HA titres and $TCID_{50}$ increased earlier the higher the MOI chosen for infection for all four strains. An earlier increase in virus titres for increasing MOI was also observed in other studies (Genzel *et al.* 2006b; Rimmelzwaan *et al.* 1998). When Aggarwal *et al.* (2011) tested different *ca* influenza virus strains, they found infectious titres to increase at the same time at different MOIs. Additionally, they described great differences in virus yields with change in the MOI. This is also apparent in the results summarised in Table 4-3. Furthermore, peak titre variations were small at low MOI in Aggarwal *et al.* (2011), which was also seen in T25-flask infections at MOI 0.0001 (Figure 4-9b). Maximum infectious titres, however, did not vary significantly in their experiments. This is in contrast to $TCID_{50}$ titres in this thesis—especially for the A/PR/8 wild type strains. These differences might be due to the different infection system used by Aggarwal *et al.* (2011). They cultivated MDCK cells in bioreactors and split them into shaker flasks for subsequent infection. Furthermore, infections were carried out at 33°C as they used live attenuated virus strains, all containing an A/AnnArbor or B/AnnArbor backbone.

Final HA titres varied only slightly at lower MOI in T25-flask infections (Figure 4-9a). Also, dynamics of the release of infectious virus particles appeared more homogeneous at lower MOI (Figure 4-9b). Concerning the maximum HA titres reached, only the Wisconsin-like HGR showed an MOI dependency. Here, the HA titre dropped significantly with the increase of the MOI to 3. The Uruguay-like reassortant could be grown to very high titres at all MOIs. In addition, the A/PR/8 RKI variant reached higher titres than the NIBSC variant, which is in accordance with previous results (Schulze-Horsel *et al.* 2009). Genzel *et al.* (2006b) investigated HA titres of equine influenza virus infections in roller bottles at MOI from 1 to 0.0001 and also found a time shift in virus particle release, but no differences in final HA titres. Rimmelzwaan *et al.* (1998) analysed HA and $TCID_{50}$ titres of infections with an influenza virus H3N2 wild type strain at different MOIs in MDCK cells. Maximum HA titres were 2–4-fold increased when lowering the MOI from 1 to 0.0001, whereas maximum infectious titres showed no significant differences (Rimmelzwaan *et al.* 1998). These discrepancies to the data presented here probably result from the different virus strain they used and differences in infection conditions, namely infecting in BSA containing medium without addition of trypsin. Furthermore, unbound virus particles were removed by washing steps in their experiments after one hour incubation at 37°C. Le Ru *et al.* (2010) investigated influenza virus A/PR/8 replication in HEK-293 cells and found higher HA titres for infections at MOI 1 x 10^{-3} and 1 x 10^{-5} compared to infections at MOI 1 and 10^{-1} after 3 days post infection. This could indicate that MOI dependency is also potentially dependent on the cell line used.

Maximum infectious titres decreased for increasing MOI, which was also seen for different influenza virus strains by others (Aggarwal *et al.* 2011; Maranga *et al.* 2003; Carinhas *et al.* 2009). While in most studies either total or infectious virus titres were determined, the data presented in Table 4-3 show that the ratio of infectious virus particles to total virus particles also decreased for the higher MOI. One explanation could be the accumulation of DIPs that might influence this ratio, a hypothesis that Nayak *et al.* (1985) and Aggarwal *et al.* (2011) proposed. In literature there are four populations of non-infectious biological active influenza virus particles (niBAP)s described, namely interferon-inducing particles (Marcus 1982), interferon induction-supressing particles (Marcus *et al.* 2005), niCKPs (Ngunjiri *et al.* 2008), and DIPs (Nayak *et al.* 1985). These non-infectious particles have the potential to influence the course of pathogenesis through their capacity to stimulate or suppress antiviral responses (Marcus *et al.* 2009). Especially DIPs are described to be generated by passaging at high MOI (Nayak *et al.* 1985). Though not directly killing cells, DIPs impair the replication of co-infecting infectious cell-killing particles. Marcus *et al.* (2009) postulated that large copy numbers of gene segments, present in high multiplicity passages, may influence replication steps in subsequent low MOI infections as well as the selective packaging of the eight gene segments required for infectivity. When comparing

percentage of infectious virus particles to the total number of virions produced in this work, values of MOI 3 infections were always lower than those of MOI 0.0001 infections (Table 4-3), and thus in line with above mentioned literature.

Flow cytometry was used to analyse populations of uninfected, infected, apoptotic, and apoptotic infected cells. Earlier investigations concerning time courses of influenza virus-induced apoptosis mostly used qualitative methods like agarosegel electrophoresis (Hornícková 1997; Kurokawa *et al.* 1999). Quantitative studies using flow cytometry were performed by Price *et al.* (1997), who identified apoptotic cells in influenza virus infections by a low DNA content and Wurzer *et al.* (2003), who measured time courses of early apoptosis with an Annexin V assay. However, both studies were performed at one single MOI only. Flow cytometric data presented here were generated after infections at different MOIs and combine information about intracellular virus protein accumulation and apoptosis induction through a double staining.

Former work in the bioprocess engineering group, comparing A/PR/8 NIBSC and RKI at a single MOI 0.025 in stirred tank infections, showed the A/PR/8 NIBSC had a faster increase in the percentage of infected cells and an earlier apoptosis induction resulting in lower titres than the A/PR/8 RKI infection (Schulze-Horsel *et al.* 2009; Heynisch *et al.* 2010). Above presented data for infections at three different MOIs gives new insights into the differences between these two variants. Only at a very low MOI, but not at a higher MOI, A/PR/8 RKI and A/PR/8 NIBSC showed similar dynamics. Noteworthy, the percentage of infectious virus particles in the seed virus strains varied from 0.16% to 1.00%, for A/PR/8 NIBSC and A/PR/8 RKI, respectively (Table 4-2). Accordingly, the RKI-derived seed virus contained six times more infectious virus particles than the NIBSC-derived seed virus. Seed viruses with a higher proportion of non-infectious virus particles, like the used A/PR/8 NIBSC, should contain more niCKPs that potentially drive cells into apoptosis (Marcus *et al.* 2009). Those niCKPs could not only explain the stronger activation of different signalling pathways and interferon expression found in A/PR/8 NIBSC infections compared to A/PR/8 RKI infections (Heynisch *et al.* 2010; Seitz *et al.* 2010) but also the stronger apoptosis induction in A/PR/8 NIBSC infections, especially at the higher MOIs.

For the two tested HGRs—which are both H3N2 subtype strains with an A/PR/8 backbone—a faster progress of infection compared to the wild type A/PR/8 strains was observed. Especially the Uruguay-like HGR had a faster increase in infected cells at all MOIs, while for the Wisconsin-like HGR this fast dynamic was lost at the high MOI. Regarding apoptosis induction, the two HGRs showed a more pronounced difference for higher MOIs. In particular, the Wisconsin-like HGR showed a much stronger induction of apoptosis at MOI 3 compared to the Uruguay-like HGR. In contrast to A/PR/8 NIBSC,

both HGRs showed only a weak induction of analysed host cell signalling molecules: namely, the signalling molecules IκBα, elF2α, Stat2 and IRF3 were less activated upon influenza virus infection in MDCK cells (Heynisch 2013). Thus, signal transduction seems unlikely to be the cause for the enhanced apoptosis induction in Wisconsin-like HGR infections at MOI 3. It seems more likely that the Wisconsin-like reassortant generates higher proportions of niCKP that are sufficiently diluted in low MOI infections but play an important role regarding apoptosis induction at higher MOIs. This hypothesis agrees with Marcus *et al.* (2010), who also described influenza virus-induced apoptosis to be mainly caused by niCKP, and not by plaque-forming particles (PFP).

Summarising, here presented experiments revealed that strain-specific differences in HA and $TCID_{50}$ titres and apoptosis induction are less pronounced with reduction of the MOI. This more homogeneous behaviour is beneficial for robustness in vaccine production processes, as process conditions and time point of harvest can be kept constant independent of the strain used. Especially, late induction of apoptosis of virus-infected cells is of interest for vaccine production as, according to the models proposed by Möhler *et al.* (2005) and Schulze-Horsel *et al.* (2009), this results in an improvement of virus yields. This can explain the high total virus titres obtained in Uruguay-like HGR and A/PR/8 RKI infections, as infections with both strains result in a slow onset of apoptosis but a fast progress in infection. Thus, for influenza vaccine production strains combining a fast progress of infection with a late induction of apoptosis are the most preferable ones, as they yield the highest titres. It would be interesting to characterise more influenza virus strains in order to confirm this hypothesis. Also, the high virus titres obtained in infections with Uruguay-like HGR suggest that yield improvements in cell culture-based influenza virus propagation might be achieved by delaying apoptosis induction as it could prolong the cells' productive lifespan.

4.4 Influence of defective interfering virus particles on virus yields

T25-flask infections with different strains and varying MOI showed the impact of seed virus composition for the outcome of an infection. It seemed that DIPs negatively affected infectious virus yield. Therefore, the question arose whether the observed differences between in-house influenza A/PR/8 variants are caused by the seed virus preparations. To clarify this, two experimental strategies were followed and are presented in sections 4.4.1 and 4.4.2. Afterwards, results are discussed in section 4.4.3. Firstly, a high $TCID_{50}$ influenza seed virus preparation should be mixed with increasing proportions of non-infectious seed virus preparation to see if and how the performance of the seed virus decreases. Secondly, different seed virus preparations from A/PR/8 NIBSC with different

$TCID_{50}$ and different percentage of infectious virions should be compared regarding their infection and apoptosis dynamics as well as virus yields.

4.4.1 Addition of inactive seed virus to high $TCID_{50}$ virus seed

At first, experiments should investigate how a higher proportion of inactive particles in a virus seed influences virus dynamics and apoptosis. For this purpose, high $TCID_{50}$ seed virus was inactivated by incubation at 37°C for 5 days, as this is an easy to handle way for virus inactivation. A $TCID_{50}$ was performed afterwards to control the generated virus was inactive. Then, infections of petri dishes with adherent MDCK cells were performed with seed virus containing 7% infectious virus particles (with a $TCID_{50}$ of 2.09 x 10^9 IVP/mL; the untreated original seed virus), 0.7%, 0.07%, and only 0.007% infectious virus particles. MOI 0.1 was used in infections with all four preparations. Following the infection the HA titre and the $TCID_{50}$ were monitored (Figure 4-13). In addition, flow cytometric analysis was performed (Figure 4-14).

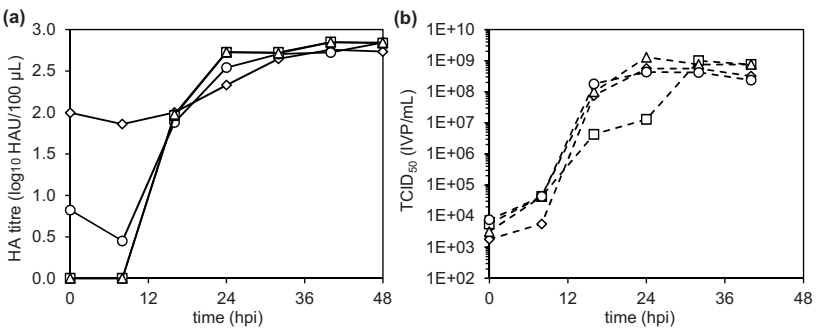

Figure 4-13 Analysis of effect of addition of inactive seed virus to a high $TCID_{50}$ seed virus. Courses of (a) HA titre and (b) $TCID_{50}$ of adherent MDCK cells infected with influenza A/PR/8 RKI seed virus containing 7% (triangles), 0.7% (squares), 0.07% (circles), and 0.007% (diamonds) infectious virus particles.

For the two seed virus preparations containing the lowest proportion of infectious particles already 0 hpi a HA titre could be detected due to the high amount of seed virus needed for MOI 0.1 adjustment (Figure 4-13a). The increase in HA titre for the 0.007% seed virus infection appeared less steep. Importantly, 48 hpi final virus titres did not differ much between all four preparations, ranging from 2.74–2.88 log_{10} HAU/100 µL. Consequently, net virus production was much lower for the 0.007% seed virus than for the other seed virus preparations. For time courses of $TCID_{50}$ 0.007% seed virus infection again showed a relatively slow increase compared to seed viruses with higher proportions of infectious virus particles (Figure 4-13b). Maximum $TCID_{50}$ ranged between 4.30 x 10^8 and 1.30 x 10^9 IVP/mL. Flow cytometric analysis showed a similar progress of infection and

virus-induced apoptosis for infections with 7%, 0.7%, and 0.07% infectious particles (Figure 4-14a, c). A maximum proportion of 72.4–83.3% infected non-apoptotic cells was reached 16 hpi. Interestingly, the infection using 0.007% infectious particles showed a delayed increase in the infected cell population with only 24.4% of the cells being infected 16 hpi, and a maximum of 71.7% infected cells 24 hpi. Also, the cells detached later (Figure 4-14b). In parallel to the increase of the concentration of cells in the supernatant the apoptotic infected cell population increased, but stayed relatively low for all tested samples with a maximum of 17.5% at 24 hpi.

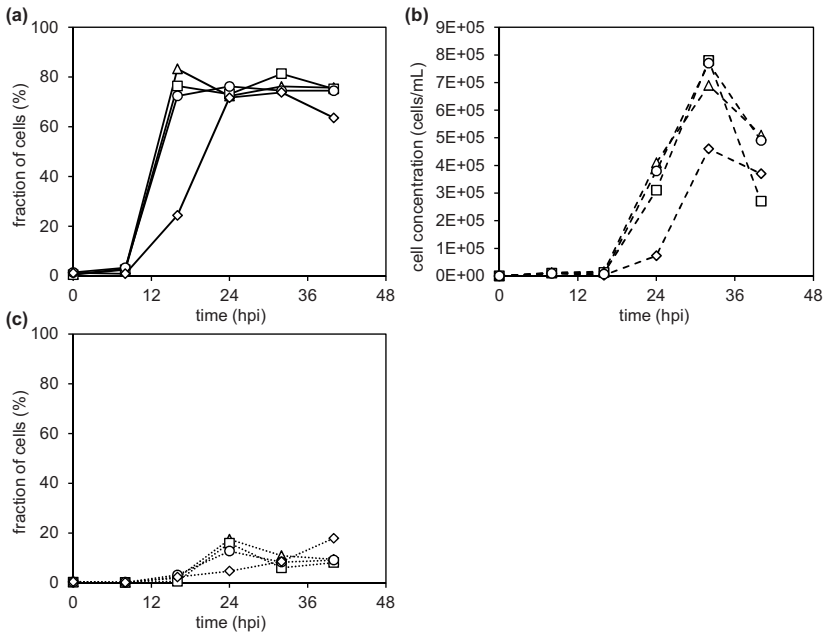

Figure 4-14 Analysis of (a) infection status and (c) apoptosis induction with flow cytometry as well as (b) supernatant cell concentration of infections of adherent MDCK cells with influenza A/PR/8 RKI seed virus containing different proportions of infectious particles: 7% (triangles), 0.7% (squares), 0.07% (circles), and 0.007% (diamonds).

4.4.2 Comparison of different influenza A/PR/8 seed viruses

As working virus banks have to be prepared every few years, there do exist several in-house A/PR/8 NIBSC seed virus preparations with different proportions of infectious particles. Four A/PR/8 NIBSC seed viruses, listed in Table 4-4, with $TCID_{50}$ ranging from 5.43 x 10^6 IVP/mL to 1 x 10^9 IVP/mL, corresponding to 0.2% to 21.3% infectious virus particles, were directly compared in the experiments described below. With these strains

infections at MOI 1 were performed in adherent MDCK cells in GMEM grown for one day in petri dishes.

Table 4-4 List of influenza A/PR/8 NIBSC seed virus preparations including $TCID_{50}$, HA titre, and proportion of infectious virions.

Date of preparation	$TCID_{50}$ (IVP/mL)	HA titre (log_{10} HAU/100 µL)	% infectious virions
16.07.2009	5.43×10^6	2.10	0.22
06.11.2007	6.32×10^6	2.08	0.26
17.02.2010	9.20×10^8	2.80	7.29
02.03.2011[a]	1.00×10^9	2.37	21.33

[a] prepared from the 6.32×10^6 IVP/mL seed virus through low MOI passage by C. Seitz

Due to the large volume of seed virus added in infections with low $TCID_{50}$ seed viruses, already 0 hpi a HA titre was detectable (Figure 4-15a). Final titres differed by at least 0.4 log_{10} HAU/100 µL between low and high $TCID_{50}$ seed virus infections, which is a difference slightly larger than the error of the method. $TCID_{50}$ time courses show extreme differences between low and high $TCID_{50}$ seed viruses. While for high $TCID_{50}$ preparations maximum $TCID_{50}$ of 2×10^9 IVP/mL were reached, infections with low $TCID_{50}$ seed virus preparations showed declining $TCID_{50}$ time courses, which means that no infectious particles were released (Figure 4-15b).

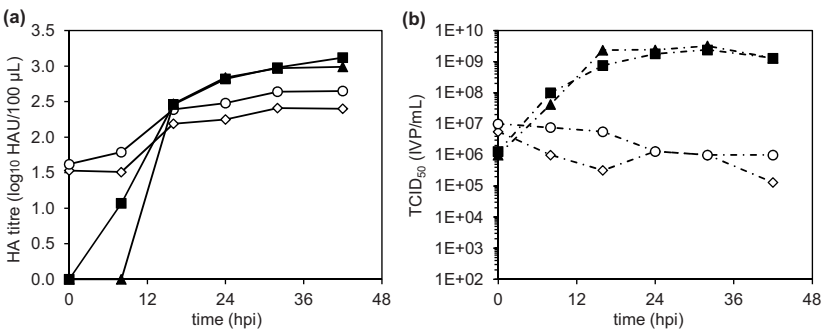

Figure 4-15 Comparison of different influenza A/PR/8 NIBSC high $TCID_{50}$ (1×10^9 IVP/mL triangles, 9.2×10^8 IVP/mL squares) and low $TCID_{50}$ (5.43×10^6 IVP/mL diamonds, 6.32×10^6 IVP/mL circles) seed virus preparations. Time courses of (a) HA titre and (b) $TCID_{50}$.

Flow cytometric analysis also showed the population of infected non-apoptotic cells to differ between low and high $TCID_{50}$ seed virus infections at 16 hpi and the second half of the infection (Figure 4-16a). Total cell concentration in the supernatant increased earlier and clearly stronger in low $TCID_{50}$ seed virus infections (Figure 4-16b). The decrease in

the proportion of infected non-apoptotic cells at 16 hpi in low $TCID_{50}$ seed virus infections corresponded to a by trend larger apoptotic infected cell population (Figure 4-16c).

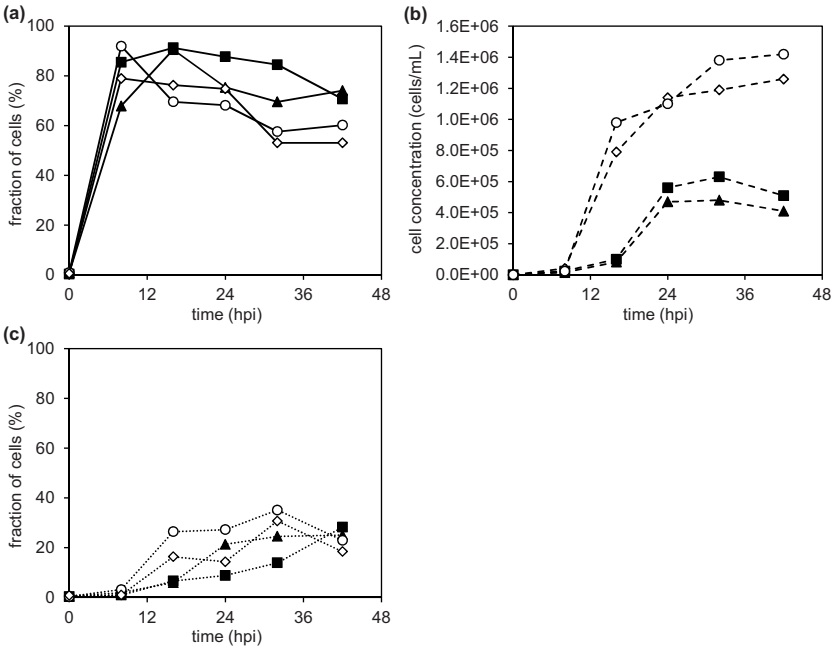

Figure 4-16 Comparison of different influenza A/PR/8 NIBSC seed virus preparations. Infections with high $TCID_{50}$ (1 x 10^9 IVP/mL triangle, 9.2 x 10^8 IVP/mL squares) and low $TCID_{50}$ (5.43 x 10^6 IVP/mL diamonds, 6.32 x 10^6 IVP/mL circles) seed strains were analysed for (a) fractions of infected cells, (b) total cell concentration in supernatant, and (c) apoptotic infected cells.

4.4.3 Discussion

Results from the T25-flask study shown in section 4.3.3 indicated that variations in infectious virus titres and seed virus performance are potentially influenced by DIPs. To further investigate this impact of DIPs on influenza virus replication in MDCK cells, seed virus preparations from the same virus strain containing different amounts of DIPs should be compared.

For this purpose, in a first attempt influenza virus A/PR/8 RKI seed virus preparations containing different proportions of infectious particles were generated through addition of temperature-inactivated seed virus. This resulted in seed viruses with 7%, 0.7%, 0.07%, and 0.007% infectious virus particles. In petri dish infections of adherent MDCK cells all of these four seed viruses reached similar final HA titres. However, due to the high 0 hpi

titre caused by the seed virus added at toi net virus production was much lower in the infection with the 0.007% seed virus. Except for the preparation with the lowest amount of infectious particles (0.007%) no differences in virus titre dynamics, NP accumulation, and apoptosis induction were detected. This low proportion of infectious virus particles could be under a threshold for reduction of virus propagation by DIPs. Samples of this infection experiment were also analysed for interferon (IFN)-β and Mx1 expression by C. Seitz. IFN expression did not differ much between the infections with the four A/PR/8 RKI preparations and also Mx1 expression was only increased at 24 hpi for the infection with the 0.007% seed virus.

These results indicate that the approach of adding temperature-inactivated seed virus to high $TCID_{50}$ seed virus was not successful in creating high amounts of DIP-containing seed viruses. Incubation of the seed virus at 37°C apparently resulted in formation of non-infectious particles other than DIPs. In literature there are several non-infectious biological active virus populations described (Marcus *et al.* 2009). However, little is known about their molecular function and how these particles induce different effects. The kind of particles produced in the presented heat-inactivated seed virus should be clarified in further studies. It was not in the scope of this work, as differentiation between the diverse populations of non-infectious biological active particles is methodically rather complex.

As high MOI conditions are described in literature to result in low infectious virus tires and based on the results from experiments with increasing MOI presented in section 4.3.3, it was tried to generate a high DIPs containing seed virus by high MOI passaging. This attempt performed in the bioprocess engineering group by N. Wynserski and T. Frensing, however, was not successful.

The second approach presented in the following used four different A/PR/8 NIBSC seed virus preparations with $TCID_{50}$ from 5.43×10^6 to 1.00×10^9 IVP/mL. In line with results for A/PR/8 NIBSC in T25-flasks (Figure 4-9f), in infections with the two low $TCID_{50}$ seed virus strains solely non-infectious particles were released. In contrast, in infections with the high $TCID_{50}$ A/PR/8 NIBSC seed virus strains $TCID_{50}$ of up to 3.2×10^9 IVP/mL were obtained. Final HA titres differed by at least 0.34 $\log_{10}$ HAU/100 µL between low and high $TCID_{50}$ seed virus infections, which means that at minimum twice the number of virus particles were released. Also percentage of infected cells differed between the seed viruses: infections with the high $TCID_{50}$ seed virus preparation resulted in higher proportions of infected cells in the second half of the infection. Both results indicated that the low $TCID_{50}$ seed virus is not able to perform a productive virus replication in the cell population. Virus-induced apoptosis also differed between the seed viruses, however, to a smaller extend.

Samples from above shown infections with low and high $TCID_{50}$ influenza A/PR/8 NIBSC seed virus (section 4.4.2) were analysed for expression of IFN-β and Mx1 by C. Seitz. Expression of both molecules was found to be higher in low $TCID_{50}$ seed virus infections compared to high $TCID_{50}$ seed virus infections: at 8 hpi Mx1 expression was increased 3.5–7.2-fold in low $TCID_{50}$ seed virus infections compared to high $TCID_{50}$ seed virus infections, IFN-β was stronger expressed by a factor of 6.5–14.9 (data not shown). This reflects a stronger antiviral host response by cells infected with the low $TCID_{50}$ seed viruses. This could be caused by the preferential binding of the cellular viral RNA sensor RIG-I to smaller influenza genome segments and subgenomic RNA (Baum *et al.* 2010). To some extend this stronger immune response could be responsible for the—by trend—higher apoptosis induction observed in low $TCID_{50}$ seed virus infections, as interferon expression is described to increase virus-induced apoptosis (Balachandran *et al.* 2000). Additionally, the low $TCID_{50}$ A/PR/8 NIBSC seed virus might also contain other kinds of biological active particles, e.g. niCKPs that influence the antiviral response and virus-induced apoptosis (Marcus *et al.* 2009).

A repetition of the second study with two of the four A/PR/8 NIBSC strains (the 5.43×10^6 and 1.29×10^9 IVP/mL virus preparations) was published by Frensing *et al.* (2014). They checked seed virus preparations for DIPs by analysing shorter gene segments, amplified by gene-specific polymerase chain reaction (PCR) and separated by gel electrophoresis. This showed that segments 1, 2, 3, and 6 of the 5.43×10^6 seed virus contained DIPs, determined as small fragments of approximately 400–700 base pair length. In contrast, the 1.29×10^9 IVP/mL virus preparation contained predominantly full-length segments and only small amounts of short PCR products. Interestingly, most deletions were identified in the polymerase-coding segments 1, 2, and 3 which is in line with descriptions of the polymerases-coding gene segments to be the most prevalently origin of DI RNAs (Davis and Nayak 1979; Saira *et al.* 2013). Furthermore, Frensing *et al.* (2014) confirmed the stronger interferon response induced by the low $TCID_{50}$ seed virus compared to the high $TCID_{50}$ seed virus. In addition to virus titre measurements and flow cytometric analysis of NP accumulation and apoptosis, RT-qPCR was performed for determination of viral mRNA, cRNA, and vRNA. They found vRNA synthesis, but not mRNA and cRNA synthesis, to be impeded by DI RNAs. Thus, DIPs influenced the second replication step (the synthesis of progeny vRNA) of the viral life cycle and had only a minor impact of on viral transcription and cRNA synthesis.

The impact of DIPs in a continuous influenza propagation process was investigated by Frensing *et al.* (2013). They showed DIPs to be responsible for virus titre fluctuations (HA and $TCID_{50}$) and fluctuations of the effective MOI in a continuous (17 day long) influenza propagation process using a two-step bioreactor set-up (one “cell bioreactor” and one “virus bioreactor”) using the duck-derived suspension cell line AGE1.CR. Even small

amounts of DIPs in the seed virus preparation rapidly accumulated and consequently affected virus yield. This demonstrated DIPs to be a challenge and a crucial factor to be considered for design and optimisation of efficient (continuous) influenza virus propagation processes.

Summing up, data presented in this section confirm the hypothesis stated in section 4.3.3 that DIPs are responsible for the low titres of infectious virions resulting from infections with low $TCID_{50}$ seed virus preparations. Furthermore, the importance of low MOI infection conditions to yield high infectious virus titres was underlined. Influenza vaccine production using cell culture should avoid DIPs formation and thus benefit from low MOI condition, which is indeed currently used by producers of cell culture-based influenza vaccine (Genzel *et al.* 2014a), as it leads to a robust and reliable production process. Special attendance should be given to seed viruses with low amounts of DIPs in order to ensure an efficient and high titre yielding infection. As the virus titre is often not tested during virus adaptation in vaccine strain generation, high MOI situations might occur favouring formation of DIPs. Also, it would be important to check older stored seed virus preparations for presence of DIPs by RT-PCR. Thereby, it could be decided if a low MOI passage should be performed in order to avoid or at least strongly reduce DIPs in the seed virus preparation. And as low MOI virus strain adaptation strategy is very laborious large lots of seed virus should be performed.

Concluding, results on MOI dependency in T25-flasks (section 4.3.3) and data presented in this section demonstrate the importance of seed virus composition and DIPs on total and infectious particle formation in cell culture-based influenza virus propagation. One low MOI passage was sufficient to increase seed virus $TCID_{50}$ and reduce the amount of DIPs in the seed virus.

4.5 Infection of adherent MDCK cells in dynamic cultivation systems

In this section results from infections of adherent MDCK cells with different influenza virus A strains in dynamic cultivations systems are shown. Different virus strains as well as different infection conditions should be compared. For this purpose, infection dynamics and virus-induced apoptosis were analysed with flow cytometry. HA and $TCID_{50}$ assay were used for determination of total and infectious virus titres, and extracellular metabolite concentration was measured with a BioProfile® Plus.

Results from infections of adherent MDCK cells in spinner flask (section 4.5.1) and stirred tank bioreactors (section 4.5.2) are shown. Bioreactors were infected with influenza

A/PR/8 RKI and NIBSC at MOI 0.025 as well with the HGR strains Wisconsin-like and Uruguay-like at MOI 0.025 and 0.05, respectively. In addition, cultivation and infection with influenza A/PR/8 RKI under serum-free conditions and at very low MOI 1 x 10^{-5} were performed. All results are discussed in section 4.5.3.

Data from low MOI infections in section 4.5.2 were also published as: "Peschel B, Frentzel S, Laske T, Genzel Y, Reichl U. 2013. Comparison of influenza virus yields and apoptosis-induction in an adherent and a suspension MDCK cell line. *Vaccine* **31**: 5693–5699". The infections with influenza A/PR/8 RKI in GMEM medium at MOI 0.025 as well as Wisconsin-like HGR at MOI 0.025 were part of the Bachelor thesis of Tanja Laske (Otto von Guericke University, Magdeburg).

4.5.1 Infections in spinner flask

Stirred cultivation systems are divided into controlled systems, i.e. bioreactors with controlled gassing and pH, and uncontrolled systems like most spinner flasks. In spinner flasks the only adjusted parameters are stirring and temperature. In contrast to bioreactors in spinner flasks gas exchange only takes place through membranes in the side caps that are in contact to the 5% CO_2 atmosphere of the incubator, and pH regulation takes place through the buffering capacity of the medium. Thus, especially oxygen supply, pH, and osmotic concentration differ for uncontrolled compared to controlled cultivation systems. In this section it should be investigated whether these differences have an influence on influenza virus infection dynamics and virus-induced apoptosis. For this purpose, spinner cultivation of adherent MDCK cells (grown in GMEM using 2 g/L microcarriers) and subsequent infection with influenza A/PR/8 RKI at MOI 0.025 was conducted with analysis of cell and extracellular metabolite concentration, infection dynamics, virus-induced apoptosis, and HA titre (Figure 4-17).

Two days after inoculation adherent cell concentration reached its plateau, due to confluence of cells on the microcarriers, probably accompanied by a switch to maintenance metabolism (Rehberg *et al.* 2013). Approximately 24 hpi adherent cell concentration started to decrease and total and viable cell concentration in the supernatant to increase (Figure 4-17a). Flow cytometric analysis of infection status and apoptosis showed 90% of the cells to be infected at 12 hpi with a declining tendency after 30 hpi (Figure 4-17b). Apoptosis induction started 24 hpi. Afterwards, a drop in the measured fraction of apoptotic cells was observed. This might be due to a poor sample treatment during sample taking thereby artificially increasing the apoptotic cell population or due to an insufficient paraformaldehyde fixation resulting in an insufficient TUNEL staining. Generally, the decrease in infected cells correlated with the increase in double positive cells, indicating that those infected cells underwent virus-induced apoptosis. Approximately 4 h after NP

positive cells were detectable, at 12 hpi, an HA titre of 1.39 $\log_{10}$ HAU/100 µL was measured, reaching a maximum of 3.30 $\log_{10}$ HAU/100 µL by the end of infection (Figure 4-17c). This corresponds to a cell-specific virus yield of 22261 virions/cell.

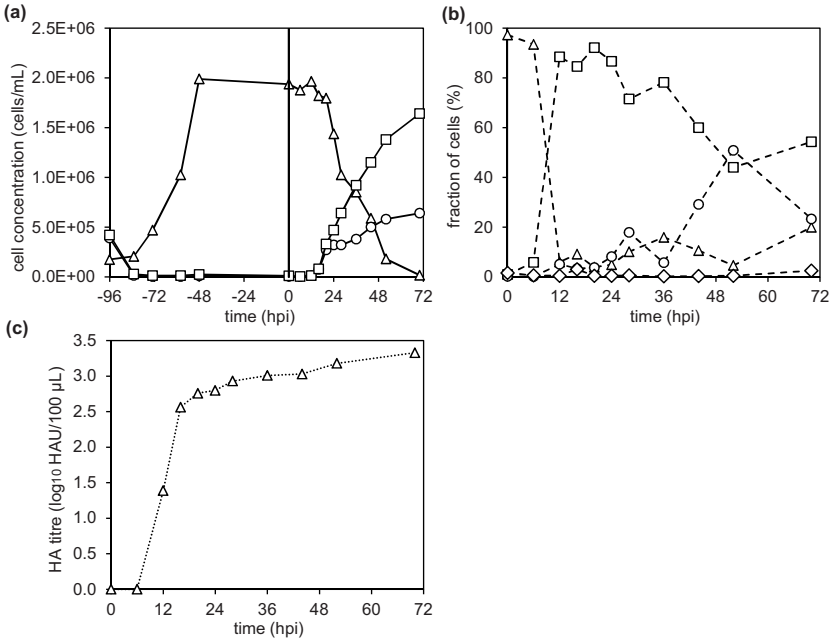

Figure 4-17 Spinner flask cultivation of adherent MDCK cells and subsequent infection with influenza A/PR/8 RKI at MOI 0.025. Analysis of (a) cell concentration, (b) infection status, and (c) HA titre: adherent cell concentration (a, triangles), total cell concentration in supernatant (a, squares), viable cells in supernatant (a, circles), uninfected cells (b, triangles), infected cells (b, squares), apoptotc infected cells (b, circles), and apoptotic uninfected cells (b, diamonds). Vertical line in (a) marks toi.

Quantification of extracellular metabolite concentration is shown in Figure 4-18. During 48 h prior to infection no measurements were performed. Thus, 48 hpi and 0 hpi sampling points were not connected in order to avoid wrong impressions of concentration time courses. Glucose was consumed during the infection phase from 29.3 mmol/L to 17.8 mmol/L, and lactate released to 27.9 mmol/L (Figure 4-18a). This corresponds to a yield coefficient of $Y'_{lac/gluc}$ = 2.43. Courses of ammonia and glutamine concentration in the supernatant behaved inverse, with ammonia being released up to 2.1 mmol/L, and glutamine being consumed to 0.7 mmol/L (Figure 4-18b). This corresponds to an ammonia yield coefficient from glutamine of $Y'_{NH4/gln}$ = 4.29. It is not clear whether the washing step did not completely remove the ammonia or during storage of the medium ammonia

formed through decomposition of glutamine. As seen in other infections of adherent MDCK cells (Genzel *et al.* 2004, 2005, 2006a; Ritter *et al.* 2010) glutamate is consumed during the first 12 hpi, and released after 33 hpi up to 0.46 mmol/L by the end of infection (Figure 4-18b). Generally, cells did not run into nutrient limitations, except for glutamate that was completely taken up temporarily. Importantly, Genzel *et al.* (2004) described lactate concentration of more than 8 mmol/L at toi to reduce HA titre by a factor of two in roller bottle infections. This critical level was exceeded 12 hpi (Figure 4-18a), thus, a negative impact of lactate on virus titre cannot be excluded.

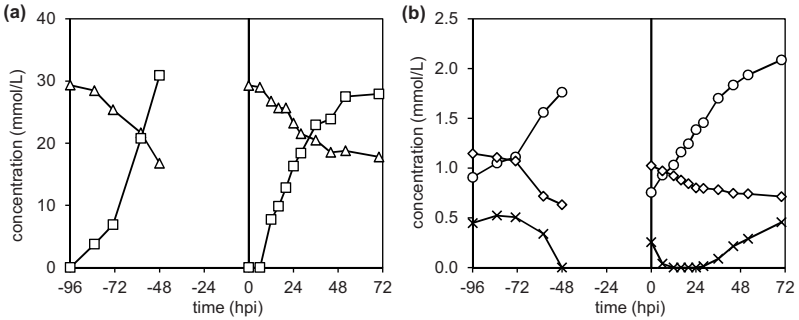

Figure 4-18 Analysis of extracellular metabolite concentration of a spinner flask cultivation of adherent MDCK cells infected with influenza A/PR/8 RKI at MOI 0.025. Analysed metabolite concentration: glucose (a, triangles), lactate (a, squares), ammonia (b, circles), glutamine (b, diamonds), and glutamate (b, crosses). Vertical lines indicate point of infection.

4.5.2 Infections in stirred tank bioreactors

Infection with influenza A/PR/8 RKI

The next step was to compare infection and apoptosis dynamics, virus titres, and metabolic profiles of the spinner infection to the dynamics and profiles in a controlled cultivation system. For this purpose, a 1 L stirred tank bioreactor cultivation with adherent MDCK cells infected with influenza virus A/PR/8 RKI at MOI 0.025 was performed (Figure 4-19). About 30 hpi adherent cell concentration started to decrease, with a parallel increase in total and viable cell concentration in the supernatant (Figure 4-19a). At 12 hpi HA titre increased, reaching up to 3.3 $\log_{10}$ HAU/100 µL at 72 hpi (Figure 4-19c). Cells expressing viral NP were detectable 4 h before HA titre increase. A maximum of 88% of the cells appeared infected non-apoptotic at 24 hpi. At this time point the apoptotic infected cell population also started to increase (Figure 4-19b, circles). $TCID_{50}$ showed its maximum of 1.33×10^9 IVP/mL at 28 hpi, which is rather late compared to the HA titre course (Figure 4-19c). In other standard infections the maximum $TCID_{50}$ was reached before the HA titre

had reached its plateau (Schulze-Horsel *et al.* 2009). Cell-specific yields were 29617 virions/cell and 917 IVP/cell.

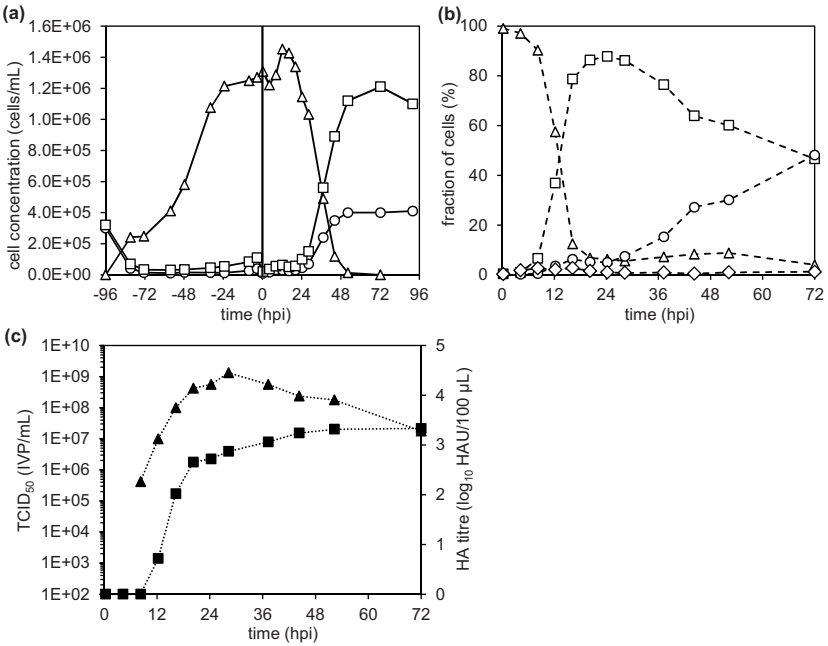

Figure 4-19 1 L stirred tank bioreactor cultivation of adherent MDCK cells and subsequent infection with influenza A/PR/8 RKI at MOI 0.025. Determination of (a) cell concentration: adherent (triangles), total (squares), and viable (circles) supernatant cells, (b) infection and apoptosis status: uninfected (triangles), infected (squares), apoptotic infected (circles), and apoptotic (diamonds) cell populations, (c) HA titre (squares), and $TCID_{50}$ (triangles). Vertical line in (a) indicates point of infection.

Analysis of extracellular metabolite concentration is shown in Figure 4-20. Glucose was consumed from 29.6 to 2.4 mmol/L, and lactate released up to 75 mmol/L ($Y'_{lac/gluc} = 2.79$) during the infection. Glutamine was consumed, and ammonia released into supernatant, with a yield coefficient $Y'_{NH4/gln} = 1.35$. As seen previously, glutamate concentration increased during the second half of the infection.

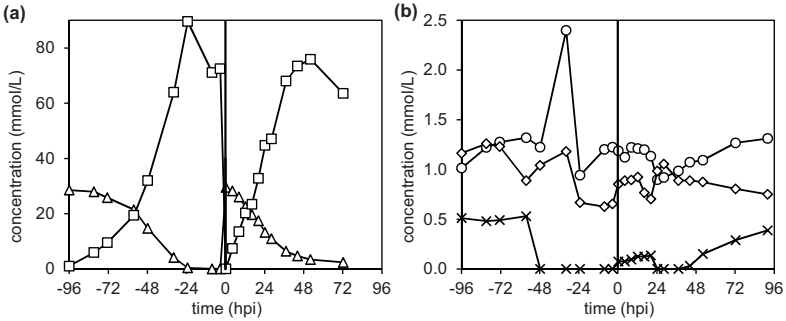

Figure 4-20 Courses of extracellular metabolite concentration in a stirred tank reactor cultivation of adherent MDCK cells infected with influenza A/PR/8 RKI at MOI 0.025. Concentration of glucose (a, triangles), lactate (a, squares), ammonia (b, circles), glutamine (b, diamonds), and glutamate (b, crosses). Vertical lines indicate point of infection.

Infection with influenza A/PR/8 NIBSC

In addition, the second in-house A/PR/8 strain from a different supplier—the influenza A/PR/8 from NIBSC—was investigated for infections of adherent MDCK cells. Earlier studies in STR had shown that A/PR/8 NIBSC infects cells faster than the A/PR/8 RKI but reaches much lower titres (Schulze-Horsel *et al.* 2009). To determine whether this difference between the seed viruses still holds true, a 1 L stirred tank cultivation of adherent MDCK cells infected with influenza A/PR/8 NIBSC at MOI 0.025 was performed (Figure 4-21).

Adherent cell concentration started to decrease at 24 hpi (Figure 4-21a), and thereby 6 h earlier than in A/PR/8 RKI bioreactor infection. Cell concentration in the supernatant increased with decreasing adherent cell concentration (Figure 4-21a). First HA titre was detectable 16 hpi (Figure 4-21b), and thus 4 h later than in the A/PR/8 RKI infection. The final HA titre of 2.7 $\log_{10}$ HAU/100 µL was clearly lower than the final titre obtained in the A/PR/8 RKI infection. Cell-specific virus yields were 9325 virions/cell. Flow cytometric analysis (Figure 4-21c) showed 10% of the cells to be infected already 4 hpi, as indicated by NP accumulation, reaching a maximum of 90% at 16 hpi. Flow cytometric determination of apoptosis induction showed a steady increase of apoptotic infected cells at 36 hpi.

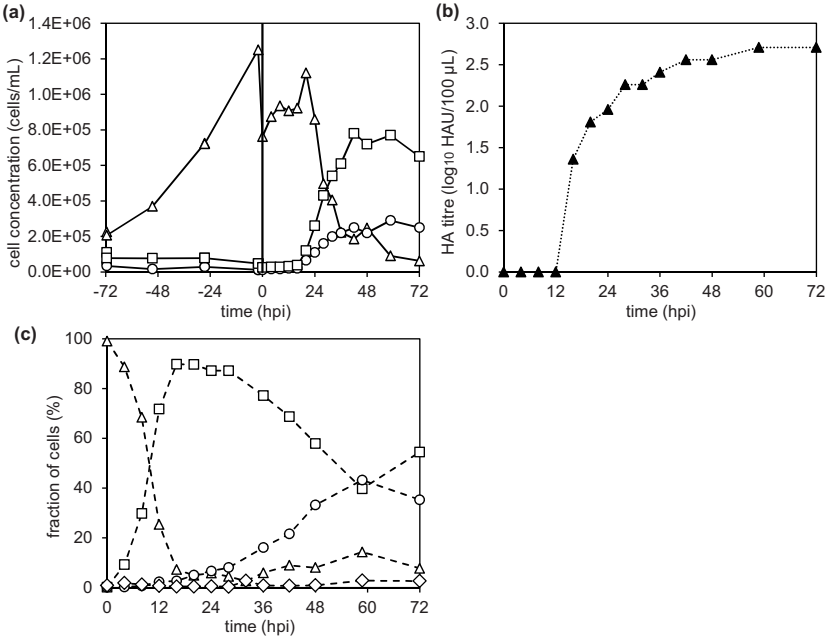

Figure 4-21 Stirred tank bioreactor cultivation of adherent MDCK cells subsequently infected with influenza A/PR/8 NIBSC at MOI 0.025. Determination of adherent cell concentration (a, triangles), total (a, squares) and viable (a, circles) cell concentration in supernatant, HA titre (b), and infected and apoptotic cell populations detected by flow cytometry (c): uninfected (triangles), infected (squares), apoptotic infected (circles), apoptotic (diamonds) cells. Vertical line in (a) indicates point of infection.

Infection with influenza A/Wisconsin/67/2007-like HGR

Another wide-spread influenza virus subtype besides H1N1 is H3N2. Therefore, a H3N2-like strain should also be characterised in terms of infection dynamics and apoptosis induction in bioreactor cultivations of adherent MDCK cells and compared to H1N1 infections. For this purpose, the influenza HGR strain A/Wisconsin/67/2007-like (containing an A/PR/8-backbone) was chosen. This strain was included in the 2007 seasonal influenza vaccine. A 1 L stirred tank bioreactor cultivation of adherent MDCK cells infected at MOI 0.025 showed a decrease in the adherent cell concentration with a parallel increase in the supernatant cell concentration at 12 hpi (Figure 4-22a). At the same time an HA titre of 1.9 $\log_{10}$ HAU/100 µL was detected, reaching its plateau of 3.05 $\log_{10}$ HAU/100 µL at 36 hpi (Figure 4-22c). This corresponds to a cell-specific virus yield of 11700 virions/cell. The $TCID_{50}$ showed its maximum of 7.5×10^8 IVP/mL at 20 hpi, staying on a high level up to 45 hpi (Figure 4-22c). This corresponds to a cell-specific yield of 417 IVP/cell. The flow cytometric detection of virus accumulation in the

cells started around 6 hpi, with a maximum of 80% infected non-apoptotic cells (Figure 4-22b). After this maximum the infected non-apoptotic cell population decreased in favour of the double positive infected apoptotic cell population. This population steadily increased up to 45% at 72 hpi.

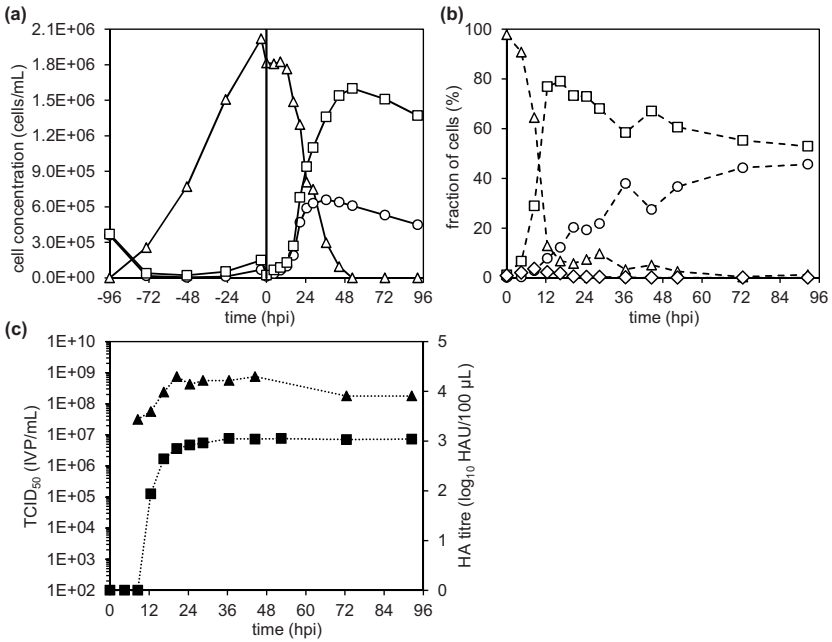

Figure 4-22 Adherent MDCK cells cultivated in a 1 L stirred tank bioreactor and infected with influenza A/Wisconsin/67/2007-like HGR (H3N2) at MOI 0.025. (a) cell concentration: adherent (triangles), total supernatant (squares), viable supernatant (circles); (b) flow cytometric determination of infection status and apoptosis induction: uninfected (triangles), infected (squares), apoptotic infected (circles), and apoptotic (diamonds) cell populations; (c) HA titre (squares) and $TCID_{50}$ (triangles). Vertical line in (a) indicates point of infection.

Profile of extracellular glucose concentration showed a complete consumption during 95 h of cell growth, with a corresponding increase in extracellular lactate up to 63 mmol/L (Figure 4-23a). After infection with influenza virus A glucose was consumed down to 8.5 mmol/L, with 50.5 mmol/L lactate being produced ($Y'_{lac/gluc}$ = 2.21). Until 72 hpi 2.3 mmol/L ammonia were released (Figure 4-23b). Glutamine was converted to ammonia to a final concentration of 0.53 mmol/L with a yield coefficient $Y'_{NH4/gln}$ of 2.60. Glutamate was consumed during cell growth, but released after 24 hpi up to 1.02 mmol/L (Figure 4-23b). At this time the HA titre reached its plateau and a significant apoptosis induction was detected compared to both A/PR/8 wild type strains.

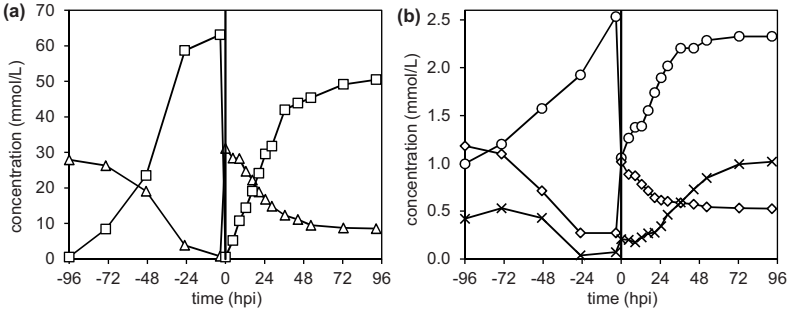

Figure 4-23 Extracellular metabolite concentration of adherent MDCK cells infected with influenza A/Wisconsin/67/2007-like HGR (H3N2). Analysis of concentration of glucose (a, triangles), lactate (a, squares), ammonia (b, circles), glutamine (b, diamonds), and glutamate (b, crosses). Vertical lines indicate point of infection.

Infection with influenza A/Uruguay/716/2007-like HGR

Another vaccine-relevant H3N2 strain is the Uruguay-like HGR, containing HA and NA from influenza virus A/Uruguay/716/2007 and the backbone from influenza virus A/PR/8. This strain was used for a 5 L cultivation of adherent MDCK cells with subsequent infection at MOI 0.05 (Figure 4-24 and Figure 4-25). Supernatant cell concentration started to increase at 24 hpi (Figure 4-24a). Already 8 hpi a HA titre of 1.6 $\log_{10}$ HAU/100 µL was detectable, finally reaching a maximum of 2.8 $\log_{10}$ HAU/100 µL (Figure 4-24c), corresponding to a cell-specific virus yield of 7464 virions/cell. The $TCID_{50}$ increased in parallel to the HA titre at 8 hpi. As the 0 hpi $TCID_{50}$ value was determined, the MOI adjustment could be checked: with 1.69 x 10^6 cells/mL at toi and MOI 0.05 the calculated 0 hpi $TCID_{50}$ value is 8.5 x 10^4 IVP/mL, which fits the measured 0 hpi value, and thus confirmed a good MOI adjustment. At 16 hpi a plateau in the infectious virus titre of 1.8 x 10^8 IVP/mL was reached that lasted up to 44 hpi (Figure 4-24c). With a maximum cell concentration of 1.73 x 10^6 cells/mL the cell-specific infectious virus yield was 104 IVP/cell. Already at 4 hpi 38% of the cells were infected, and the maximum of infection was reached 16 hpi with 95% infected non-apoptotic cells (Figure 4-24b). At 40 hpi 56% of the cells were apoptotic and infected. The metabolic profile shown in Figure 4-25 looked similar to earlier described profiles. It appears that concentrations determined at 20 and 24 hpi eventually overestimate concentration for some metabolites. This might be due to evaporated liquid, e.g. through not fully closed cap lids of sample vials during heating at 80°C. Up to 24 hpi glucose was consumed and lactate released by the cells ($Y'_{lac/gluc}$ = 2.30) (Figure 4-25a). Ammonia was released continuously by the cells (Figure 4-25b). Glutamate behaved inversely to ammonia, however, as the data points fluctuate a clear tendency is not determinable. Glutamine showed the earlier described decreasing

concentration in the first half of the infection, but increasing concentration at 20 hpi (Figure 4-25b).

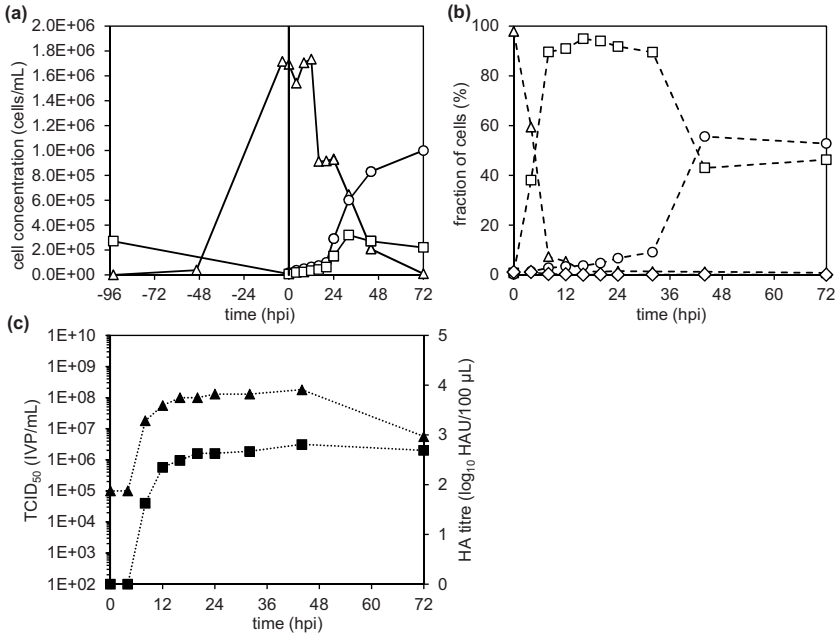

Figure 4-24 Infection of adherent MDCK cells with Uruguay-like HGR in a stirred tank bioreactor at MOI 0.05. Adherent cell concentration (a, triangles), total cell concentration supernatant (a, circles), viable cell concentration supernatant (a, squares); population of uninfected cells (b, triangles), infected cells (b, squares), apoptotic infected cells (b, circles), apoptotic cells (b, diamonds); time courses of HA titre (c, squares) and $TCID_{50}$ (c, triangles). Vertical line in (a) indicates point of infection.

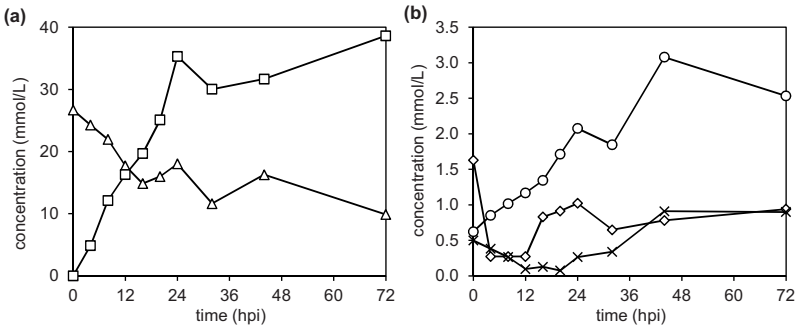

Figure 4-25 Extracellular metabolite concentration of influenza Uruguay-like HGR-infected MDCK cells (stirred tank bioreactor, MOI 0.05): glucose (a, triangles), lactate (a, squares), ammonia (b, circles), glutamine (b, diamonds), and glutamate (b, crosses).

Infection at MOI 1 x 10^{-5}

Previous shown infections were performed at an intermediate MOI of 0.025, which is the internal "standard MOI" in the bioprocess engineering group. However, industrial influenza vaccine production using cell culture for virus propagation uses MOIs as low as 1 x 10^{-5}–1 x 10^{-8} (Genzel *et al.* 2014a). Also T25-flask experiments showed very low MOI to be very attractive (section 4.3.3). Thus, in the next step, the influence of a drastic reduction of the MOI on infection dynamics and virus-induced apoptosis in stirred tank bioreactor systems should be investigated. As an example A/PR/8 RKI was used for infection of adherent MDCK cells in GMEM medium at MOI 1 x 10^{-5} in a 1 L stirred tank bioreactor. As these infections were performed three times (in three completely independent experiments), in Figure 4-26 median ± MAD of time courses of HA titre, $TCID_{50}$, and flow cytometric evaluation of infection status and apoptosis induction are shown. For courses of cell concentration median ± MAD are not plotted because of variations in the starting concentration, instead, all three single runs are shown.

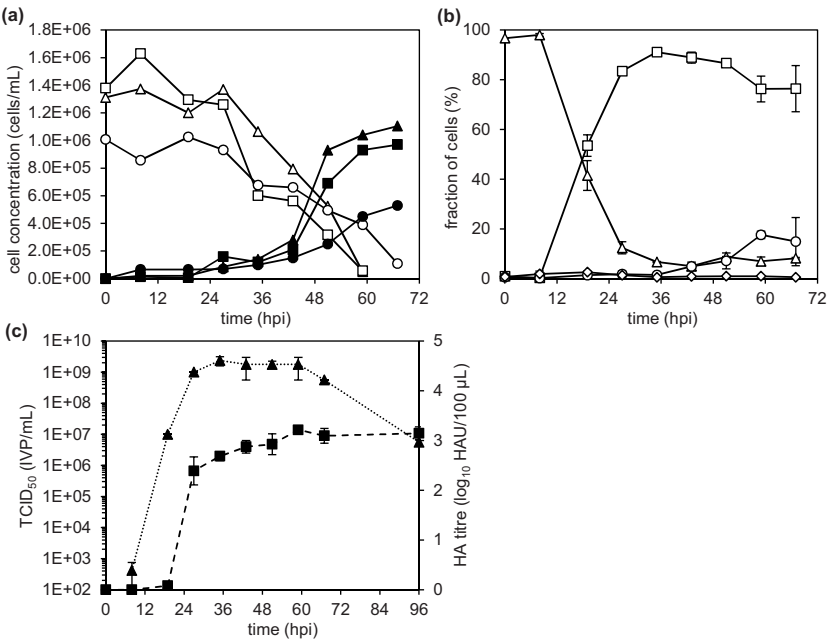

Figure 4-26 Cultivation of MDCK cells in GMEM medium in a stirred tank bioreactor and infected with influenza A/PR/8 RKI at MOI 1 x 10^{-5} (n = 3). (a) adherent (open symbols) and total (filled symbols) cell concentration in supernatant; (b) flow cytometric determination of uninfected cells (triangles), infected cells (squares), apoptotic infected (circles), and apoptotic uninfected (diamonds) cells; (c) $TCID_{50}$ and HA titre. Median ± MAD are shown for cytometric evaluation of cell populations as well as for HA titre and $TCID_{50}$.

Adherent cell concentration showed a decrease starting at 30 hpi in all three cultivations, with a corresponding increase in the supernatant cell concentration (Figure 4-26a). At that time point the maximum percentage of the infected non-apoptotic cell population was reached (91%) (Figure 4-26b). The infected non-apoptotic cell population stayed at a level above 76% until 67 hpi. Apoptosis induction appeared late at 60 hpi and only to a maximum around 20%. HA titres were above 2 $\log_{10}$ HAU/100 µL 24 hpi, and increased up to 3.15 ± 0.13 $\log_{10}$ HAU/100 µL (median ± MAD) (Figure 4-26c). $TCID_{50}$ reached its maximum of 2.37 x 10^9 IVP/mL at 36 hpi. The corresponding cell-specific virus yields were 22891 ± 2747 virions/cell and 2887 ± 1217 IVP/cell (median ± MAD).

Analysis of metabolite concentration was performed for one of the three performed experiments (represented in Figure 4-26a as circles) and is shown in Figure 4-27. Glucose was consumed during the infection from 25.1 to 14.9 mmol/L, while lactate was released up to 23.3 mmol/L at 96 hpi (Figure 4-27a), corresponding to a yield coefficient $Y'_{lac/gluc}$ of 2.27. Glutamate was taken up by the cells during the first 20 hpi, but released again at 60 hpi (Figure 4-27b). This glutamate release corresponded to apoptosis induction and the HA titre reaching its plateau. Ammonia was continuously released during the infection up to 2.35 mmol/L, glutamine consumed from 1.58 to 1.05 mmol/L ($Y'_{NH4/gln}$ = 3.44) (Figure 4-27b).

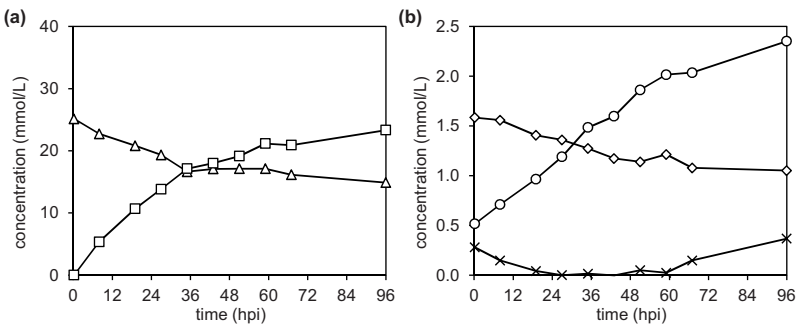

Figure 4-27 Extracellular metabolite concentration of a MOI 1 x 10^{-5} infection of adherent MDCK cells in GMEM with influenza A/PR/8 RKI in a stirred tank bioreactor. Shown are glucose (a, triangles), lactate (a, squares), ammonia (b, circles), glutamine (b, diamonds), and glutamate (b, crosses) concentration.

Infection under serum-free conditions

Influenza virus propagation using adherent cells requires washing steps when changing from serum-containing to serum-free medium, because the protease trypsin is added with the seed virus. Furthermore, spent medium and remaining serum are removed through this washing step. However, those washing steps are laborious, time consuming, and bear the

risk of contamination. Besides, production processes using mammalian cell culture seek to omit animal components to reduce risks of contaminations (like prions) and increase batch-to-batch reproducibility. Serum-free media, like EpiSerf (by Gibco®) are available which can also be used to cultivate adherent MDCK cells, enabling a production process without medium exchange and washing steps. However, in a direct infection spent medium and potential inhibitory molecules are not removed. To investigate if the omitting of a washing step influences infection dynamics and virus-induced apoptosis, adherent MDCK cells were directly infected after the cell growth phase. For this purpose, a 5 L stirred tank cultivation with serum-free grown MDCK cells was infected directly (without medium exchange) only by addition of trypsin, glucose, and A/PR/8 RKI seed virus at MOI 0.025 at toi (Figure 4-28).

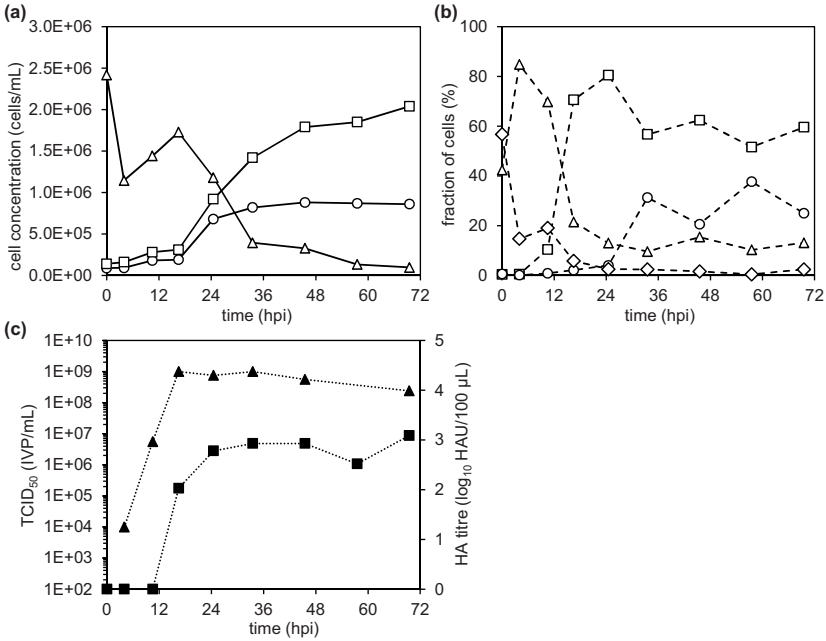

Figure 4-28 Adherent MDCK cells grown in serum-free EpiSerf medium in a stirred tank bioreactor infected without a medium exchange with influenza A/PR/8 RKI at MOI 0.025. Adherent cell concentration (a, triangles), total cells in supernatant (a, squares), viable cells in supernatant, populations of uninfected (b, triangles), infected (b, squares), apoptotic infected (b, circles), and apoptotic uninfected (b, diamonds) cells; time courses of HA titre (c, squares) and $TCID_{50}$ (triangles).

Cell concentration in the supernatant started to increase 16 hpi, with a corresponding decrease in the adherent cell concentration (Figure 4-28a). Also, 16 hpi an HA titre of 2.03 log_{10} HAU/100 µL was detected, ending in a final titre of 3.09 log_{10} HAU/100 µL at

72 hpi (Figure 4-28c). $TCID_{50}$ showed a strong increase already 4 hpi (Figure 4-28c), and thereby earlier than the increase in HA titre. A maximum of 1 x 10^9 IVP/mL was reached 16 hpi, at that time point the HA titre was still increasing. Cell-specific production was 14223 virions/cell and 578 IVP/cell, respectively.

Results from flow cytometric analysis of infection and apoptosis are plotted in Figure 4-28b. Especially in the beginning of infection the apoptotic uninfected population made up more than the half of the present cells (56.7%), while in infections with a medium exchange this population never exceeded 4%. Importantly, within 15 hpi this population decreased down to less than 10%, presumably due to cell lysis or infection of already apoptotic cells. Surprisingly, measurements of supernatant cell concentration did not show an increased concentration of dead cells shortly after infection. Proportion of infected cells reached its maximum of 80.5% at 24 hpi. At 33 hpi a significant proportion of the cells appeared apoptotic and infected, corresponding again to the HA titre reaching its plateau.

4.5.3 Discussion

Four different influenza virus A strains, A/PR/8 RKI, A/PR/8 NIBSC, Wisconsin-like HGR, and Uruguay-like HGR, were characterised regarding infection dynamics, apoptosis induction, total and infectious virus titres, and concentration of five extracellular metabolites, namely glucose, lactate, glutamate, glutamine, and ammonia. Furthermore, for A/PR/8 RKI, a direct infection without medium exchange was investigated as well as an infection in a spinner flask and at very low MOI. An overview of all performed stirred tank cultivations including infection conditions, maximum virus titres, and cell-specific yields is given in Table 4-5.

Comparison of influenza A/PR/8 RKI to A/PR/8 NIBSC

The first comparison of A/PR/8 RKI to A/PR/8 NIBSC was motivated by differences earlier observed in infection dynamics and final virus titres (Schulze-Horsel *et al.* 2009). Influenza A/PR/8 NIBSC showed a faster infection of the cells by approximately 8 h, and virus titres up to 1 $\log_{10}$ HAU/100 µL lower compared to infection at the same MOI with A/PR/8 RKI. These observations were very surprising at this point, as the seed virus strain should be the same only derived by two different suppliers.

The stirred tank infections with influenza A/PR/8 RKI and A/PR/8 NIBSC performed in this work showed a reduced time delay in the onset of infection determined, with the A/PR/8 NIBSC being not as fast as described in earlier studies; only approx. 4 h faster than the A/PR/8 RKI (Figure 4-29a), which is not significant taking into account biological variations of bioreactor experiments. Interestingly, HA titre increased simultaneously in

infections with both A/PR/8 strains. In addition, compared to previous studies with influenza A/PR/8 NIBSC, the final HA titres were increased by 0.2 $\log_{10}$ HAU/100 µL now yielding a maximum HA titre of 2.7 $\log_{10}$ HAU/100 µL. Correspondingly, cell-specific virus yields were increased, yielding more than 9000 virions/cell, compared to earlier reported 3000–4000 virions/cell (Schulze-Horsel *et al.* 2009). This is still lower than yields of 29000 virions/cell in A/PR/8 RKI infection, but a clear increase compared to earlier studies. Thus, although A/PR/8 NIBSC spread faster in the cell population and had a longer time window from NP accumulation to the first detectable increase in HA titre, virus titres and cell-specific yields were lower than in A/PR/8 RKI infections.

The reason for this changed behaviour of A/PR/8 NIBSC is most likely due to a different lot of seed virus used for infection compared to experiments by Schulze-Horsel *et al.* (2009). Only a limited volume of seed virus is generated during working bank preparation, and every few years original seed virus from the supplier is used to prepare a new virus working bank. Unfortunately, those infections for seed virus preparations are performed with standard volumes and harvest at eventually different time points, resulting in undefined infection conditions (such as potential high MOI) during seed virus propagation. Furthermore, it is not possible to use infectious virus titres for determination of the best harvest time point, as only the HA assay gives results within few hours. All of this finally results in significant lot to lot variations and different seed virus qualities between virus working banks. This becomes apparent when comparing $TCID_{50}$ and HA titres of the seed virus lots from the same master banks in the bioprocess engineering group. A/PR/8 NIBSC seed viruses used in former studies had different $TCID_{50}$ and different ratios of infectious virus particles to total virus particles. A/PR/8 RKI seed virus preparations used in the last years did not differ much in $TCID_{50}$, however, as the non-infectious virus population in the seed virus aliquots has not been determined, no clear conclusion can be drawn. Still, the different seed virus composition is most likely the reason for here observed different behaviour of the A/PR/8 NIBSC and emphasises the need for controlled low MOI seed virus generation procedures to minimise lot to lot differences and to draw valid conclusions on the impact of other cultivation parameters modified. Consequently, when comparing different infection conditions (such as vessel or MOI) it is of utmost importance to use identical lots of seed virus. Otherwise, potential observed differences might be caused by seed virus quality and not be due to the changed culture conditions. Consequently, for all infections shown in this work, the same lot of seed viruses were used (if possible) for all virus strains investigated.

Table 4-5 Overview of performed stirred tank cultivations with adherent MDCK cells: virus strain, MOI, cultivation vessel, medium, maximum HA titre, maximum $TCID_{50}$, total cell-specific yield (ratio HA titre to maximum cell concentration), infectious cell-specific virus yield (ratio maximum $TCID_{50}$ to maximum cell concentration), and percentage infectious virions produced.

Virus strain	MOI	Vessel	Medium	Maximum HA titre (log_{10}HAU/100µL)	Maximum $TCID_{50}$ (IVP/mL)	Cell-specific yield (virions/cell)	Cell-specific inf. yield (IVP/cell)	% infectious virions
A/PR/8 RKI	0.025	Stirred tank	GMEM	3.33	1.33×10^9	29617	917	3.1
A/PR/8 NIBSC	0.025	Stirred tank	GMEM	2.71	n.a.	9158	n.a.	n.a.
Wisconsin-like HGR	0.025	Stirred tank	GMEM	3.05	7.50×10^8	11700	417	3.1
Uruguay-like HGR	0.05	Stirred tank	GMEM	2.81	1.80×10^8	7552	104	1.4
A/PR/8 RKI	0.00001	Stirred tank	GMEM	3.28	2.37×10^9	22891	2887	12.6
A/PR/8 RKI	0.025	Spinner	GMEM	3.33	n.a.	20800	n.a.	n.a.
A/PR/8 RKI	0.025	Stirred tank	EpiSerf	3.09	1.00×10^9	14223	578	4.1

Analysis of the genetic differences between A/PR/8 RKI and NIBSC was also performed. Rödig *et al.* (2011) published results from pyrosequencing analyses of the HA-coding gene segment 4, revealing that the A/PR/8 RKI seed virus preparation was very homogeneous. In contrast, the A/PR/8 NIBSC seed virus preparation comprised several quasispecies, some possibly linked to the lower virus yield obtained.

Influenza high growth reassortants compared to wild type A/PR/8

For seasonal influenza vaccine production not wild type but HGR influenza virus strains are used. Thus, it was interesting to compare vaccine relevant reassortants to A/PR/8 wild type strains in stirred tank bioreactor infections.

Infections of MDCK cells with the Wisconsin-like HGR showed infection dynamics comparable to A/PR/8 NIBSC infections. The Uruguay-like HGR was even faster, with 8 hpi having 90% of the cells infected (Figure 4-29a). Thus, bioreactor cultivations of the two HGR strains and the two A/PR/8 variants showed similar tendencies as low MOI infections in T25-flask, with the A/PR/8 RKI showing the latest progress of infection and the Uruguay-like HGR infecting very fast (Figure 4-11). The differences in infection dynamics are very remarkable since the gene segments coding for the polymerases, and thus for the main determinants of replication speed, should be identical between all four strains. Thus, steps like virus attachment, incorporation, release into cytoplasm, and entering the nucleus that also affect onset of virus replication and that are influenced by HA and NA might be reasons for differences between the A/PR/8 wild type and A/PR/8-based HGR strains. Plant *et al.* (2012) described mutations in influenza PB1 gene to influence growth kinetics of reassorted H3N2 strains containing an A/PR/8 backbone. Reasons for observed differences in infection dynamics could be elucidated by genetic analyses clarifying the molecular differences between the virus strains or microscopic analyses of virus attachment and internalisation dynamics.

Apoptosis induction appeared somewhat increased for the HGR strains in comparison to the A/PR/8 wild type strains (Figure 4-29b). Mohsin *et al.* (2002) described (H3/H2)N2 influenza virus strains to induce higher levels of apoptosis than (H1/Hsw1)N1 strains. They compared apoptosis induction in adherent MDCK cells infected with seven N2 and four N1 strains and emphasised the role of NA for this process. However, they analysed only one time point, thereby not revealing infection dynamics and possible differences in apoptosis dynamics. In addition, they tested only one MOI, and results of T25-flask experiments in this work demonstrated an additional influence of MOI on apoptosis induction. Additionally, in a later work they failed to modify apoptosis induction of influenza strains by inserting NA genes of high apoptosis inducing strains into low

apoptosis inducing strains and vice versa. This demonstrated the role of NA for apoptosis induction to be limited (Morris *et al.* 2005).

A comparison of HA and $TCID_{50}$ time courses is shown in Figure 4-29c and d. All final HA titres ranged between 2.71 and 3.33 $\log_{10}$ HAU/100 µL (Table 4-5), which demonstrates again adherent MDCK cells to be suitable for propagation of a wide range of influenza virus strains to high HA titres. Interestingly, final HA titres were higher for all tested strains in bioreactor infections than in T25-flask infections. This is presumably caused by the higher maximum percentage of infected cells: between 5.3% and 24.8% more infected non-apoptotic cells were reached in infections in stirred tank bioreactors compared to T25-flasks. This tendency was already visible in the data shown in Figure 4-5.

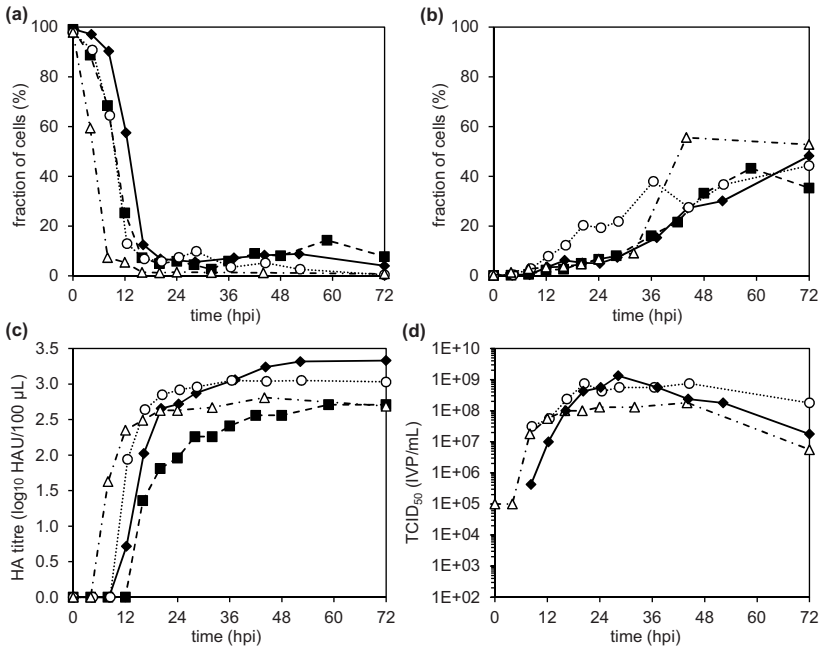

Figure 4-29 Stirred tank cultivations of MDCK cells infected with influenza A/PR/8 RKI (diamonds), A/PR/8 NIBSC (squares), Uruguay-like HGR (triangles), and Wisconsin-like HGR (circles) at MOI 0.025 (Uruguay-like HGR: MOI 0.05). (a) fraction of uninfected non-apoptotic cells; (b) fraction of apoptotic infected cells; (c) HA titre time courses; (d) $TCID_{50}$ time courses.

$TCID_{50}$ increased similar between all strains and reached maxima between 1.3 x 10^8 and 2.4 x 10^9 IVP/mL, which is in the same range as maximum $TCID_{50}$ obtained in low MOI infections in T25-flasks. In A/PR/8 RKI infections the highest $TCID_{50}$ was measured,

while in Uruguay-like HGR infections the lowest maximum $TCID_{50}$ was detected. The only study describing cell culture propagation of Uruguay-like HGR were performed in a MDCK suspension cell line (MDCK-*siat7e*) at MOI 0.01, in which maximum infectious titres of 8 $\log_{10}$ $TCID_{50}$/ml (= 1 x 10^8 IVP/mL) were described (Chu *et al.* 2010). Overall, high $TCID_{50}$ were obtained in STR infections with all four tested virus strains.

Effect of low MOI for infections in stirred tank bioreactors

Established industrial cell culture-based influenza vaccine production processes use very low MOI (Genzel *et al.* 2014a). Results from T25-flask infections and studies on DIPs performed here also demonstrated a beneficial effect of low MOI (section 4.3 and 4.4). For these reasons, the influence of lowering the MOI from 0.025 down to 1 x 10^{-5} for stirred tank bioreactor cultivations of adherent MDCK cells was investigated. Through this lower virus concentration at toi the onset of infection was about 10 h later than in MOI 0.025 infections (Figure 4-30a). Importantly, at 36 hpi the percentage of infected non-apoptotic cells was highest in this low MOI infection compared to all MOI 0.025 infections with influenza A/PR/8 RKI. This corresponded to a later and slower increase of the apoptotic infected cell population (Figure 4-30b). Nevertheless, maximum HA titres were very similar between MOI 1 x 10^{-5} and MOI 0.025 infections. Comparing time courses of HA titres and point of maximum $TCID_{50}$ it seemed that at standard MOI maximum $TCID_{50}$ was reached comparatively late. Eventually, the low MOI results in an earlier release of infectious virus particles compared to the release of non-infectious virus particles in here presented stirred tank infections. Importantly, maximum $TCID_{50}$ was higher compared to MOI 0.025 infection, as was cell-specific yield. The highest cell-specific virus yield in terms of total virus particles released was obtained in infections with influenza A/PR/8 RKI under all tested conditions compared to A/PR/8 NIBSC, Uruguay-like HGR, or Wisconsin-like HGR (Table 4-5). And also the highest infectious cell-specific yield of all performed stirred tank infections was obtained in the low MOI infections with influenza A/PR/8 RKI: 12.6% infectious virus particles were obtained, which is a factor 4 higher than at MOI 0.025. This result matches observations in T25-flask infections at different MOIs in which increased proportions of infectious virus particles were released at very low MOI. Thus, results obtained in T25-flasks could be confirmed for stirred tank systems and further support the hypotheses on the role of DIPs in influenza virus propagation.

In comparison to standard MOI infections, low MOI infections revealed not only a later release of infectious particles, but also a more constant infectious virus titre (a later decrease). This indicates that under low MOI conditions infectious virus particles are released for a longer time period, while in higher MOI infections more non-infectious particles are released, especially later in infection. Again, this demonstrates the importance

of low MOI infections for seed virus generation and LAIV production, both aiming at harvesting at time points with high proportions of infectious particles.

Influence of direct infection without medium exchange

Direct infection of adherent MDCK cells in serum-free EpiSerf medium showed infection dynamics in terms of HA titre and populations of infected cells determined with flow cytometry not to be significantly slower compared to infection with a medium exchange (Figure 4-30a, c). A difference in this direct infection is the presence of an apoptotic uninfected cell population in the beginning of the infection, reflecting a lower viability of the culture. Interestingly, 24 hpi this population disappeared, presumably due to secondary necrosis (lysis of the cells) or infection of apoptotic cells. Final HA titre was comparable to infection with medium exchange (3.09 $\log_{10}$ HAU/100 µL), and a high maximum $TCID_{50}$ of 1 x 10^9 IVP/mL was reached (Figure 4-30c, d). Thus, virus titres obtained with adherent MDCK cells under serum-free infection conditions were comparable to those obtained with cells grown in serum-containing medium. Also, flow cytometric characterisation of infection and apoptosis showed—despite the significant apoptotic non-infected cell population right after the infection—very similar profiles (Figure 4-30a, b). As metabolic profiles were not monitored in the serum-free infection experiment (Figure 4-28), it is unclear whether ammonia and lactate eventually reached critical levels.

Genzel *et al.* (2006a) also described similar yields for serum-containing and serum-free influenza virus propagation in 5 L stirred tank bioreactor infections of adherent MDCK cells in Ex-Cell® medium. Their infections with influenza A/PR/8 NIBSC at MOI 0.05 reached titres up to 2.9 $\log_{10}$ HAU/100 µL and cell-specific yields of approx. 12200 virions/cell. In a different study they obtained maximum HA titre of 3.3 $\log_{10}$ HAU/100 µL, corresponding to 33255 virions/cell, when infecting adherent MDCK cells in EpiSerf medium in a wave bioreactor with influenza A/PR/8 RKI at MOI 0.018 (Genzel *et al.* 2010). This is very similar to results for stirred tank infections of MDCK cells with influenza A/PR/8 RKI obtained in this work (Table 4-5).

Tree *et al.* (2001) reached higher titres under serum-free compared to serum-containing conditions when infecting adherent MDCK cells in roller bottles with influenza A/PR/8 at MOI 0.001. For MDCK cells grown in EpiSerf medium and infected in EpiSerf plus 5 µg/mL trypsin they reached 1 x 10^9 PFU/mL. When cells were grown in FCS supplemented DMEM and infected in virus maintenance medium containing 5 µg/mL trypsin only 7.9 x 10^7 PFU/mL were obtained. Liu *et al.* (2009) tested seven *ca* influenza virus strains for propagation in MDCK cells grown in serum-containing DMEM or serum-free MediV100 medium (a supplemented SF-DME/F12 medium). Four *ca* influenza virus A strains (A/New Caledonia/20/99, A/Panama/2007/99, A/Sydney/05/97, and

A/Texas/36/91) reached higher titres in serum-containing medium, while three *ca* influenza virus B strains (B/Brisbane/32/2002, B/Hong Kong/330/01, and B/Victoria/504/2000) reached higher titres in serum-free cultivated MDCK cells. Differences in titres were less than 0.6 $\log_{10}$ $TCID_{50}$/mL, except for influenza *ca* A/Texas/36/91 that reached 1.2 $\log_{10}$ $TCID_{50}$/mL higher titres in serum-containing compared to serum-free infection conditions.

Concluding, cultivation of adherent MDCK cells in serum-free media like EpiSerf is a good alternative to processes with serum-containing cell growth phases, enabling a completely serum-free, facilitated process with no need for washing of microcarriers and medium exchange, still yielding almost unchanged infection dynamics and acceptable yields. Indeed, as for human vaccine manufacturing regulatory authorities require omitting of serum, serum-free production processes for influenza virus propagation were established (Genzel *et al.* 2014a).

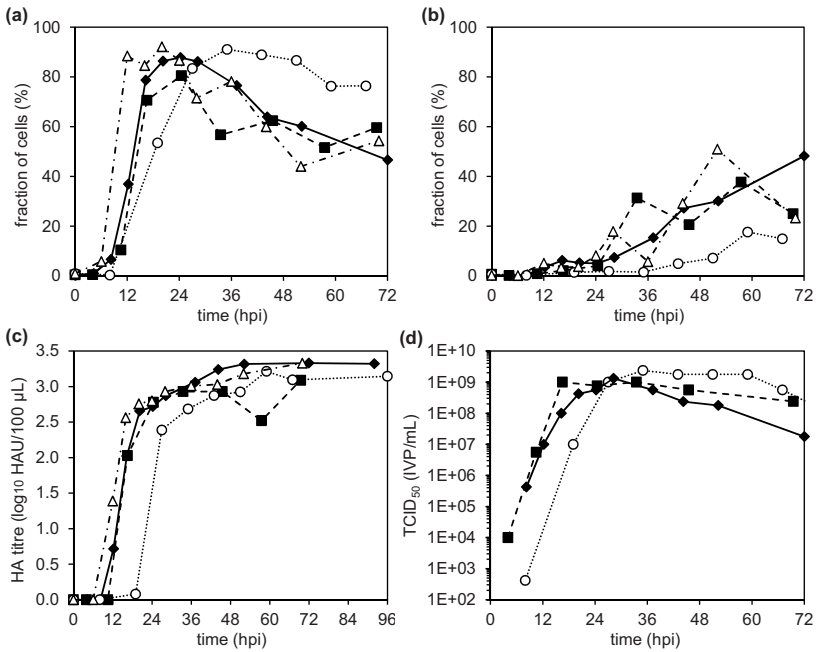

Figure 4-30 Comparison of A/PR/8 RKI infections of adherent MDCK cells in stirred systems performed under different conditions. Infection in spinner flask at MOI 0.025 (triangles); infection in stirred tank bioreactor at MOI 0.025 (diamonds); infection in bioreactor at MOI 1 x 10^{-5} (circles); direct infection in serum-free EpiSerf medium at MOI 0.025 (squares). Flow cytometric analysis of (a) infected non-apoptotic cells and (b) apoptotic infected cells; time courses of (c) HA titre and (d) $TCID_{50}$.

Spinner flask infection compared to stirred tank bioreactor infection

While in bioreactor systems many parameters such as pH and dissolved oxygen are controlled, in spinner flasks only temperature and stirrer speed are typically controlled. Oxygen and carbon dioxide are influenced through the atmosphere of the incubator and pH is kept in the physiologic range by the buffering capacity of the medium. Consequently, the not constant pH might have an influence on cell viability, apoptosis, and virus infection dynamics.

A direct comparison of spinner and bioreactor infection dynamics, virus-induced apoptosis, and HA titres is shown in Figure 4-30. Infection dynamics appeared very similar in both experiments; the slightly earlier increase of infected cells and HA titre in the spinner cultivation is in the range of biological variation. Also, maximum percentage of infected cells was very similar (88% and 92%). The apoptotic infected cell populations seemed also comparable. However, measured percentage of infected non-apoptotic and infected apoptotic cell populations in the spinner infection fluctuate. This was also seen in infections of adherent MDCK cells with influenza A/PR/8 RKI under serum-free conditions and STR infection with Wisconsin-like HGR. Reasons for those fluctuations are not clear, but are most likely a measuring artefact caused by sample taking, sample treatment, or measurement errors, as biological processes like apoptosis induction are irreversible and thus do not fluctuate within few hour intervals. Variations between percentage of infected and apoptotic infected cell populations were also observed by Schulze-Horsel *et al.* (2009) and also explained by misclassification. Importantly, TUNEL-fluorescence histograms of these fluctuating samples did not show abnormalities in the distribution shape (like multimodalities).

HA titre time courses increased almost simultaneously in spinner and STR infections and reached identical final titres of 3.33 $\log_{10}$ HAU/100 µL. While in the stirred tank cultivation pH was kept constant at 7.3, pH in spinner was influenced by lactate and glutamate release by the cells. Importantly, in the spinner infection pH ranged from 7.61 to 7.05 at 70 hpi (data not shown). Thus, pH stayed close enough to the optimal range of 7.2–7.4, and a negative effect on titre or cell viability was not detected. In contrast, a negative impact of a low pH value during influenza virus propagation was described by Genzel *et al.* (2006b, 2010). Adherent MDCK cells grown serum-free in Ex-Cell® medium in a Wave bioreactor system without pH control infected with equine influenza A/eq/Newmarket/1/93 at MOI 0.04 showed a drop in the pH below levels of 6.8, caused by lactate release and glutamate release of up to 2 mmol/L (Genzel *et al.* 2006b). This drop in pH was speculated to be responsible for a final titre of only 1.7 $\log_{10}$ HAU/100 µL. A drop in pH of below 6.4 was seen at the very end of infection in adherent MDCK cells cultivated in EpiSerf medium in uncontrolled wave bioreactor systems and infected with

influenza A/PR/8 RKI at MOI 0.018 (Genzel *et al.* 2010). Although this drop is stronger than the drop in pH observed in here performed uncontrolled infection, Genzel *et al.* (2010) reached a final titre of 3.3 $\log_{10}$ HAU/100 µL and high cell-specific yield, thus, this late drop in pH did not negatively affect virus titre.

Concluding, although low pH values can negatively affect influenza virus titres this is not the case for MDCK cells cultivated in GMEM in spinner flasks. Also infection dynamics and apoptosis induction did not seem to be influenced by the decreasing pH or headspace aeration. In the spinner cultivation, a plateau in cell concentration was reached during cell growth and infection was performed at a higher cell concentration at toi compared to the bioreactor cultivation, in which confluency probably had not been reached at toi. To a certain extent, these factors limit the comparability of the two cultivations as both factors potentially influence onset of infection.

Extracellular metabolite profiles

Comparing metabolic profiles, for cell growth (analysed in cultivations subsequently infected with A/PR/8 RKI and Wisconsin-like HGR) typical time courses were found: with glucose being consumed and lactate being released. In here presented cultivations, yield coefficients $Y'_{lac/gluc}$ of 2.3–2.5 were found, which is higher than earlier described yield coefficients (Genzel *et al.* 2004). As according to described metabolic pathways for MDCK cells two molecules lactate are formed per molecule glucose, corresponding to a maximum yield coefficient of 2. Reasons for here determined coefficients larger than 2 could be overestimation of lactate concentration, or that lactate formed by other pathways than reduction of glucose-derived pyruvate. The by-product ammonia was released during cell growth, while glutamine and glutamate were taken up by the cells or decomposed. With the medium exchange performed for infection of adherent MDCK cells, consumed glucose, glutamine, and glutamate were replenished and potential inhibitors like lactate and ammonia were removed. As no high MOI was used for infection, glucose was consumed during the early infection phase, and lactate and ammonia were released.

Importantly, glutamate profiles differed from that of other metabolites during infection: in the first hours after infection glutamate levels stayed constant or decreased, while in the second half of the infection cells released glutamate. Genzel *et al.* (2004) described this release to correlate with HA titre and speculate it to correspond to cell death and glutamate being released via permeabilised mitochondrial and cellular membranes. Here presented data additionally show this increase also to correlate with apoptosis induction, which would support the hypothesis of glutamate being released by dying cells. The uptake of glutamine correlated to the release of ammonia, as the latter is one product of glutamine

metabolism. The yield coefficients $Y'_{NH4/gln}$ for this conversion varied in here presented infections between 1.35 and 3.44.

Interpretation of glutamine to ammonia conversion is, however, difficult, as different pathways can be used by the cell for glutamine metabolism, only some of which result in ammonia formation. This, and the variations in the calculated values higher than 2, show that this yield coefficient is not very reliable. In addition, this could also indicate that pathways other than deamination of glutamine resulting in ammonia formation might play a role. For different infection experiments, though not exact values, but time courses of the determined metabolic concentration generally did not differ much. In literature, there are several critical concentrations described to have a negative impact on cell growth or virus propagation. For example, 20 mmol/L ammonia chloride are described to inhibit HA-mediated fusion with the endosomes (Morris *et al.* 1999; Jakeman *et al.* 1991), 8 mmol/L lactate at toi to negatively impact HA titre (Genzel *et al.* 2004), 7–10 mmol/L NH_4Cl to reduce cell growth by 50% (Glacken *et al.* 1986), and 5 mmol/L ammonium chloride in virus maintenance medium at toi to reduce influenza virus yields in MDCK cells (Genzel *et al.* 2005). In here presented cultivations, ammonia concentration were uncritical, however, lactate concentration exceeded in most infections critical values, thus, a negative effect on HA titre cannot be excluded.

Loss of productivity

The time point when an infected culture becomes unproductive is highly interesting for influenza virus propagation. The loss of productivity in this thesis is regarded as the end of release of virions due to dying of cells. In this context, apoptosis determined by a TUNEL assay was investigated, as late apoptotic cells are unlikely to release virions. Indeed, apoptosis induction determined by flow cytometry correlated to three measured indicators in cell culture infections with influenza virus, namely detached cell concentration, HA titre plateau, and glutamate release. Afterwards, the ratio of infected non-apoptotic to infected apoptotic cells as indicator to determine the time point when the cell culture becomes unproductive is introduced.

As dead cells detach from their growth surface, concentration of cells in the supernatant correlates to apoptotic infected cells detected by flow cytometry. Accordingly, in a separate analysis of adherent and detached cells in STR cultivations infected with influenza A/PR/8 NIBSC (MOI 0.025) apoptotic cells were almost solely found in the supernatant, but not attached to microcarriers (Isken *et al.* 2009). In T25-flasks increases of total cell concentration in supernatant and apoptotic infected cells were perfectly simultaneous (Figure 4-12), in STR systems it appeared that cell concentration in supernatant increased some hours before apoptotic infected cells were detected by flow cytometry. Apparently,

shear stress present in stirred systems but not in static cultivation systems led to an earlier detachment of dying cells from the growth surface. This is in agreement with the concept of dead adherent cells to detach from microcarriers (Schulze-Horsel *et al.* 2009; Isken *et al.* 2009).

Regarding the connection between apoptosis and HA titre, Schulze-Horsel *et al.* (2009) found induction of apoptosis to correlate to the HA titre reaching its plateau for three cultivations. This was interpreted as the end of the high productive virus release phase. For most of all (74%) of infection experiments with adherent MDCK cells presented in this work, apoptosis induction and HA titre reaching its plateau correlated very well. However, no correlation was found for the following infection experiments:

- T25-flask infections at MOI 3 with A/PR/8 RKI, A/PR/8 NIBSC, and Wisconsin-like HGR
- Spinner infection of adherent MDCK cells with A/PR/8 RKI at MOI 0.025
- STR infections with Uruguay-like HGR (MOI 0.05) and A/PR/8 RKI (MOI 1 x 10^{-5})

In T25-flasks correlation of HA titre plateau and apoptosis was given for low MOI infections, while for MOI 3 infections only Uruguay-like HGR fulfilled the correlation. Especially as A/PR/8 NIBSC and Wisconsin-like HGR at MOI 3 showed a strong and early apoptosis induction, the correlation between apoptosis and HA titre plateau was not observed. Furthermore, no correlation between apoptosis induction and HA titre plateau could be determined in spinner infection with influenza A/PR/8 RKI at MOI 0.025 because percentage of infected and infected apoptotic cells fluctuated. Interestingly, in STR infections with Uruguay-like HGR (MOI 0.05) and A/PR/8 RKI (MOI 1 x 10^{-5}) increase in apoptotic infected cells and HA titre did not correlate due to the very late apoptosis induction in those infections. Summing up, except for high MOI infections and spinner infection with fluctuating data points, the increase of apoptotic infected cells indicated that the HA titre is reaching its plateau or has reached its plateau (when apoptosis induction is very late). Thus, these data support that apoptotic cells do not productively release virions anymore (Schulze-Horsel *et al.* 2009).

Finally, correlation of glutamate release to apoptosis induction was analysed. It appeared that apoptotic infected cells detected by a flow cytometric TUNEL assay increased up to 10 h earlier than extracellular glutamate concentration. Thus, data show that the increase in extracellular glutamate observed later in infection is presumably caused by dead and lysed cells. However, glutamate release depends on the permeability of the cell membrane, and deviations in cell membrane permeability directly affect glutamate release.

Concluding, there is no general one single indicator for the end of the productive phase. For different cultivation conditions, different indicators should be applied to determine time point when productivity is lost.

As an additional indicator for the loss of productivity the ratio infected non-apoptotic to infected apoptotic cells (inf./apop.inf.) can be used. The time point when the ratio exceeds one indicates more apoptotic infected cells than infected cells to be present. The ratios of flow cytometrically determined infected and apoptotic infected cell populations over the infection period are shown in Figure 4-31. These ratios were calculated only for time points after onset of infection, as very low percentage of infected cells falsifies the ratio. The time point when this ratio starts to increase indicates the shift from predominantly infected productive cells to less productive apoptotic infected cells. Comparing MOI 1 x 10^{-5} to 0.025 infections a clearly earlier and stronger increase in the ratio apopt.inf./inf. is observed, as the three MOI 0.025 infections reach a ratio apopt.inf./inf. of 1 between 58 and 72 hpi. Thus, a lower proportion of apoptotic infected cells relative to infected cells is present in the culture broth in the low MOI infections. This eventually prolongs the productive time window and could be responsible for higher $TCID_{50}$ and higher cell-specific infectious virus yields reached.

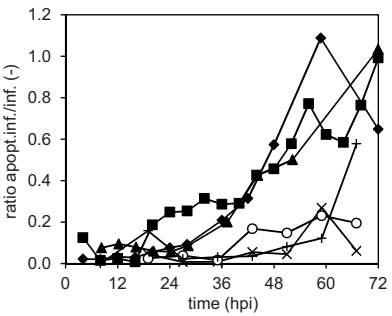

Figure 4-31 Calculation of ratio apoptotic infected to infected non-apoptotic cells for stirred tank cultivations of adherent MDCK cells infected with influenza A/PR/8: comparison of MOI 0.025 (filled symbols, three experiments) to MOI 1 x 10^{-5} infections (open symbols, three experiments).

The time window from NP accumulation to the time when the inf./apop.inf.-ratio exceeds 1 is proportional to the productive lifespan of the cells. Indeed, Uruguay-like HGR with the lowest output in virions per cell had only 36 h for virus production, while in A/PR/8 RKI MOI 0.025 infection 29617 virions/cell within 62 h productive infection were obtained. However, no strict correlation is determinable, indicating that other factors like virus replication or release efficiency might also play a role. Mathematical models can give hints for elucidating such additional factors that influence the productive lifespan of virus-infected cells (Heldt *et al.* 2013).

Concluding remarks

All tested virus strains replicated well to high titres, proving adherent MDCK cells again to be a very suitable substrate for propagation of a broad range of influenza virus strains. Interestingly, differences between the virus strains in terms of infection dynamics, apoptosis induction, and cell-specific virus yields were detected, even though all strains contained the same genetic backbone, confirming earlier observations in T25-flask infections. These results demonstrate flow cytometric characterisation of infection dynamics and virus-induced apoptosis to be a powerful tool to understand high titre-yielding virus propagation processes and can help to improve industrial vaccine production by identifying ways for optimisation like low MOI seed virus adaptation.

4.6 MDCK.SUS2 cells for influenza virus propagation

Adherent MDCK cells are a high virus titre-yielding substrate for influenza virus propagation, and able to replicate a broad range of different influenza virus strains (Gaush and Smith 1968; Merten *et al*. 1996). However, production processes using adherent cells rely on the usage of microcarriers to offer a growth surface in dynamic cultivation systems. This complicates scale-up of the process and causes additional costs. Furthermore, serum-free processes are required for production of human vaccines. Therefore, cells growing in suspension in serum-free medium are considered to be an attractive alternative to adherently growing cells (Feng *et al.* 2011). Thus, in cooperation with Klaus Scharfenberg from FH Emden/Leer an adaptation of adherent MDCK cells to growth in suspension in chemically-defined serum-free Smif8 medium was performed (Lohr *et al.* 2010). Those cells were named MDCK.SUS1–MDCK.SUS3.

In this thesis MDCK.SUS2 cells were used for infection experiments. Characterisation of infections dynamics and apoptosis induction was performed in order to develop strategies for usage of MDCK.SUS2 cells in influenza virus propagation in a vaccine production process. Firstly, a comparison of infection dynamics and cell-specific virus yields using different infection strategies was performed (section 4.6.1). Secondly, trypsin activity was determined (section 4.6.2). Finally, two influenza virus A strains (A/PR/8 RKI and Uruguay-like HGR) should be propagated in MDCK.SUS2 cells with analysis of infection dynamics and virus-induced apoptosis using flow cytometry and virus titre determination using HA and $TCID_{50}$ assays (sections 4.6.3 and 4.6.4). All results are finally discussed in section 4.6.5.

Parts of this section, namely results and discussion of low MOI shake flask and stirred tank infections (sections 4.6.1 and 4.6.3), have been published as “Peschel B, Frentzel S,

Laske T, Genzel Y, Reichl, U. 2013. Comparison of influenza virus yields and apoptosis-induction in an adherent and a suspension MDCK cell line. *Vaccine* **31**: 5693–5699". Stirred tank cultivations of MDCK.SUS2 cells and subsequent infection with influenza A/PR/8 RKI and Wisconsin-like HGR at MOI 0.025 without medium exchange as well as spinner flask infection with influenza A/PR/8 at MOI 0.025 (section 4.6.1) were part of the Bachelor thesis of Tanja Laske (Otto von Guericke University, Magdeburg). Trypsin activity measurements shown in section 4.6.2 as well as low MOI spinner infections (section 4.6.1) were part of Sarah Frentzel's Bachelor thesis (Otto von Guericke University, Magdeburg).

4.6.1 Infection conditions for MDCK.SUS2 cells

MDCK.SUS2 cells were tested for replication of two different influenza virus A strains by a direct infection as performed by Lohr *et al*. (2010). For this purpose, MDCK.SUS2 cells were grown in stirred tank bioreactors and infected by addition of 1 x 10^{-5} units porcine trypsin per cell and influenza virus A/PR/8 RKI as well as the Wisconsin-like HGR, both at MOI 0.025. Additionally, glucose at a final concentration of 5 mmol/L was added at toi to compensate for nutrient depletion. In Figure 4-32 and Figure 4-33 results for stirred tank bioreactor infections are shown.

Infections were performed at cell concentrations of 3.8 and 4.0 x 10^6 cells/mL, thus, twice as high as cell concentration reached with adherent MDCK cells using 2 g/L microcarriers. To infect the culture no medium exchange was performed, only glucose, trypsin, and seed virus were added to the culture broth at toi. Immediately after infection viable cell concentration started to decrease and 90 hpi only 5 x 10^5 viable cells/mL were present (Figure 4-32a).

HA titre in A/PR/8 RKI infection was only detectable 48 hpi and increased until the end of infection to only 2.15 $\log_{10}$ HAU/100 µL (Figure 4-32c), corresponding to 819 virions/cell. Infection with Wisconsin-like showed a 12 h earlier increase in HA titre, but only a final titre of 1.56 $\log_{10}$ HAU/100 µL (Figure 4-32c), this is equivalent to a cell-specific yield of only 214 virions/cell. Maximum $TCID_{50}$ were detected 44 and 32 hpi with 1.0 x 10^8 and 2.4 x 10^7 IVP/mL for A/PR/8 and Wisconsin-like infections, respectively (Figure 4-32c). Flow cytometric analyses of NP accumulation confirmed this late onset of infection: in A/PR/8 RKI infection the infected cell population started to increase at 40 hpi, in Wisconsin-like HGR infection at 12 hpi (Figure 4-32b). Interestingly, the infected apoptotic population started to increase in parallel to the infected non-apoptotic cell population. This very early onset of apoptosis plus the very small fraction of infected cells indicates a loss of productive cells and is presumably the reason for the low titres and the low cell-specific virus yields determined in these infections. Importantly, a significant

proportion of the cells were not infected even by 72 hpi as seen in the uninfected cell populations not falling below 30% until the end of the experiments. Importantly, even when considering this low fraction of infected cells for calculation of cell-specific yields, yields are much lower than those obtained in adherent MDCK cells.

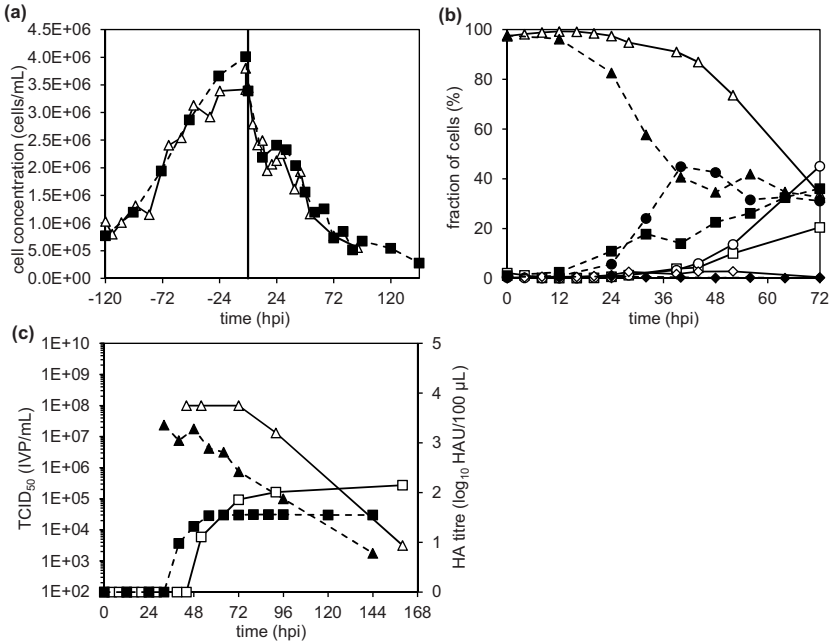

Figure 4-32 MDCK.SUS2 cells cultivated in 1 L stirred tank bioreactors and infected with influenza A/PR/8 RKI (open symbols) and Wisconsin-like HGR (filled symbols) at MOI 0.025. (a) viable cell concentration; (b) flow cytometric determination of infection status and apoptosis induction: uninfected cells (triangles), infected cells (squares), and apoptotic infected cells (circles). For a better visualisation of the infection dynamics, apoptotic uninfected cells were excluded from the analysis. The vertical line in (a) indicates point of infection.

In addition, metabolic profiles of extracellular glucose, lactate, ammonia, glutamine, and glutamate were recorded (Figure 4-33). Glucose was almost completely consumed in both cultivations during cell growth, but replenished to half of the starting concentration by addition of glucose at toi (Figure 4-33a). Lactate was released by the cells up to 40–45 mmol/L at the end of the infections (Figure 4-33a). Ammonia was released during cell growth up to 3.42–3.70 mmol/L, and increased further during infection up to 4.74–5.12 mmol/L (Figure 4-33b). Glutamine was continuously taken up or decomposed during cell growth and further during infection, while glutamate was consumed in the later phase of cell growth, and released from 12 hpi on (Figure 4-33b).

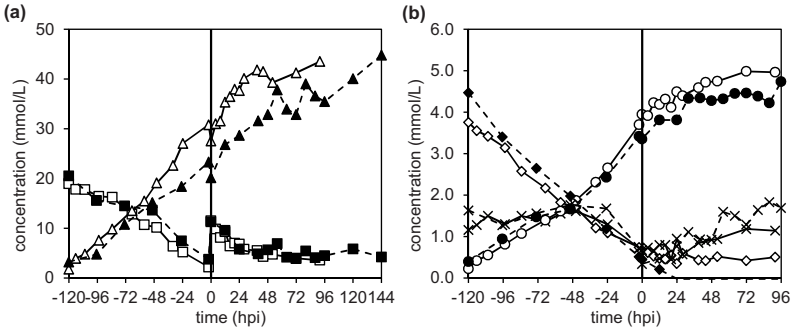

Figure 4-33 Metabolic profiles of MDCK.SUS2 cell infections in stirred tank bioreactors at MOI 0.025 with influenza A/PR/8 RKI (open symbols) and Wisconsin-like (filled symbols) at MOI 0.025. Glucose (a, triangles), lactate (a, squares), ammonia (b, circles), glutamine (b, diamonds), and glutamate (b, crosses) concentration. Vertical lines indicate point of infection.

Generally, the metabolic profiles of MDCK.SUS2 cells looked similar to those of infected adherent MDCK cells, as recorded by Lohr *et al*. (2010). Absolute concentrations can of course not be directly compared as infection were performed at a twofold higher cell concentration and in a different medium. Ammonia concentration increased during the infection with A/PR/8 RKI from 4.0–5.0 mmol/L and from 3.5–4.4 mmol/L in Wisconsin-like HGR infection. Thus, by the end of infection ammonia concentration was close to the critical level of 5 mmol/L that was described to negatively affect influenza virus yields in adherent MDCK cells (Genzel *et al.* 2005). Thus, ammonia eventually had a negative effect on virus yields in these cultivations. It has to be mentioned that this critical value for ammonia was only determined for adherent MDCK cells, thus, additional tests to determine critical ammonia concentration for MDCK.SUS2 cells would be necessary.

In infections of adherent cells extracellular glutamate concentration increase correlated to apoptosis induction and cell lysis, which is also true for the MDCK.SUS2 cell infection. However, it is less explicit because of the high amount of apoptotic uninfected cells present in the culture broth at toi due to the omitted medium exchange at toi.

Concluding, directly infected MDCK.SUS2 cells showed a delayed infection dynamic with lower virus titres and lower cell-specific virus yields compared to adherent MDCK cells. Reasons for this observation might be the presence of inhibitory molecules and cell debris that are not washed away prior to infection as in adherent MDCK infections. Furthermore, although a suspension cell line, MDCK.SUS2 cells showed a tendency for cell clogging especially at higher cell concentration. Those agglomerates might have hindered efficient spreading of the virus. Eventually, only cells on the surface of the agglomerates might be infected. Analysis of extracellular metabolite concentration showed the same general

tendencies as observed in adherent MDCK cell cultivations, thus implying that no severe changes in metabolism have occurred during the adaptation process.

As the obtained virus titres and infection dynamics in MDCK.SUS2 cell infections were not satisfying when compared to adherent MDCK cells, strategies were tested to improve infection dynamics and yields. Parameters considered were: cell concentration at toi, a reduced volume for infection, increasing trypsin activity, medium supplementation, and addition of fresh medium to the culture broth at toi. Above discussed infections were performed in stirred tank bioreactors to enable a direct comparison to adherent MDCK cell infections. Therefore, scouting experiments testing different parameters to improve infection dynamics and virus titres were performed in 100 mL shake flasks.

Firstly, it was investigated whether the delay in infection dynamic was caused by an insufficient trypsin activity. For this purpose, the trypsin activity of 1 x 10^{-5} units/cell used previously was compared to 5 x 10^{-5} and 1 x 10^{-4} units/cell in A/PR/8 RKI infections at MOI 0.025 in shake flasks. As an indicator for virus replication only the HA titre was monitored (Figure 4-34). In all infections approx. 25 hpi an HA titre of 2.1–2.25 $\log_{10}$ HAU/100 µL was detected, increasing up to 2.75–2.9 $\log_{10}$ HAU/100 µL at 120 hpi. Importantly, no large differences between the different trypsin activities were detected. Thus, trypsin activity was not limiting infection spreading. Hence, an trypsin activity of 1 x 10^{-5} units/cell was used for subsequent infections. Interestingly, final HA titres in these shake flask infections were higher than final HA titres obtained in infections with influenza A/PR/8 RKI in STR. This could be caused by smaller cell agglomerates observed when cultivating MDCK.SUS2 cells in shake flask compared to STR (data not shown).

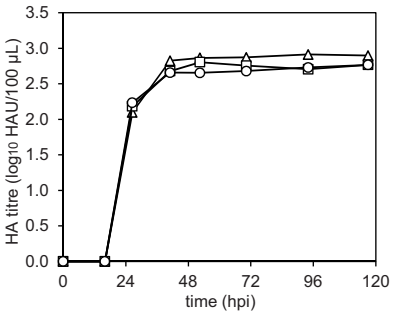

Figure 4-34 Testing of different trypsin activities for MDCK.SUS2 cell infections with influenza A/PR/8 RKI at MOI 0.025 in shake flasks. HA titre time courses for infection with 1 x 10^{-5} units/cell (triangles), 5 x 10^{-5} units/cell (squares), and 1 x 10^{-4} units/cell (circles).

In the next experiment, it was investigated whether infection dynamics can be accelerated by temporarily reducing the culture volume for infection. For this purpose, infections with influenza A/PR/8 RKI at MOI 0.025 were performed in which the culture broth was concentrated via centrifugation prior to seed virus and trypsin addition (Figure 4-35). One hour after infection the culture volume was replenished with the stored supernatant. HA titre time courses showed a faster increase when the culture broth was concentrated for infection, but the difference was small. At 48 hpi identical HA titres were reached. Thus, for the tested conditions, a higher cell and virus concentration at toi had no effect on infection dynamics. Also, studies testing different supplementations of Smif8 medium and different cell concentration at toi were not successful in improving infection dynamics and cell-specific virus-yields (data not shown).

The disadvantage of a direct infection strategy without a medium exchange (hereinafter: w/oME) is accumulation of inhibitory molecules and cell debris that are not washed away prior to infection. To evaluate whether those factors might be responsible for the slowed infection dynamic, direct infections performed in a reduced or normal culture volume were compared to infections with a medium exchange prior to infection (hereinafter: wME).

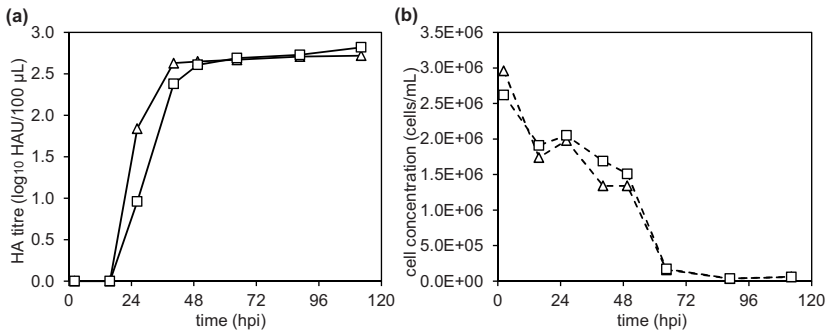

Figure 4-35 Comparison of normal (squares) and reduced (triangles) culture volume for infection of MDCK.SUS2 cells with influenza A/PR/8 RKI at MOI 0.025 in shake flasks. (a) HA titre time courses; (b) viable cell concentration.

For this purpose, culture broth was centrifuged, the used medium discarded, and the cells were resuspended in fresh medium. In Figure 4-36 HA titres and cell concentration for w/oME (open symbols) and wME (filled symbols) infections performed in reduced (triangles) or normal (squares) culture volume are shown. HA titre courses clearly showed an improvement of at least 12 h with an HA titre of 2.30 $\log_{10}$ HAU/100 µL 12 hpi (Figure 4-36a). By the end of infection even 3.21 $\log_{10}$ HAU/100 µL were reached. Importantly, both wME infections looked very similar in their HA titre time courses. The same holds true for cell concentration (Figure 4-36b). As a consequence of the higher final virus titre

also cell-specific virus yields were improved through the medium exchange. Compared to 3500 and 4800 virions/cell in w/oME infections, 9600 and 11000 virions/cell were obtained in wME infections.

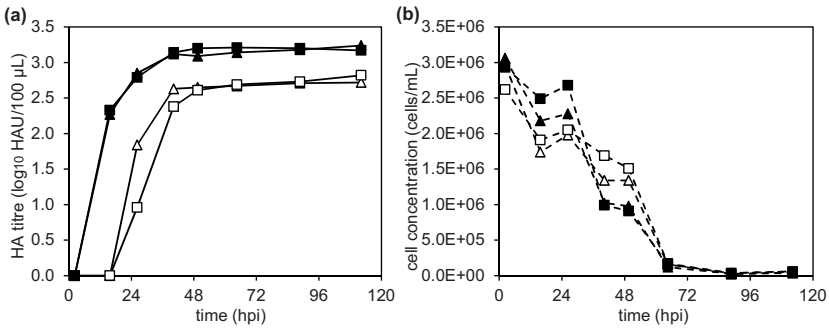

Figure 4-36 Influence of a medium exchange on (a) HA titre dynamics and (b) viable cell concentration of influenza A/PR/8 RKI infected MDCK.SUS2 cells. Infection conditions: wME (filled symbols), w/oME (open symbols), reduced volume (triangles), and normal volume (squares).

However, the finding of wME infection strategy to be beneficial for infection dynamics, virus titres, and cell-specific yields, bears the problem of being very labour-intensive: with suspension cells the culture broth has to be centrifuged, which is already in small-scale bioreactors cumbersome. For these reasons, a 1:2 dilution of the culture broth at toi (hereinafter: 1:2dil) was additionally tested as this is much easier to perform—especially at large scale—than a full medium exchange with the need for cell retention by centrifugation or other means. Also, as addition of fresh medium at toi reduces cell concentration, it might also reduce the problem of cell agglomeration that was observed especially at higher cell concentration.

In Figure 4-37 a comparison of wME, 1:2dil, and w/oME infection strategies in A/PR/8 RKI infections at MOI 0.025 in shake flasks is shown. HA titre courses showed very similar profiles with titres of 1.96 and 2.15 $\log_{10}$ HAU/100 µL at 16 hpi when comparing 1:2dil and wME infections. Also, final HA titres did not differ much (2.93 and 3.02 $\log_{10}$ HAU/100 µL, respectively). As seen before, w/oME infections resulted in a 12 h delay in HA titre increase. Thus, a 1:2dil infection procedure seems like a good compromise between laborious medium exchange and improved infection dynamics. Also for industrial vaccine production processes, diluting the culture broth of suspension cells should be more feasible than performing a complete medium exchange.

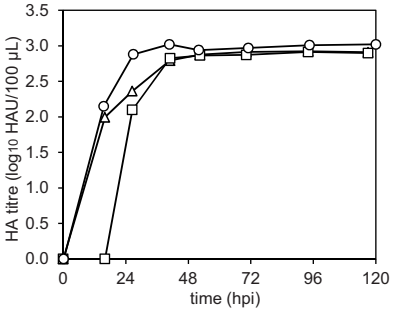

Figure 4-37 Comparison of a complete medium exchange (circles), a 1:2 dilution (triangles), and no medium exchange (squares) for MOI 0.025 infection of MDCK.SUS2 cells with influenza A/PR/8 RKI in shake flasks. Determination of HA titre time courses.

All infections of MDCK.SUS2 cells shown above were performed at MOI 0.025. With the results shown in section 4.3.3 that a low MOI in adherent MDCK cell infection was beneficial for infectious virus titres, reduced apoptosis induction, and a robust virus production in mind, the effect of a low MOI should also be investigated for MDCK.SUS2 cells. For this purpose, w/oME, 1:2dil, and wME shake flask infections at MOI 1 x 10^{-5} were performed three times. HA titre profiles with median ± MAD are shown in Figure 4-38a. Despite of the low MOI, 27 hpi HA titres of 1.4 for 1:2dil and 2.85 $\log_{10}$ HAU/100 µL for wME infections were detected. Final titres reached 3.01 and 3.27 $\log_{10}$ HAU/100 µL. In w/oME infections the increase in HA titre was delayed significantly and final titres of only 1.65 $\log_{10}$ HAU/100 µL (23-fold lower than wME) were obtained. The differences in HA titres were also reflected in lower cell-specific virus yields, with comparable cell-specific yields of 9575 and 9178 virions/cell for wME and 1:2dil infections, respectively, and only 289 virions/cell for w/oME infections.

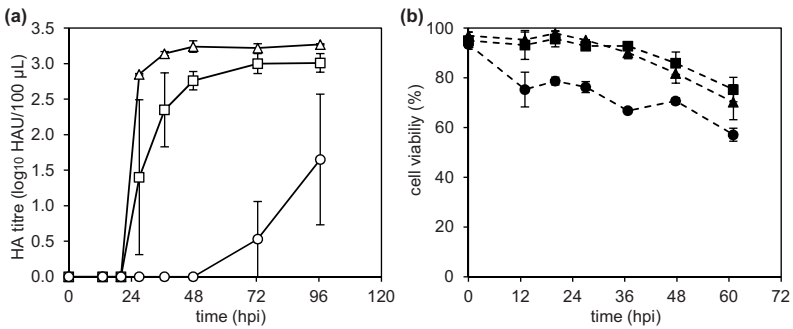

Figure 4-38 MOI 1 x 10^{-5} infection of MDCK.SUS2 cells with influenza A/PR/8 RKI in shake flasks. Comparison of wME (triangles), 1:2dil (squares), and w/oME (circles) infection conditions. Determination of (a) HA titre and (b) cell viability. Shown are median ± MAD of three independent experiments.

The improved performance of wME and 1:2dil infections might be caused by a better cell viability of the culture, as cell viabilities of w/oME infections and 1:2dil were much higher than in w/oME infections throughout the infection (Figure 4-38b).

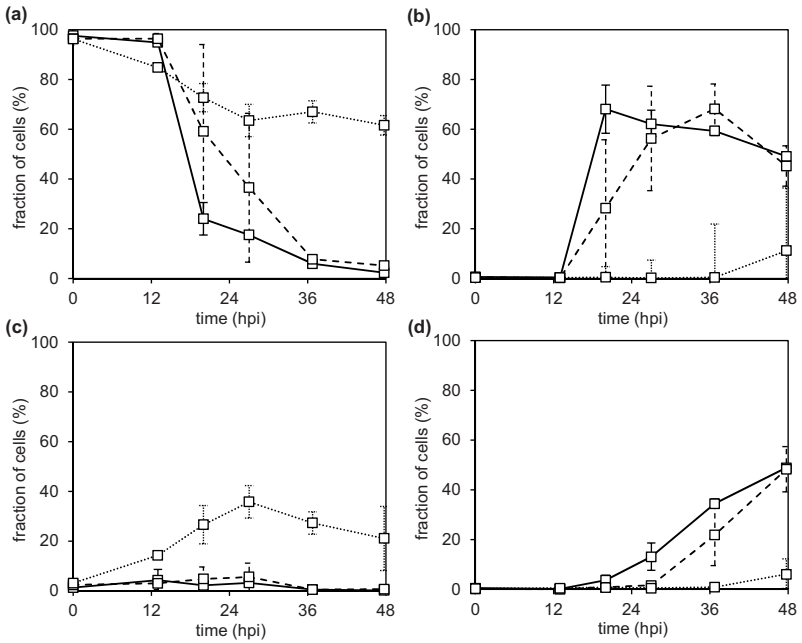

Figure 4-39 MDCK.SUS2 cells infected with influenza A/PR/8 RKI at MOI 1 x 10^{-5} in shake flasks. Comparison of wME (solid lines), 1:2dil (dashed lines), and w/oME (dotted lines) infection conditions. Determination of infection status and apoptosis induction using flow cytometry: (a) uninfected cells, (b) infected cells, (c) apoptotic uninfected cells, and (d) apoptotic infected cells. Shown are median ± MAD of three independent experiments.

For the performed shake flask infections of MDCK.SUS2 cells the effect of low MOI and different medium exchange conditions at toi on infected and apoptotic cell populations was investigated additionally using flow cytometry (Figure 4-39). Time courses of uninfected non-apoptotic cells showed a faster decrease in wME and 1:2dil infections than in w/oME infections (Figure 4-39a). Again, the difference between wME and 1:2dil was not large. Populations of infected non-apoptotic cells (Figure 4-39b) showed the same tendencies as seen in the uninfected cell population. In addition, the w/oME infection was clearly delayed (below 20% until 48 hpi) with 60% of uninfected cells at 48 hpi. At this time point, in wME infections HA titre had already reached its plateau. In case no medium exchange was performed, a poor viability during the infection was observed, as reflected in an apoptotic uninfected cell population that was significantly higher compared to wME and 1:2dil infections (Figure 4-39c). Temporarily, 35.8 ± 6.5% (median ± MAD) of the cells

were apoptotic, while in wME and 1:2dil infections this population never exceeded 6%. The infected apoptotic cell population started to increase later in infection. Again, no large difference between wME and 1:2dil infections was observed (Figure 4-39d), while the population of infected apoptotic cells increased only slightly at 48 hpi in the w/oME infection.

The next step was to investigate whether above observed tendencies for MOI lowering and 1:2 dilution prior to infection are also valid for uncontrolled systems, in which a drop in pH, e.g. caused by release of lactate, might influence infection dynamics and cell death. Indeed, the same tendencies seen in shake flask infections were found for infections of MDCK.SUS2 cells in spinner flasks (Figure 4-40a, b). A direct infection with influenza A/PR/8 RKI at MOI 0.025 resulted in an increase of HA titre at 36 hpi, to a final value of 2.28 $\log_{10}$ HAU/100 µL at 113 hpi. This corresponds to a cell-specific yield of 1050 virions/cell.

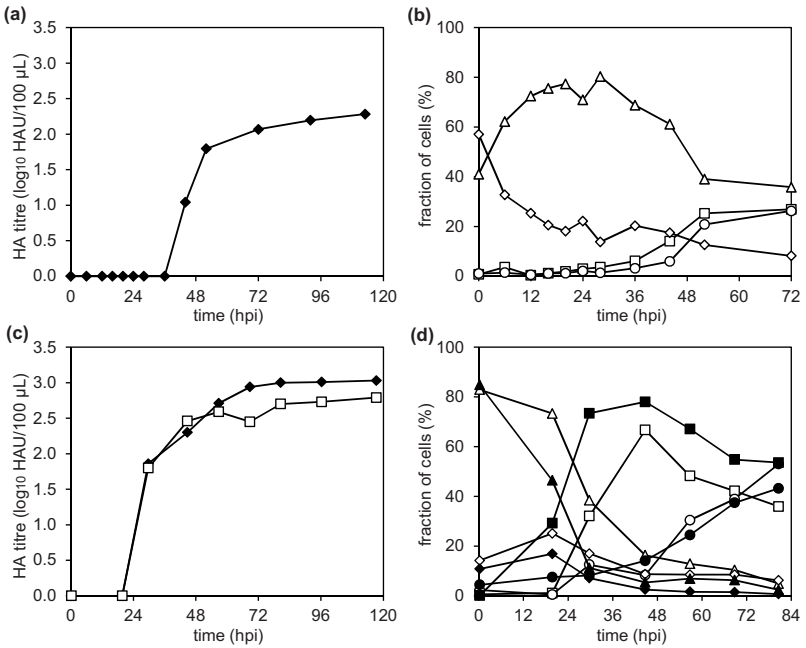

Figure 4-40 Spinner flask cultivation of MDCK.SUS2 cells infected with (a, b) influenza A/PR/8 RKI at MOI 0.025 w/oME and (c, d) influenza A/PR/8 RKI at MOI 10^{-4} wME (filled symbols) and 1:2dil (open symbols). (a, c) HA titre and (b, d) flow cytometric determination of uninfected (triangles), infected (squares), apoptotic infected (circles), and apoptotic uninfected cells (diamonds).

The flow cytometric analysis showed that apoptotic uninfected cells made up a significant proportion of the total cell population reflecting the low viability of the culture at toi (58%). Still, only 36 hpi infected non-apoptotic cells are detectable, shortly followed by an increasing infected apoptotic cell population. This parallel increase was already seen in w/oME stirred tank infections; however, in the latter the infected apoptotic population even outran the infected non-apoptotic cell population which is not the case in the spinner flask infection. Still, an overall maximum of only 53% (sum of infected non-apoptotic and infected apoptotic) of the cells were infected at 72 hpi.

In Figure 4-40c and d the subsequently performed infections of MDCK.SUS2 cells at MOI 1 x 10^{-4} using a wME and 1:2dil infection strategy are shown. HA titre increased at about 24 hpi for both conditions, with the wME infection reaching a final titre of 3.03 $\log_{10}$ HAU/100 µL, and 2.79 $\log_{10}$ HAU/100 µL in 1:2dil infection. This corresponds to cell-specific yields of 11487 and 8113 virions/cell, respectively. Interestingly, HA titres started to increase simultaneously, but ended up at different final titres. Flow cytometric evaluation of infection status showed a faster progress of infection in wME infection with a maximum of 92.1% infected cells (sum of infected non-apoptotic and infected apoptotic cells). In the 1:2dil infection a maximum of only 75.0% of the cells was infected. Virus-induced apoptosis was detected at 44 hpi for both infection conditions.

4.6.2 Measurement of trypsin activity throughout the infection

A sufficient trypsin activity is essential for cleavage of influenza virus HA0 into HA1 and HA2 and efficient virus propagation in cell culture systems (Klenk *et al.* 1975). Trypsin stock solutions used for here presented infection experiments were adjusted to activities of 500 and 5000 U/mL according to the manufacturer's recommendations. However, trypsin activity was not confirmed after stock solution preparation. An insufficient trypsin activity can result in delayed infection dynamics or impaired infection (Kaverin and Webster 1995; Seitz *et al.* 2012). The delayed infection dynamics observed in w/oME infections of MDCK.SUS2 cells raised concerns whether sufficient trypsin activity was present in the culture supernatant. To clarify this, trypsin activity present during infection experiments was determined.

For analysis of trypsin activity in infection supernatants the commercial "trypsin activity colorimetric assay kit" (BioVision) was used. It is based on cleavage of the substrate BAPNA by trypsin to form the yellow dye pNA that can be detected in a fluorescence plate reader. The read-out pNA units/mL was converted into the more common BAEE units/mL by equation (6) in section 3.4.5.

Firstly, the internal trypsin stock used in the bioprocess engineering group for infection experiments was tested for its actual activity. Values detected with the assay kit for stock solutions were in the range of the expected activity of 500 U/mL (data not shown). Next, it was investigated if different medium exchange conditions affect trypsin activity. Thus, supernatant of shake flask infections of MDCK.SUS2 cells with influenza A/PR/8 RKI at MOI 1 x 10^{-5} and a calculated adjusted trypsin activity of 1 x 10^{-5} units/cell was analysed with the assay kit. In Figure 4-41 trypsin activity in BAEE units/mL of one set of parallel infected shake flasks either under wME, 1:2dil, or w/oME infection conditions is shown. Data clearly showed that trypsin activity was present with 23–30 BAEE units/mL under all infection conditions over the complete infection period. Thus, omitting of a medium exchange had no negative effect on trypsin activity. Taking the cell concentration at toi, target trypsin activity of 1 x 10^{-5} units/cell correspond to 28, 29, and 30 BAEE units/mL. Thus, the determined 0 hpi values of 28.0, 30.3, and 30.5 BAEE units/mL met the expected corresponding calculated values very well (Figure 4-41).

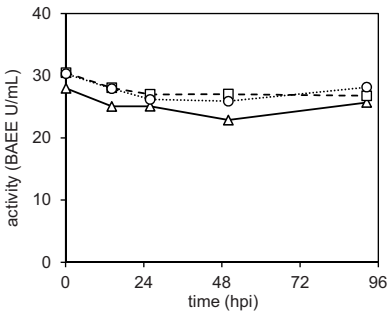

Figure 4-41 Trypsin activity in MDCK.SUS2 cell shake flask infections with influenza A/PR/8 RKI (MOI 1 x 10^{-5}). Comparison of wME (triangles), 1:2dil (squares), and w/oME (circles) infection conditions using the commercial "trypsin activity colorimetric assay kit" (BioVision).

Trypsin activity was also determined for 1:2dil infections at MOI 1 x 10^{-5} and 1 x 10^{-4} in stirred tank and spinner flasks, respectively. For the bioreactor infection (Figure 4-42a) trypsin activity decreased during the infection duration: 16 BAEE units/mL at 0 hpi to 7 BAEE units at 60 hpi. Afterwards, determined activity was stable. With a calculated activity of 25 BAEE units/mL at toi, the adjustment of the activity did not work well in this infection experiment. In Figure 4-42b trypsin activity from MDCK.SUS2 cell infections in spinner flasks is depicted. In this experiment the adjusted value of 23 BAEE units/mL was met very well, with the assay determining an activity of 26 BAEE units/mL at toi. Afterwards, a drop in activity was observed (8 BAEE units/mL at 26 hpi), but recovering to activities around 18 BAEE units/mL. It is not clear whether this behaviour is due to assay error or a poor sample preparation.

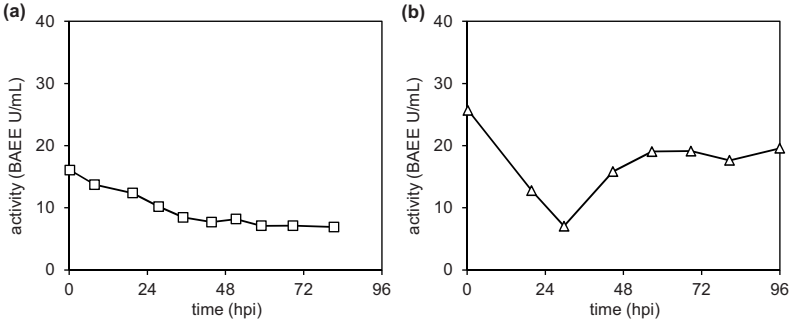

Figure 4-42 Trypsin activity determined with a commercial assay kit of (a) stirred tank and (b) spinner flask infections of MDCK.SUS2 cells (influenza A/PR/8 RKI at MOI 1 x 10^{-5} and 1 x 10^{-4}, respectively).

In summary, the commercial kit worked, although absolute values should be treated with care until a validation has been performed. Measurements showed that even without a medium exchange no limitation in trypsin activity is observed, and that the tested infections with 1:2dil at toi did not show low trypsin activity during the course of infection.

4.6.3 Infections in stirred tank bioreactors

As the next step, the performance of MDCK.SUS2 cells was compared to adherent MDCK cells. For this purpose, three stirred tank cultivations with MDCK.SUS2 cells were performed under 1:2dil conditions and infected with influenza virus A/PR/8 RKI at MOI 1 x 10^{-5}. In Figure 4-43 median values ± MAD of these three infections are shown. HA titres of these 1 L stirred tank bioreactor infections (Figure 4-43a) showed a similar time course and comparable maximum virus titres compared to infections under the same conditions in shake flasks (2.94 ± 0.02 $\log_{10}$ HAU/100 µL). With 11411 ± 949 virions/cell (median ± MAD) cell-specific virus yields were also comparable to shake flask infections in which 9178 ± 1400 virions/cell were obtained (Figure 4-48). Additionally, a maximum $TCID_{50}$ of 1 x 10^9 ± 3 x 10^8 IVP/mL at 43 hpi was determined (Figure 4-43a). This corresponds to a cell-specific infectious virus yield of 633 ± 227 IVP/cell (median ± MAD).

Flow cytometric analysis of the infection status and apoptosis showed the uninfected cell population to decrease at 24 hpi (Figure 4-43b). Likewise, the infected non-apoptotic cell population started to increase at that time point reaching a maximum of 88.2 ± 3.6% at 35 hpi. The subsequent decrease in the proportion of infected non-apoptotic cells corresponded to an increase of the apoptotic infected population up to 55.2 ± 1.4%. The apoptotic uninfected cell population remained more or less constant at a level below 5% during the entire infection period, as seen before in shake flask infections (Figure 4-39).

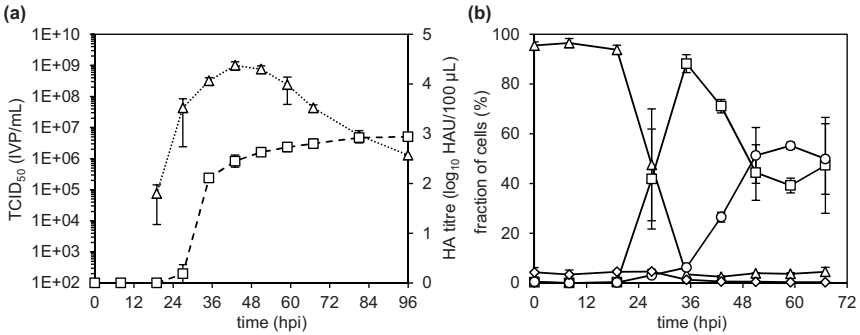

Figure 4-43 Stirred tank cultivation of MDCK.SUS2 cells infected with influenza A/PR/8 RKI at MOI 1 x 10^{-5} using 1:2dil. Determination of (a) HA titre and $TCID_{50}$, as well as (b) infection status and apoptosis induction with flow cytometry: uninfected cells (triangles), infected cells (squares), apoptotic infected cells (circles), and apoptotic uninfected cells (diamonds). Median ± MAD from three independent experiments are shown.

Also, concentration of extracellular metabolites was compared (Figure 4-44). During the first 94 h of cell growth glucose was consumed by the cells to a final concentration of 4.6 mmol/L, but replenished after medium addition at toi to 8.8 mmol/L (Figure 4-44a). Lactate reached a concentration of 23.1 mmol/L prior to infection (Figure 4-44a). This level was reduced to 12.5 mmol/L by 1:2 dilution with fresh medium. With 15.2 mmol/L lactate being released until the end of infection, and consumption of glucose from 8.7 to 2.3 mmol/L, yield coefficient $Y'_{lac/gluc}$ was 2.34.

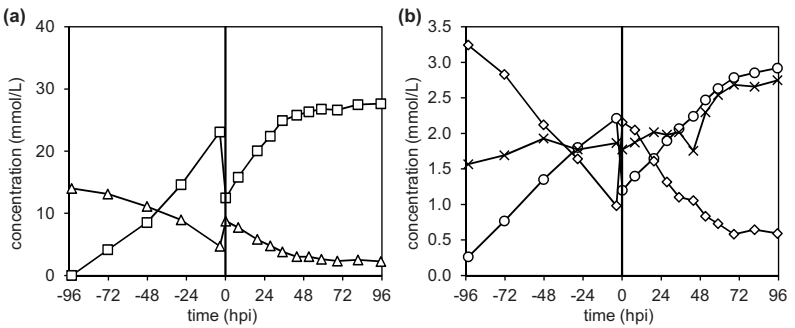

Figure 4-44 Stirred tank infection of MDCK.SUS2 cells with influenza A/PR/8 RKI at MOI 1 x 10^{-5} using 1:2dil. Determination of extracellular metabolite concentration: glucose (a, triangles), lactate (a, squares), ammonia (b, circles), glutamine (b, diamonds), and glutamate (b, crosses). Vertical lines indicate point of infection.

Ammonia concentration was reduced after dilution at toi from 2.2 to 1.2 mmol/L (Figure 4-44b). After infection its concentration increased again up to 3.0 mmol/L. Glutamine was consumed during cell growth from 3.3 to 1.0 mmol/L (Figure 4-44b). 1:2 dilution at toi

replenished glutamine concentration to 2.2 mmol/L. During infection glutamine was once more taken up by the cells, resulting in a final concentration of 0.6 mmol/L at 96 hpi. Yield coefficient $Y'_{NH4/gln}$ was 1.1. Glutamate concentration showed only minor changes during cell growth (from 1.6 to 1.9 mmol/L). In the second half of the infection (at 44 hpi) glutamate concentration increased again up to 2.9 mmol/L (Figure 4-44b).

4.6.4 Infections with Uruguay-like HGR seed virus

Above shown infections of MDCK.SUS2 cells were all performed with influenza virus A/PR/8 RKI. Studies in adherent MDCK cells demonstrated the influenza Uruguay-like HGR strain to perform very well in T25-flask infections. It showed a fast progress of infection and a late apoptosis induction resulting in high virus titres and high cell-specific virus yields. Thus, it should be analysed whether this strains performs equally well in MDCK.SUS2 cells. For this purpose, shake flask infections were performed (1:2dil, 1 x 10^{-5} units trypsin/cell) and HA titres were analysed (Figure 4-45).

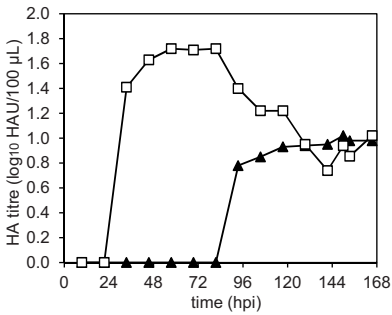

Figure 4-45 Shake flask cultures of MDCK.SUS2 cells infected with influenza Uruguay-like HGR at MOI 0.025 (triangles) and MOI 1 (squares). Determination of HA titre time courses.

Surprisingly, even using MOI 1, 58 hpi a maximum HA titre of only 1.72 $\log_{10}$ HAU/100 µL was reached, and in MOI 0.025 infection it took even 93 h to have a detectable HA titre that only increased up to 1.02 $\log_{10}$ HAU/100 µL. This corresponds to cell-specific yields of only 446 virions/cell and 89 virions/cell, respectively.

As the influenza Uruguay-like HGR seed virus used for infection had been adapted to adherent MDCK cells, it should be investigated whether an adaptation of this seed virus to MDCK.SUS2 cells could improve infection dynamics, virus titres, and cell-specific virus yields. Standard seed virus adaptation in the bioprocess engineering group uses fixed standard volumes per flask, thus, no concrete MOI is adjusted, and eventually high MOI situations might occur. Previous experiments in this thesis had shown a low MOI to be

beneficial for achieving high infectious virus titres (section 4.3.3) and generating a high quality seed virus. Consequently, a different SOP for the adaptation of the Uruguay-like HGR seed virus to MDCK.SUS2 cells was used. In this procedure, the seed virus was highly diluted over 5 passages (up to a dilution of 10^{-8}), thereby achieving very low MOIs resulting in a seed virus with a high proportion of infectious virus particles. The adaptation of the Uruguay-like HGR virus to MDCK.SUS2 cells generated a seed virus containing 9.2% infectious virus particles, with a $TCID_{50}$ of 1 x 10^9 IVP/mL. This is identical to $TCID_{50}$ of the best adherent cell-adapted seed virus used in this work, which was the influenza A/PR/8 NIBSC seed virus generated by a low MOI passage.

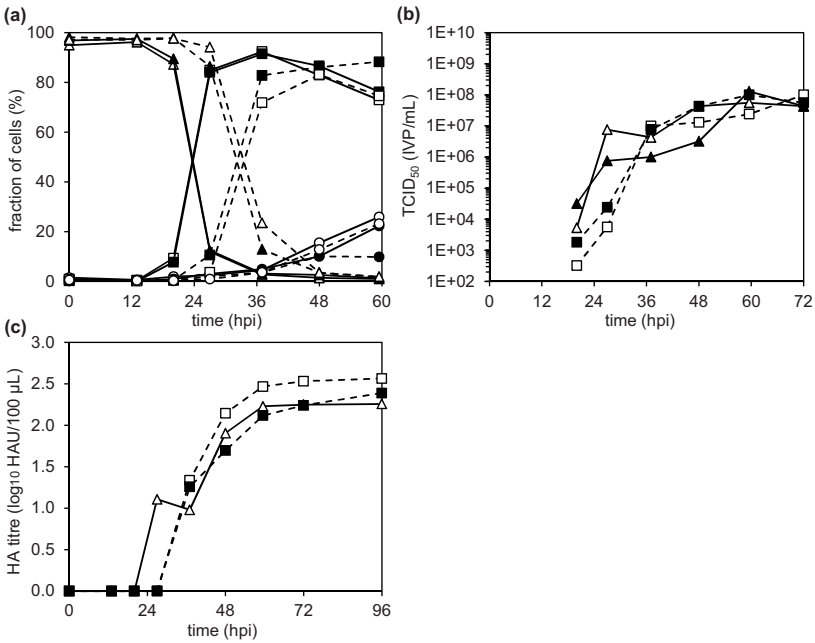

Figure 4-46 Infections of MDCK.SUS2 cells with MDCK.SUS2 cell-adapted Uruguay-like HGR seed virus at MOI 1 x 10^{-5} using wME (solid lines) and 1:2dil (dashed lines) infection conditions in shake flasks. Results of two experiments are shown (open and filled symbols): (a) flow cytometric determined uninfected (triangles), infected non-apoptotic (squares), and apoptotic infected (circles) cell populations; time courses of (b) $TCID_{50}$ and (c) HA titre.

This adapted Uruguay-like HGR seed virus was then used for two low MOI infections of MDCK.SUS2 cell shake flask cultures (Figure 4-46). To obtain a better impression of the new seed virus, wME as well as 1:2dil conditions were compared for MOI 1 x 10^{-5} infections (n = 2). Uninfected non-apoptotic cells were absent 36 hpi in wME infections (Figure 4-46a). Under 1:2dil conditions this took about 10–12 h longer. Correspondingly,

the maximum of infected non-apoptotic cells was reached at these time points. Apoptosis was induced late in these infections, with the apoptotic infected cell population starting to increase at 40 hpi. Importantly, apoptotic uninfected cells did not play a role during the experiment (constantly below 3%). Maximum $TCID_{50}$ reached were 6×10^7 to 1.3×10^8 IVP/mL (Figure 4-46b). Interestingly, maxima were reached very late during infection. HA titre increased up to 2.3 and 2.6 $\log_{10}$ HAU/100 µL (Figure 4-46c). Cell-specific yields were 497–2938 virions/cell and 13–40 IVP/cell.

4.6.5 Discussion

Testing of medium exchange strategies for infections of MDCK.SUS2 cells

Cell-specific virus yields of MDCK.SUS2 cells presented by Lohr *et al.* (2010) were much lower than those obtained in adherent MDCK cells. Additionally, progress of infection was delayed significantly compared to infections in microcarrier cultures. In line with this, first infections with MDCK.SUS2 cells presented in this work showed a weaker performance of MDCK.SUS2 cells compared to adherent MDCK cells. Thus, in order to improve virus titre and cell-specific yields, MDCK.SUS2 cells infection conditions should be optimised. First attempts tried higher trypsin concentration, different medium supplementation (data not shown), or reduced culture volume at toi (higher cell and virus concentration) but achieved no significant improvement. An insufficient trypsin activity could be excluded as a cause for delayed infection dynamics, as trypsin activity was high in all shake flask infections throughout the complete infection phase (Figure 4-41).

Further attempts for improving infection dynamics included addition of fresh medium to the culture broth at toi and medium exchange. Although cultivation in serum-free medium enables a direct infection, also vaccine industry performs washing steps in order to remove spent medium. Furthermore, in direct infections of MDCK.SUS2 cells inhibiting metabolites like ammonia and lactate had accumulated and glucose had been consumed during cell growth (Figure 4-33). Therefore, performing a full medium exchange at toi should be compared to direct infections with only glucose being added. Additionally, infections in which the culture broth was 1:2 diluted with fresh medium at toi were included, as this is more feasible than a full medium exchange. Furthermore, the MOI was reduced to 1×10^{-5} as it was shown previously that low MOI infections can improve infectious virus titres (section 4.3.3). Also industrial cell culture-based influenza vaccine productions use very low MOI. Aggarwal *et al.* (2011) described the MOI to be an important parameter for optimisation of influenza virus production, and showed a low MOI to be not only beneficial for process productivity, but also for process robustness. Shake flask infection experiments performed under low MOI conditions showed that 1:2dil at toi

improved the viability of the culture (Figure 4-38) and reduced the apoptotic uninfected cell population (Figure 4-39c). This might be caused by dilution of potential inhibitors and supply of fresh nutrients. In contrast, in w/oME infections the viable cell concentration steadily decreased (Figure 4-38b). Importantly, virus propagation started earlier under wME and 1:2dil conditions. Possible explanations might be the dilution of substances inhibiting virus entry and intracellular virus replication, or the activation of cellular metabolism and cell growth after addition of fresh medium. The latter is supported by an increasing viable cell concentration and a better cell viability after infection in 1:2dil but not in w/oME infections (Figure 4-38b). The lower cell concentration in 1:2dil infections compared to w/oME infections might also be responsible for the faster onset of infection: MDCK.SUS2 cells tend to form cell aggregates at higher cell concentration eventually hindering an efficient spreading of the virus through the whole cell population. While for Modified Vaccinia Ankara virus in AGE1.CR cell cultures cell agglomerates support virus spreading (Lohr *et al.* 2009), MDCK.SUS2 cells eventually still release virus particles via their former apical side, thereby hindering an infection of cells within cell agglomerates.

Most likely, in wME and 1:2dil infections the early onset of virus replication together with the late induction of apoptosis resulted in higher cell-specific virus yields because the virus production time window was extended. Importantly, a 1:2 dilution was already sufficient to achieve this beneficial effect, as infection dynamics and virus titres did not differ much between wME and 1:2dil infections (in maximum by 0.26 $\log_{10}$ HAU/100µL). Similar results were obtained in spinner flask infections of MDCK.SUS2 cells. Here, w/oME infection with influenza A/PR/8 RKI at MOI reached a final HA titre of 2.28 $\log_{10}$ HAU/100 µL (1050 virions/cell). Interestingly, this value is higher than the final HA titre obtained in stirred tank infections under these conditions. Performance of a 1:2dil and wME infection strategy clearly improved infection dynamics and virus titres. A first HA titre was detectable 15 h earlier in wME and 1:2dil infections than in the w/oME MOI 0.025 infection. Final HA titre improved 3.2-fold when comparing w/oME infection to 1:2dil infection, and a factor 5.6 improvement compared to wME infection. For cell-specific yields improvement factors were even higher: 7.7 and 10.9 when comparing wME and 1:2dil infection yields to w/oME infection yields, respectively.

A comparison of the former infection strategy (also used by Lohr *et al.* 2010) to the 1:2dil infection strategy is shown in Figure 4-47. Infected cells (apoptotic plus non-apoptotic NP-positive cells in flow cytometric measurements) and HA titres of direct w/oME infections of MDCK.SUS2 cells with influenza A/PR/8 RKI at MOI 0.025 showed a later progress of infection than infections with the same virus strain under 1:2dil infection conditions at MOI 1 x 10^{-5}. Also, cell-specific virus yields in 1:2dil and wME infections were higher than yields obtained in w/oME infections (Figure 4-48).

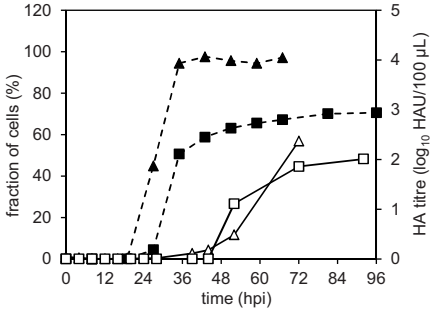

Figure 4-47 Improved infection conditions for MDCK.SUS2 cells. Comparison of w/oME MOI 0.025 (open symbols) to 1:2dil MOI 1 x 10^{-5} (filled symbols) infections. Infected cell populations (triangles) (sum of non-apoptotic as well as apoptotic infected cells) and HA titre time courses (squares) of MDCK.SUS2 cells grown in stirred tank reactors and infected with influenza A/PR/8 RKI.

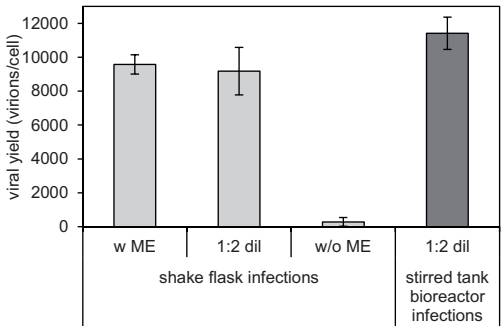

Figure 4-48 Cell-specific virus yields of w/oME, 1:2dil, and wME shake flask infections and 1:2dil stirred tank infections of MDCK.SUS2 cells with influenza A/PR/8 at MOI 1 x 10^{-5}. Median ± MAD of three independent experiments are shown.

Similar results were obtained by Genzel *et al.* (2013), who investigated the influence of a wME and 1:2dil in comparison to w/oME infections in influenza infections using CAP cells. In shake flask infections using CAP cell-adapted influenza A/PR/8 seed virus, the 1:2dil infection strategy also improved HA titres by at least 0.4 $\log_{10}$ HAU/100 µL compared to w/oME infections. Here, a full medium exchange at toi resulted in even further increased final HA titres of 3.0 $\log_{10}$ HAU/100µL and earlier onset of infection.

In summary, though a direct infection w/oME of MDCK.SUS2 cells is possible, a 1:2dil was necessary to achieve fast infection dynamics, high virus titres, and increased cell-specific virus yields in MDCK.SUS2 cell infections.

Infection of MDCK.SUS2 cells in stirred tank reactors and spinner flasks

A 1:2dil infection of MDCK.SUS2 cells with influenza A/PR/8 RKI at MOI 1 x 10^{-5} in STR cultivations was subsequently performed to enable a direct comparison to adherent MDCK cells. Diluting the culture broth 1:2 at toi successfully reduced ammonia concentration and replenished substrates like glucose (Figure 4-44). Yield coefficient $Y'_{lac/gluc}$ was identical to coefficients determined in adherent MDCK cell infections in this work (2.27 and 2.34 in adherent and MDCK.SUS2 cell infections, respectively). Conversion of glutamine to ammonia was lower compared to adherent MDCK cell infections ($Y'_{NH4/Gln}$ = 1.1 in MDCK.SUS2 cells and 3.44 in adherent MDCK cells). Genzel *et al.* (2005) described ammonia concentration of 5 mmol/L at toi to inhibit virus propagation in adherent MDCK cell infections. Thus, maximum ammonia concentration of 2.35 mmol/L obtained in low MOI MDCK.SUS2 cell infections was most likely below critical levels, assuming critical concentration for MDCK.SUS2 cells to be in the same range as for adherent cells. It needs to be clarified whether the lower yield coefficient of ammonia from glutamine is caused by the different medium composition used for the two cell lines or by a change in metabolism through the adaptation process. MDCK.SUS2 cell infections showed a release of glutamate during the second half of the infection, comparable to tendencies in here presented experiments with adherent MDCK cells and results described by Genzel *et al.* (2004). This increase in extracellular glutamate correlated with flow cytometrically determined virus-induced apoptosis (Figure 4-43b) and decreasing viable cell concentration (data not shown). Interestingly, net release of glutamate (calculated as difference between concentration at the end of infection minus concentration at toi) was 2.6 times higher in MDCK.SUS2 cell infections than in the low MOI infection of adherent MDCK cells.

Lohr *et al.* (2010) found A/PR/8 virus-infected MDCK.SUS2 cells to reach maximum $TCID_{50}$ of 7.6 x 10^8 IVP/mL and a maximum HA titre of 2.9 $\log_{10}$ HAU/100 µL in wave-bioreactor cultivations, which is in the range of values obtained in this work. However, cell-specific yields were 7000 virions/cell, which is below the 11400 virions/cell reached in 1:2dil infections presented in this work.

Recently, Tapia *et al.* (2014) used MDCK.SUS2 cells for influenza virus A/PR/8 and A/Mexico/4108/2009 (H1N1) propagation (MOI 0.001) in a hollow fibre bioreactor system. They estimated yields of 11000–19000 virions/cell, thus, proving the potential of MDCK.SUS2 cells. Van Wielink *et al.* (2011) showed for infections of MDCK-SFS cells with egg-adapted influenza virus A/PR/8 a $TCID_{50}$ of approximately 6.3 x 10^8 IVP/mL, and HA titres of 2.6 $\log_{10}$ HAU/100 µL. However, as the authors do not provide cell-specific virus yields, a direct comparison of the cultivations is difficult.

Nevertheless, for infections of adherent MDCK cells with influenza A/PR/8 virus at MOI 1 x 10^{-5} titres of 3.15 $\log_{10}$ HAU/100 µL and 2.37 x 10^9 IVP/mL (22000 virions/cell and 2900 IVP/cell) were obtained (Figure 4-43). While this demonstrates that there is further room for improvement of cell-specific yields in MDCK.SUS2 cells, one has to keep in mind that concentration of cells in suspension cultures can be increased relatively easily. For example, similar to Pohlscheidt *et al.* (2008), perfusion or volume-extended fed batch strategies might be used as in adherent MDCK cells for further improvement of virus production. Another option was demonstrated by Petiot *et al.* (2011). They increased total virus titres as well as infectious virus titres for influenza virus production in a HEK-293 suspension cell line in perfusion cultures (using an acoustic filter system for cell retention) compared to batch cultivations.

Alternating tangential flow (ATF) cultivation systems, as used by Genzel *et al.* (2014) for influenza virus propagation in AGE1.CR and CAP cells, should be considered, too. They found the ATF system—that combines perfusion with filtration strategies—to positively influence the ratio of infectious to total virions released and increased cell-specific infectious virus yield compared to batch cultivation. Total number of virions/cell were constant, thus, no high cell density effect occurred.

Regarding other cell lines, Petiot and Kamen (2013) showed maximum infectious titres of 10^8–10^{12} IVP/mL in HEK-293 suspension cells infected with influenza A/PR/8 at MOI 0.01 in batch cultivations. With human CAP cells 2.5 $\log_{10}$ HAU/100 µL (up to 6400 virions/cell) and 7.7 x 10^7 IVP/mL were obtained when infected with influenza A/PR/8 virus (seed virus adapted to the cells) (Genzel *et al.* 2013). Per.C6 cells reached 10^{10} $TCID_{50}$/mL in bioreactor infections with influenza A/Sydney/95 virus at MOI 1 x 10^{-4} (Pau *et al.* 2001). Lohr *et al.* (2012) described influenza A/PR/8 virus propagation in AGE1.CR cells to reach $TCID_{50}$ of 1.8 x 10^8 IVP/mL and 2.1 $\log_{10}$ HAU/100 µL. Genzel *et al.* (2010) showed Vero cells to yield HA titres of 2.6–2.9 $\log_{10}$ HAU/100 µL and $TCID_{50}$ of 5.6 x 10^6 to 1.8 x 10^8 IVP/mL for MOI 0.001 and MOI 1 influenza A/PR/8 virus infections in small-scale stirred tank systems under serum-containing and serum-free conditions. Hu *et al.* (2008) demonstrated Vero cells to yield 1 x 10^8 to 1.65 x 10^9 IVP/mL when infected with an influenza A/Vietnam/1194/2004 (H5N1)-HGR virus containing a A/PR/8 backbone in a 1 L-scale bioreactor with 3 x 10^6 cells/mL at toi. Concluding, with titres of 1 x 10^9 IVP/mL and HA titres of 2.94 $\log_{10}$ HAU/100 µL MDCK.SUS2 cells thus performed well compared to other cell lines.

Comparison of w/oME, 1:2dil, and w/ME infection strategies for MDCK.SUS2 cells in spinner flasks showed similar tendencies as in shake flasks. 1:2dil and wME infections showed a faster onset of infection compared to w/oME of 20 h despite the 2500-fold lower

MOI used. Final HA titres were 0.5 log_{10} HAU/100 µL higher and cell-specific yields increased almost 8-fold when comparing 1:2dil infections with w/oME infections.

When comparing the controlled to the uncontrolled cultivation system for MDCK.SUS2 cell infections, stirred tank infections were still faster (90% infected cells in 36 h), especially taking into account that a 10-fold lower MOI was used than in spinner flask infections. Cell-specific yields in stirred tank reactor and spinner flask infections differed only slightly: 11411 virions/cell in stirred tank, 8113 virions/cell in spinner flasks. Data presented here suggest similar performance of MDCK.SUS2 cells in stirred tank and spinner systems. However, as spinner infections were not performed in biological replicates the comparison shall not be over-interpreted.

Trypsin activity in MDCK.SUS2 cell infections

Trypsin activity was determined in infection supernatants to exclude delayed infection dynamics being caused insufficient trypsin activity during infection. Comparing trypsin activity in w/oME, 1:2dil, and wME shake flask infections of MDCK.SUS2 cells similar trypsin activities were determined. Thus, trypsin activity is not limiting virus activation and spreading in infections without medium exchange.

Although trypsin is described to self-digest itself (Bier *et al.* 1956), trypsin activity of shake flask infections did not show a decrease in trypsin activity over time. Thus, self-digestion doesn't seem to play a role in cell culture infection experiments. The assay could be used to check trypsin activity of in-house-prepared trypsin stock solutions used for infection experiments. Furthermore, it might be interesting to monitor trypsin activity during continuous influenza virus cultivations (Frensing *et al.* 2013), to check if trypsin activity is affected by such infection conditions. Also, high cell density situations like in ATF or hollow fibre bioreactor systems (Tapia *et al.* 2014; Genzel *et al.* 2014b) should be analysed for trypsin activity, as with high cell densities secreted protease inhibitors could play a more prominent role and might decrease trypsin activity. The importance of trypsin addition for influenza virus propagation in cell culture was reported by Le Ru *et al.* (2010) who found no influenza virus replication in HEK-293 cells even 4 days post infection when infecting without trypsin added at toi. For adherent MDCK cells, Seitz *et al.* (2012) described absence of trypsin in adherent MDCK cell infections with influenza virus A/PR/8 NIBSC at MOI 0.025 to result in delayed increase and lower final HA titre, stronger IFN-β expression, and higher fractions of apoptotic cells later in infection. However, a too high trypsin activity can also have negative effects on cell viability and/or virus titres (Pau *et al.* 2001; Le Ru *et al.* 2010). Thus, testing for the optimal trypsin activity is important when aiming at improving influenza virus propagation in cell culture.

Comparison of MDCK.SUS2 cells to adherent MDCK cells

Compared to adherent MDCK cell infections in bioreactor at MOI 1 x 10^{-5} with influenza A/PR/8 RKI, analysis of infected cell populations in bioreactor infections of MDCK.SUS2 cells showed a delay in the increase of infected non-apoptotic cells and HA titre of about 8 h. Reasons for this delay might be related to altered lipid composition of MDCK.SUS2 cell membranes caused by adaptation of the cells to growth in suspension. This could affect steps like virus attachment, internalisation, and virus budding, thereby influencing onset of infection and time of virus particle release. Also, in stirred cultivation systems cell agglomerates of MDCK.SUS2 cells were observed that eventually hindered an efficient spreading of the virus. Rodriguez-Boulan *et al.* (1983) analysed influenza virus budding of adherent MDCK cells that were brought into suspension by trypsin-EGTA treatment. While single cells in suspension lost their structural and functional polarisation and released influenza virus particles from the entire cell surface, cells in agglomerates showed cell polarisation features and asymmetric virus budding (as in cells attached to a surface).

In addition, the adaptation process eventually changed other cellular factors that affect virus replication. Evaluation of changes between adherent and MDCK suspension cells on the proteome level could give hints on such altered cellular factors that potentially influence virus replication. Van Wielink *et al.* (2011) performed a comparison of influenza virus infection in MDCK-SFS suspension cells to the parental adherent MDCK cells, however, they only provide final virus titres and do not comment on infection dynamics. Tapia *et al.* (2014) performed infection experiments with both, adherent MDCK cells and MDCK.SUS2 cells. However, as they performed perfusion cultivations in hollow fibre bioreactors for 200 hours or longer, differences in the onset of infection between the two cell lines were not in the scope of their work.

Importantly, apoptosis induction after influenza virus infection was much more pronounced in MDCK.SUS2 cells than in adherent MDCK cells, shown in percentage of apoptotic cells and the ratio apopt.inf./inf. cells (Figure 4-49). This indicates an early loss in the proportion of virus-producing cells in MDCK.SUS2 cell infections, as TUNEL positive cells do not contribute significantly to virus production anymore (Schulze-Horsel *et al.* 2009). Importantly, this was only true for virus-induced cell death, as levels of uninfected apoptotic cell populations were equally low in infections of both cell lines. Interestingly, despite the stronger apoptosis induction, increase of apoptotic infected cells and the HA titre reaching its plateau correlated, as previously observed for most infections of adherent MDCK cells.

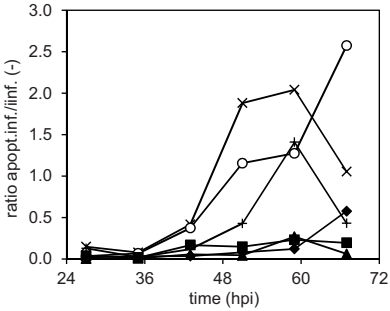

Figure 4-49 Comparison of adherent MDCK (filled symbols) to MDCK.SUS2 cells (open symbols) in stirred tank infections with influenza A/PR/8 RKI at MOI 1 x 10^{-5}: ratio apopt.inf./inf. cell populations determined with flow cytometry of three cultivations each.

Adaptation of adherent cells to growth in suspension requires overcoming anoikis. Thus, suspension-adapted cells should have a lower susceptibility for programmed cell death and, possibly, also for virus-induced cell death. In contrast, here presented data show that during the adaptation to suspension growth the cells became more susceptible to virus-induced apoptosis. Signalling pathways leading to cell death are described to be also connected to adhesion molecules (reviewed by Zhong and Rescorla 2012; Mitra and Schlaepfer 2006). Furthermore, the interplay of influenza virus proteins with molecules involved in cell adhesion is described, e.g. Gaur *et al.* (2012) showed the interaction of influenza virus neuraminidase with the adhesion molecule CEACAM6 to result in activation of the Protein Kinase B (Akt) cell survival pathway. Thus, alterations in protein expression levels or structure of adhesion molecules might alter cell survival signalling pathways that also interact with influenza virus proteins. This might explain the observed susceptibility of MDCK.SUS2 cells for virus-induced apoptosis. This hypothesis might be supported by Coombs *et al.* (2010) describing proteins associated with cell adhesion to be downregulated upon influenza virus A infection in A549 cells. If this is also true for MDCK.SUS2 cells, influenza virus infection might result in down-regulation of various cell-survival signalling pathways, thereby possibly facilitating virus-induced apoptosis. Another factor could be that the chemically-defined Smif8 medium used for cultivation of MDCK.SUS2 cells might not sufficiently protect the cells from virus-induced cell stress. Finally, mathematical models can be used to estimate the lifetime of productively infected cells and help to understand the underlying molecular mechanisms (Schulze-Horsel *et al.* 2009; Heldt *et al.* 2013).

Propagation of influenza Uruguay-like HGR in MDCK.SUS2 cells

The low MOI adaptation of influenza Uruguay-like HGR successfully generated a seed virus with a high $TCID_{50}$ and a high proportion of infectious virus particles. This adapted virus showed improved infection dynamics, virus titres of 2.6 $\log_{10}$ HAU/100 µL, and $TCID_{50}$ of 1.3 x 10^8 IVP/mL in low MOI infections in MDCK.SUS2 cells. This corresponds to an HA titre improvement by a factor of 8, and improvement of cell-specific yields by a factor of 33 compared to the adherent-adapted seed virus. This is clearly an improvement to beforehand observed infection dynamics, titres, and cell-specific yields with the adherent MDCK cell-adapted seed virus.

However, compared to infections with influenza A/PR/8 RKI (Figure 4-50a) this is still lower by a factor 2.6. Also, infection dynamics is delayed by 6–12 h when comparing the adapted influenza Uruguay-like HGR to the A/PR/8 RKI. It would be interesting to additionally test the fourth passage of the Uruguay-like HGR adaptation for propagation in MDCK.SUS2 cells.

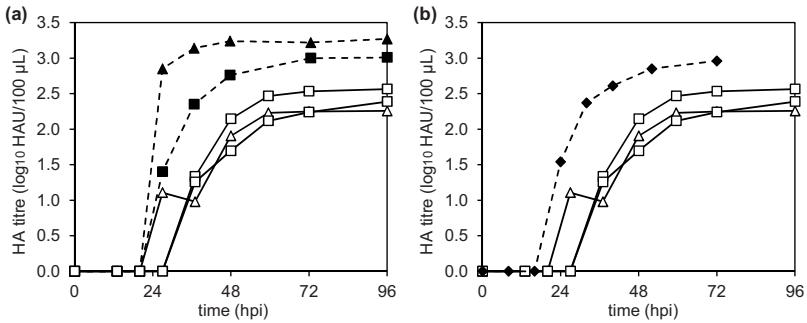

Figure 4-50 Comparison of HA titre time courses of shake flasks infections of MDCK.SUS2 cells with adapted influenza Uruguay-like HGR at MOI 1 x 10^{-5} (open squares: 1:2dil, open triangles: wME) to (a) infections of MDCK.SUS2 cells with influenza A/PR/8 RKI at MOI 1 x 10^{-5} (median of three independent experiments; filled squares: 1:2dil, filled triangles: wME) and to (b) infections of adherent MDCK cells with Uruguay-like HGR (adapted to adherent MDCK cells) at MOI 1 x 10^{-4} in T25-flaks (diamonds).

Finally, despite of the adaptation to the suspension cell line, influenza Uruguay-like HGR still performed better in adherent MDCK cells compared to infections in MDCK.SUS2 cells (Figure 4-50b). HA titre increased 4–12 h earlier in adherent cells and reached titres at least 0.4 $\log_{10}$ HAU/100 µL higher than in MDCK.SUS2 cells. $TCID_{50}$ reached a maximum of 4 x 10^8 IVP/mL in adherent MDCK cell infections, which is higher than the obtained 6 x 10^7 and 1.3 x 10^8 IVP/mL in here shown MDCK.SUS2 cell infections. It has to be noted that adherent MDCK cells in this comparison have been cultivated in a different cultivation system and were infected with a factor 10 higher MOI, which might

influence infection dynamics. A complete direct comparison was not possible in these small vessels as adherent MDCK cells cannot be grown in shake flasks with baffles. Still, comparing cell-specific virus yields adherent MDCK cells replicated the Uruguay-like HGR better than MDCK.SUS2 cells by a factor of 10.

Chu *et al.* (2010) used MDCK-*siat7e* suspension cells that were generated out of CCL-34 MDCK cells for propagation of the Uruguay-like HGR. They performed a low culture volume infection strategy with 10-fold dilution of the culture with fresh medium 1 hpi in shake flaks using MOI 0.01. Maximum HA titre was reached 8 hpi of 8 $\log_2$ HA/50 µL (approx. 2.7 $\log_{10}$ HAU/100 µL), corresponding to approximately 5900 virions/cell and 8 $\log_{10}$ $TCID_{50}$/mL (= 1 x 10^8 IVP/mL). Furthermore, they performed a 2 L stirred tank bioreactor cultivation using a perfusion strategy, thereby achieving a viable cell concentration of 4 x 10^6 cells/mL during 10 days of cell growth. Infection was performed at MOI 0.2 and reached 512 HAU/50 µL (approx. 3 $\log_{10}$ HAU/100 µL). They did not compare these yields to the parental adherent CCL-34 MDCK cell line, but compared it to HA titres obtained in chicken eggs. In that study, they found three of four tested influenza virus strains to yield higher titres in MDCK-*siat7e* cells, with the Uruguay-like HGR being the only one reaching lower titres in MDCK-*siat7e* cells than in chicken eggs.

Nakowitsch *et al.* (2014) investigated the influence of influenza virus propagation in eggs, Vero cells, and MDCK cells and found for influenza A/Uruguay/716/2007 and other H3N2 strains an increased pH threshold of HA conformational change and impaired virus stability. Thus, adaptation of the Uruguay-like HGR is sensitive to the system it is adapted to. This might explain the only moderate titres obtained with the influenza Uruguay-like reassortant in MDCK suspension cells, as the seed virus adaptation potentially influenced virus properties. In-depth analyses would be necessary to clarify whether genetic changes between the original seed virus, adherent MDCK cell-adapted seed virus, and MDCK.SUS2 cell-adapted seed virus are present. However, this was beyond the scope of this work.

An interesting observation is the $TCID_{50}$ time course of the Uruguay-like HGR which showed a very late maximum titre. This is an unusual $TCID_{50}$ time course, as infected cells are thought to first release intact virions, and later in infection mostly defective particles. Furthermore, virus particles become non-infectious through incubation at 37°C and degradation through proteases that are released by lysed cells. Importantly, this late $TCID_{50}$ peak behaviour of the Uruguay-like HGR was not only observed in MDCK.SUS2 cells, but also in adherent MDCK cells (Figure 4-51), and thus seems to be a characteristic of the Uruguay-like reassortant strain. Also in infections of MDCK-*siat7e* cells with influenza Uruguay-like HGR, $TCID_{50}$ and HA titre time courses showed the $TCID_{50}$ to reach its maximum approximately 30 h after the HA titre had reached its plateau (Chu *et al.* 2010),

thus confirming observations with MDCK.SUS2 cells. Further investigation would be necessary to clarify the reasons for this interesting behaviour of the Uruguay-like reassortant but were beyond the scope of this work.

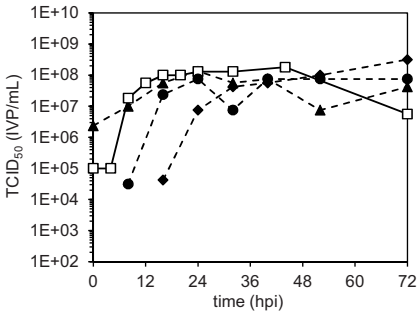

Figure 4-51 Courses of $TCID_{50}$ in infections of adherent MDCK cells with influenza Uruguay-like HGR. Results from MOI 0.05 stirred tank reactor cultivation (open symbols) as well as T25-flask infections (filled symbols) at MOI 0.0001 (diamonds), MOI 0.1 (circles), and MOI 3 (triangles).

As a concluding remark, the protocol used to adapt the Uruguay-like HGR seed virus to MDCK.SUS2 cells is still not optimal. Due to its high limit of detection HA titre increases rather late. Hence, it is not optimal as indicator for the next passage in seed virus adaptation, since maximum of infectious particles is potentially passed over. Concluding, the here found late $TCID_{50}$ peak behaviour makes the Uruguay-like HGR a highly interesting strain for future studies such as further investigations on DIPs and continuous virus cultivations.

5 Summary

Scope of this work was to investigate influenza virus propagation in two MDCK cell lines in terms of infection dynamics and virus-induced apoptosis for an influenza vaccine production process. An overview of most important studies performed in this work is given in Figure 5-1.

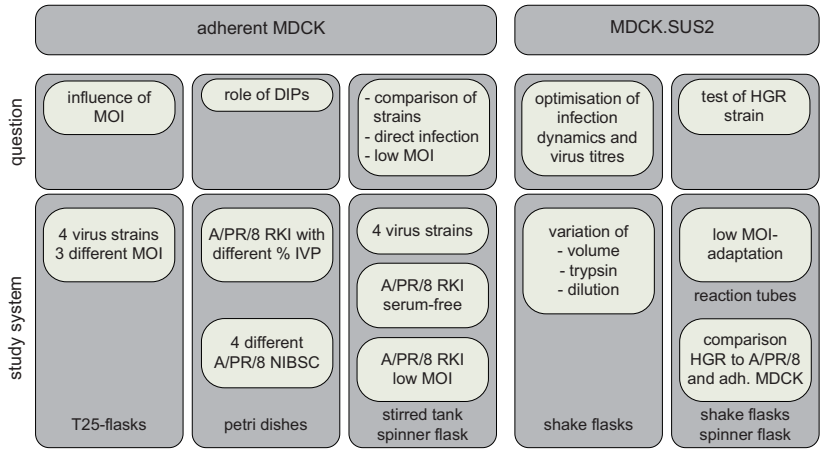

Figure 5-1 Overview of most important studies performed in this work: cell lines used, question addressed, and system chosen.

To extend the range of testable virus strains and to test different MOIs, a large number of experiments are necessary, especially, as due to batch-to-batch variations three repetitions would be eligible. Hence, the use of bioreactor cultivation systems as used in previous studies was not feasible. Thus, a T25-flask-based system which allows to analyse four virus strains or four MOIs in parallel in one experiment was established and demonstrated a good biological variance and reproducibility.

In this T25-flask system, studies on infected and apoptotic cell populations, virus titres, and cell concentration for infection adherent MDCK cells was performed. Therefore, cell were infected with four influenza virus strains (influenza A/PR/8 RKI, A/PR/8 NIBSC, A/Uruguay/716/2007-like HGR, and A/Wisconsin/67/2005-like HGR) at three different MOIs (0.0001, 0.1, and 3). The HGR strains showed an early release of virus particles. Importantly, in infections with the Uruguay-like HGR the highest HA titres of all four tested strains at all three MOIs were obtained. For $TCID_{50}$ courses, the increase in MOI not

only resulted in an earlier increase with lower maximum values, but strains reacted differently. Infections with influenza A/PR/8 NIBSC at MOI 3 showed no increase in $TCID_{50}$, thus no production of infectious virus particles. This corresponded to a 920-fold decrease in infectious particles released per cell compared to MOI 0.0001 infection. Also, flow cytometric analysis of virus-induced apoptosis in A/PR/8 NIBSC infections showed, especially at higher MOI, a strong apoptosis induction. Hence, four influenza virus A strains, that should be identical or differ in maximum in the two surface proteins-coding gene segments, revealed remarkable differences in their behaviour on an increased MOI. In all infections, lower maximum $TCID_{50}$ and lower cell-specific virus yields were reached at high MOI compared to low MOI. Most likely, this is caused by DIPs present in different amounts in the seed virus preparations. Especially in infections with influenza A/PR/8 NIBSC, the seed virus with the lowest content of infectious particles, the most severe drop in $TCID_{50}$ appeared, with no production of infectious virions at MOI 3. Results demonstrated influenza virus strains that show a fast progress in infection combined with a late onset of apoptosis to yield the highest virus titres.

Demonstrating hypotheses on DIPs, a subsequent study with four influenza A/PR/8 NIBSC seed virus preparations containing 5.43×10^6 to 1.00×10^9 IVP/mL (0.22 to 21.33% infectious particles) revealed the high $TCID_{50}$ seed virus to reach much higher $TCID_{50}$ and higher cell-specific virus yields in petri dish infection experiments. In addition, it seemed that the infected non-apoptotic cell population stayed on a higher level till the end of infection. This again confirmed results from the T25-flask study that seed virus composition is of utmost importance. Frensing *et al.* (2014) confirmed the low $TCID_{50}$ A/PR/8 NIBSC seed virus to contain more DIPs than the high $TCID_{50}$ A/PR/8 NIBSC seed virus. In summary, low MOI situations in seed virus generation were demonstrated to be of great importance in order to minimise DIPs.

In stirred tank bioreactor systems, infections of adherent MDCK cells with influenza A/PR/8 RKI and NIBSC showed fewer differences in infection dynamics compared to earlier studies (Schulze-Horsel *et al.* 2009). This is presumably due to a different seed virus stock used and emphasises the importance of using the same seed virus preparation for repetitions of experiments.

A direct infection of adherent MDCK cells grown in serum-free medium showed infection dynamics not to be delayed compared to infections with a medium exchange. Maximum HA titre and $TCID_{50}$ were only slightly lower compared to medium exchange infection. Thus, growth of adherent cells under serum-free conditions was shown to be an attractive alternative to serum-containing process with washing steps and presents an option for process simplification.

Lowering the MOI down to 1 x 10^{-5} resulted in increased maximum $TCID_{50}$, increased percentage of infected cells as well as delayed and reduced apoptosis induction. Thus, results for low MOI infections obtained in T25-flasks were confirmed, and hereby advantages of low MOI infections for infectious virus titres were verified.

As adherent cells are difficult to scale-up, suspension cell lines should be established whenever possible. Here, the MDCK.SUS2 cell line established by K. Scharfenberg (FH Emden/Leer) was chosen for characterisation of influenza virus infection dynamics and virus-induced apoptosis. A first optimisation study to improve infection dynamics and virus titres—including medium supplementation, trypsin activity, and cell concentration at toi—failed. However, a medium exchange at toi resulted in an earlier increase in HA titre by at least 12 h. As a medium exchange is relatively cumbersome for suspension cells, other options for infections were investigated, and a 1:2dil of the culture broth at toi was identified to result in an HA titre increase only slightly later than with a medium exchange. Thus, 1:2dil at toi was demonstrated to be a good compromise to improve infection dynamics in MDCK.SUS2 cells without a laborious medium exchange step.

A study on shake flask infections of MDCK.SUS2 cells with influenza A/PR/8 RKI at MOI 1 x 10^{-5} confirmed 1:2dil at toi to be only few hours delayed compared to infection with medium exchange. In addition, flow cytometry confirmed an only slightly slower infection dynamic for 1:2dil compared to wME infections. Importantly, w/o infections showed a significant larger population of apoptotic uninfected cells, reflecting the bad viability of the culture. Hence, 1:2dil infection strategy was identified to be an effective way for improvement of infection dynamics.

Transfer of the optimised infection conditions of 1:2dil and MOI 1 x 10^{-5} to a stirred tank bioreactor system showed an almost complete infection (90% infected non-apoptotic cells) at 36 hpi. Final HA titre was 2.94 $\log_{10}$ HAU/100 µL (11411 virions/cell), and maximum $TCID_{50}$ was 1 x 10^{9} IVP/mL. Thus, titres and yields were improved to first w/oME cultivations at MOI 0.025 in which an HA titre of 2.15 $\log_{10}$ HAU/100 µL (819 virions/cell) and 1 x 10^{8} IVP/mL had been obtained. However, compared to titres and yields of infections in adherent MDCK cells (final HA titre: 3.33 $\log_{10}$ HAU/100 µL, maximum $TCID_{50}$: 1.33 x 10^{9} IVP/mL) there is still optimisation potential, which will be discussed in the outlook.

Propagation of the influenza Uruguay-like HGR strain in MDCK.SUS2 cells in shake flasks showed very late increase and low final HA titres. Through the use of a low MOI, maximum HA titre of 2.57 $\log_{10}$ HAU/100 µL and maximum $TCID_{50}$ of 1.3 x 10^{8} IVP/mL were obtained, together with an earlier increase in infected cells. Despite these improved yields, titres obtained with influenza A/PR/8 RKI in MDCK.SUS2 cells were still higher, as were yields with the Uruguay-like HGR in adherent MDCK cells.

Concluding, this work contributes to the understanding of influenza virus infections of host cells by characterising infection dynamics and virus-induced apoptosis. The influence of MOI, characteristics of high titre yielding virus strains, the role of DIPs, and differences between adherent and suspension MDCK cells were identified. Thereby, options for optimisation of upstream processing were disclosed, with special respect to industrial application and improvement of viral yields.

6 Outlook

In this work four different influenza virus A strains were used for infection experiments characterising virus titres, infection dynamics, and virus-induced apoptosis. Expanding investigations on more influenza virus strains such as vaccine-relevant strains from the B lineage can help to deepen the understanding of virus propagation in cell culture for vaccine production. Also, strains that were problematic in MDCK cell-adaptation would be worthy to be analysed for infection dynamics and virus-induced apoptosis (eventually before and after low MOI adaptation) to reveal characteristics of low yield influenza virus strains.

Results gained in this work emphasised the influence of seed virus quality on infection outcome and highlighted the beneficial effect of low MOI conditions on infectious virus yields. One consequence is to reduce the MOI used for bioreactor infections experiments in the bioprocess engineering group from 0.025 to levels below 1 x 10^{-4}. The second consequence is the revision of the previously performed seed virus generation protocol using a volume-based adaptation with potential high MOI situations. Instead, a low MOI protocol such as used for adaptation of the influenza Uruguay-like HGR to MDCK.SUS2 cells would be recommendable for seed virus adaptations. Although it is more laborious, the high dilutions guarantee low MOI situations, thereby resulting in high $TCID_{50}$ seed virus preparations with low contents of DIPs. In addition, the question to quantify proportions of DIPs in seed virus stocks used in this work remains to be answered, as it would help to obtain a better inside on seed virus quality for previously performed infection experiments. Performing a PCR as described by Frensing *et al.* (2014) is a step in that direction. Of course, a detailed analysis of seed virus composition comprising several virus particle species (refer to Marcus *et al.* 2009) would be very interesting and could help to further understand background of good and poor seed virus preparations. In addition, as the influenza Uruguay-like HGR showed an interesting behaviour in terms of $TCID_{50}$ time courses it would be interesting to include this strain in future studies on DIPs formation and continuous virus cultivation.

MDCK.SUS2 cells were shown to be a promising substrate for influenza virus propagation. However, as only two different influenza virus strains were characterised in this work, further strains should be tested for their performance in MDCK.SUS2 cells to confirm and extend their suitability for influenza virus propagation. In addition, it would be interesting to compare MDCK.SUS2 cells to other suspension cells. A comparison of MDCK.SUS2 cells to other MDCK suspension cell lines would be of special interest to see how prominent virus-induced apoptosis is in other MDCK cell lines adapted to growth in

suspension. Furthermore, new reactor designs like ATF or hollow fibre bioreactors were shown to be able to improve cell-specific yields (Genzel *et al.* 2014b; Tapia *et al.* 2014) and should be further tested for influenza virus propagation in MDCK.SUS2 cells. Also, further medium additives able to eventually reduce cell agglomerates (e.g. EDTA) should be tested for improvement of cell-specific virus yield in MDCK.SUS2 cells.

In addition, new technologies like image stream flow cytometry should be included in future studies on influenza virus infection dynamics and apoptosis, as this method allows addressing further questions: through an increased number of detector channels and additional lasers for excitation more complex simultaneous stainings are possible. This enables evaluation of additional features such as necrosis, other cellular factors, or viral M1 proteins. M1 detection was already tested for analysis in an Epics XL cytometer, however, discrimination of M1-positive from M1-negative cells did not work well (Schulze-Horsel 2011). Using new cytometers with higher sensitivity, M1 staining should be tested again, as models on influenza virus replication emphasised the regulatory role of M1 in viral RNA synthesis. Additionally, image stream flow cytometry offers information on localisation of target molecules within the cell enabling co-localisation studies. Thereby, information on special distribution, e.g. of viral components, can be gained that are not accessible with conventional flow cytometry, thereby supporting a deeper understanding of molecular processes of virus replication and spreading. Also, the expansion of flow cytometry to single-cell tracking was described by Sitton and Srienc (2011). They showed this technique to be applicable for analysis of drug export in human cancer cells and measurement of yeast cells expressing a mutant of the green fluorescent protein. Such a reversing flow cytometer enables acquisition of data on changes of single-cell rates. These kinds of data sets are highly interesting for mathematical modelling, e.g. determination of NP-fluorescence distributions on the single-cell level would enable calculation of NP accumulation rates on the single-cell level.

Bringing together experimental data and mathematical models showed already great potential but may even be further improved. Models established by Heldt *et al.* (2013) and Müller *et al.* (2013) gave already hints towards bottlenecks in virus replication and propagation. Experiments testing different anti-viral drugs proposed by the model of Heldt *et al.* (2013) could be performed to verify the model's predictivity of effects on virus titres. For the single-cell model (Heldt *et al.* 2012) intracellular factors influencing apoptosis are of special interest. The single influencing factors can best be determined by perturbation experiments like infection in cells with knocked-down of RIG-I or treated with apoptosis inhibitors. Alternatively, other proteins (like viral M1 (see paragraph above)) and also viral RNAs, which are linked by the model to the apoptosis influencing factors, could be measured to test the underlying hypotheses of the model. In addition, the knowledge of deviations (e.g. of NP-fluorescence) in single cells can also be used for population balance

modelling. Here, experiments analysing the behaviour of many single cells may enable conclusions on the population behaviour.

From an experimental point of view, models able to display effects of medium exchange conditions would be desirable to help finding optimal infection strategies. The simulation model by Heldt *et al.* (2013) predicted that most cells die before the end of the productive phase. Therefore, models on cell metabolism, similar to those published by Ritter *et al.* (2010) and Rehberg *et al.* (2014), could suggest medium supplementation or substrate dosage strategies in order to improve cell viability (e.g. of MDCK.SUS2 cells) thereby eventually delaying apoptosis and prolonging productive lifetime of the cells finally resulting in increased virus release. Furthermore, transport of virions differs in static and dynamic cell culture systems influencing onset of infection dynamics. To investigate this, models on flow conditions in cell culture vessels (Oncül *et al.* 2010) could be combined with models on virus release and virus spreading, thereby helping to understand delays in the onset of infection between static and dynamic cultivation systems. All above mentioned models would help to reduce number of laborious and cost-intensive experiments enabling more target-oriented experiment design.

Concluding, this thesis is a valuable contribution to the understanding of virus replication, virus-host cell interaction, and optimisation of upstream processing. Collaborations between modellers and experimenters may enhance both the models as well as design of experiments, and thereby even further improve the understanding of influenza virus propagation in cell culture.

7 Lists and bibliography

7.1 List of figures

7.2 List of tables

7.3 Bibliography

Adar Y, Singer Y, Levi R, Tzehoval E, Perk S, Banet-Noach C, Nagar S, Arnon R, Ben-Yedidia T. 2009. A universal epitope-based influenza vaccine and its efficacy against H5N1. *Vaccine* **27**: 2099–2107.

Aggarwal K, Jing F, Maranga L, Liu J. 2011. Bioprocess optimization for cell culture based influenza vaccine production. *Vaccine* **29**: 3320–3328.

Aguilar-Yáñez JM, Portillo-Lara R, Mendoza-Ochoa GI, García-Echauri SA, López-Pacheco F, Bulnes-Abundis D, Salgado-Gallegos J, Lara-Mayorga IM, Webb-Vargas Y, León-Angel FO, et al. 2010. An influenza A/H1N1/2009 hemagglutinin vaccine produced in Escherichia coli. *PloS One* **5**: e11694.

Ambrose CS, Levin MJ. 2012. The rationale for quadrivalent influenza vaccines. *Human Vaccines & Immunotherapeutics* **8**: 81–88.

An Y, Rininger JA, Jarvis DL, Jing X, Ye Z, Aumiller JJ, Eichelberger M, Cipollo JF. 2013. Comparative glycomics analysis of influenza Hemagglutinin (H5N1) produced in vaccine relevant cell platforms. *Journal of Proteome Research* **12**: 3707–3720.

Arden N, Betenbaugh MJ. 2004. Life and death in mammalian cell culture: strategies for apoptosis inhibition. *Trends in Biotechnology* **22**: 174–180.

Arden N, Betenbaugh MJ. 2006. Regulating apoptosis in mammalian cell cultures. *Cytotechnology* **50**: 77–92.

Arif B, Pavlik L. 2013. Insect cell culture: Virus replication and applications in biotechnology. *Journal of Invertebrate Pathology* **112**: S138–S141.

Arriaga EA. 2009. Determining biological noise via single cell analysis. *Analytical and Bioanalytical Chemistry* **393**: 73–80.

Baez M, Palese P, Kilbourne ED. 1980. Gene composition of high-yielding influenza vaccine strains obtained by recombination. *The Journal of Infectious Diseases* **141**: 362–365.

Balachandran S, Roberts PC, Kipperman T, Bhalla KN, Compans RW, Archer DR, Barber GN. 2000. Alpha/beta interferons potentiate virus-induced apoptosis through activation of the FADD/Caspase-8 death signaling pathway. *Journal of Virology* **74**: 1513–1523.

Barrett PN, Portsmouth D, Ehrlich HJ. 2013. Vero cell culture-derived pandemic influenza vaccines: preclinical and clinical development. *Expert Review of Vaccines* **12**: 395–413.

Baum A, Sachidanandam R, García-Sastre A. 2010. Preference of RIG-I for short viral RNA molecules in infected cells revealed by next-generation sequencing. *Proceedings of the National Academy of Sciences of the United States of America* **107**: 16303–16308.

Bedner E, Smolewski P, Amstad P, Darzynkiewicz Z. 2000. Activation of caspases measured in situ by binding of fluorochrome-labeled inhibitors of caspases (FLICA): correlation with DNA fragmentation. *Experimental Cell Research* **259**: 308–313.

Bier M, Nord FF, Terminiello L. 1956. On the mechanism of enzyme action. LXI. The self digestion of trypsin, calcium-trypsin and acetyltrypsin. *Archives of Biochemistry and Biophysics* **65**: 120–131.

Bock A, Sann H, Schulze-Horsel J, Genzel Y, Reichl U, Möhler L. 2009. Growth behavior of number distributed adherent MDCK cells for optimization in microcarrier cultures. *Biotechnology Progress* **25**: 1717–1731.

Bock A, Schulze-Horsel J, Schwarzer J, Rapp E, Genzel Y, Reichl U. 2011. High-density microcarrier cell cultures for influenza virus production. *Biotechnology Progress* **27**: 241–250.

Brands R, Visser J, Medema J, Palache AM, van Scharrenburg GJ. 1999. Influvac: a safe Madin Darby Canine Kidney (MDCK) cell culture-based influenza vaccine. *Developments in Biological Standardization* **98**: 93–100; discussion 111.

Brooke CB, Ince WL, Wrammert J, Ahmed R, Wilson PC, Bennink JR, Yewdell JW. 2013. Most influenza a virions fail to express at least one essential viral protein. *Journal of Virology* **87**: 3155–3162.

Brown SW, Mehtali M. 2010. The Avian EB66(R) Cell Line, Application to Vaccines, and Therapeutic Protein Production. *PDA Journal of Pharmaceutical Science and Technology / PDA* **64**: 419–425.

Carinhas N, Bernal V, Yokomizo AY, Carrondo MJT, Oliveira R, Alves PM. 2009. Baculovirus production for gene therapy: the role of cell density, multiplicity of infection and medium exchange. *Applied Microbiology and Biotechnology* **81**: 1041–1049.

Chaïbi C, Cotte-Laffitte J, Sandré C, Esclatine A, Servin AL, Quéro A-M, Géniteau-Legendre M. 2005. Rotavirus induces apoptosis in fully differentiated human intestinal Caco-2 cells. *Virology* **332**: 480–490.

Chan CY-Y, Tambyah PA. 2012. Preflucel®: a Vero-cell culture-derived trivalent influenza vaccine. *Expert Review of Vaccines* **11**: 759–773.

Chen H, Yuan H, Gao R, Zhang J, Wang D, Xiong Y, Fan G, Yang F, Li X, Zhou J, et al. 2014. Clinical and epidemiological characteristics of a fatal case of avian influenza A H10N8 virus infection: a descriptive study. *Lancet* **383**: 714–721.

Chen W, Calvo PA, Malide D, Gibbs J, Schubert U, Bacik I, Basta S, O'Neill R, Schickli J, Palese P, et al. 2001. A novel influenza A virus mitochondrial protein that induces cell death. *Nature Medicine* **7**: 1306–1312.

Chou Y, Vafabakhsh R, Doğanay S, Gao Q, Ha T, Palese P. 2012. One influenza virus particle packages eight unique viral RNAs as shown by FISH analysis. *Proceedings of the National Academy of Sciences of the United States of America* **109**: 9101–9106.

Christensen ME, Jansen ES, Sanchez W, Waterhouse NJ. 2013. Flow cytometry based assays for the measurement of apoptosis-associated mitochondrial membrane depolarisation and cytochrome c release. *Methods (San Diego, Calif.)* **61**: 138–145.

Chu C, Lugovtsev V, Golding H, Betenbaugh M, Shiloach J. 2009. Conversion of MDCK cell line to suspension culture by transfecting with human siat7e gene and its application for influenza virus production. *Proceedings of the National Academy of Sciences of the United States of America* **106**: 14802–14807.

Chu C, Lugovtsev V, Lewis A, Betenbaugh M, Shiloach J. 2010. Production and antigenic properties of influenza virus from suspension MDCK-siat7e cells in a bench-scale bioreactor. *Vaccine* **28**: 7193–7201.

Coombs KM, Berard A, Xu W, Krokhin O, Meng X, Cortens JP, Kobasa D, Wilkins J, Brown EG. 2010. Quantitative proteomic analyses of influenza virus-infected cultured human lung cells. *Journal of Virology* **84**: 10888–10906.

Cox MMJ, Hashimoto Y. 2011. A fast track influenza virus vaccine produced in insect cells. *Journal of Invertebrate Pathology* **107 Suppl**: S31–41.

Cox MMJ, Hollister JR. 2009. FluBlok, a next generation influenza vaccine manufactured in insect cells. *Biologicals: Journal of the International Association of Biological Standardization* **37**: 182–189.

Cox RJ, Madhun AS, Hauge S, Sjursen H, Major D, Kuhne M, Höschler K, Saville M, Vogel FR, Barclay W, et al. 2009. A phase I clinical trial of a PER.C6 cell grown influenza H7 virus vaccine. *Vaccine* **27**: 1889–1897.

Crucell. 2014. Influenza Seasonal Vaccine. http://www.crucell.com/R_AND_D_CLINICAL_DEVELOPMENT_EP.HTM (accessed 2014-10-17).

Davis AR, Nayak DP. 1979. Sequence relationships among defective interfering influenza viral RNAs. *Proceedings of the National Academy of Sciences of the United States of America* **76**: 3092–3096.

Dimmock NJ. 2008. Defective interfering virus. WO 2007/135420 A3.

Dimmock NJ, Dove BK, Scott PD, Meng B, Taylor I, Cheung L, Hallis B, Marriott AC, Carroll MW, Easton AJ. 2012. Cloned defective interfering influenza virus protects ferrets from pandemic 2009 influenza A virus and allows protective immunity to be established. *PloS One* **7**: e49394.

Dimmock NJ, Easton AJ. 2014. Defective interfering influenza virus RNAs: time to re-evaluate their clinical potential as broad spectrum antivirals? *Journal of Virology* **88**: 5217–5227.

Doroshenko A, Halperin SA. 2009. Trivalent MDCK cell culture-derived influenza vaccine Optaflu (Novartis Vaccines). *Expert Review of Vaccines* **8**: 679–688.

Du L, Zhou Y, Jiang S. 2010. Research and development of universal influenza vaccines. *Microbes and Infection / Institut Pasteur* **12**: 280–286.

Dürr R, Müller T, Isken B, Schulze-Horsel J, Reichl U, Kienle A. 2012. Distributed modeling and parameter estimation of influenza virus replication during vaccine production. In *MATHMOD 2012 – full paper reprint volume*, Inge T, Breitenecker F (eds). Vienna; 320–325.

Ehrhardt C, Marjuki H, Wolff T, Nürnberg B, Planz O, Pleschka S, Ludwig S. 2006. Bivalent role of the phosphatidylinositol-3-kinase (PI3K) during influenza virus infection and host cell defence. *Cellular Microbiology* **8**: 1336–1348.

Ehrhardt C, Wolff T, Pleschka S, Planz O, Beermann W, Bode JG, Schmolke M, Ludwig S. 2007. Influenza A virus NS1 protein activates the PI3K/Akt pathway to mediate antiapoptotic signaling responses. *Journal of Virology* **81**: 3058–3067.

Elmore S. 2007. Apoptosis: a review of programmed cell death. *Toxicologic Pathology* **35**: 495–516.

Van Engeland M, Nieland LJ, Ramaekers FC, Schutte B, Reutelingsperger CP. 1998. Annexin V-affinity assay: a review on an apoptosis detection system based on phosphatidylserine exposure. *Cytometry* **31**: 1–9.

Erlanger BF, Kokowsky N, Cohen W. 1961. The preparation and properties of two new chromogenic substrates of trypsin. *Archives of Biochemistry and Biophysics* **95**: 271–278.

FDA. 2013. FDA approves new seasonal influenza vaccine made using novel technology. http://www.fda.gov/NewsEvents/Newsroom/PressAnnouncements/ucm335891.htm (accessed: 2014-08-16).

Feng S-Z, Jiao P-R, Qi W-B, Fan H-Y, Liao M. 2011. Development and strategies of cell-culture technology for influenza vaccine. *Applied Microbiology and Biotechnology* **89**: 893–902.

Fernandes F, Teixeira AP, Carinhas N, Carrondo MJT, Alves PM. 2013. Insect cells as a production platform of complex virus-like particles. *Expert Review of Vaccines* **12**: 225–236.

Figueroa B Jr, Ailor E, Osborne D, Hardwick JM, Reff M, Betenbaugh MJ. 2007. Enhanced cell culture performance using inducible anti-apoptotic genes E1B-19K and Aven in the production of a monoclonal antibody with Chinese hamster ovary cells. *Biotechnology and Bioengineering* **97**: 877–892.

Filip AA, Ciseł B, Wąsik-Szczepanek E. 2013. Guilty bystanders: nurse-like cells as a model of microenvironmental support for leukemic lymphocytes. *Clinical and Experimental Medicine* **15**: 73–83.

Frensing T, Heldt FS, Pflugmacher A, Behrendt I, Jordan I, Flockerzi D, Genzel Y, Reichl U. 2013. Continuous influenza virus production in cell culture shows a periodic accumulation of defective interfering particles. *PloS One* **8**: e72288.

Frensing T, Pflugmacher A, Bachmann M, Peschel B, Reichl U. 2014. Impact of defective interfering particles on virus replication and antiviral host response in cell culture-based influenza vaccine production. *Applied Microbiology and Biotechnology* **98**: 8999–9008.

Frisch SM, Francis H. 1994. Disruption of epithelial cell-matrix interactions induces apoptosis. *The Journal of Cell Biology* **124**: 619–626.

Gannagé M, Dormann D, Albrecht R, Dengjel J, Torossi T, Rämer PC, Lee M, Strowig T, Arrey F, Conenello G, et al. 2009. Matrix protein 2 of influenza A virus blocks autophagosome fusion with lysosomes. *Cell Host & Microbe* **6**: 367–380.

García-Sastre A, Schmolke M. 2014. Avian influenza A H10N8--a virus on the verge? *Lancet* **383**: 676–677.

Gaur P, Ranjan P, Sharma S, Patel JR, Bowzard JB, Rahman SK, Kumari R, Gangappa S, Katz JM, Cox NJ, et al. 2012. Influenza A virus neuraminidase protein enhances cell survival through interaction with carcinoembryonic antigen-related cell adhesion molecule 6 (CEACAM6) protein. *The Journal of Biological Chemistry* **287**: 15109–15117.

Gaush CR, Smith TF. 1968. Replication and plaque assay of influenza virus in an established line of canine kidney cells. *Applied Microbiology* **16**: 588–594.

Gavina M, Za L, Molteni R, Pardi R, de Curtis I. 2010. The GIT-PIX complexes regulate the chemotactic response of rat basophilic leukaemia cells. *Biology of the Cell / Under the Auspices of the European Cell Biology Organization* **102**: 231–244.

Gavrieli Y, Sherman Y, Ben-Sasson SA. 1992. Identification of programmed cell death in situ via specific labeling of nuclear DNA fragmentation. *The Journal of Cell Biology* **119**: 493–501.

Genzel Y, Behrendt I, König S, Sann H, Reichl U. 2004. Metabolism of MDCK cells during cell growth and influenza virus production in large-scale microcarrier culture. *Vaccine* **22**: 2202–2208.

Genzel Y, Behrendt I, Rödig J, Rapp E, Kueppers C, Kochanek S, Schiedner G, Reichl U. 2013. CAP, a new human suspension cell line for influenza virus production. *Applied Microbiology and Biotechnology* **97**: 111–122.

Genzel Y, Dietzsch C, Rapp E, Schwarzer J, Reichl U. 2010. MDCK and Vero cells for influenza virus vaccine production: a one-to-one comparison up to lab-scale bioreactor cultivation. *Applied Microbiology and Biotechnology* **88**: 461–475.

Genzel Y, Fischer M, Reichl U. 2006a. Serum-free influenza virus production avoiding washing steps and medium exchange in large-scale microcarrier culture. *Vaccine* **24**: 3261–3272.

Genzel Y, Olmer RM, Schäfer B, Reichl U. 2006b. Wave microcarrier cultivation of MDCK cells for influenza virus production in serum containing and serum-free media. *Vaccine* **24**: 6074–6087.

Genzel Y, Reichl U. 2009. Continuous cell lines as a production system for influenza vaccines. *Expert Review of Vaccines* **8**: 1681–1692.

Genzel Y, Ritter JB, König S, Alt R, Reichl U. 2005. Substitution of glutamine by pyruvate to reduce ammonia formation and growth inhibition of mammalian cells. *Biotechnology Progress* **21**: 58–69.

Genzel Y, Rödig J, Rapp E, Reichl U. 2014a. Vaccine production: upstream processing with adherent or suspension cell lines. In *Animal Cell Biotechnology: Methods and Protocols*, Pörtner R (ed). Springer Science+Business; 371–393.

Genzel Y, Vogel T, Buck J, Behrendt I, Ramirez DV, Schiedner G, Jordan I, Reichl U. 2014b. High cell density cultivations by alternating tangential flow (ATF) perfusion for influenza A virus production using suspension cells. *Vaccine* **32**: 2770–2781.

Gerdil C. 2003. The annual production cycle for influenza vaccine. *Vaccine* **21**: 1776–1779.

Glacken MW, Fleischaker RJ, Sinskey AJ. 1986. Reduction of waste product excretion via nutrient control: Possible strategies for maximizing product and cell yields on serum in cultures of mammalian cells. *Biotechnology and Boengineering* **28**: 1376–1389.

Govorkova EA, Murti G, Meignier B, de Taisne C, Webster RG. 1996. African green monkey kidney (Vero) cells provide an alternative host cell system for influenza A and B viruses. *Journal of Virology* **70**: 5519–5524.

Gregersen J-P, Schmitt H-J, Trusheim H, Bröker M. 2011. Safety of MDCK cell culture-based influenza vaccines. *Future Microbiology* **6**: 143–152.

Hacker DL, De Jesus M, Wurm FM. 2009. 25 years of recombinant proteins from reactor-grown cells – where do we go from here? *Biotechnology Advances* **27**: 1023–1027.

Hale BG, Jackson D, Chen Y-H, Lamb RA, Randall RE. 2006. Influenza A virus NS1 protein binds p85beta and activates phosphatidylinositol-3-kinase signaling. *Proceedings of the National Academy of Sciences of the United States of America* **103**: 14194–14199.

Hamamoto I, Takaku H, Tashiro M, Yamamoto N. 2013. High yield production of influenza virus in Madin Darby canine kidney (MDCK) cells with stable knockdown of IRF7. *PloS One* **8**: e59892.

Hatada E, Saito S, Fukuda R. 1999. Mutant influenza viruses with a defective NS1 protein cannot block the activation of PKR in infected cells. *Journal of Virology* **73**: 2425–2433.

He B. 2006. Viruses, endoplasmic reticulum stress, and interferon responses. *Cell Death and Differentiation* **13**: 393–403.

Heldt FS, Frensing T, Pflugmacher A, Gröpler R, Peschel B, Reichl U. 2013. Multiscale modeling of influenza A virus infection supports the development of direct-acting antivirals. *PLoS Computational Biology* **9**: e1003372.

Heldt FS, Frensing T, Reichl U. 2012. Modeling the intracellular dynamics of influenza virus replication to understand the control of viral RNA synthesis. *Journal of Virology* **86**: 7806–7817.

Herold S, Ludwig S, Pleschka S, Wolff T. 2012. Apoptosis signaling in influenza virus propagation, innate host defense, and lung injury. *Journal of Leukocyte Biology* **92**: 75–82.

Hess RD, Weber F, Watson K, Schmitt S. 2012. Regulatory, biosafety and safety challenges for novel cells as substrates for human vaccines. *Vaccine* **30**: 2715–2727.

Heynisch B. 2013. Impact of innate immunity of MDCK cells on virus replication in an influenza vaccine production process. In *Forschungsberichte aus dem Max-Planck-Institut für Dynamik komplexer technischer Systeme.* Shaker Verlag, Aachen.

Heynisch B, Frensing T, Heinze K, Seitz C, Genzel Y, Reichl U. 2010. Differential activation of host cell signalling pathways through infection with two variants of influenza A/Puerto Rico/8/34 (H1N1) in MDCK cells. *Vaccine* **28**: 8210–8218.

Hinshaw VS, Olsen CW, Dybdahl-Sissoko N, Evans D. 1994. Apoptosis: a mechanism of cell killing by influenza A and B viruses. *Journal of Virology* **68**: 3667–3673.

Hoffmann E, Krauss S, Perez D, Webby R, Webster RG. 2002. Eight-plasmid system for rapid generation of influenza virus vaccines. *Vaccine* **20**: 3165–3170.

Hornícková Z. 1997. Different progress of MDCK cell death after infection by two different influenza virus isolates. *Cell Biochemistry and Function* **15**: 87–93.

Hütter J, Rödig JV, Höper D, Seeberger PH, Reichl U, Rapp E, Lepenies B. 2013. Toward animal cell culture-based influenza vaccine design: viral hemagglutinin N-glycosylation markedly impacts immunogenicity. *Journal of Immunology (Baltimore, Md.: 1950)* **190**: 220–230.

IFPMA. 2013. Influenza vaccine research and development. http://www.ifpma.org/resources/influenza-vaccines/influenza-vaccines-rd/about-influenza-vaccine-rd.html (accessed: 2013-08-29).

Ikeda H, Kato K, Suzuki T, Kitani H, Matsubara Y, Takase-Yoden S, Watanabe R, Kitagawa M, Aizawa S. 2000. Properties of the naturally occurring soluble surface glycoprotein of ecotropic murine leukemia virus: binding specificity and possible conformational change after binding to receptor. *Journal of Virology* **74**: 1815–1826.

Isken B, Genzel Y, Reichl U. 2012. Productivity, apoptosis, and infection dynamics of influenza A/PR/8 strains and A/PR/8-based reassortants. *Vaccine* **30**: 5253–5261.

Isken B, Schulze-Horsel J, Bock A, Genzel Y, Reichl U. 2009. Monitoring of host-cell infection and virus-induced apoptosis in influenza vaccine production. In *Proceedings of the 21st Annual Meeting of the European Society for Animal Cell Technology (ESACT)*, Jenkins N, Barron N, Alves P (eds). Springer Netherlands; 675–683.

Jagger BW, Wise HM, Kash JC, Walters K-A, Wills NM, Xiao Y-L, Dunfee RL, Schwartzman LM, Ozinsky A, Bell GL, et al. 2012. An overlapping protein-coding region in influenza A virus segment 3 modulates the host response. *Science (New York, N.Y.)* **337**: 199–204.

Jakeman KJ, Smith H, Sweet C. 1991. Influenza virus enhancement of membrane leakiness induced by staphylococcal alpha toxin, diphtheria toxin and streptolysin S. *The Journal of General Virology* **72 (Pt 1)**: 111–115.

Jayapal KR, Wlaschin KF, Hu W-S, Yap MG. 2007. Recombinant protein therapeutics from CHO cells – 20 years and counting. *Chemical Engineering Progress* **103**: 40–47.

Jayaraman S. 2003. Intracellular determination of activated caspases (IDAC) by flow cytometry using a pancaspase inhibitor labeled with FITC. *Cytometry. Part A: The Journal of the International Society for Analytical Cytology* **56**: 104–112.

Jendrossek V, Handrick R, Belka C. 2003. Celecoxib activates a novel mitochondrial apoptosis signaling pathway. *FASEB Journal: Official Publication of the Federation of American Societies for Experimental Biology* **17**: 1547–1549.

Jenkins N, Barron N, Alves P (Eds.). 2012. Proceedings of the 21st Annual Meeting of the European Society for Animal Cell Technology (ESACT), Dublin, Ireland, June 7-10, 2009. Springer Netherlands: Dordrecht.

Kalbfuss B, Knöchlein A, Kröber T, Reichl U. 2008. Monitoring influenza virus content in vaccine production: precise assays for the quantitation of hemagglutination and neuraminidase activity. *Biologicals: Journal of the International Association of Biological Standardization* **36**: 145–161.

Kalmbach A, Bordás R, Oncül AA, Thévenin D, Genzel Y, Reichl U. 2011. Experimental characterization of flow conditions in 2- and 20-L bioreactors with wave-induced motion. *Biotechnology Progress* **27**: 402–409.

Kaufmann SH, Desnoyers S, Ottaviano Y, Davidson NE, Poirier GG. 1993. Specific proteolytic cleavage of poly(ADP-ribose) polymerase: an early marker of chemotherapy-induced apoptosis. *Cancer Research* **53**: 3976–3985.

Kaverin NV, Webster RG. 1995. Impairment of multicycle influenza virus growth in Vero (WHO) cells by loss of trypsin activity. *Journal of Virology* **69**: 2700–2703.

Kawabata S, Miura T, Morita T, Kato H, Fujikawa K, Iwanaga S, Takada K, Kimura T, Sakakibara S. 1988. Highly sensitive peptide-4-methylcoumaryl-7-amide substrates for blood-clotting proteases and trypsin. *European Journal of Biochemistry / FEBS* **172**: 17–25.

Keating GM, Plosker GL, Lyseng-Williamson KA. 2012. A/H5N1 prepandemic influenza vaccine (Vepacel®): a guide to its use. *BioDrugs: Clinical Immunotherapeutics, Biopharmaceuticals and Gene Therapy* **26**: 425–430.

Kelso JM. 2014. Administering influenza vaccine to egg-allergic persons. *Expert Review of Vaccines* **13**: 1049–1057.

Kerr JF, Wyllie AH, Currie AR. 1972. Apoptosis: a basic biological phenomenon with wide-ranging implications in tissue kinetics. *British Journal of Cancer* **26**: 239–257.

Kilbourne ED. 1969. Future influenza vaccines and the use of genetic recombinants. *Bulletin of the World Health Organization* **41**: 643–645.

Kilbourne ED, Schulman JL, Schild GC, Schloer G, Swanson J, Bucher D. 1971. Related studies of a recombinant influenza-virus vaccine. I. Derivation and characterization of virus and vaccine. *The Journal of Infectious Diseases* **124**: 449–462.

Kistner O, Barrett PN, Mundt W, Reiter M, Schober-Bendixen S, Dorner F. 1998. Development of a mammalian cell (Vero) derived candidate influenza virus vaccine. *Vaccine* **16**: 960–968.

Klenk HD, Rott R, Orlich M, Blödorn J. 1975. Activation of influenza A viruses by trypsin treatment. *Virology* **68**: 426–439.

Knipe DM, Howley PM. 2013. *Fields virology*. Wolters Kluwer/Lippincott Williams & Wilkins Health: Philadelphia, PA.

Koudstaal W, Hartgroves L, Havenga M, Legastelois I, Ophorst C, Sieuwerts M, Zuijdgeest D, Vogels R, Custers J, de Boer-Luijtze E, et al. 2009. Suitability of PER.C6 cells to generate epidemic and pandemic influenza vaccine strains by reverse genetics. *Vaccine* **27**: 2588–2593.

Krumbholz A, Philipps A, Oehring H, Schwarzer K, Eitner A, Wutzler P, Zell R. 2011. Current knowledge on PB1-F2 of influenza A viruses. *Medical Microbiology and Immunology* **200**: 69–75.

Kurokawa M, Koyama AH, Yasuoka S, Adachi A. 1999. Influenza virus overcomes apoptosis by rapid multiplication. *International Journal of Molecular Medicine* **3**: 527–530.

Kuzelová K, Grebenová D, Hrkal Z. 2007. Labeling of apoptotic JURL-MK1 cells by fluorescent caspase-3 inhibitor FAM-DEVD-fmk occurs mainly at site(s) different from caspase-3 active site. *Cytometry. Part A: The Journal of the International Society for Analytical Cytology* **71**: 605–611.

Langlois RA, Legge KL. 2010. Plasmacytoid dendritic cells enhance mortality during lethal influenza infections by eliminating virus-specific CD8 T cells. *Journal of Immunology (Baltimore, Md.: 1950)* **184**: 4440–4446.

Lasunskaia EB, Fridlianskaia II, Darieva ZA, da Silva MSR, Kanashiro MM, Margulis BA. 2003. Transfection of NS0 myeloma fusion partner cells with HSP70 gene results in higher hybridoma yield by improving cellular resistance to apoptosis. *Biotechnology and Bioengineering* **81**: 496–504.

Le Ru A, Jacob D, Transfiguracion J, Ansorge S, Henry O, Kamen AA. 2010. Scalable production of influenza virus in HEK-293 cells for efficient vaccine manufacturing. *Vaccine* **28**: 3661–3671.

Lee M-S, Hu AY-C. 2012. A cell-based backup to speed up pandemic influenza vaccine production. *Trends in Microbiology* **20**: 103–105.

Legge KL, Braciale TJ. 2005. Lymph node dendritic cells control CD8+ T cell responses through regulated FasL expression. *Immunity* **23**: 649–659.

Li J, Arévalo MT, Zeng M. 2013. Engineering influenza viral vectors. *Bioengineered* **4**: 9–14.

Li S, Min J-Y, Krug RM, Sen GC. 2006. Binding of the influenza A virus NS1 protein to PKR mediates the inhibition of its activation by either PACT or double-stranded RNA. *Virology* **349**: 13–21.

Li X, Darzynkiewicz Z. 2000. Cleavage of Poly(ADP-ribose) polymerase measured in situ in individual cells: relationship to DNA fragmentation and cell cycle position during apoptosis. *Experimental Cell Research* **255**: 125–132.

Lindsay DA, Betenbaugh MJ. 1992. Quantification of cell culture factors affecting recombinant protein yields in baculovirus-infected insect cells. *Biotechnology and Bioengineering* **39**: 614–618.

Liu J, Shi X, Schwartz R, Kemble G. 2009. Use of MDCK cells for production of live attenuated influenza vaccine. *Vaccine* **27**: 6460–6463.

Liu T, Hannafon B, Gill L, Kelly W, Benbrook D. 2007. Flex-Hets differentially induce apoptosis in cancer over normal cells by directly targeting mitochondria. *Molecular Cancer Therapeutics* **6**: 1814–1822.

Lockshin RA, Beaulaton J. 1974. Programmed cell death. *Life Sciences* **15**: 1549–1565.

Loewer A, Lahav G. 2011. We are all individuals: causes and consequences of non-genetic heterogeneity in mammalian cells. *Current Opinion in Genetics & Development* **21**: 753–758.

Lohr V, Genzel Y, Behrendt I, Scharfenberg K, Reichl U. 2010. A new MDCK suspension line cultivated in a fully defined medium in stirred-tank and wave bioreactor. *Vaccine* **28**: 6256–6264.

Lohr V, Genzel Y, Jordan I, Katinger D, Mahr S, Sandig V, Reichl U. 2012. Live attenuated influenza viruses produced in a suspension process with avian AGE1.CR.pIX cells. *BMC Biotechnology* **12**: 79.

Lohr V, Rath A, Genzel Y, Jordan I, Sandig V, Reichl U. 2009. New avian suspension cell lines provide production of influenza virus and MVA in serum-free media: studies on growth, metabolism and virus propagation. *Vaccine* **27**: 4975–4982.

Lonsdale R, Pau MG, Oerlemans M, Ophorst C, Vooys A, Havenga M, Goudsmit J, UytdeHaag F, Marzio G. 2003. A rapid method for immunotitration of influenza viruses using flow cytometry. *Journal of Virological Methods* **110**: 67–71.

Loo DT. 2011. In situ detection of apoptosis by the TUNEL assay: an overview of techniques. *Methods in Molecular Biology (Clifton, N.J.)* **682**: 3–13.

Luchini ND, Broderick GA, Combs DK. 1996. Characterization of the proteolytic activity of commercial proteases and strained ruminal fluid. *Journal of Animal Science* **74**: 685–692.

Luo M. 2012. Influenza virus entry. *Advances in Experimental Medicine and Biology* **726**: 201–221.

Madin SH, Darby NB Jr. 1958. Established kidney cell lines of normal adult bovine and ovine origin. *Proceedings of the Society for Experimental Biology and Medicine. Society for Experimental Biology and Medicine (New York, N.Y.)* **98**: 574–576.

Von Magnus P. 1954. Incomplete forms of influenza virus. *Advances in Virus Research* **2**: 59–79.

Mahy B, Kangro H. 1996. *Virology Methods Manual*. Academic press: London.

Maranga L, Brazão TF, Carrondo MJT. 2003. Virus-like particle production at low multiplicities of infection with the baculovirus insect cell system. *Biotechnology and Bioengineering* **84**: 245–253.

Marcus PI. 1982. Interferon induction by viruses. IX. Antagonistic activities of virus particles modulated interferon production. *Journal of Interferon Research* **2**: 511–518.

Marcus PI, Ngunjiri JM, Sekellick MJ. 2009. Dynamics of biologically active subpopulations of influenza virus: plaque-forming, noninfectious cell-killing, and defective interfering particles. *Journal of Virology* **83**: 8122–8130.

Marcus PI, Ngunjiri JM, Sekellick MJ, Wang L, Lee C-W. 2010. In vitro analysis of virus particle subpopulations in candidate live-attenuated influenza vaccines distinguishes effective from ineffective vaccines. *Journal of Virology* **84**: 10974–10981.

Marcus PI, Rojek JM, Sekellick MJ. 2005. Interferon induction and/or production and its suppression by influenza A viruses. *Journal of Virology* **79**: 2880–2890.

Matrosovich MN, Matrosovich TY, Gray T, Roberts NA, Klenk H-D. 2004. Neuraminidase is important for the initiation of influenza virus infection in human airway epithelium. *Journal of Virology* **78**: 12665–12667.

Mehtali M, Champion-Arnaud P, Leon A. 2006. Process of manufacturing viral vaccines in suspension avian embryonic derived stem cell lines. WO 2006/108846 A1.

Mei Y, Thompson MD, Cohen RA, Tong X. 2013. Endoplasmic Reticulum Stress and Related Pathological Processes. *Journal of Pharmacological & Biomedical Analysis* **1**: 1000107.

Mercille S, Jolicoeur P, Gervais C, Paquette D, Mosser DD, Massie B. 1999. Dose-dependent reduction of apoptosis in nutrient-limited cultures of NS/0 myeloma cells transfected with the E1B-19K adenoviral gene. *Biotechnology and Bioengineering* **63**: 516–528.

Mercille S, Massie B. 1999. Apoptosis-resistant E1B-19K-expressing NS/0 myeloma cells exhibit increased viability and chimeric antibody productivity under perfusion culture conditions. *Biotechnology and Bioengineering* **63**: 529–543.

Merten OW, Hannoun C, Manuguerra JC, Ventre F, Petres S. 1996. Production of influenza virus in cell cultures for vaccine preparation. *Advances in Experimental Medicine and Biology* **397**: 141–151.

Mitra SK, Schlaepfer DD. 2006. Integrin-regulated FAK-Src signaling in normal and cancer cells. *Current Opinion in Cell Biology* **18**: 516–523.

Moeller A, Kirchdoerfer RN, Potter CS, Carragher B, Wilson IA. 2012. Organization of the influenza virus replication machinery. *Science (New York, N.Y.)* **338**: 1631–1634.

Möhler L, Flockerzi D, Sann H, Reichl U. 2005. Mathematical model of influenza A virus production in large-scale microcarrier culture. *Biotechnology and Bioengineering* **90**: 46–58.

Mohsin MA, Morris SJ, Smith H, Sweet C. 2002. Correlation between levels of apoptosis, levels of infection and haemagglutinin receptor binding interaction of various subtypes of influenza virus: does the viral neuraminidase have a role in these associations. *Virus Research* **85**: 123–131.

Molinari N-AM, Ortega-Sanchez IR, Messonnier ML, Thompson WW, Wortley PM, Weintraub E, Bridges CB. 2007. The annual impact of seasonal influenza in the US: measuring disease burden and costs. *Vaccine* **25**: 5086–5096.

Montagnon BJ. 1989. Polio and rabies vaccines produced in continuous cell lines: a reality for Vero cell line. *Developments in Biological Standardization* **70**: 27–47.

Montomoli E, Khadang B, Piccirella S, Trombetta C, Mennitto E, Manini I, Stanzani V, Lapini G. 2012. Cell culture-derived influenza vaccines from Vero cells: a new horizon for vaccine production. *Expert Review of Vaccines* **11**: 587–594.

Müller T, Dürr R, Isken B, Schulze-Horsel J, Reichl U, Kienle A. 2011. Population balance modelling of influenza virus replication during vaccine production – Influence of apoptosis. In *21st European Symposium on Computer Aided Process Engineering – ESCAPE 21,* Pistikopoulos E, Georgiadis M, Kokossis A (eds). Elsevier Science BV; 1336–1340.

Müller T, Dürr R, Isken B, Schulze-Horsel J, Reichl U, Kienle A. 2013. Distributed modeling of human influenza A virus-host cell interactions during vaccine production. *Biotechnology and Bioengineering* **110**: 2252–2266.

Muramoto Y, Noda T, Kawakami E, Akkina R, Kawaoka Y. 2013. Identification of novel influenza A virus proteins translated from PA mRNA. *Journal of Virology* **87**: 2455–2462.

Nafziger AN, Pratt DS. 2014. Seasonal influenza vaccination and technologies. *Journal of Clinical Pharmacology* **54**: 713–731.

Nakowitsch S, Waltenberger AM, Wressnigg N, Ferstl N, Triendl A, Kiefmann B, Montomoli E, Lapini G, Sergeeva M, Muster T, et al. 2014. Egg- or cell culture-derived hemagglutinin mutations impair virus stability and antigen content of inactivated influenza vaccines. *Biotechnology Journal* **9**: 405–414.

Nayak DP, Chambers TM, Akkina RK. 1985. Defective-interfering (DI) RNAs of influenza viruses: origin, structure, expression, and interference. *Current Topics in Microbiology and Immunology* **114**: 103–151.

Neumann G, Fujii K, Kino Y, Kawaoka Y. 2005. An improved reverse genetics system for influenza A virus generation and its implications for vaccine production. *Proceedings of the National Academy of Sciences of the United States of America* **102**: 16825–16829.

Ngunjiri JM, Sekellick MJ, Marcus PI. 2008. Clonogenic assay of type a influenza viruses reveals noninfectious cell-killing (apoptosis-inducing) particles. *Journal of Virology* **82**: 2673–2680.

Nichols JE, Mock DJ, Roberts NJ Jr. 1993. Use of FITC-labeled influenza virus and flow cytometry to assess binding and internalization of virus by monocytes-macrophages and lymphocytes. *Archives of Virology* **130**: 441–455.

Nishiyama K, Sugawara K, Nouchi T, Kawano N, Soejima K, Abe S-I, Mizokami H. 2008. Purification and cDNA cloning of a novel protease inhibitor secreted into culture supernatant by MDCK cells. *Biologicals: Journal of the International Association of Biological Standardization* **36**: 122–133.

Nivitchanyong T, Martinez A, Ishaque A, Murphy JE, Konstantinov K, Betenbaugh MJ, Thrift J. 2007. Anti-apoptotic genes Aven and E1B-19K enhance performance of BHK cells engineered to express recombinant factor VIII in batch and low perfusion cell culture. *Biotechnology and Bioengineering* **98**: 825–841.

Noda T, Kawaoka Y. 2012. Packaging of influenza virus genome: robustness of selection. *Proceedings of the National Academy of Sciences of the United States of America* **109**: 8797–8798.

Ohmit SE, Victor JC, Rotthoff JR, Teich ER, Truscon RK, Baum LL, Rangarajan B, Newton DW, Boulton ML, Monto AS. 2006. Prevention of antigenically drifted influenza by inactivated and live attenuated vaccines. *The New England Journal of Medicine* **355**: 2513–2522.

Ohuchi M, Asaoka N, Sakai T, Ohuchi R. 2006. Roles of neuraminidase in the initial stage of influenza virus infection. *Microbes and Infection / Institut Pasteur* **8**: 1287–1293.

Olsen CW, Kehren JC, Dybdahl-Sissoko NR, Hinshaw VS. 1996. bcl-2 alters influenza virus yield, spread, and hemagglutinin glycosylation. *Journal of Virology* **70**: 663–666.

Oncül AA, Kalmbach A, Genzel Y, Reichl U, Thévenin D. 2010. Characterization of flow conditions in 2 L and 20 L wave bioreactors using computational fluid dynamics. *Biotechnology Progress* **26**: 101–110.

Orita Y, Ando A, Urakabe S, Abe H. 1976. A metal complexing property of furosemide and bumetanide: determination of pK and stability constant. *Arzneimittel-Forschung* **26**: 11–13.

Oyadomari S, Araki E, Mori M. 2002. Endoplasmic reticulum stress-mediated apoptosis in pancreatic beta-cells. *Apoptosis: an International Journal on Programmed Cell Death* **7**: 335–345.

Paillet C, Forno G, Kratje R, Etcheverrigaray M. 2009. Suspension-Vero cell cultures as a platform for viral vaccine production. *Vaccine* **27**: 6464–6467.

Paillet C, Forno G, Soldano N, Kratje R, Etcheverrigaray M. 2011. Statistical optimization of influenza H1N1 production from batch cultures of suspension Vero cells (sVero). *Vaccine* **29**: 7212–7217.

Palese P, Compans RW. 1976. Inhibition of influenza virus replication in tissue culture by 2-deoxy-2,3-dehydro-N-trifluoroacetylneuraminic acid (FANA): mechanism of action. *The Journal of General Virology* **33**: 159–163.

Parry J. 2014. H10N8 avian flu virus claims its first known human casualty. *BMJ (Clinical Research ed.)* **348**: g1360.

Partridge J, Kieny MP. 2013. Global production capacity of seasonal influenza vaccine in 2011. *Vaccine* **31**: 728–731.

Paterson D, Fodor E. 2012. Emerging roles for the influenza A virus nuclear export protein (NEP). *PLoS Pathogens* **8**: e1003019.

Pau MG, Ophorst C, Koldijk MH, Schouten G, Mehtali M, Uytdehaag F. 2001. The human cell line PER.C6 provides a new manufacturing system for the production of influenza vaccines. *Vaccine* **19**: 2716–2721.

Pau MG, Uytdehaag AGC. 2003. Use of recombinant trypsin for vaccine production. WO 2003076462 A1.

Peschel B, Frentzel S, Laske T, Genzel Y, Reichl U. 2013. Comparison of influenza virus yields and apoptosis-induction in an adherent and a suspension MDCK cell line. *Vaccine* **31**: 5693–5699.

Petiot E, Jacob D, Lanthier S, Lohr V, Ansorge S, Kamen AA. 2011. Metabolic and kinetic analyses of influenza production in perfusion HEK293 cell culture. *BMC Biotechnology* **11**: 84.

Petiot E, Kamen A. 2013. Real-time monitoring of influenza virus production kinetics in HEK293 cell cultures. *Biotechnology Progress* **29**: 275–284.

Petsch B, Schnee M, Vogel AB, Lange E, Hoffmann B, Voss D, Schlake T, Thess A, Kallen K-J, Stitz L, et al. 2012. Protective efficacy of in vitro synthesized, specific mRNA vaccines against influenza A virus infection. *Nature Biotechnology* **30**: 1210–1216.

Plant EP, Liu TM, Xie H, Ye Z. 2012. Mutations to A/Puerto Rico/8/34 PB1 gene improves seasonal reassortant influenza A virus growth kinetics. *Vaccine* **31**: 207–212.

Pleschka S. 2013. Overview of influenza viruses. *Current Topics in Microbiology and Immunology* **370**: 1–20.

Plosker GL. 2012. A/H5N1 prepandemic influenza vaccine (whole virion, vero cell-derived, inactivated) [Vepacel®]. *Drugs* **72**: 1543–1557.

Pohlscheidt M, Langer U, Minuth T, Bödeker B, Apeler H, Hörlein H-D, Paulsen D, Rübsamen-Waigmann H, Henzler H-J, Reichl U. 2008. Development and optimisation of a procedure for the production of Parapoxvirus ovis by large-scale microcarrier cell culture in a non-animal, non-human and non-plant-derived medium. *Vaccine* **26**: 1552–1565.

Porter M, Karp M, Killedar S, Bauer SM, Guo J, Williams D, Breysse P, Georas SN, Williams MA. 2007. Diesel-enriched particulate matter functionally activates human dendritic cells. *American Journal of Respiratory Cell and Molecular Biology* **37**: 706–719.

Pozarowski P, Huang X, Halicka DH, Lee B, Johnson G, Darzynkiewicz Z. 2003. Interactions of fluorochrome-labeled caspase inhibitors with apoptotic cells: a caution in data interpretation. *Cytometry. Part A: The Journal of the International Society for Analytical Cytology* **55**: 50–60.

Price GE, Smith H, Sweet C. 1997. Differential induction of cytotoxicity and apoptosis by influenza virus strains of differing virulence. *The Journal of General Virology* **78 (Pt 11)**: 2821–2829.

Reed C, Meltzer MI, Finelli L, Fiore A. 2012. Public health impact of including two lineages of influenza B in a quadrivalent seasonal influenza vaccine. *Vaccine* **30**: 1993–1998.

Rehberg M, Rath A, Ritter JB, Genzel Y, Reichl U. 2014. Changes in intracellular metabolite pools during growth of adherent MDCK cells in two different media. *Applied Microbiology and Biotechnology* **98**: 385–397.

Rehberg M, Ritter JB, Genzel Y, Flockerzi D, Reichl U. 2013. The relation between growth phases, cell volume changes and metabolism of adherent cells during cultivation. *Journal of Biotechnology* **164**: 489–499.

Reynales H, Astudillo P, de Vallière S, Hatz C, Schlagenhauf P, Rath B, Velentgas P, Fariña A, Sales-Carmona V, Groth N. 2012. A prospective observational safety study on MF59(®) adjuvanted cell culture-derived vaccine, Celtura(®) during the A/H1N1 (2009) influenza pandemic. *Vaccine* **30**: 6436–6443.

Rimmelzwaan GF, Baars M, Claas EC, Osterhaus AD. 1998. Comparison of RNA hybridization, hemagglutination assay, titration of infectious virus and immunofluorescence as methods for monitoring influenza virus replication in vitro. *Journal of Virological Methods* **74**: 57–66.

Ritter JB, Wahl AS, Freund S, Genzel Y, Reichl U. 2010. Metabolic effects of influenza virus infection in cultured animal cells: Intra- and extracellular metabolite profiling. *BMC Systems Biology* **4**: 61.

Roberson EC, Tully JE, Guala AS, Reiss JN, Godburn KE, Pociask DA, Alcorn JF, Riches DWH, Dienz O, Janssen-Heininger YMW, et al. 2012. Influenza induces endoplasmic reticulum stress, caspase-12-dependent apoptosis, and c-Jun N-terminal kinase-mediated transforming growth factor-β release in lung epithelial cells. *American Journal of Respiratory Cell and Molecular Biology* **46**: 573–581.

Robertson JS. 1993. Clinical influenza virus and the embryonated Hen's egg. *Reviews in Medical Virology* **3**: 97–106.

Robertson JS, Bootman JS, Newman R, Oxford JS, Daniels RS, Webster RG, Schild GC. 1987. Structural changes in the haemagglutinin which accompany egg adaptation of an influenza A(H1N1) virus. *Virology* **160**: 31–37.

Rodriguez-Boulan E, Paskiet KT, Sabatini DD. 1983. Assembly of enveloped viruses in Madin-Darby canine kidney cells: polarized budding from single attached cells and from clusters of cells in suspension. *The Journal of Cell Biology* **96**: 866–874.

Roedig JV, Rapp E, Höper D, Genzel Y, Reichl U. 2011. Impact of host cell line adaptation on quasispecies composition and glycosylation of influenza A virus hemagglutinin. *PloS One* **6**: e27989.

Rollié S. 2010. Heteroaggregation processes in colloidal particle and cell systems. In *Forschungsberichte aus dem Max-Planck-Institut für Dynamik komplexer technischer Systeme*. Shaker Verlag, Aachen.

Roose K, Fiers W, Saelens X. 2009. Pandemic preparedness: toward a universal influenza vaccine. *Drug News & Perspectives* **22**: 80–92.

Rudolf M, Kuhlisch W. 2008. *Biostatistik: eine Einführung für Biowissenschaftler*. Pearson Studium, München.

Sacks H, Bank S, Kramer I, Novis B, Marks IN. 1971. A comparison between spectrophotometric and titrimetric methods of estimating trypsin. *Gut* **12**: 727–728.

Saira K, Lin X, DePasse JV, Halpin R, Twaddle A, Stockwell T, Angus B, Cozzi-Lepri A, Delfino M, Dugan V, et al. 2013. Sequence analysis of in vivo defective interfering-like RNA of influenza A H1N1 pandemic virus. *Journal of Virology* **87**: 8064–8074.

Sakahira H, Enari M, Nagata S. 1998. Cleavage of CAD inhibitor in CAD activation and DNA degradation during apoptosis. *Nature* **391**: 96–99.

Sanders BP, Edo-Matas D, Custers JHHV, Koldijk MH, Klaren V, Turk M, Luitjens A, Bakker WAM, Uytdehaag F, Goudsmit J, et al. 2013. PER.C6(®) cells as a serum-free suspension cell platform for the production of high titer poliovirus: a potential low cost of goods option for world supply of inactivated poliovirus vaccine. *Vaccine* **31**: 850–856.

Sanders MT, Brown LE, Deliyannis G, Pearse MJ. 2005. ISCOMTM-based vaccines: The second decade. *Immunology and Cell Biology* **83**: 119–128.

Sandig V, Jordan I. 2005. Immortalized avian cell lines for virus production. WO 2005/042728 A2.

Saraste A, Pulkki K. 2000. Morphologic and biochemical hallmarks of apoptosis. *Cardiovascular Research* **45**: 528–537.

Schneider J, Wolff T. 2009. Nuclear functions of the influenza A and B viruses NS1 proteins: do they play a role in viral mRNA export? *Vaccine* **27**: 6312–6316.

Schultz-Cherry S, Dybdahl-Sissoko N, Neumann G, Kawaoka Y, Hinshaw VS. 2001. Influenza virus ns1 protein induces apoptosis in cultured cells. *Journal of Virology* **75**: 7875–7881.

Schulze-Horsel J. 2011. Zellphysiologische Charakterisierung von Zellkulturen in der Influenza-Impfstoffproduktion. In *Forschungsberichte aus dem Max-Planck-Institut für Dynamik komplexer technischer Systeme*. Shaker Verlag, Aachen.

Schulze-Horsel J, Genzel Y, Reichl U. 2008. Flow cytometric monitoring of influenza A virus infection in MDCK cells during vaccine production. *BMC Biotechnology* **8**: 45.

Schulze-Horsel J, Schulze M, Agalaridis G, Genzel Y, Reichl U. 2009. Infection dynamics and virus-induced apoptosis in cell culture-based influenza vaccine production-Flow cytometry and mathematical modeling. *Vaccine* **27**: 2712–2722.

Scott PD, Meng B, Marriott AC, Easton AJ, Dimmock NJ. 2011. Defective interfering influenza virus confers only short-lived protection against influenza virus disease: evidence for a role for adaptive immunity in DI virus-mediated protection in vivo. *Vaccine* **29**: 6584–6591.

Seitz C, Frensing T, Höper D, Kochs G, Reichl U. 2010. High yields of influenza A virus in Madin-Darby canine kidney cells are promoted by an insufficient interferon-induced antiviral state. *The Journal of General Virology* **91**: 1754–1763.

Seitz C, Isken B, Heynisch B, Rettkowski M, Frensing T, Reichl U. 2012. Trypsin promotes efficient influenza vaccine production in MDCK cells by interfering with the antiviral host response. *Applied Microbiology and Biotechnology* **93**: 601–611.

Selman M, Dankar SK, Forbes NE, Jia J-J, Brown EG. 2012. Adaptive mutation in influenza A virus non-structural gene is linked to host switching and induces a novel protein by alternative splicing. *Emerging Microbes & Infections* **1**: e42.

Shaw A. 2012. New technologies for new influenza vaccines. *Vaccine* **30**: 4927–4933.

Shoji Y, Farrance CE, Bautista J, Bi H, Musiychuk K, Horsey A, Park H, Jaje J, Green BJ, Shamloul M, et al. 2012. A plant-based system for rapid production of influenza vaccine antigens. *Influenza and other Respiratory Viruses* **6**: 204–210.

Sitailo LA, Tibudan SS, Denning MF. 2002. Activation of caspase-9 is required for UV-induced apoptosis of human keratinocytes. *The Journal of Biological Chemistry* **277**: 19346–19352.

Sitton G, Srienc F. 2011. Single-cell tracking with a reversing flow cytometer. *Cytometry. Part A: The Journal of the International Society for Analytical Cytology* **79**: 66–76.

Smith GJD, Vijaykrishna D, Bahl J, Lycett SJ, Worobey M, Pybus OG, Ma SK, Cheung CL, Raghwani J, Bhatt S, et al. 2009. Origins and evolutionary genomics of the 2009 swine-origin H1N1 influenza A epidemic. *Nature* **459**: 1122–1125.

Snijder B, Pelkmans L. 2011. Origins of regulated cell-to-cell variability. *Nature Reviews. Molecular Cell Biology* **12**: 119–125.

Snijder B, Sacher R, Rämö P, Damm E-M, Liberali P, Pelkmans L. 2009. Population context determines cell-to-cell variability in endocytosis and virus infection. *Nature* **461**: 520–523.

Somorin O, Tokura S, Nishi N, Noguchi J. 1979. The action of trypsin on synthetic chromogenic arginine substrates. *Journal of Biochemistry* **85**: 157–162.

Steele-Mortimer OA, Meier-Ewert H, Löser R, Hasmann MJ. 1990. Flow cytometric analysis of virus-infected cells and its potential use for screening antiviral agents. *Journal of Virological Methods* **27**: 241–252.

Suphaphiphat P, Keiner B, Trusheim H, Crotta S, Tuccino AB, Zhang P, Dormitzer PR, Mason PW, Franti M. 2010. Human RNA polymerase I-driven reverse genetics for influenza a virus in canine cells. *Journal of Virology* **84**: 3721–3725.

Suzuki T, Takahashi T, Guo C-T, Hidari KI-PJ, Miyamoto D, Goto H, Kawaoka Y, Suzuki Y. 2005. Sialidase activity of influenza A virus in an endocytic pathway enhances viral replication. *Journal of Virology* **79**: 11705–11715.

Takizawa T, Matsukawa S, Higuchi Y, Nakamura S, Nakanishi Y, Fukuda R. 1993. Induction of programmed cell death (apoptosis) by influenza virus infection in tissue culture cells. *The Journal of General Virology* **74 (Pt 11)**: 2347–2355.

Tapia F, Vogel T, Genzel Y, Behrendt I, Hirschel M, Gangemi JD, Reichl U. 2014. Production of high-titer human influenza A virus with adherent and suspension MDCK cells cultured in a single-use hollow fiber bioreactor. *Vaccine* **32**: 1003–1011.

Tetsutani K, Ishii KJ. 2012. Adjuvants in influenza vaccines. *Vaccine* **30**: 7658–7661.

Tey BT, Singh RP, Piredda L, Piacentini M, Al-Rubeai M. 2000. Influence of bcl-2 on cell death during the cultivation of a Chinese hamster ovary cell line expressing a chimeric antibody. *Biotechnology and Bioengineering* **68**: 31–43.

Thomassen YE, Rubingh O, Wijffels RH, van der Pol LA, Bakker WAM. 2014. Improved poliovirus D-antigen yields by application of different Vero cell cultivation methods. *Vaccine* **32**: 2782–2788.

To KKW, Tsang AKL, Chan JFW, Cheng VCC, Chen H, Yuen K-Y. 2014. Emergence in China of human disease due to avian influenza A(H10N8)–cause for concern? *The Journal of Infection* **68**: 205–215.

Tobita K. 1975. Permanent canine kidney (MDCK) cells for isolation and plaque assay of influenza B viruses. *Medical Microbiology and Immunology* **162**: 23–27.

Tobita K, Sugiura A, Enomote C, Furuyama M. 1975. Plaque assay and primary isolation of influenza A viruses in an established line of canine kidney cells (MDCK) in the presence of trypsin. *Medical Microbiology and Immunology* **162**: 9–14.

Toovey S. 2007. Preventing rabies with the Verorab vaccine: 1985-2005 Twenty years of clinical experience. *Travel Medicine and Infectious Disease* **5**: 327–348.

Topham DJ, Tripp RA, Doherty PC. 1997. CD8+ T cells clear influenza virus by perforin or Fas-dependent processes. *Journal of Immunology (Baltimore, Md.: 1950)* **159**: 5197–5200.

Tree JA, Richardson C, Fooks AR, Clegg JC, Looby D. 2001. Comparison of large-scale mammalian cell culture systems with egg culture for the production of influenza virus A vaccine strains. *Vaccine* **19**: 3444–3450.

Trifonov V, Khiabanian H, Greenbaum B, Rabadan R. 2009. The origin of the recent swine influenza A(H1N1) virus infecting humans. *Euro Surveillance: Bulletin Européen sur les Maladies Transmissibles = European Communicable Disease Bulletin* **14**.

Tsutsumi R, Fujisaki S, Shozushima M, Saito K, Sato S. 2006. Anoikis-resistant MDCK cells carrying susceptibilities to TNF-alpha and verotoxin that are suitable for influenza virus cultivation. *Cytotechnology* **52**: 71–85.

Tudela J, Garcia-Canovas F, Garcia-Carmona F, Iborra JL, Lozano JA. 1986. Irreversible inhibition of trypsin by TLCK. A continuous method for kinetic study of irreversible enzymatic inhibitors in the presence of substrate. *The International Journal of Biochemistry* **18**: 285–288.

Valneva. 2014. EB66® cell-based pandemic influenza vaccine manufacturing. http://www.valneva.com/?page=82 (accessed 2014-08-16).

Varga ZT, Ramos I, Hai R, Schmolke M, García-Sastre A, Fernandez-Sesma A, Palese P. 2011. The influenza virus protein PB1-F2 inhibits the induction of type I interferon at the level of the MAVS adaptor protein. *PLoS Pathogens* **7**: e1002067.

Vasin AV, Temkina OA, Egorov VV, Klotchenko SA, Plotnikova MA, Kiselev OI. 2014. Molecular mechanisms enhancing the proteome of influenza A viruses: An overview of recently discovered proteins. *Virus Research* **185C**: 53–63.

Vigerust DJ, Shepherd VL. 2007. Virus glycosylation: role in virulence and immune interactions. *Trends in Microbiology* **15**: 211–218.

Voeten JT, Brands R, Palache AM, van Scharrenburg GJ, Rimmelzwaan GF, Osterhaus AD, Claas EC. 1999. Characterization of high-growth reassortant influenza A viruses generated in MDCK cells cultured in serum-free medium. *Vaccine* **17**: 1942–1950.

De Vries RP, Smit CH, de Bruin E, Rigter A, de Vries E, Cornelissen LAHM, Eggink D, Chung NPY, Moore JP, Sanders RW, et al. 2012. Glycan-dependent immunogenicity of recombinant soluble trimeric hemagglutinin. *Journal of Virology* **86**: 11735–11744.

Wahl A, Sidorenko Y, Dauner M, Genzel Y, Reichl U. 2008. Metabolic flux model for an anchorage-dependent MDCK cell line: characteristic growth phases and minimum substrate consumption flux distribution. *Biotechnology and Bioengineering* **101**: 135–152.

Walls HH, Harmon MW, Slagle JJ, Stocksdale C, Kendal AP. 1986. Characterization and evaluation of monoclonal antibodies developed for typing influenza A and influenza B viruses. *Journal of Clinical Microbiology* **23**: 240–245.

WHO. 2014. Influenza (seasonal) – Fact sheet N° 211. http://www.who.int/mediacentre/factsheets/fs211/en/ (accessed: 2014-04-11).

Van Wielink R, Kant-Eenbergen HCM, Harmsen MM, Martens DE, Wijffels RH, Coco-Martin JM. 2011. Adaptation of a Madin-Darby canine kidney cell line to suspension growth in serum-free media and comparison of its ability to produce avian influenza virus to Vero and BHK21 cell lines. *Journal of Virological Methods* **171**: 53–60.

Wise HM, Foeglein A, Sun J, Dalton RM, Patel S, Howard W, Anderson EC, Barclay WS, Digard P. 2009. A complicated message: Identification of a novel PB1-related protein translated from influenza A virus segment 2 mRNA. *Journal of Virology* **83**: 8021–8031.

Wise HM, Hutchinson EC, Jagger BW, Stuart AD, Kang ZH, Robb N, Schwartzman LM, Kash JC, Fodor E, Firth AE, et al. 2012. Identification of a novel splice variant form of the influenza A virus M2 ion channel with an antigenically distinct ectodomain. *PLoS Pathogens* **8**: e1002998.

Wlodkowic D, Telford W, Skommer J, Darzynkiewicz Z. 2011. Apoptosis and beyond: cytometry in studies of programmed cell death. *Methods in Cell Biology* **103**: 55–98.

Wong KT, Peter CH, Greenfield PF, Reid S, Nielsen LK. 1996. Low multiplicity infection of insect cells with a recombinant baculovirus: The cell yield concept. *Biotechnology and Bioengineering* **49**: 659–666.

Wood HA, Johnston LB, Burand JP. 1982. Inhibition of Autographa californica nuclear polyhedrosis virus replication in high-density Trichoplusia ni cell cultures. *Virology* **119**: 245–254.

Wu X, Liang H, Tan Y, Yuan C, Li S, Li X, Li G, Shi Y, Zhang X. 2014b. Cell-SELEX aptamer for highly specific radionuclide molecular imaging of glioblastoma in vivo. *PloS One* **9**: e90752.

Wu Y, Wu Y, Tefsen B, Shi Y, Gao GF. 2014a. Bat-derived influenza-like viruses H17N10 and H18N11. *Trends in Microbiology* **22**: 183–191.

Wurm FM. 2004. Production of recombinant protein therapeutics in cultivated mammalian cells. *Nature Biotechnology* **22**: 1393–1398.

Wurzer WJ, Planz O, Ehrhardt C, Giner M, Silberzahn T, Pleschka S, Ludwig S. 2003. Caspase 3 activation is essential for efficient influenza virus propagation. *The EMBO Journal* **22**: 2717–2728.

Wyllie AH. 1980. Glucocorticoid-induced thymocyte apoptosis is associated with endogenous endonuclease activation. *Nature* **284**: 555–556.

Yang LPH. 2013. Recombinant trivalent influenza vaccine (flublok(®)): a review of its use in the prevention of seasonal influenza in adults. *Drugs* **73**: 1357–1366.

Yee L, Blanch HW. 1993. Recombinant trypsin production in high cell density fed-batch cultures in Escherichia coli. *Biotechnology and Bioengineering* **41**: 781–790.

Young F, Marra F. 2011. A systematic review of intradermal influenza vaccines. *Vaccine* **29**: 8788–8801.

Zamarin D, García-Sastre A, Xiao X, Wang R, Palese P. 2005. Influenza virus PB1-F2 protein induces cell death through mitochondrial ANT3 and VDAC1. *PLoS Pathogens* **1**: e4.

Zeiger RS. 2002. Current issues with influenza vaccination in egg allergy. *The Journal of Allergy and Clinical Immunology* **110**: 834–840.

Zhang C, Yang Y, Zhou X, Yang Z, Liu X, Cao Z, Song H, He Y, Huang P. 2011. The NS1 protein of influenza A virus interacts with heat shock protein Hsp90 in human alveolar basal epithelial cells: implication for virus-induced apoptosis. *Virology Journal* **8**: 181.

Zheng W, Tao YJ. 2013. Structure and assembly of the influenza A virus ribonucleoprotein complex. *FEBS Letters* **587**: 1206–1214.

Zhirnov OP, Klenk H-D. 2007. Control of apoptosis in influenza virus-infected cells by up-regulation of Akt and p53 signaling. *Apoptosis: an International Journal on Programmed Cell Death* **12**: 1419–1432.

Zhirnov OP, Konakova TE, Wolff T, Klenk H-D. 2002. NS1 protein of influenza A virus down-regulates apoptosis. *Journal of Virology* **76**: 1617–1625.

Zhong X, Rescorla FJ. 2012. Cell surface adhesion molecules and adhesion-initiated signaling: understanding of anoikis resistance mechanisms and therapeutic opportunities. *Cellular Signalling* **24**: 393–401.

8 Appendix

8.1 Equipment and consumables

A list of all used equipment and consumables is given in Table 8-1.

Table 8-1 Used equipment.

Equipment	Manufacturer	Model
Autoclave	Thermo Scientific	Varioklav 135S
Balances	Sartorius	Cubis® precision MSU62029
Biological safety cabinet	Thermo Scientific	Safe 2020 Heraeus HERAsafe HS15
Bioreactors	Sartorius DasGip	Biostat® Bplus, Cplus Cellferm-pro® system
Cell counter	Beckman Coulter	Vi-Cell™ XR
Cell filter	Partec	CellTrics® 50 µm
Centrifuges	Beckman Coulter Thermo Scientific Grant bio	Avanti J-20 XP Heraeus Biofuge PrimoR PCV 3000
CO_2 Incubator	Thermo Scientific Integra Biosciences	Heracell™ NU-5510E
Dispenser	Eppendorf	Multipette
Flow cytometer	Beckman Coulter	Coulter Epics® XL
Flow cytometer tubes	Sarstedt	FACSCAN, 5 mL
Glass bottles	Schott	0.05–5 L
Heating block thermostat	neoLab	neoBlock Mono 1
Haemocytometer	Marienfeld	Fuchs-Rosenthal
Incubation shaker	Infors HT	Multitron
Light optical microscope	Carl Zeiss	Axiovert S100, 40C, Axioskop2
Metabolite analyser	Nova Biomedical	BioProfile® 100 Plus
Manual pipettes	Eppendorf	10, 100, 200, 1000 µL, 10 mL
Microplate reader	Tecan	Infinite® M200
Microtitre plates	Greiner bio-one	96-well plates, flat or U-bottom shape
Multichannel pipettes	Eppendorf	100, 300 µL
pH meter	WTW	inoLab®
O_2 sensors	Mettler Toledo Broadley James	InPro 6100 OxyProbe D140
pH sensor	Mettler Toledo Broadley James	405-DPAS-SC-K85 FermProbe®
Pipette aid	Hirschmann Laborgeräte	pipetus®
Pipette tips	Greiner bio-one, Brand	10 µL–10 mL
Roller bottle incubator	Bellco Biotechnology	Benchtop incubator

Reaction tubes (screw-topped)	Greiner bio-one	15, 50 mL
Rotator	Stuart Scientific Bibby	Culture Tube Rotator SC1
Shaker flask	VWR	125, 250 mL
Single-use pipettes	Greiner bio-one	Cellstar® 1, 2, 5, 10, 25, 50 mL
Single-use cell culture flasks	Greiner bio-one	Cellstar® 25, 75, 175 cm^2, Cellmaster™ 850 cm^2 roller bottle
Small reaction tubes	Greiner bio-one	1.5, 2 mL
Spinner flask	Wheaton	Celstir® 250 mL, 500 mL
Syringes	B Braun	Omnifix 5, 10, 20 mL
Syringe filters (single-use)	Sartorius Neolab	Midisart® 0.2 µm 0.2 µm
Ultrapure water purification system	Millipore	Milli-Q Advantage A10
Vortexer	VWR	Analog Vortex Mixer

8.2 Chemicals

All used chemicals are listed in Table 8-2.

Table 8-2 Used chemicals.

Chemical	Manufacturer	Catalogue number
Acetic acid	Carl Roth Merck	3738.1 818755.1000
Acetone	Carl Roth	CP40.4
Alexa Fluor® 488 donkey anti-sheep IgG	Invitrogen	A-11015
Benzonase	Sigma-Aldrich	E1014-25KU
BioProfile® reagent pack	Nova Biomedical	38291
BSA	Sigma-Aldrich	A2153
Coulter CLENZ®	Beckman Coulter	8448222
Coulter® ISOTON® II Diluent	Beckman Coulter	8448011
Cytodex™ 1	GE Healthcare	17-0448-01
D-(+)-glucose	Carl Roth	X997.3
Disodium hydrogen phosphate (Na_2HPO_4)	Merck	106585
EDTA	Sigma-Aldrich	ED2SS
Ethanol	Carl Roth	T868.3
Ethanolamine	Sigma-Aldrich	E9508
Flow-Check™ Fluorospheres	Beckman Coulter	6605359
FCS	Gibco Pan Biotech	10270-106 P30-3302
Gentamicin	Invitrogen	11130-036
Glycine	Carl Roth	3790.2
GMEM powder medium	Gibco	22100-093

Hydrochloric acid (HCl)	Carl Roth	4625.2
HEPES (4-(2-hydroxyethyl)-1-piperazineethanesulfonic acid)	Carl Roth	9105.3
Influenza anti A/PR/8/34 (H1N1) HA serum (sheep)	NIBSC	03/242
Influenza anti A/Wisconsin/67/2005-like HA serum (sheep)	NIBSC	05/236
Influenza anti A/Brisbane/10/2007 (H3N2)-like HA	NIBSC	08/246
In situ cell death detection kit, TMR red	Roche	12156792910
Isopropanol	Carl Roth	6752.4
L-Alanine	Sigma-Aldrich	05130
L-Asparagine	Sigma-Aldrich	A8381
L-Aspartic acid	Merck	100129.1000
L-Glutamine	Sigma-Aldrich	G3126
L-Glutamic acid	Merck	100291.0250
Magnesium chloride hexahydrate ($MgCl_2$ x 6 H_2O)	Carl Roth	2189.2
Mouse anti influenza A Nucleoprotein (FITC-labelled)	AbD Serotec	MCA400
O2 Electrolyte	Broadley James	AS-3140-C30-0025
Paraformaldehyde	Sigma-Aldrich	P6148
Peptone	LabM Ltd.	MC033
pH 7.0 buffer solution for pH sensor calibration	Mettler Toledo	51350006
pH 9.21 buffer solution for pH sensor calibration	Mettler Toledo	51350008
Pluronic® F-68	Gibco	24040-032
Potassium chloride (KCl)	Merck	104935.5000
Potassium dihydrogen phosphate (KH_2PO_4)	Merck	104877.1000
Quantum™ FITC-5 MESF beads	Bangs Laboratories	555A
Smif8 and Smif8-PG powder medium	K. Scharfenberg (FH Emden/Leer)	through personal contact
Sodium bicarbonate ($NaHCO_3$)	Carl Roth	6885.3
Sodium chloride (NaCl)	Merck Carl Roth	106400.5000 P029.3
Sodium hydroxide (pellets)	Sigma-Aldrich	S8045
Sodium pyruvate	Sigma-Aldrich	P8574
Trisodium citrate dihydrate	Merck	106448.0500
Triton™ X-100	Sigma-Aldrich	X100
Trypan blue	Merck	111732
Trypsin	Gibco Sigma-Aldrich	27250-018 T7409
Trypsin activity colorimetric assay kit	BioVision	K771-100

8.3 List of SOPs

A list of SOPs of methods used in this work is given in Table 8-3.

Table 8-3 List of relevant SOPs.

SOP Name	Number	Date
Preparation of PBS solution	M/01	2007-09-26
Preparation of Glasgow full medium from ready-to-use solutions	M/02	2006-09-11
Preparation of Glasgow-MEM medium from powder	M/03	2010-08-19
Preparation of Smif8 medium	M/03.3	2012-05-16
Preparation of trypsin-EDTA (10x) solution	M/07	2010-05-20
Preparation of 2% paraformaldehyde	M/08	2009-11-30
Preparation of glutamine solution	M/09	2007-09-25
Preparation of glycine solution	M/10	2008-06-04
Preparation of pyruvate solution	M/11	2007-09-25
Preparation of FACS buffer washing solution	M/12	2007-01-04
Preparation of glucose solution	M/14	2008-03-26
Preparation of trypan blue solution	M/15	2011-04-28
Manual counting of total cells and viable cells	Z/01	2005-11-10
Adherent cell concentration determination	Z/01.1	2005-03-07
Unfreezing of adherent MDCK cells	Z/02	2005-10-25
Medium exchange MDCK cells	Z/03	2003-06-25
Passage of MDCK cells in serum-containing medium	Z/04	2006-09-11
Passage of MDCK cells in serum-free medium	Z/05	2006-09-11
Unfreezing and cultivation of MDCK suspension cells	Z/10	2008-07-17
Preparation of trypsin solution for virus infection	V/02	2007-01-17
Haemagglutination assay	V/05	2011-01-20
Preparation of erythrocyte solution	V/07	2007-06-07
$TCID_{50}$ assay	V/08	2008-06-02
Flow cytometric double staining for NP and TUNEL assay	-	2007-02-11

8.4 Analysis of NP-fluorescence distributions

A Gaussian fit of NP histograms was performed and mean fluorescence intensity, the according SD, and the 95% confidence interval of the SD were determined. Analysis of a three times repeated T25-flask infection of adherent MDCK cells with influenza virus A/PR/8 RKI at MOI 3. Values plotted in Figure 4-8 (section 4.3.2) are listed in Table 8-4.

Table 8-4 Mean fluorescence intensities (FI) with corresponding uncertainties (± SD), and SD in positive and negative direction with corresponding uncertainties (95% confidence interval) determined by a Gaussian Fit of NP-fluorescence distributions of T25-flasks infected with influenza A/PR/8 RKI at MOI 3 (n = 3).

		mean FI	+ SD	- SD
24 hpi	**Exp. 1**	2469 (1269–4804)	2335 (2292–2379)	1200 (1189–1223)
	Exp. 2	1902 (839–4313)	2411 (2372–2489)	1063 (1048–1071)
	Exp. 3	2138 (1079–4236)	2098 (2011–2136)	1059 (1049–1079)
32 hpi	**Exp. 1**	1662 (781–3539)	1876 (1845–1941)	881 (867–888)
	Exp. 2	1937 (847–4431)	2494 (2454–2574)	1090 (1083–1098)
	Exp. 3	1937 (1051–3571)	1634 (1602–1666)	886 (877–896)
40 hpi	**Exp. 1**	3635 (2158–6125)	2490 (2327–2545)	1478 (1458–1497)
	Exp. 2	2537 (1281–5025)	2489 (2444–2580)	1256 (1233–1268)
	Exp. 3	1868 (910–3837)	1968 (1934–2003)	959 (950–967)

The analysis of NP-fluorescence distributions was also performed for three parallel T25-flasks of adherent MDCK cells infected with influenza virus A/PR/8 RKI at MOI 0.016 and is displayed in Table 8-5. The according courses of cell concentrations, HA titres, and flow cytometric analysis of infection status and apoptosis were shown in Figure 4-6.

Table 8-5 Analysis of NP-fluorescence distributions of three parallel infected T25-flasks (also displayed in Figure 4-6). Mean FI with corresponding uncertainties (± SD) as well as SD in positive and negative direction with corresponding uncertainties (95% confidence interval).

		mean FI	+ SD	- SD
32 hpi	**Exp. 1**	3907 (2277–6702)	2795 (2675–2917)	1629 (1589–1671)
	Exp. 2	4274 (2447–7465)	3191 (2992–3395)	1827 (1762–1894)
	Exp. 3	4198 (2606–6762)	2564 (2443–2749)	1592 (1522–1639)
40 hpi	**Exp. 1**	3234 (1692–6236)	3002 (2891–3058)	1542 (1512–1557)
	Exp. 2	2852 (1506–5400)	2549 (2500–2647)	1346 (1319–1359)
	Exp. 3	3148 (1575–6293)	3145 (3032–3201)	1573 (1559–1602)
52 hpi	**Exp. 1**	2560 (1304–5025)	2466 (2421–2557)	1256 (1244–1268)
	Exp. 2	2726 (1340–5548)	2822 (2723–2872)	1387 (1375–1411)
	Exp. 3	2382 (1160–4892)	2510 (2466–2554)	1222 (1212–1243)
72 hpi	**Exp. 1**	4160 (2340–7399)	3238 (3106–3305)	1821 (1800–1863)
	Exp. 2	3872 (2158–6947)	3075 (2952–3138)	1714 (1695–1753)
	Exp. 3	3978 (2257–7010)	3032 (2907–3096)	1721 (1700–1762)